Synthesis And Coordination Of Phosphorus-Nitrogen Ligands.

By

Matthew Victor Wheatley

A Thesis submitted in partial fulfilment for the award of

Doctor of Philosophy

School of Chemistry

University of St. Andrews

North Haugh

St. Andrews

Fife

KY16 9ST.

1 April 2004.

DECLARATION.

I, Matthew Victor Wheatley, hereby certify that this thesis, which is approximately 35,000 words in length, has been written by me, that it is the record of work carried out by me and that it has not been submitted in any previous application for a higher degree.

Date 3/12/04 signature of candidate.

I was admitted as a research student in September 2000 and as a candidate for the degree of Doctor of Philosophy in September 2001; the higher study for which this is a record was carried out in the University of St. Andrews between 2000 and 2003.

Date 3/12/04 signature of candidate..

I hereby certify that the candidate has fulfilled the conditions of the Resolution and Regulations appropriate for the degree of Doctor of Philosophy in the University of St. Andrews and that the candidate is qualified to submit this thesis in application for that degree.

Date 3/12/04 signature of supervisor

UNRESTRICTED ACCESS

In submitting this thesis to the University of St. Andrews I understand that I am giving permission for it to be made available for use in accordance with the regulations of the University Library for the time being in force, subject to any copyright vested in the work not being affected thereby. I also understand that the title and abstract will be published, and that a copy of the work may be made and supplied to any *bona fide* library or research worker.

Date 3/12/04 signature of candidate.

ASTRACT

This thesis describes the synthesis and coordination of a range of phosphorus-nitrogen ligands.

2-(Diphenylphosphino)picolinoamide (dpppa) was prepared and oxidised to form dpppa-E (E = O, S and SE) or reacted with metal complexes such as $[MCl_2(cod)]$ (M = Pt and Pd), $[\{PdCl(\mu\text{-}Cl)(\eta^3\text{-}C_3H_5)\}_2]$, $[\{MCl(\mu\text{-}Cl)(Cp^*)\}_2]$ (M = Rh or Ir), $[\{Rh(\mu\text{-}Cl)(cod)\}_2]$, $[\{RuCl(\mu\text{-}Cl)(\eta^6\text{-}p\text{-}MeC_6H_4{}^iPr)\}_2]$ and [AuCl(tht)] to generates a range of new monodentate complexes. Treatment of these monodentate complexes with base provides a bidentate, chelated ligand bound by O^-, and whereas treatment with halide abstractors provides a bidentate, chelated ligand bound by the pyridyl nitrogen and the phosphorus.

2-(Diphenylphosphino)thiophenecarboxamide (dpptc) was prepared and oxidised to form dpptc-E (E = O and S), or reacted with appropriate metal complexes such as $[MCl_2(cod)]$ (M = Pt and Pd), $[\{PdCl(\mu\text{-}Cl)(\eta^3\text{-}C_3H_5)\}_2]$, $[\{MCl(\mu\text{-}Cl)(Cp^*)\}_2]$ (M = Rh or Ir), $[\{Rh(\mu\text{-}Cl)(cod)\}_2]$, $[\{RuCl(\mu\text{-}Cl)(\eta^6\text{-}p\text{-}MeC_6H_4{}^iPr)\}_2]$ and [AuCl(tht)] to generate a range of new monodentate complexes. Treatment of $[RuCl_2(p\text{-}Cymene)(dpptc\text{-}P)]$ with a halide abstractor generates the chelated complex with the carbonyl oxygen binding to the metal.

Bis(2,6-diphenylphosphino)dipicolinamide (bdpppa) was prepared and can be unsymmetrically oxidised to give bdpppa-EE' (E = E' = S and Se). It can also react with $[\{PdCl(\mu\text{-}Cl)(\eta^3\text{-}C_3H_5)\}_2]$ and $[\{Pt(\mu\text{-}Cl)(\eta^3\text{-}C_3H_6)\}_4]$ to give bridged complexes of the type $[M_2Cl_2(\eta^3\text{-}C_3H_6)_2(bdpppa\text{-}P,P)]$ (M = Pt and Pd), it also reacts with [AuCl(tht)] to either give [AuCl(bdpppa-*P*)] or $[Au_2Cl_2(bdpppa\text{-}P)]$.

7-diphenylphosphinoazaindole (dppai) was synthesised and oxidised to give dppai-S, or was reacted with [MCl_2(cod)] (M = Pd and Pt)] to give the 1:1, chelated complex [MCl_2(dppai-*P,N*)], it was also reacted with [PtClR(cod)] (R = Me and Ph) to generate the analogous complex.

2-(diphenylphosphino)aminothiazole (dppat), 2-(diphenylphosphino)amino-4-methylthiazole (Me-dppat) and 2-(diphenylphosphino)amino-4-tert-butylthiazole (b-dppat) were synthesised and dppat and Me-dppat subsequently oxidised to give the sulfur derivative. Reaction of these ligands with [$PtCl_2$(cod)] showed that dppat and Me-dppat have the ability to bind both monodentate and bidentate and b-dppat only has the ability to bind in a monodentate style.

AKNOWLEDGEMENTS.

I must thank Jo for helping me in every way throughout the last few years; hopefully I wasn't too much hard work. I can't say enough about how much Derek has been amazing to helping me get this done, always supportive, always enthusiastic and always very patient, thanks for everything. Also I must thank Alex, not just all the X-ray crystal work (which was excellent), but also for being a pleasure to bump into for a cheery chat. Also thanks to Heather for her Crystal Magic.

The guys in the lab deserve a mention, especially Steve, Prav, Petr and Matt for their help and guidance over the three (and a half) years, the lab couldn't have had a better set of Post Doc's. My fellow lab mates also squeeze in, thanks to Rehan, Zubie, the Frenchman, Gary Oober, the Monk and Maurice for all the good times and the bad, memorable moments must include studies on reaction of metals with water, bleach and various solvents, along with reaction of acid with ned kegs.

Also a big thanks to all the staff in the department, there's too many to mention, but many have helped me get through.

Finally I have to thank my folks, they too have helped more than they know.

CONTENTS

List Of Figures

LIST OF TABLES

ABBREVIATIONS.

Å	Angstrom unit 10^{-10} m
Acac	acetylacetonate, $[CH_3C(O)CHC(O)CH_3]^-$
AIBN	azobis(isobutyronitrile)
Bn	benzyl, $-CH_2C_6H_5$
^{n}Bu	*n*-Butyl, $-(CH_2)_3CH_3$
^{t}Bu	*t*-Butyl, $-C(CH_3)_3$
cm^{-1}	wavenumber
cod	1,5-cyclooctadiene, C_8H_{12}
Cy	cyclohexyl, $-C_6H_{11}$
dcm	dichloromethane, CH_2Cl_2
dmpm	bis(dimethylphosphino)methane, $Me_2PCH_2PMe_2$
dmpe	bis(dimethylphosphino)ethane, $Me_2PCH_2CH_2PMe_2$
dmso	dimethyl sulfoxide, $(CH_3)_2SO$
dppa	bis(diphenylphosphino)amine, $Ph_2PNHPPh_2$
dppap	2-(diphenylphosphinoamino)pyridine, Ph_2PNHpy
dppb	bis(diphenylphosphino)butane, $Ph_2PCH_2CH_2CH_2CH_2PPh_2$
dppe	bis(diphenylphosphino)ethane. $Ph_2PCH_2CH_2PPh_2$
dppm	bis(diphenylphosphino)methane, $Ph_2PCH_2PPh_2$
dppp	bis(diphenylphosphino)propane, $Ph_2PCH_2CH_2CH_2PPh_2$
ee	enantiomeric excess
Et	ethyl, $-C_2H_5$
FAB	Fast Atom Bombardment

FT	Fourier transform (for NMR or IR)
HH	head-to-head
HT	head-to –tail
Hz	Hertz, s^{-1}
IR	Infra-red
J	coupling constant, Hz
Me	methyl, $-CH_3$
m/z	mass-to-charge ratio
nbd	2,5-norbornadiene, C_7H_8
NMR	Nuclear Magnetic Resonance
P~O	A generic Phosphorus-Oxgyen Ligand.
Ph	phenyl, $-C_6H_5$
ppm	parts per million
^{n}Pr	*n*-propyl, $-(CH_2)_2CH_3$
^{i}Pr	*i*-propyl, $-CH(CH_3)_2$
PR_3	phosphine
py	pyridyl, $-C_5H_4N$
thf	tetrahydrofuran, C_4H_8O
tht	tetrahydrothiophene, C_4H_8S

CHAPTER ONE: Introduction.

1.1 Hemilabile Ligands.

During the course of this work the term 'Hemilabile Ligands' will appear regularly. This class of ligand is very useful today with regard to homogeneous catalysts containing transition metals, and has many other useful applications. This is because these types of ligands offer a huge amount of selectivity in terms of coordination. Hemilabile ligands are considered 'Hybrid Ligands' and generally consist of 'hard' donors (oxygen, nitrogen etc.), and 'soft' donors (phosphorus, sulfur), (fig. 1.1).

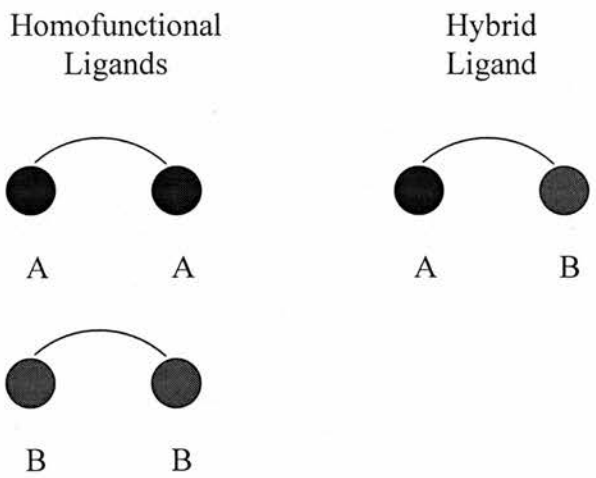

***Figure 1.1**: Pictorial Description of Homofunctional/Hybrid Ligands.*

These functionalities are chosen to be so different to each other to increase the differentiation between their resulting interactions with metal centres. The

differences influence the bonding and reactivity of the other ligands surrounding the metal centre, particularly those *trans* to the ligand. One essential aspect of these hybrid, hemilabile ligands in catalysis is to have one substitutionally labile donor function (B), while the other donor atom (A) remains firmly bound to the metal centre. (Fig. 1.2)

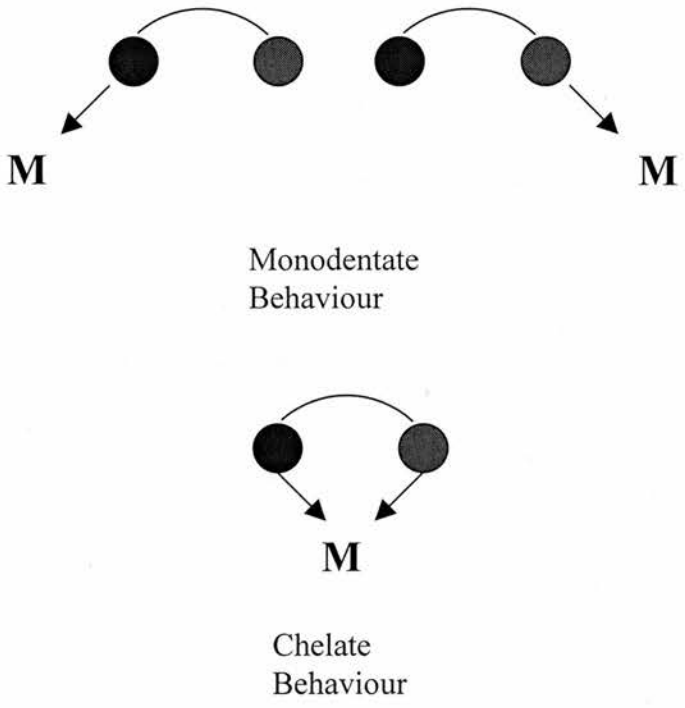

***Figure 1.2**: Monodentate and Chelate binding.*

During the course of this work a number of new hemilabile, hybrid ligands will be described. Pyridylphosphines are the most well know variety that will be considered, however thiophenylphosphines are also discussed, (fig 1.3).

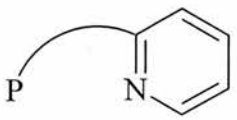

Generic Pyridylphosphine

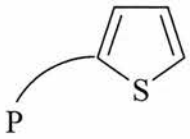

Generic Thiophenylphosphine

***Figure 1.3**: Generic Pyridyl/Thiophenyl phosphines.*

1.2 Synthesis of pyridylphosphine ligands.

Pyridylphosphine ligands are the most common phosphorus nitrogen ligands used in complexes. The first synthesis, was reported in 1944 by Davies and Mann[1]. Treatment of phenyl(4-bromophenyl)chlorophosphine with (2/3)-pyridylmagnesium bromide produced 2-[phenyl(4-bromophenyl)phosphino]pyridine **1** (5%) or the 3-isomer **2** (7%), (equation 1.1).

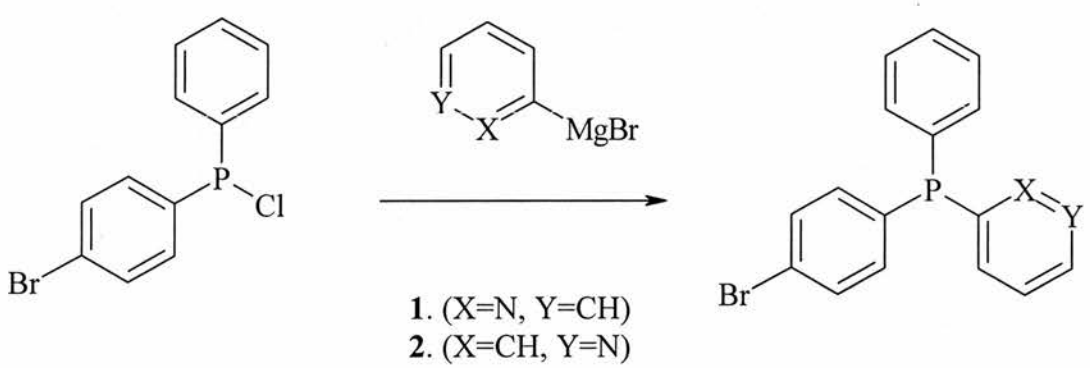

1. (X=N, Y=CH)
2. (X=CH, Y=N)

Equation 1.1

This procedure was extended to produce the tri-2-pyridylphosphine **3** (13%), from PCl_3 and in 1948[2] the synthesis of di-2-(phenylphosphino)pyridine **4** and 2-(diphenylphosphino)pyridine **5** was reported. (fig. 1.4).

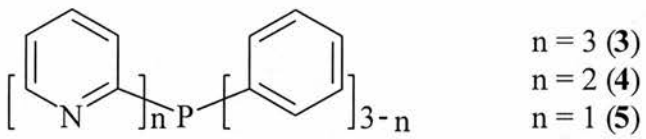

Figure 1.4: *Mono, di and tri-2-pyridyl substituted phosphines.*

These yields were improved dramatically when the halophosphines were exposed to 2-lithiopyridines at low temperatures (-65°C to –100°C). The best example of this was found when **3** was re-synthesised *via* this method. This synthesis reports a 66% yield[3] of tris-2-pyridylphosphine. The phosphines **6**, **7**, **8**[4] and **9**[5] have been synthesised via reaction of PCl_3 or $MePCl_2$ with the corresponding pyridyllithium reagent. (fig. 1.5)

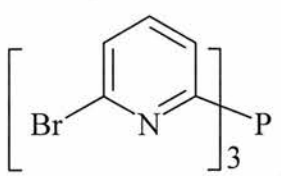

6

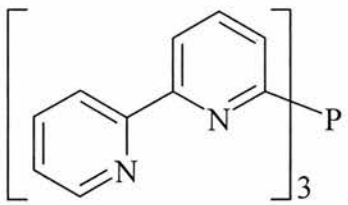

7

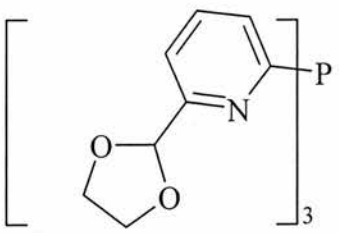

8

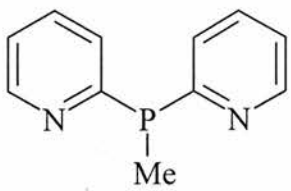

9

Figure 1.5: *Pyridylphosphines: from reaction of halophosphines with 2-lithiopyridines.*

In 1965 direct nucleophilic substitution by a metal phosphide on a halopyridine was first reported[6]. This involved treatment of 9-chloroacridine with $KPPh_2$ in dioxane. The reaction produced phosphine **10** (48% yield), (Equation 1.2).

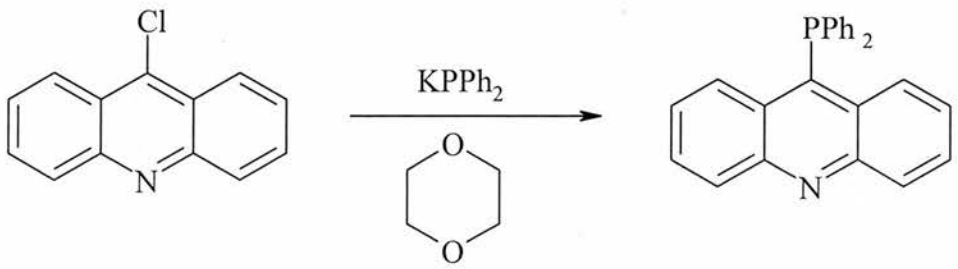

Equation 1.2

This procedure has proved extremely useful, and has been applied further in the synthesis of various phosphine substituted pyridines, as well as their α-phosphinomethyl derivatives and this has resulted in a huge variety of (potentially) polydentate P-N donor ligands being made available to chemists. (scheme 1.1.).

Synthesis of 1-(diphenylphosphino)-2-(2-pyridyl)ethane **11**[7], was reported in 1966. The reaction involved an ethane unit being introduced between the P and H of diphenylphosphine, the reaction required catalysis by glacial acetic acid (AcOH), (equation 1.3).

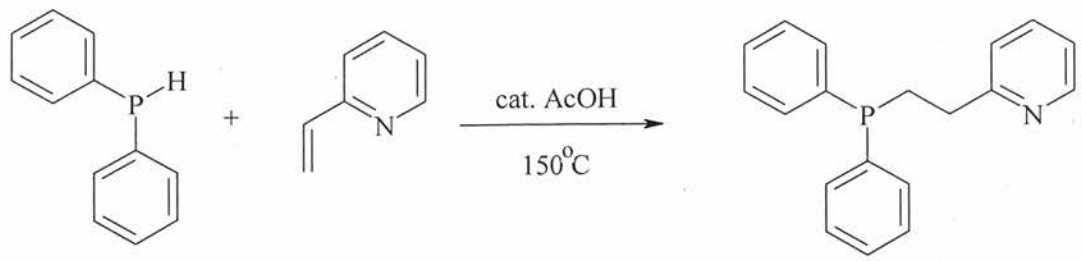

11

Equation 1.3

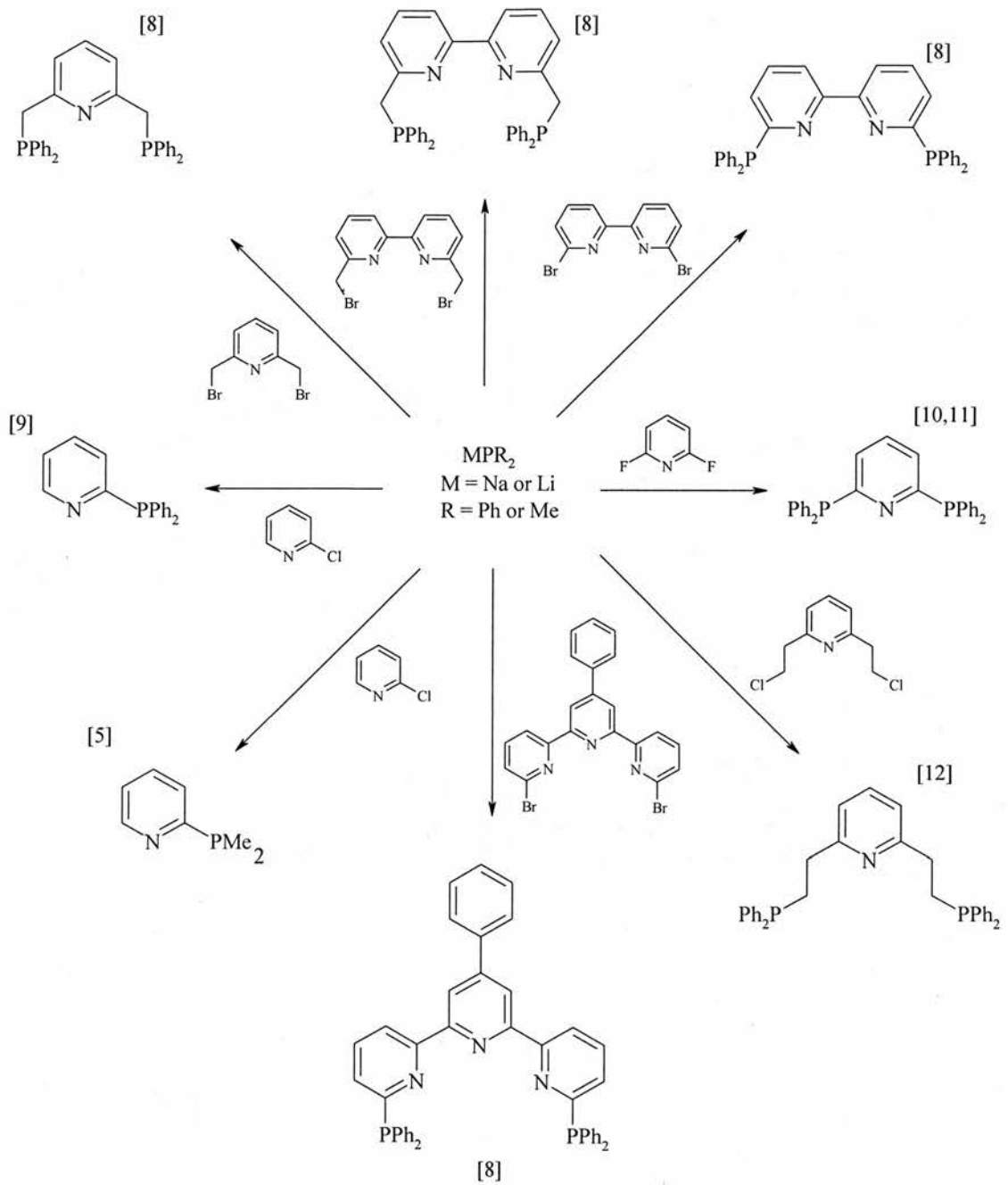

***Scheme 1.1**: Synthesis of some phosphine substituted pyridines. (References in []).*

Further relatives of **11**, $P(CH_2CH_2py)_2Ph$ and $P(CH_2CH_2py)_3$ have been synthesised, following a method laid down by King *et al*[13], this method involved base-catalysed addition of P-H bonds to 2-vinylpyridine.

1.3. Co-ordination Chemistry of 2-(diphenylphosphino)pyridine.

As mentioned above a wide range of pyridylphosphines have been synthesised and fully characterised, but the phosphine that has received the most attention is 2-(diphenylphosphino)pyridine (Ph_2Ppy, **12**) (fig. 1.6), which is undoubtedly the most simple of the range.

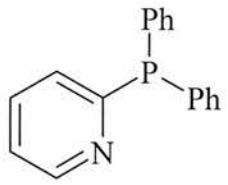

***Figure 1.6**: 2-(diphenylphosphino)pyridine (**12**).*

As can be seen, Ph_2Ppy is structurally very similar to triphenylphosphine Ph_3P, which is the archetypal phosphine ligand. So, in theory the two ligands should be readily interchangeable in many of the complexes that contain Ph_3P. The main difference comes in that the (Ph_2Ppy), can be a bidentate ligand due to its extra donor atom.

Monodentate Ph_2Ppy complexes (bound by phosphorus), can generally be synthesised via standard substitution reactions involving, metal carbonyls[14-19], metal olefins[20-22], and metal nitriles[23-26], they are also produced when hydrated metal chlorides (e.g. $NiCl_2.6H_2O$) are reacted with (Ph_2Ppy) in the presence of zinc powder[27]. Another, well-established method of formation of these phosphorus bound complexes is via reaction with halide-bridged binuclear complexes which involves cleavage at the bridging halide[5, 12, 20, 28-31], (equation 1.4).

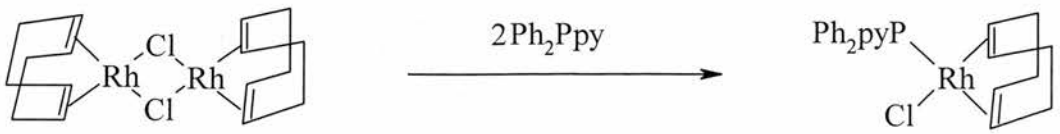

Equation 1.4

As has been mentioned before, pyridylphosphine ligands are potentially bidentate, and even taking into account the strain involved in forming four membered metallacycles, such rings have been formed. A common route for the synthesis is treatment of the phosphorus bound metal complex with a halide abstractor[20-22, 25]. This removes the halide atom, which is replaced by a very poor ligand compared to X^- (eg. PF_6^-), this forces the metal to bind with the N of the Ph_2Ppy, and thus forms the metallacycle.

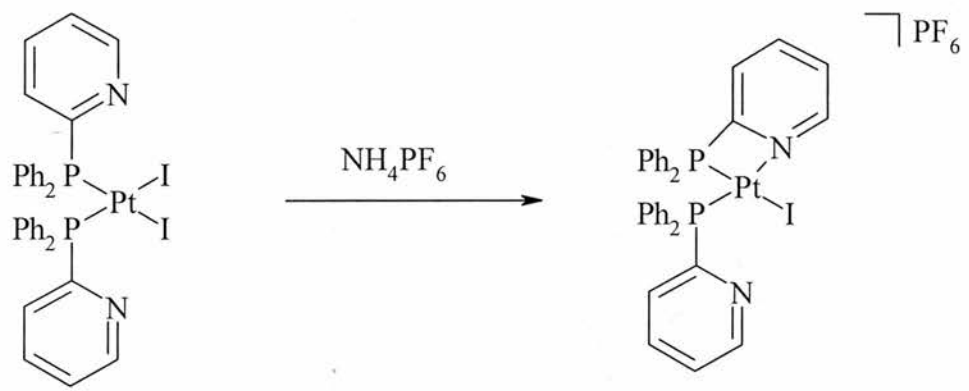

Figure 1.7: *Formation of a four-membered metallacycle.*

Other complexes where the pyridyl nitrogen is also bound have been prepared. A common method for this is simple addition of Ph_2Ppy to $[UCl_3(\eta^5\text{-Cp})]$ in thf[32], or the substitution of loosely bound solvent molecules, metal complexes of this type are $[U(BH_4)_3(THF)_x]$ and $[Rh(cod)(solv)_2)][X]$, (where X can be $[ClO_4^-]$ or $[PF_6]^-$. These reactions generate $[UCl_3(\eta^5\text{-Cp})(Ph_2Ppy\text{-}P,N)]$[32], $[U(Ph_2Ppy\text{-}P,N)_2][(BH_4)_3]$[32] and

[Rh(cod)(Ph_2Ppy-*P,N*)][X] (where X = [ClO_4^-] or [PF_6]$^-$)[23] respectively. Interestingly reactions involving [$PdCl_2(PhCN)_2$] and [$PdCl_2$(cod)] with equivalent amounts of Ph_2Ppy produced [$PdCl_2$(Ph_2Ppy-*P,N*)][23] instead of the expected P bound complex. When Ph_2Ppy was reacted with $Mn_2(CO)_{10}$, the binuclear compound [$Mn_2(CO)_8$(Ph_2Ppy-*P,N*)] resulted[33]. The mononuclear compound [Ru(Ph_2Ppy-*P,N*)$(CO)_2(Cl)_2$][28] was prepared by addition of a saturated dichloromethane solution of chlorine to the cluster complex [Ru_3(Ph_2Ppy-P)$_3(CO)_9$] also in dichloromethane. Interestingly, only one geometric isomer was found, even though it is quite possible that others could have been formed. Many other examples of complexes with chelating Ph_2Ppy ligands have been reported, including [Ru(Ph_2Ppy-*P,N*)$(CO)_2(Cl)_2$][28], [PtCl(Ph_2Ppy-*P,N*)(Ph_2Ppy-*P*)][Ru$(CO)_2(Cl)_2$][20], [PtMe(Ph_2Ppy-*P,N*)(Ph_2Ppy-*P*)][BPh_4][22] and [U(Ph_2Ppy-*P,N*)$_2$][BH_4]$_3$[34]. Due to the small bite angle of the Ph_2Ppy ligand, all of these complexes display 'abnormal' geometry at the metal centres. For example, the P-M-N angles in the two $Pt^{(II)}$ and $Ru^{(II)}$ complexes are reduced from the 'normal' 90° to about 70°. An even more extreme example is found in the complex [U(Ph_2Ppy-*P,N*)$_2$][BH_4]$_3$, the P-U-N angle here is an amazing 52.8°. This is a consequence of the two BH_4 groups in the equatorial positions. Angular compression also occurs in the P-C-N-M rings. The P-C-N angle is reduced from the ideal 120° to 101.3-104.1° in the Pt and Ru complexes, and the C-N-M angle is compressed to 103.1-106.0° (again from the expected angle of 120°). Variance is also found in the P-C bond lengths, the length found in the chelating complex is appreciably larger than in the monodentate analogue. Bearing this in mind, the chelating Ph_2Ppy complexes are quite unstable, and readily undergo ring opening. The ring is usually split at the more weakly bound N position. An example is equation 1.6[28].

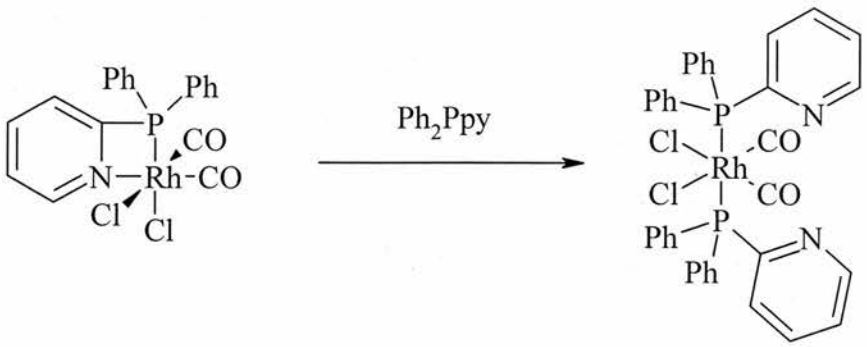

Equation 1.6

A further option is the reaction involving another metal complex, this may result in the formation of a binuclear species, with the Ph_2Ppy ligand bridging. Equation 1.7 is an example[23].

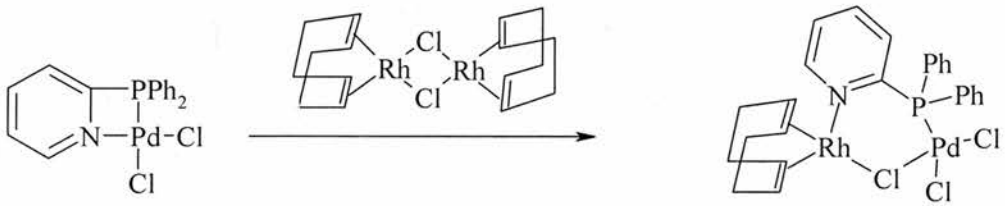

Equation 1.7

The study of such bimetallic compounds is beneficial with regards to organometallic chemistry. The close proximity of the two metals can have diverse effects on the reactivity, this is particularly pronounced in hetero-systems. Here again we can see the usefulness of Ph_2Ppy.

A further example of the chemistry of Ph_2Ppy in homo and hetero-binuclear complexes can be shown following the reaction of $[PdCl_2(cod)]$ with bis[2-diphenylphosphinopyridine]rhodium(I) carbonyl chloride. This reaction shows that

the rhodium atom had oxidatively added in the Pd-Cl bond. This means the product could be considered to be a bimetallic Rh(II) Pd(I) species[30].

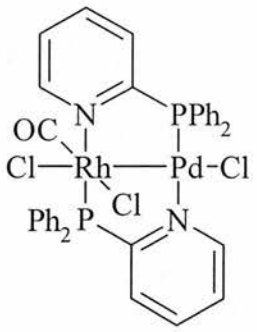

A second reaction of bis[2-diphenylphosphinopyridine]rhodium(I) carbonyl chloride with a half molar equivalent of the chloride bridged dimer [{Rh(μ-Cl)$(CO)_2$}$_2$][30]. This reaction generates the homo-binuclear Ph_2Ppy bridging complex [Rh_2(μ-Ph_2Ppy)$_2$(μ-CO)(Cl_2)], this is a similar product (as to the previous reaction) but also contains a bridging carbonyl group as well as the 'head to tail' arrangement as seen previously.

A beneficial property of these binuclear complexes is their potential for small molecule activation. The reasoning behind this is that the first metal centre may act to bind to the substrate molecule and the second metal may either remove or supply electrons as required to the binding site. An example of this type of chemistry is found in the reaction of [Rh_2(μ-Ph_2Ppy)$_2$(μ-CO)(Cl_2)] with either SO_2 or alkynes (with electron withdrawing R groups such as R = CO_2CH_3) results in displacement of the bridging CO group and formation of a species with the substrate bridging in its place, eg [Rh_2(μ-Ph_2Ppy)$_2$(μ-SO_2)(Cl_2)][30].

Also the catalytic activity of Ph_2Ppy with Pd has been investigated. Success in this area would provide a cheaper alternative to the established Pt catalysis. This being the goal, many hetero-binuclear complexes with Ph_2Ppy bridging ligands have

been synthesised and tested. An example is the carbonylation of EtOH to form ethyl propionate, studied by Zhang *et al*[100]. This involved a series of iron based heteronuclear systems including, $[FeMo(\mu\text{-}Ph_2Ppy)_2(CO)_6]$, $[FeNi(\mu\text{-}Ph_2Ppy)_2(CO)_3(NCS)_2]$, $[FeRh(\mu\text{-}Ph_2Ppy)_2(CO)_4Cl]$ and $[FeCu(\mu\text{-}Ph_2Ppy)_2(CO)_3Cl]$. Comparison of the catalytic behaviour of $[Rh(PPh_3)_3Cl]$ to that of $[FeRh(\mu\text{-}Ph_2Ppy)_2(CO)_4Cl]$ at a variety of temperatures. At 200 °C the mixed species complex demonstrated superior conversion rates compared to $[Rh(PPh_3)_3Cl]$, 99.6 % compared to 96.4 %. Also the selectivity was improved, with 98.6 % ethyl propionate, 1.4 % ethyl ether generated, compared to 67.7 % and 32.3 % respectively for $[Rh(PPh_3)_3Cl]$.

1.4. Co-ordination Chemistry of other, Chelating pyridylphosphine ligands.

As already discussed the pyridylphosphine family is very large, here we will consider some other members of the family. Ph_2Ppy has a small distance between the P and N. When one moves to compounds where this distance is increased, chelation becomes very prevalent. An example of this was reported by Uhlig and Schafer in 1969[35], the phosphine in question is 2-(diphenylphosphino)methylpyridine (Ph_2PCH_2py, Fig. 1.8, **13**).

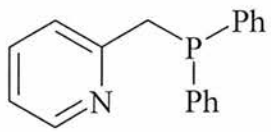

***Figure 1.8**: 2-(diphenylphosphino)methylpyridine (**13**).*

The first compounds produced where neutral octahedral complexes containing nickel(II) and cobalt(II), of the type $[M(Ph_2PCH_2py\text{-}P,N)2(X)_2]$, where M = Ni, X =

NCS, Cl and M = Co, X = NCS, Cl, Br, or I. Also the charged complexes $[Co(Ph_2PCH_2py\text{-}P,N)_2(ClO_4)][ClO_4]$ and $[Ni(Ph_2PCH_2py\text{-}P,N)_2(X)][X]$, where X = Br or I, these complexes have a reported co-ordination number of 5. The dicationic form was also synthesised: $[Ni(Ph_2PCH_2py\text{-}P,N)_2][ClO_4]_2$.

Ph_2PCH_2py has also been chelated to chromium, molybdenum and tungsten, via reaction with the relevant carbonyls[36]. The molybdenum analogue has been shown, via kinetic studies, to have some interesting properties (Equation 1.8)[37]. Via a reaction with CO, the chelate ring is opened to give the monodenate P-bound ligand. Fluxionality (in this case) is where the N site of the pyridylphosphine switches between being bound and not bound. Usually it is replaced by a different ligand, quite often the counter ion.

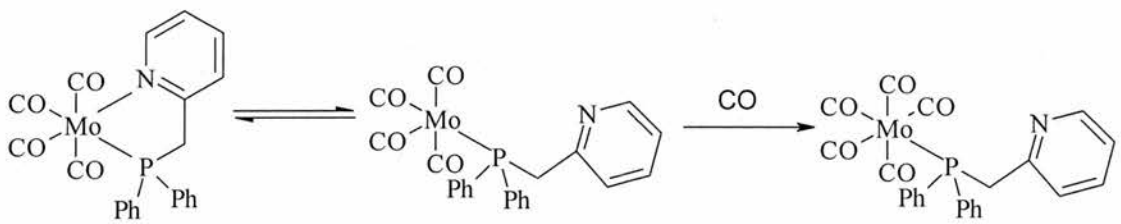

Equation 1.8

A further series of functionalised PH pyridylphosphanes were reported by Speigel and Stelzer together with their complexation to molybdenum[38], fig 1.9.

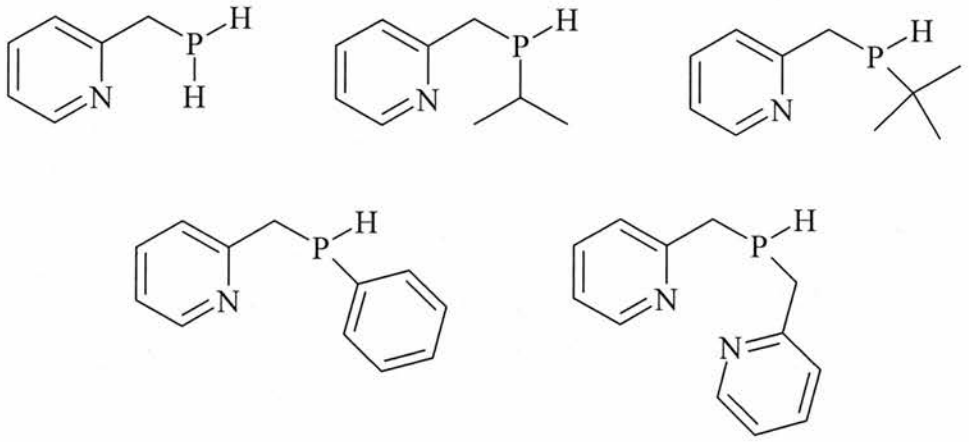

***Figure 1.9**: Primary and secondary 2-methylpyridyl substituted phosphines.*

A reaction involving Ph_2PCH_2py and norbornadiene molybdenum tetracarbonyl produced the PN chelate complex $[Mo(Ph_2PCH_2py\text{-}P,N)(CO)_4]$ (**14**). In a reaction between Ph_2PCH_2py and $[(\pi\text{-}C_3H_5)Mo(CO)_2(CH_3CN)_2Br]$, the acetonitrile ligands were easily exchanged, and the Ph_2PCH_2py co-ordinated via both P and N giving the complex $[(\pi\text{-}C_3H_5)Mo(CO)_2(Ph_2PCH_2py\text{-}P,N)Br]$ (**15**). This complex easily undergoes reductive de-allyation with more Ph_2PCH_2py to produce the bis-chelate complex *cis*-$[(Ph_2PCH_2py\text{-}P,N)_2Mo(CO)_2]$ (**16**). Also reductive de-allyation of **15** with triphenylphosphine gives rise to the *cis-trans*-$[(CO)_2(PPh_3)_2Mo(Ph_2PCH_2py\text{-}P,N)]$ (**17**), figure 1.10[39].

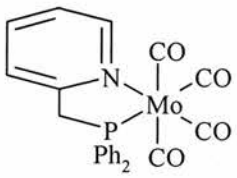

14

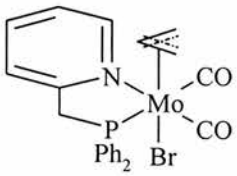

15

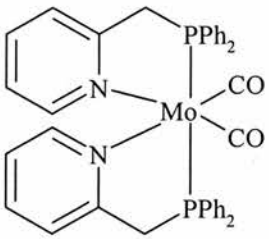

16

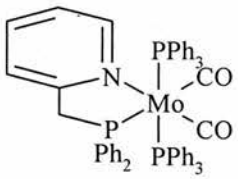

17

***Figure 1.10**: Molybdenum Complexes of **13**.*

1.5 Pyridylaminophosphines.

There has been a lot of interest in pyridylphosphines based on phosphorus-nitrogen bond containing motifs (pyridylaminophosphines).

Generic P-N bond containing Pyridylphosphine

***Figure 1.11**: P-N Pyridylphosphines.*

The simplest example of this type of molecule is 2-(diphenylphosphinoamino)pyridine (dppap) (**18**), which was first synthesised in 1967 along with its di- (**19**) and tri- (**20**) substituted derivatives[40].

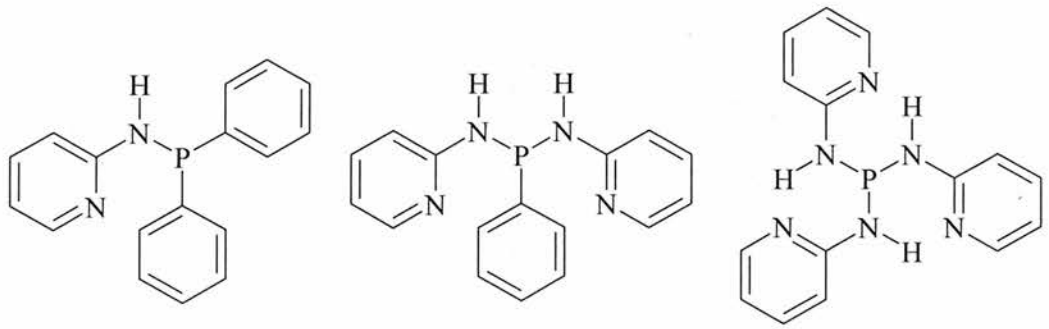

18 **19** **20**

***Figure 1.12**: mono-, di- and tri- 2-aminopyridyl substituted phosphine ligands.*

When one considers the ease of formation for phosphorus-nitrogen bonds it seems odd that so many complex phosphorus-carbon bond-containing ligands were studied during this time whilst no phosphorus-nitrogen bond containing ligands were considered. Dppap was originally complexed with a variety of metals including Cr^{III}, Mn^{III}, Fe^{II}, Co^{II}, Ni^{II}, Cu^{I} and Zn^{II} [40]. Further studies on the nickel complexes were initiated[41], this generated the first example of a neutral complex with the deprotonated ligand. This deprotonation and subsequent complexation was achieved by treatment of the ligand with phenyllithium followed by addition of $NiBr_2$. The product was isolated in 20% yield as **21** (equation 1.9).

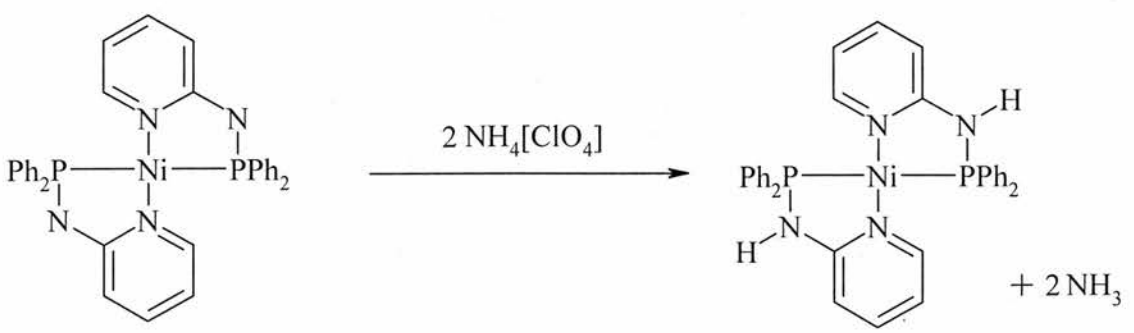

Equation 1.9

As can be seen in equation 1.9 re-protonation of the ligand was achieved by treatment of the deprotonated complex with ammonium perchlorate (or ammonium thiocyanate).

Later Ainscough and Peterson introduced an alternative synthesis of dppap, along with the thio- and seleno derivatives[42]. This work also contained characterisation of various complexes by conductivity, magnetic moment, solution molecular weight, IR, visible absorption spectra and ^{1}H NMR measurements.

Aucott *et al* have performed a thorough study of the coordination chemistry of dppap[43] (scheme 1.2). This work illustrates the many possible coordination modes of dppap. For example, dppap reacts with $[MCl_2(cod)]$ (M = Pt or Pd) in warm acetonitrile to generate the cationic species *cis*-[MCl(dppap-*P,N*)(dppap-*P*)][Cl] (M = Pt (**22**) or Pd (**23**)) with yields in excess of 90%. These compounds display fluxional behaviour with the second ligand that is only *phosphorus* bound coming on an off the metal centre, this behaviour is confirmed by observing line broadening in the ^{31}P NMR spectra.

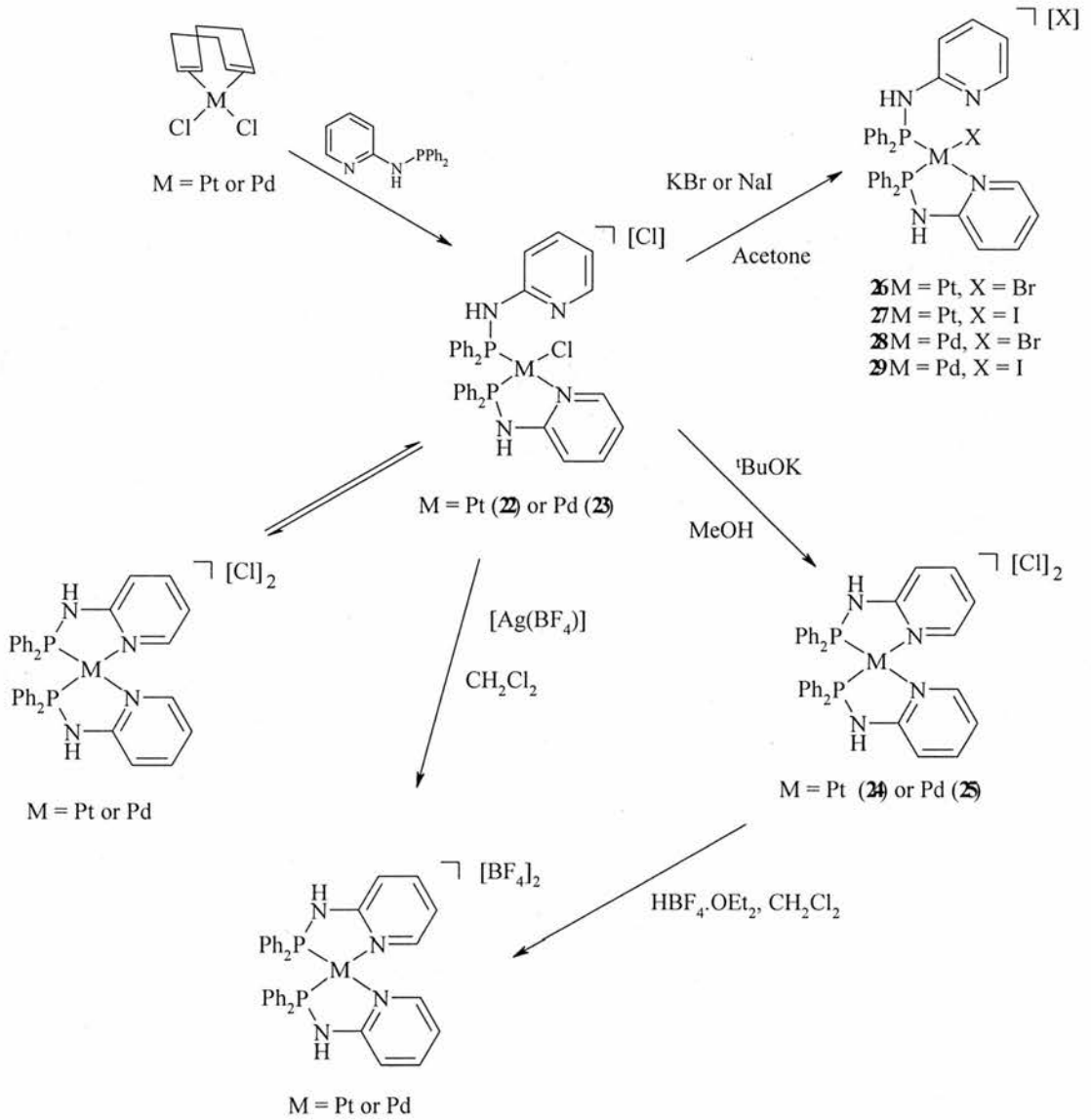

***Scheme 1.2**: Pt and Pd complexes of dppap.*

Treatment of **22** or **23** with base generates complexes **24** (Pt) and **25** (Pd) which have two chelating ligands around the metal centre with each ligand being deprotonated, further treatment of these compounds with $HBF_4.OEt_2$, in CH_2Cl_2 generates the protonated product. **24** and **25** can also be generated through reaction of **22** or **23** with $AgBF_4$. Metathasis of the chloride atom on **22** or **23** can be performed by reaction of the relevant starting complex with KBr or NaI, generating the expected complexes (**26-29**) with Br and I replacing the Cl.

The synthesis of the potentially tridentate ligand N,N-bis(diphenylphosphino)-2-aminopyridine **26** and some group 6 complexes e.g., *cis*-$[M(CO)_4(NPP)]$ (M = Cr, Mo or W) **27-29** have been reported[44].

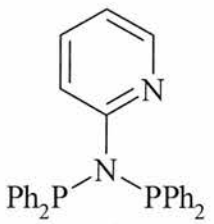

26

M = Cr (**27**), Mo (**28**) or W (**29**).

Figure 1.13*: Group Six Complexes of N,N-bis(diphenylphosphino)-2-aminopyridine.*

The bonding in these complexes is interesting, as there is formation of four membered MP_2N rings instead of the possible competitive five membered chelate ring involving a single phosphorus and the pyridyl nitrogen. The formation of bimetallic, phosphido-bridged species containing similar four-membered MP_2N chelate rings was also described. These reactions proceed as ligand substitution reactions between **26** and the dinuclear co-ordination compounds $[MM'(CO)_8(\mu\text{-}PPh_2)_2]$ (M = M' = W and M = Mo, M' = W), figure 14.

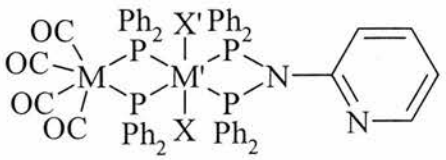

M = M' = W, X = X' = CO
M = M' = Mo, X = X' = CO
M = W, M' = Ir, X= H, X' = CO

Figure 1.14*: Di-nuclear Complexes of N,N-bis(diphenylphosphino)-2-aminopyridine.*

1.6. Coordination chemistry of tridentate (PNP) bridging pyridylphosphine ligands.

Use of the potentially tridentate PNP ligand 2,6-bis(diphenylphosphino)pyridine ($(Ph_2P)_2py$) has generated a range of bi, tri and tetranuclear complexes. Through reaction of a variety of platinium and palladium precursors four individual complex motifs have been isolated (scheme 1.3). The solution stable, non-planar, 18 membered ring, trimeric species *cis,cis,trans*-$[Pd_3\{\mu\text{-}(Ph_2P)_2py\}_3X_6]$ **30** (X = Cl[45,46] or Br[46]) were readily isolated from reaction of $(Ph_2P)_2py$ with $[PdCl_2(cod)]$, $[PdCl_2(PhCN)_2]$ or $[PdBr_2(cod)]$. On addition of further $(Ph_2P)_2py$ to **30** the expected thermodynamically favoured isomerisation was not recorded, instead ^{31}P NMR revealed that **30** was in equilibrium with the monomeric species $[Pd\{(Ph_2P)_2py\}Cl_2]$ **31**[46] (geometry not reported).

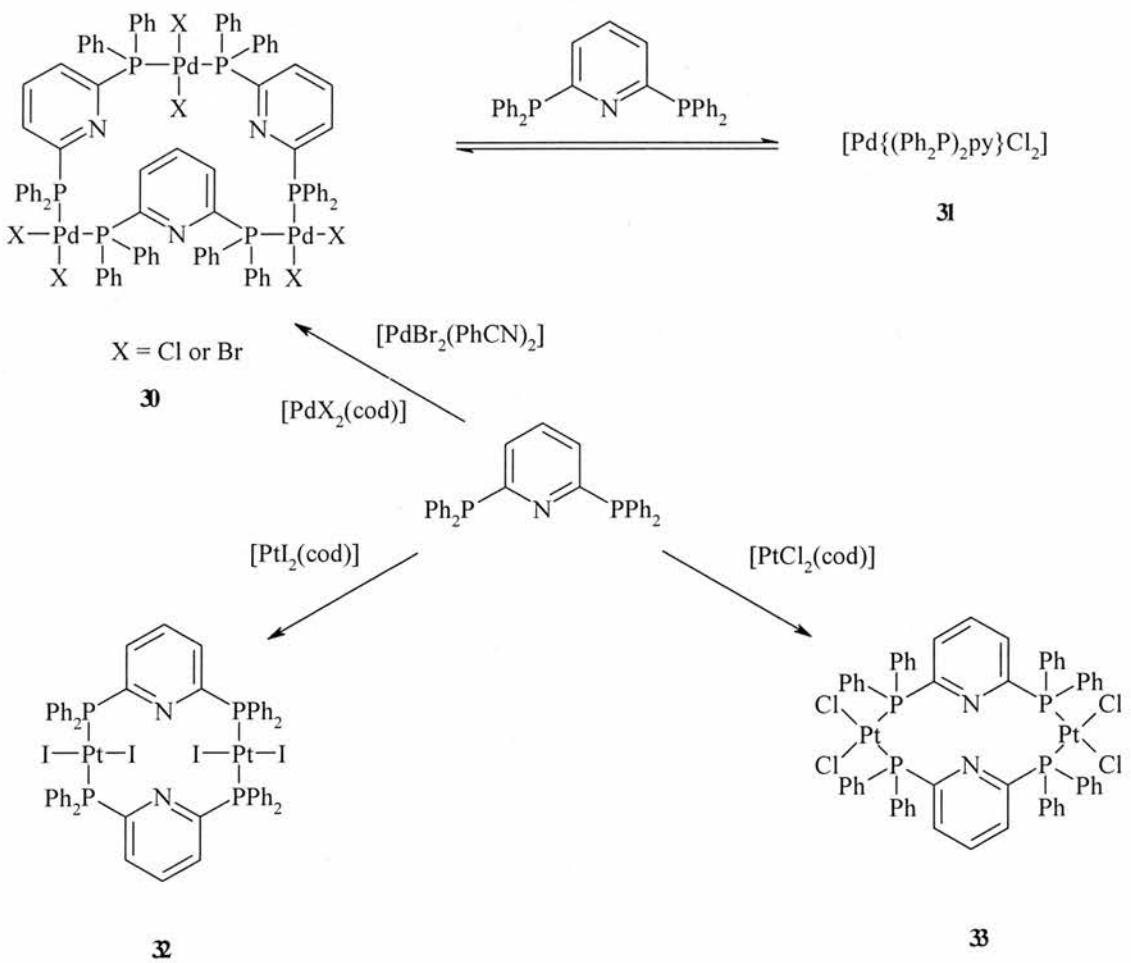

***Scheme1.3**: Palladium and Platinum complexes of $(Ph_2P)_2py$ (PNP).*

The twelve membered macrocyclic ring dimers *cis,cis*-[Pt{μ-$(Ph_2P)_2py$}$_2Cl_4$] **32** and *trans,trans*-[Pt{μ-$(Ph_2P)_2py$}$_2I_4$] **33** were prepared by addition of an equimolar quantity of $(Ph_2P)_2py$ in CH_2Cl_2 to solutions of $[PtCl_2(cod)]$ and $[PtI_2(cod)]$ respectively[46]

An extension of this chemistry led to the tridentate PNP ligand 2,6-bis(diphenylphosphinomethyl)pyridine **34**. This is a rigid ligand and shows no inclination to be hemilabile, and only 1:1 complexes have been reported. It was discussed in conjunction with magnetic cross-over point studies on Fe(II), Co(II) and Ni(II). The Ni complexes [Ni(PNP)X][Y] (X = Cl or Br, Y = Cl or ClO_4) were assessed as potential homogeneous catalysts in the water-gas shift reaction[47]. More recently some Ru complexes have been reported where the reaction conditions in particular the solvent had an important bearing on the product generated. Reflux of a small excess of **34** with $[RuCl_2(PPh_3)_3]$ in CH_2Cl_2 generated **35**, however if the same reaction is preformed in acetonitrile **36** is formed as the sole product. However if **36** is dissolved in $CDCl_3$ for 24 hours it undergoes a quantitative conversion to **35**, eq 1.10.

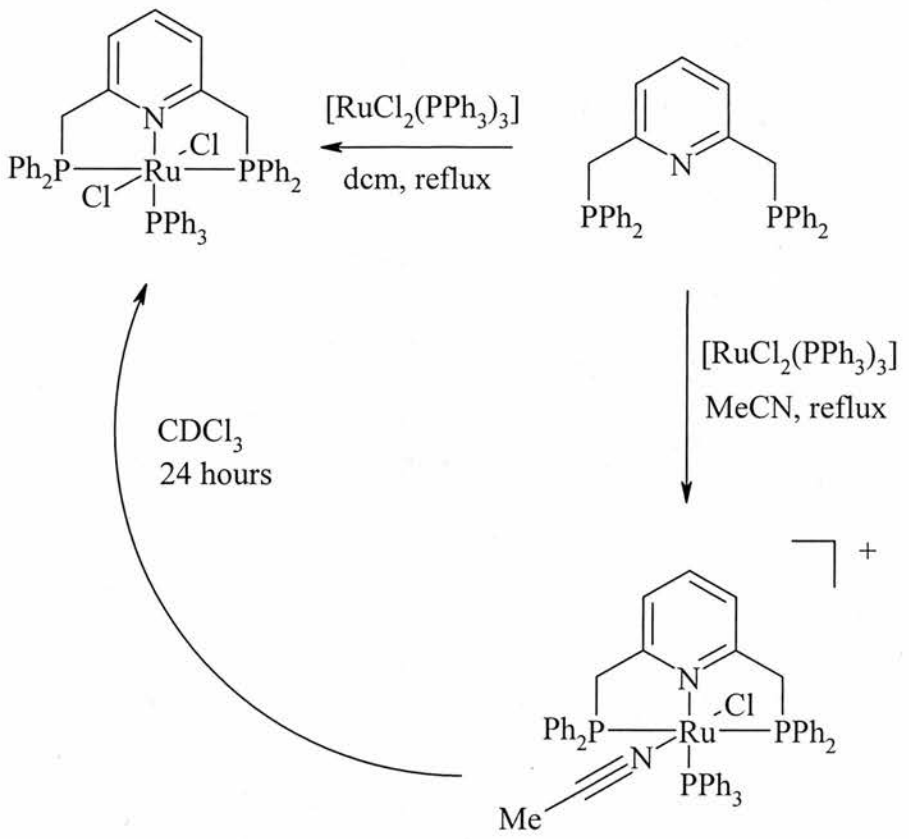

Equation 1.10

The (NH) analogue of 2,6-(diphenylphosphinomethyl)pyridine **34** (N,N'-bis(diphenylphosphino)-2,6-diaminopyridine **37**) was synthesised, and was shown to react with group 6 carbonyls of the type *fac*-$[M(CO)_3(NCMe)_3]$ and group 10 chlorides. These reactions generated two types of complex, the group 6 metals produced complexes of the type *mer*-$[M(CO)_3(PNP)]$ (**38**), the group 10 metals however showed a square planar motif ($[MCl(PNP)][Cl]$, **39**)[48], figure 1.15.

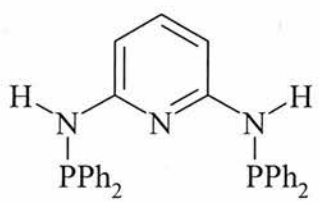

37

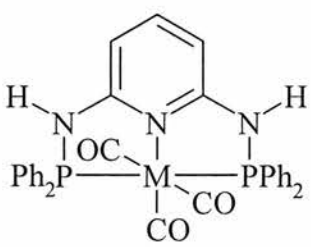

38

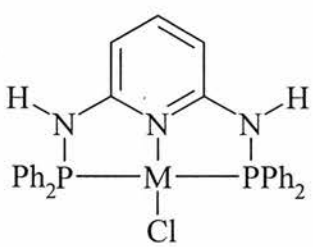

39

***Figure 1.15**: Structure and complexes of N,N'-bis(diphenylphosphino)-2,6-diaminopyridine.*

The reaction of **37** with the group 6 hexacarbonyls and trimethylamine oxide failed to generate the expected *mer*-$[M(CO)_3(PNP)]$ as seen before (e.g. **38**), but instead generated products which had one phosphorus of the PNP ligand oxidised, and the other phosphorus forming a bidentate chelate ring with the pyridyl N (eq. **1.11**). P-N bond rupture was witnessed in the *mer*-$[Mo(CO)_3(PNP)]$ complex following aerial oxidation in tetramethylbenzene. This generated the cubane like product $[Mo_4O_4(\mu^3\text{-}O)_4(\mu\text{-}O_2PPh_2)_4]$ in 48% yield[44].

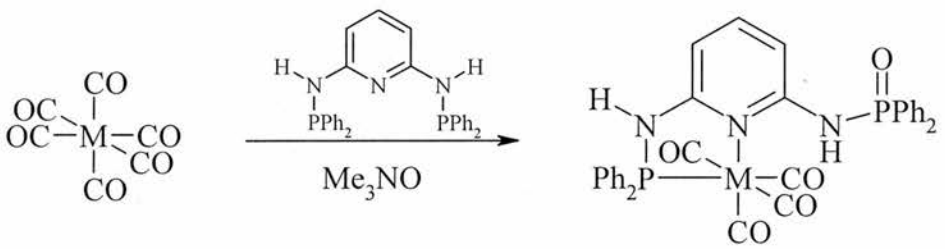

***Equation 1.11**: Formation of mono-oxidised bidentate PNP complex.*

1.7 Phosphorus-Oxgyen (P-O) Ligands.

P-O ligands are currently of considerable interest, in particular with regards to development of novel homogeneous catalysts. P-O ligands have been shown to exhibit an unusual selectivity enhancing effect in various nickel catalysed systems including oligomerization and polymerisation of ethene[48] and the carbonylation and hydrocarbonylation of methanol to a variety of oxygen containing C_2-products such as acetic acid[49, 50], acetaldehyde[50,51], ethanol[52] or diacetate[53]. This class of ligand has

also been found useful in stereoselective hydrogenations[54], hydrosilylations[55] and hydroformylations[56].

The basis of these ligands is a P^{III} bound tightly to the metal centre, and a oxygen containing subunit, either ketonic, alcoholic, carboxylic or oxidic. Some consider these oxygen molecules as being akin to intramolecular solvent molecules that form only weak metal-oxygen bonds that may be cleaved reversibly. This process has been termed an 'opening and closing mechanism'[57]. Furthermore the oxygen may increase the electron density at the coordination centre by direct metal-oxygen interaction allowing oxidative addition of a substrate as well as reductive elimination.

1.8 Ether-phosphines and furylphosphines.

Ether-phosphines are one of the most extensively studied class of P-O ligands. The most common types of these ligands have the oxygen donors as part of simple acyclic[58,59], or cyclic[52,60] ether moieties.

The synthesis of these ligands (equation 1.12) is straightforward and involves the addition of the respective lithio-phosphine to the desired chloro-ether to generate the P-O ligands[50,59-62].

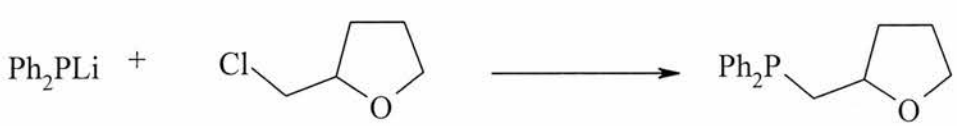

48

Equation 1.12

A similar class of compound are the phosphino ethers endowed with a polyether chain, they are potentially multidentate ligands, and have some phase-transfer properties[63].

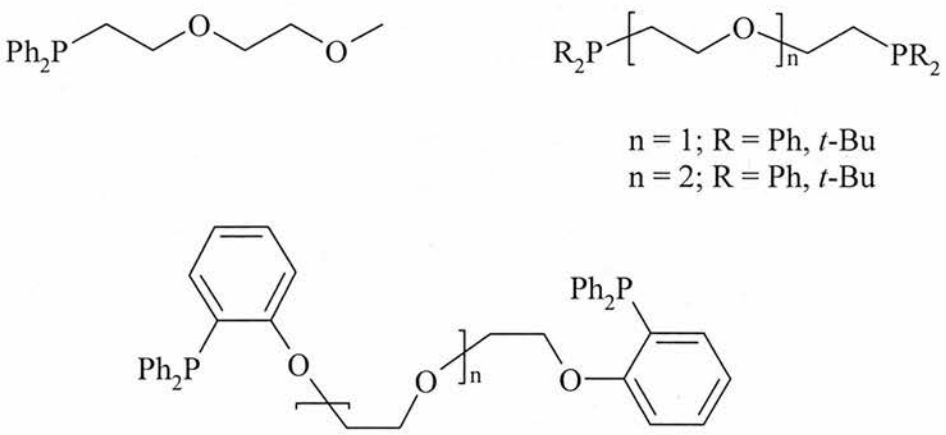

***Figure 1.16**: Ether-Phosphines.*

Ligands of particular note are the ones where the appearance of chirality is apparent. This is due to the presence of asymmetric carbon or phosphorus atoms. Examples include *o*-phosphinoanisols PAMP (**40**), CAMP[64] (**41**) and DIPAMP[63]. (**42**)

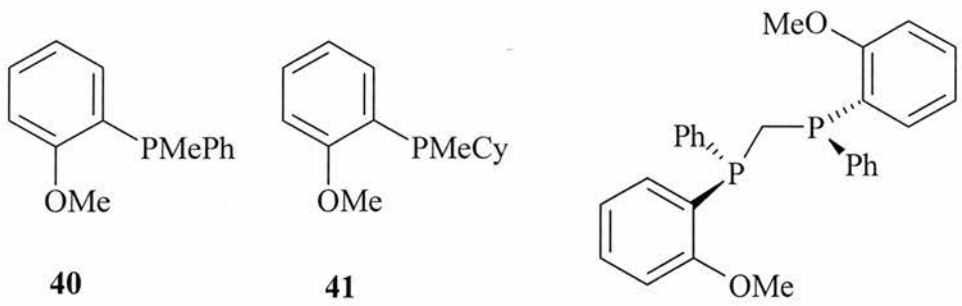

40 **41** **42**

***Figure 1.17**: Chiral ether-phosphines.*

Some derivatives of 1,3-dioxolane also display similar chiral properties, specifically DIOP (**43**)[65], PAMOP (**44**)[66] and DIOXOP (**45**)[67,68].

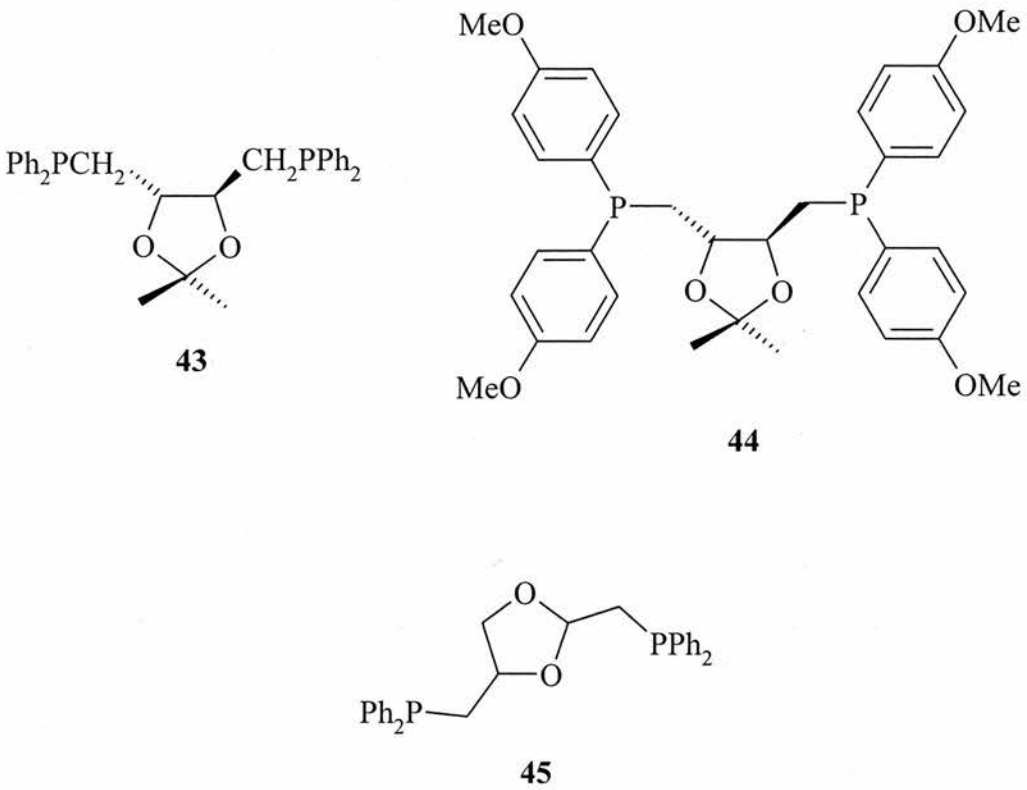

***Figure 1.18**: Derivatives of 1,3-Dioxolane as ligands.*

Unfortunately compounds containing dioxolane rings are readily hydrolysed in acidic conditions and are therefore not available for study under such conditions[49,69].

1.9 Phosphino-enolate ligands.

Another way of providing oxygen donor sites is to provide a carbonyl functionality, usually in the form of ketones or aldehydes. In the case of *β*-ketophosphines of the type $R_2PCH_2C(O)R'$ (**46**), stable five membered chelate rings can be formed by complexation of a metal species. Selected syntheses are shown in scheme 1.4.

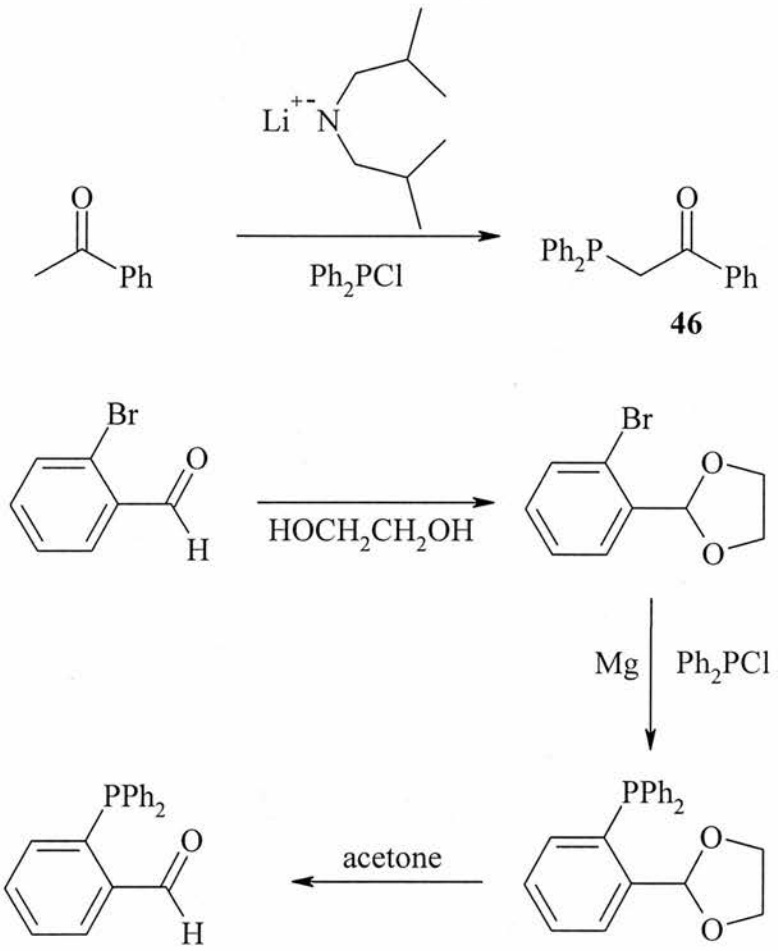

***Scheme 1.4**: Synthesis of Phosphino-enolate ligands.*

1.10 Complexes with P-O ligands.

A a large number of Cr, Mo and W compounds with oxygen or phosphorus donor ligands have been described[70-72], but complexes of these metals containing P-O chelating systems are rare. These limited examples are of the type MCl_3L_3[73] and $ML(CO)_5$[74,75] where M = Cr, Mo, W and L = amines, nitriles, ethers, ketones and water.

An effective route to such P-O systems starts by using complexes with weakly bound ligands e.g. $[M(CO)_5(thf)]$ (M = Mo, W) as starting materials. Such materials are easily accessible by UV irradiation of $M(CO)_6$ in thf[76]. Subsequent reaction of

$[W(CO)_5(thf)]$ with ether phosphines[59,52,77] leads to the respective monodentate pentacarbonyl(monophosphine)-tungsten complexes of the type $(CO)_5M(P\text{-}O)$, where P-O = ether phosphines. An example is reaction of the tetrahydrofurylphosphine **48** with $[W(CO)_5(thf)]$ (equation 1.13). Synthesis of the chelated $(CO)_4M(P\text{-}O)$ complexes is performed by the photochemically induced elimination of (CO) from $[(CO)_5M(P\text{-}O)]$.

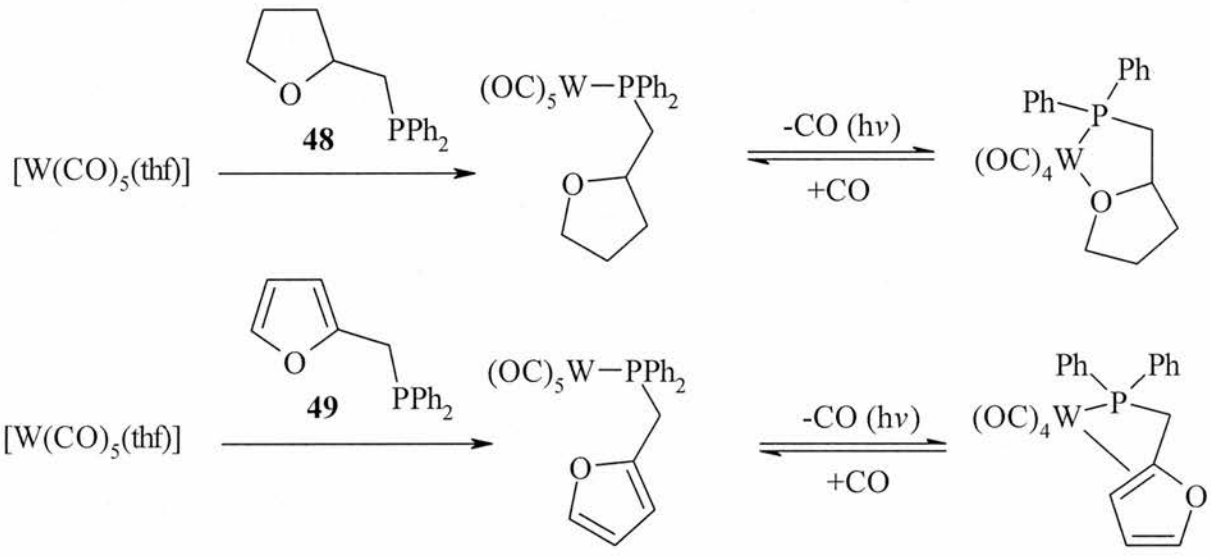

Equation 1.13

An available coordination atom occupies the vacant coordination site generated by the elimination of a CO molecule. In general this is the O of the ether phosphine ligands. However in the case of **49** the ligand chelates via a η^2-interaction between the π-system of the furan ring, suggesting that this is a better ligand than the O in the ring[77]. The coordination of the O results in a low-frequency shift of 40-60cm^{-1} in the ν(C-O-C) vibration observed in the IR spectra.

These ligands display typical hemilabile behaviour[57] in their complexes, and have been shown to be fluxional. For example, the highly reactive complex **50** will

readily re-coordinate a CO molecule, and again this reaction can be reversed photochemically. If this system is exposed to a strong ligand e.g. PR_3 ring opening can be effected (equation 1.14).

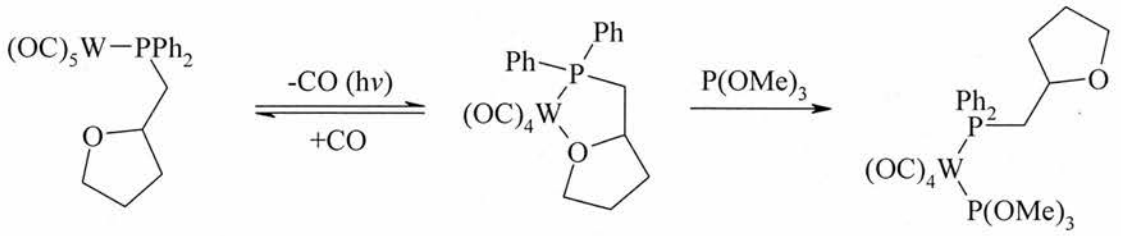

Equation 1.14

1.11 Ruthenium complexes.

Due to the preferred coordination number of ruthenium(II) being six, a great number of isomeric compounds are generated on reaction with P-O ligands, especially if the ligands are potentially hemilabile. The most important types are shown in scheme 3 along with their various synthetic transformations.

A convenient synthetic route to compounds of the type *trans,cis*-$RuCl_2(P\text{-}O)_2$ (**50**) is to reflux a solution of $RuCl_3.3H_2O$ in EtOH or 2-methoxyethanol with a slight stoichiometric excess of the desired ligand[58,78]. This method is quite robust with ligands which are not basic (see scheme 1.5) but it fails with a dioxanyl-containing ligand[79], as well as a variety of more basic ligands (figure 1.19). If one begins with the Ru starting material $[RuCl_2(PPh_3)_3]$ substitution of PPh_3 with the desired ligand can be achieved generating complex **50**. The scope of this reaction is far more extensive than the previous example, and can be extended to synthesise complexes of the type **54** by the addition of three equivalents of the P-O ligand[80].

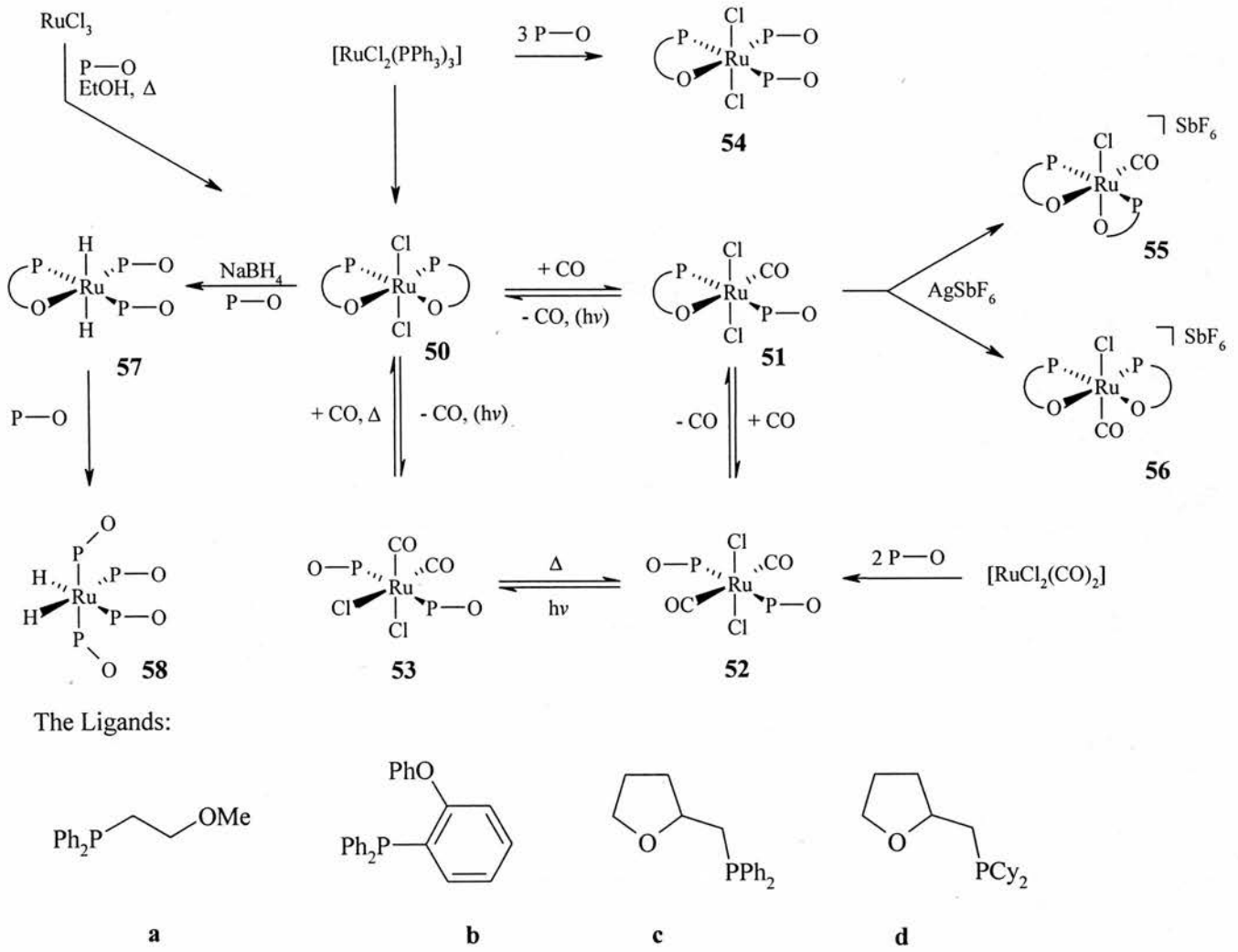

***Scheme 1.5**: Ruthenium Complexes of P-O Ligands.*

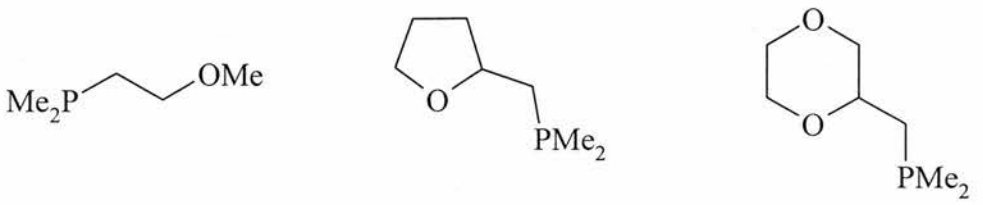

***Figure 1.19**: P-O Ligands.*

Complexes like **50** are very oxygen and heat stable, their red colour is somewhat surprising, as other hexacoordinate Ru(II) phosphine compounds are either yellow or colourless. Structures **50a,b** have been crystalographically analysed[58,78], the two co-planar chelate rings have bite angles in the region of 80°, and has *cis* oxygen and phosphorus atoms. These complexes also show unusually short Ru-P distances of 221-222 pm, these values are comparable with the *quasi*-five coordinate Ru complex $[RuH(OAc)(PPh_3)_3]$ and the actual five coordinate complexes $[RuCl_2(PPh_3)_3]$ and $[RuHCl(PPh_3)_3]$. It has been postulated that this small bond length is attributed to the very low *trans* influence exhibited by the ether oxygen atoms.

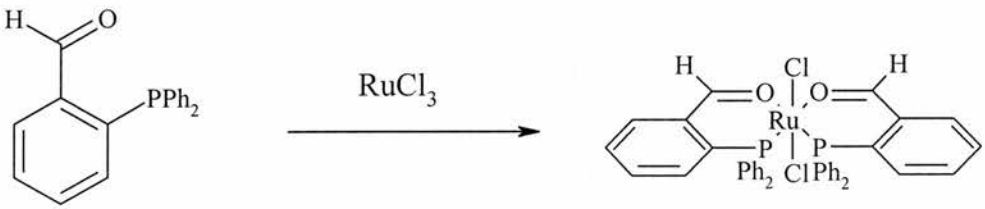

***Equation 1.15**: Reaction of $RuCl_3$ with a phosphine-aldehyde*

The bisaldehyde complex **50** obtained on reaction of $RuCl_3$ and phosphino-aldehyde is remarkably inert, Ru-O bond rupture cannot be accomplished even with CO, dppe or pyridine[81]. This is the only example of such inertness, complexes of the type *trans,cis*-$RuCl_2$(P~O-*P*,*O*) readily take up CO to generate the monocarbonyl

species $[RuCl_2(CO)(P\sim O\text{-}P,O)(P\sim O\text{-}P)]$ **51**, and after prolonged exposure to CO *trans*-$[RuCl_2(CO)_2(P\sim O\text{-}P)_2]$ **52** is generated[58,78]. Another synthetic route to **52** is the reaction of the P~O ligand with $[RuCl_2(CO)_2]_n$. Compounds **50-53** can be mutually interconverted as seen in scheme 1.5.

Complexes **55** and **56** can be obtained when complexes such as **51** are exposed to a halide abstractor (e.g. $AgSbF_6$)[82]. The isostructural complex **57** ($[RuH_2(P\sim O\text{-}P,O)(P\sim O\text{-}P)_2]$) (P~O = **a** only) is generated on treatment of analogous **50** complex with $NaBH_4$ in the presence of **a**.

1.12 Complexes with Rh and Ir.

Olefin complexes of dimeric rhodium(I) such as $[\{Rh(\mu\text{-}Cl)(cod)\}_2]$ are commonly used starting materials for the preparation of further Rh(I) complexes. Also subsequent removal of the olefin moiety can provide further opportunity for reaction. Scheme 1.6 shows the extent of these reactions.

If $[\{Rh(\mu\text{-}Cl)(cod)\}_2]$ reacts with two equivalents of an ether-phosphine **59** is obtained[83-87]. Chloride abstraction of these complexes in tetrahydrofuran can transform such compounds into the cationic Rh species **60** in which chelation of the ether-phosphine is apparent, again this interaction results in a shift to a lower frequency in the IR spectra in the region of 30-40cm^{-1}.

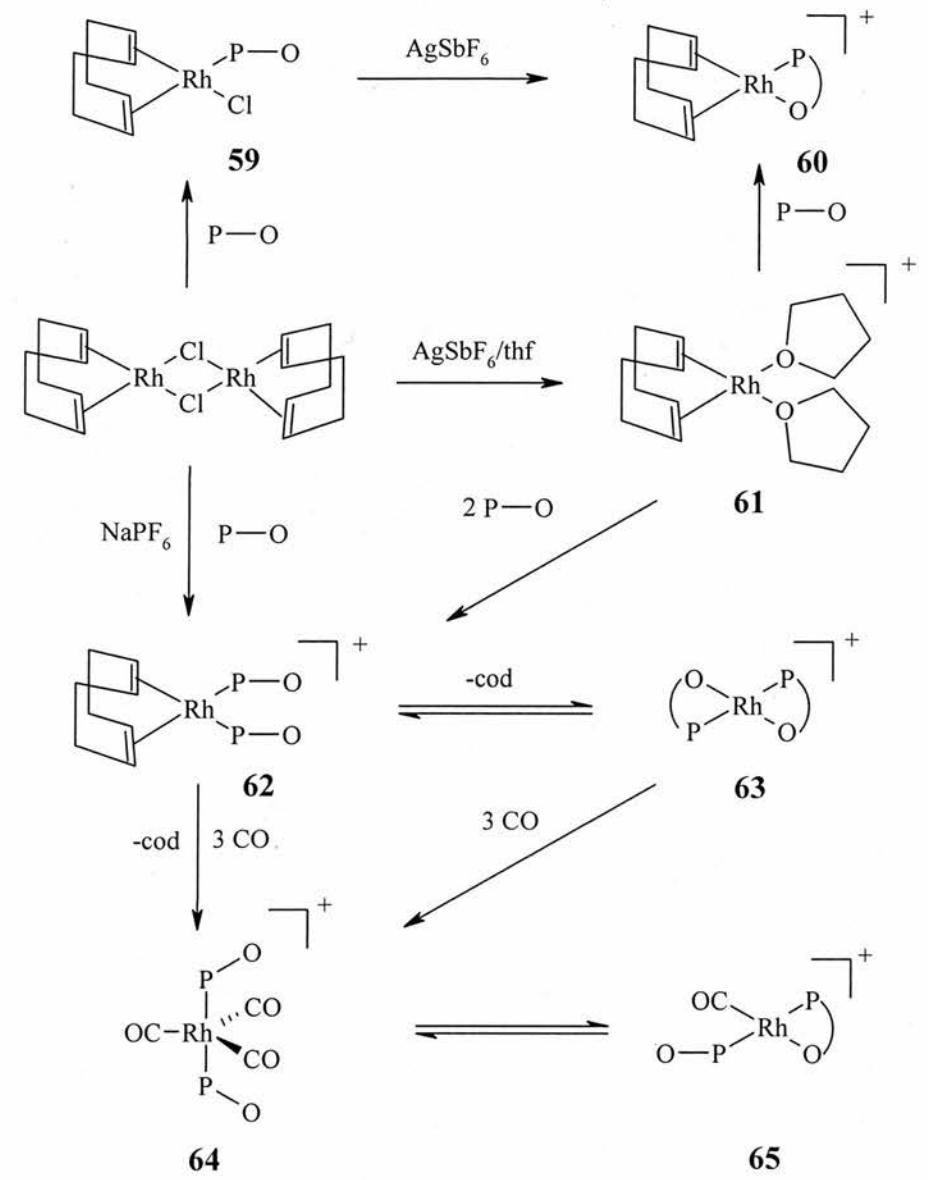

The Ligands:

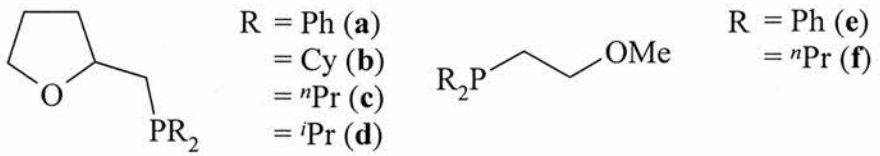

***Scheme 1.6**: Rh Complexes with various P-O ligands.*

Reaction of $NaPF_6$ with $[\{Rh(\mu\text{-}Cl)(cod)\}_2]$ generates the corresponding olefin complex **62**, subsequent addition of CH_2Cl_2 instigates loss of cod to generate complexes of the type **63**, this reaction is reversible on the addition of excess cod. If

one uses a very bulky phosphine one can disrupt this reaction, ligand **b** (with cyclohexyl R groups) forms at –40°C the monodentate complex [Rh(cod)(P~O-*P,O*)]$^+$ as opposed to the bis(mondentate) complex seen with the non-bulky ligands. At room temperature this reaction proceeds straight through to **63b** *cis*-[Rh(P~O-*P,O*)$_2$]$^+$, these chelate rings are stable to cod addition. This is in contrast to **63a**. [Rh(cod)(P~O-*P*)$_2$]$^+$ (**62**) can be produced directly from [{Rh(μ-Cl)(cod)}$_2$] if polar solvents such as acetonitrile or acetone are used[87].

Generally P~O ligands offer a considerable degree of stability to Rh(I) species. Even considering this, **63** will decompose at –30°C in the solid state, the presence of the π-acidic cod can stabilise these Rh(I) species. [Rh(cod)(P~O-*P,O*)] is much more stable than its bis(P~O) counterpart due to this electronic effect[83].

Cleavage of the Rh-O bond by CO occurs readily[88]. Passing of CO through solutions of *cis*-[Rh(P~O-*P,O*)$_2$]PF$_6$ (**63a,b**) at –40°C affords the corresponding tricarbonylrhodium(I) compounds *trans*-[Rh(P-O-*P*)$_2$(CO)$_3$]$^+$ (**64a,b**)[83].

1.13 Complexes with Pd and Pt.

Pd(II) and Pt(II) have rather straightforward coordination chemistry and form a wide range of stable complexes. Due to their preferred square-planar geometry, the number of isomers expected for a given complex is much lower than what is seen for the likes of ruthenium with its octahedral geometry.

If one considers the reactions of the ether phosphines, the essential reactions and complexes of Pt and Pd can be explored, along with the fundermantal reaction pathways which link them. As we can see from scheme 1.7, these involve mostly substitutions.

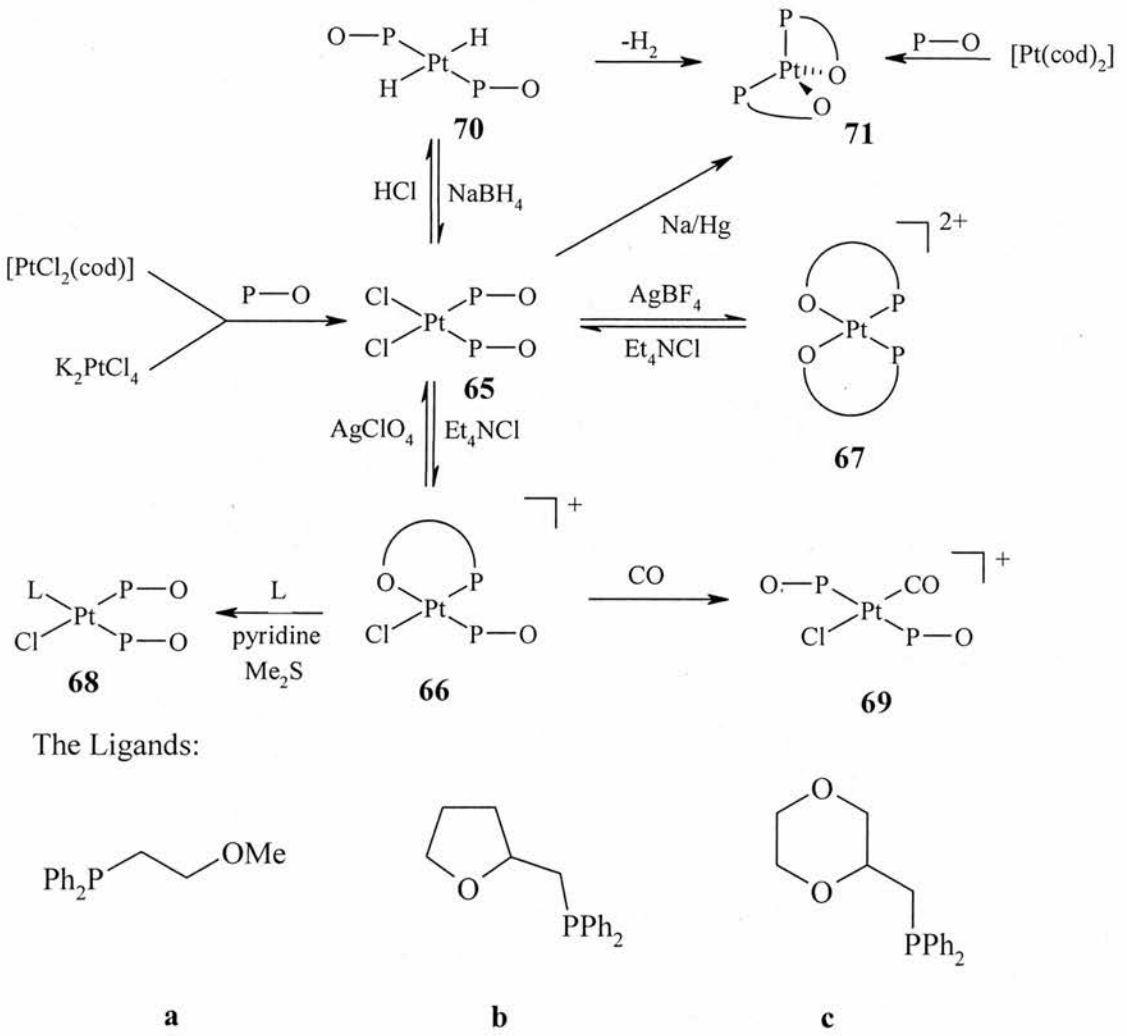

***Scheme 17**: Pt reactions with various P-O Ligands.*

As can be seen, entrance into this chemistry is relatively easy, reaction of two equivalents of ligand with $[PtCl_2(cod)]$ $[PdCl_2(cod)]$ provides the most straightforward route generating complexes of the type $[MCl_2(P\sim O\text{-}P)_2]$ (M = Pt and Pd). The stabilities of the *cis* and *trans* isomers of $[MX_2(PR_3)_2]$ depends heavily on the nature of X, PR_3 and the metal. Of particular interest is that the Pd analogue of **65** is in fact *trans* not *cis*, this is confirmed by X-ray analysis[89].

Halide abstraction of **65** with $AgClO_4$ generated *cis*-$[PtCl(P\sim O\text{-}P)(P\sim O\text{-}P,O)][ClO_4]$[62,89-91]. However if one uses $AgSbF_6$ or $AgBF_4$ as the halide abstractor the dicationic bischelate *cis*-$[Pt(P\sim O\text{-}P,O)_2][X]$ (where X = SbF_6 or BF_4) is

formed[62,89-90]. The palladium analogue has been shown to adopt the *trans*-configuration[91]. Again IR can follow the coordination of the oxygen atom. A shift of about 20 cm^{-1} is observed in the ν(C-O-C) band.

In order to study the chemistry of these reactions attention must focus on the ability of the complexes to undergo chelate rupture induced by other ligands. For example **65** *cis*-[$PtCl_2$(P~O-*P*)$_2$] will immediately regenerate from the monocation (**66**) and dication (**67**) on addition of [Et_3NH][Cl] as a source of Cl^- ions[62]. Further reaction of **66** with an incoming ligand (L = pyridine or Me_2S) yields complexes of the type *cis*-[PtCl(P~O-*P*)$_2$(L)] **68**[62]. However addition of CO leads to the formation of *trans*-[PtCl(P~O-*P*)$_2$Cl(CO)] **69**, this *trans* configuration is most likely due to the isomerization of an initially generated *cis* adduct[62]. Weaker donors such as ethane, methanol and thf undergo no reaction. This may be explained by focusing on the chelate effect that suggests that binding the ligand's oxygen is preferential to binding a discrete oxygen atom from a separate ligand.

As one would expect, these compounds are capable of enolization promoted by a strong electron-withdrawing substituents R'. Treatment with a strong base e.g. TlOEt[92] or NaH leads to the corresponding bidentate P,O ligands. There are examples of the non-deprotonated ligands binding both mono and bidentate to a variety of transition metals. The first monodentate complex formed was [$W(CO)_4(Ph_2POH)(Ph_2CH_2COPh)$] obtained in 20% yield upon photohydrolysis of [$W(CO)_4\{Ph_2PCHC(Ph)OPPh_2\}$][93].

Monodentate complexes of Ph_2PCH_2COPh (**72**) were prepared by reacting **72** with the appropriate palladium(II) starting materials[93], equation 1.16.

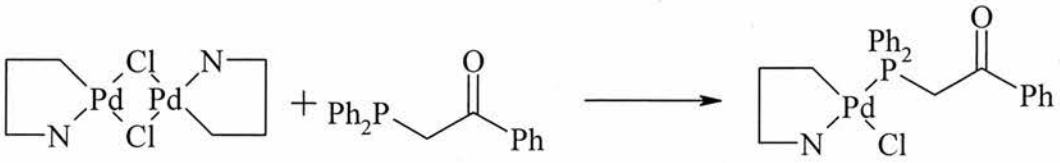

72

$\overset{\frown}{C\ N}$ = *o*-$C_6H_4CH_2NMe_2$

$\overset{\frown}{C\ N}$ = *o*-$C_{10}H_8N$

$\overset{\frown}{C\ N}$ = *o*-$C_{14}H_{13}N_2$

Equation 1.16

These monodentate complexes can be forced to chelate on addition of a halide abstractor or a base, figure 1.20.

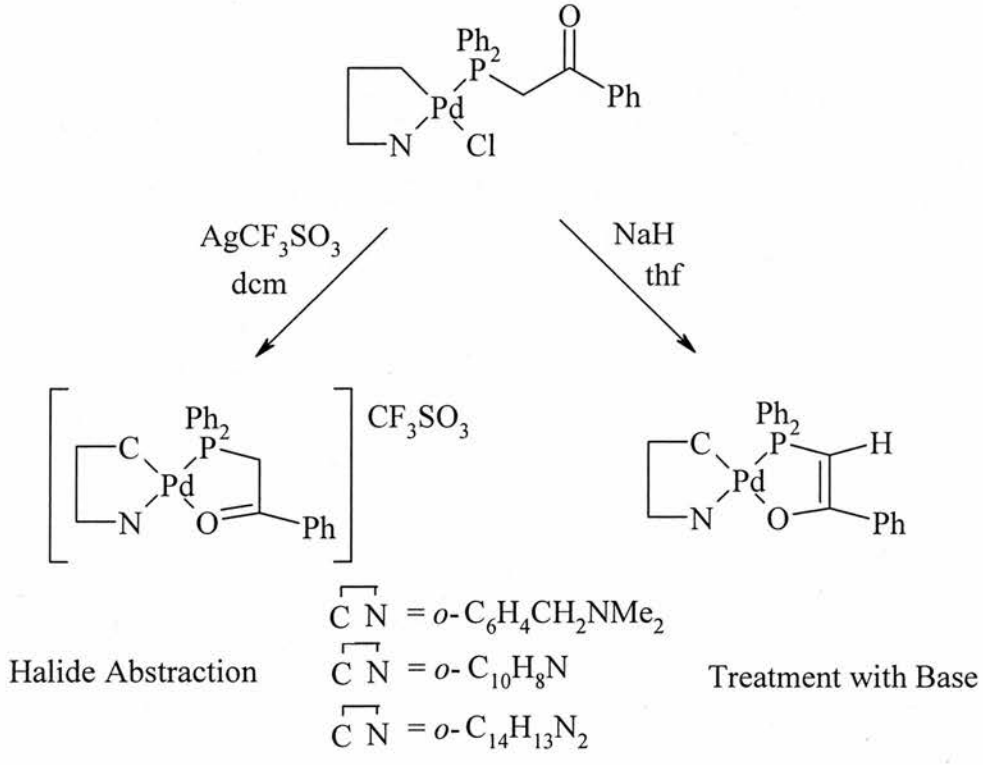

$\overset{\frown}{C\ N}$ = *o*-$C_6H_4CH_2NMe_2$

$\overset{\frown}{C\ N}$ = *o*-$C_{10}H_8N$

$\overset{\frown}{C\ N}$ = *o*-$C_{14}H_{13}N_2$

***Figure 1.20**: Two methods for chelation of Ph_2PCH_2COPh.*

IR provides an interesting insight into these reactions, the ν(C=O) stretching frequency of the monodentate complexes are all in the region of 1665 to 1680 cm^{-1}.

However on treatment with the halide abstractor this peak shifts to ca. 1570 cm^{-1} which is considered to be due to the carbonyl binding to the metal centre. Also on the addition of base to the monodentate complexes the peak shifts to 1477-1511 cm^{-1}, and this band is attributable to the ν(C-O)/ν(C=O) enolate system binding to the metal centre. The deprotonation and halide abstraction proceeds with the retention of the *trans*-N-Pd-P arrangement around the metal. All these bidentate complexes were air stable.

1.14 Ligands containing P, N and O.

Hemilabile Phosphorus-Oxazoline Hybrid Ligands.

The first example of a oxazoline based ligand was described by Braunstein[94], it was synthesised by reaction of a 2-methyl-2-oxazoline in thf at –78°C, followed by the addition at this temperature of TMS-Cl to form the N-silyl derivative which finally reacts with Ph_2PCl to give 2-diphenylphosphinomethyl-2-oxazoline (**73**), equation 1.17.

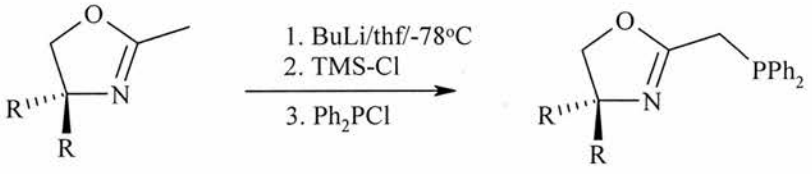

73

R = H or Me

Equation 1.17

The reported chemistry of this ligand centres around four-coordinate Pd(II) complexes, initially formation of [PdMeCl(L-*P,N*)] and [PdMe(Me_2S)(L-

P,N)][O_3SCF_3] where L = **73**[94] is described. As can be seen the chelate complexes are formed without the addition of a halide abstractor. Reaction of the ligand with the Pd dimer [{Pd(dmba)(μ-Cl)}$_2$] generates a rapid hemilabile style equilibrium between the mono and bidentate form of the complex. Treatment with base generates the deprotonated product as a stable bidentate chelate, fig 1.21.

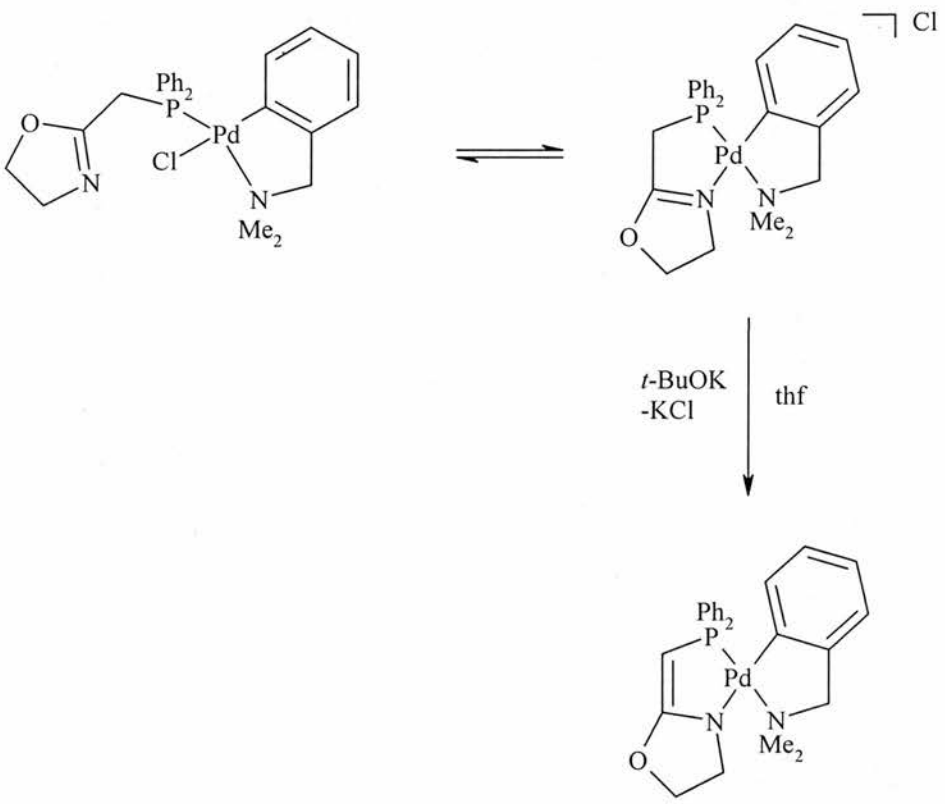

***Figure 1.21**: Fluxionality and deprotonation of 2-diphenylphosphinomethyl-2-oxazoline.*

This behaviour is not mirrored in reaction with the Ru dimer [{RuCl(μ-Cl)(*p*-Cy)}$_2$] which produces the bidentate complex [RuCl(*p*-Cy)(L-*P,N*)][Cl] (L = **73**) only and exhibits no hemilabile behaviour. There is no evidence that the O is involved in binding to the metal. This is an interesting example of O, N competition for one binding site on a metal, one in which N dominates.

1.15 Phosphino-thiophene (P-S) ligands.

There are few known examples of thiophene-metal coordination, and even fewer with a phosphorus-sulfur chelate motif. The first such example was described by Clot *et al* in 2000[95]. Reaction of 2-(2'-bromophenyl)thiophene with magnesium (to generate the Grignard), followed by reaction with chlorodiphenylphosphine generated the potential P-S chelate ligand 2-(2'-{diphenylphosphino}phenyl)thiophene (dpppth) (equation 1.18).

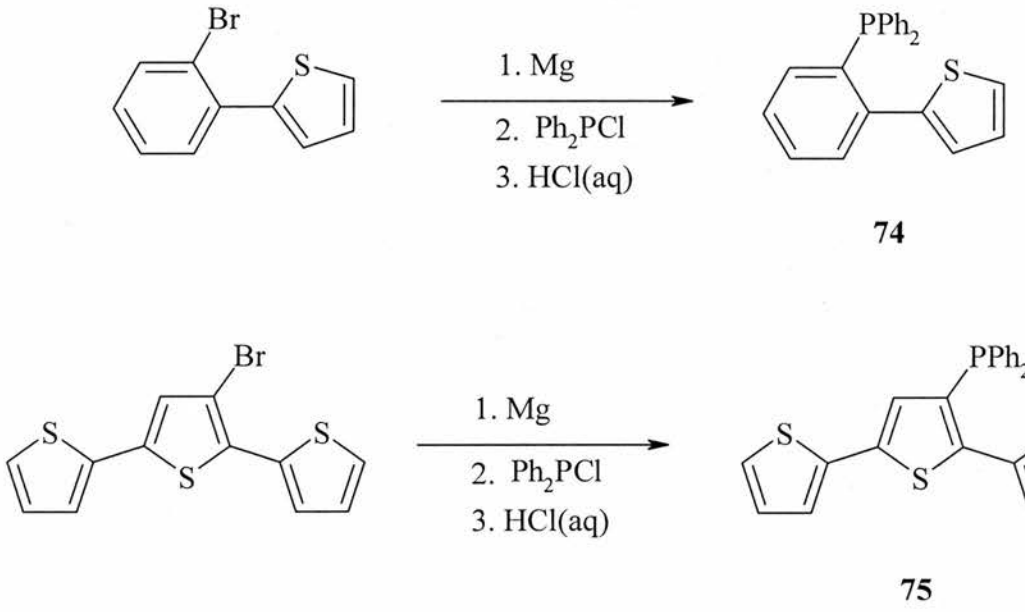

74

75

***Equation** 1.18:*

Also seen in equation 1.18 is the synthesis of 3'-diphenylphosphino-2,2':5',2''-terthiophene (dppterth) is described. This is an analogous reaction to that of dpppth and also produces a potential P-S chelate ligand.

The only metal that these two ligands have been bound to is ruthenium, reaction of two equivalents of the ligand with $[RuCl_2(PPh_3)_3]$ generated complexes **76** and **77**(figure 1.22).

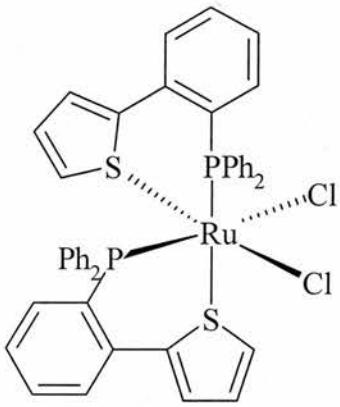

76

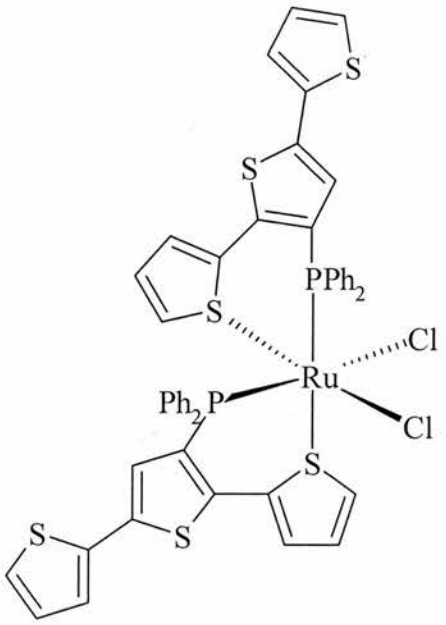

77

***Figure 1.22**: Ruthenium complexes of thiophene based ligands.*

The *cis* arrangement in **76** was confirmed by the presence of two doublets in the ^{31}P NMR spectra, however a small singlet was also noticed, indicating the presence of a possible *trans* complex. Also this complex is not air stable in a dichloromethane solution, and turned green after 15 min. In comparison **77** are air stable but it also display equivalent doublets, and a small singlet as seen for **76**.

On reaction with carbon monoxide the thiophene arm of the ligand is removed with one CO molecule replacing the sulfur. This occurs only for one arm in **77** generating a single product, however this happens in both ligands for **76** and generates a mixture of isomers (figure 1.23).

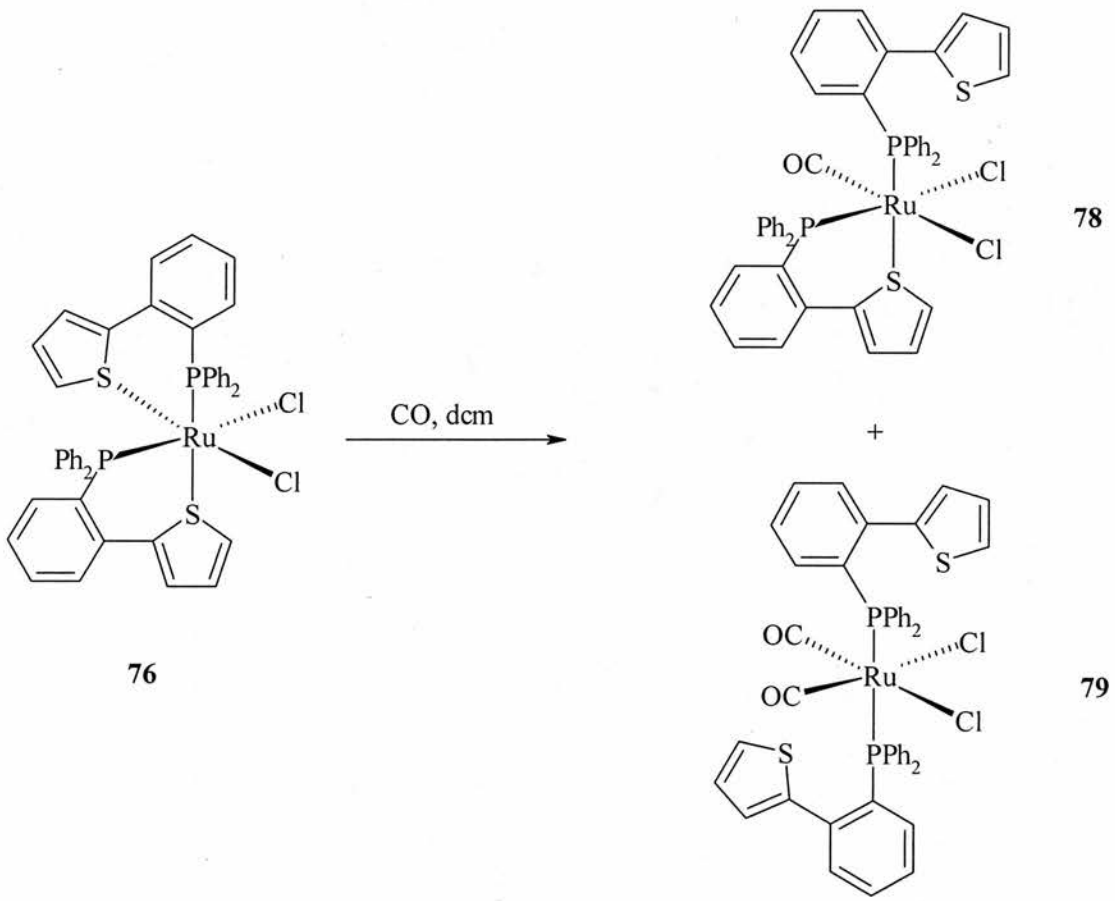

***Figure 1.23**: Ring opening at the thiophene sulfur.*

In 2001 Field *et al* reported the synthesis and coordination of a number of thiophene containing ligands, some in conjunction with pyridine[96] (fig 1.24).

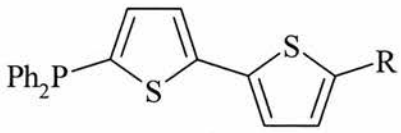

R = PPh_2
R = H

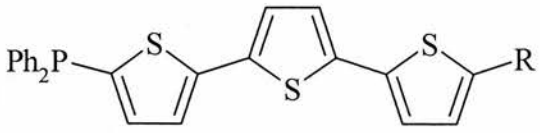

R = PPh_2
R = H

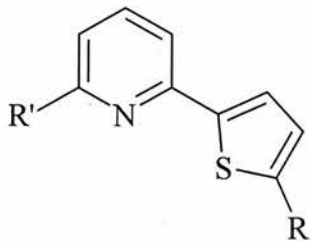

R = PPh_2; R' = H
R = H; R' = PPh_2
R = PPh_2; R' = PPh_2

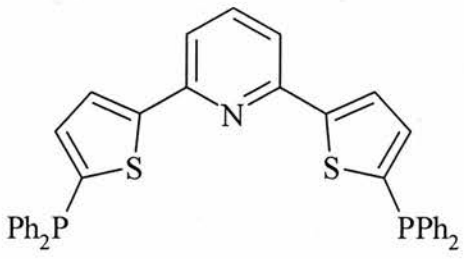

***Figure 1.24**: A further range of thiophene ligands.*

This synthesis involves initial lithiation of a halide starting material and either subsequent coupling with a derived Grignard reagent or reaction of the lithiated species with chlorodiphenylphosphine. Example syntheses are shown in figure 1.25.

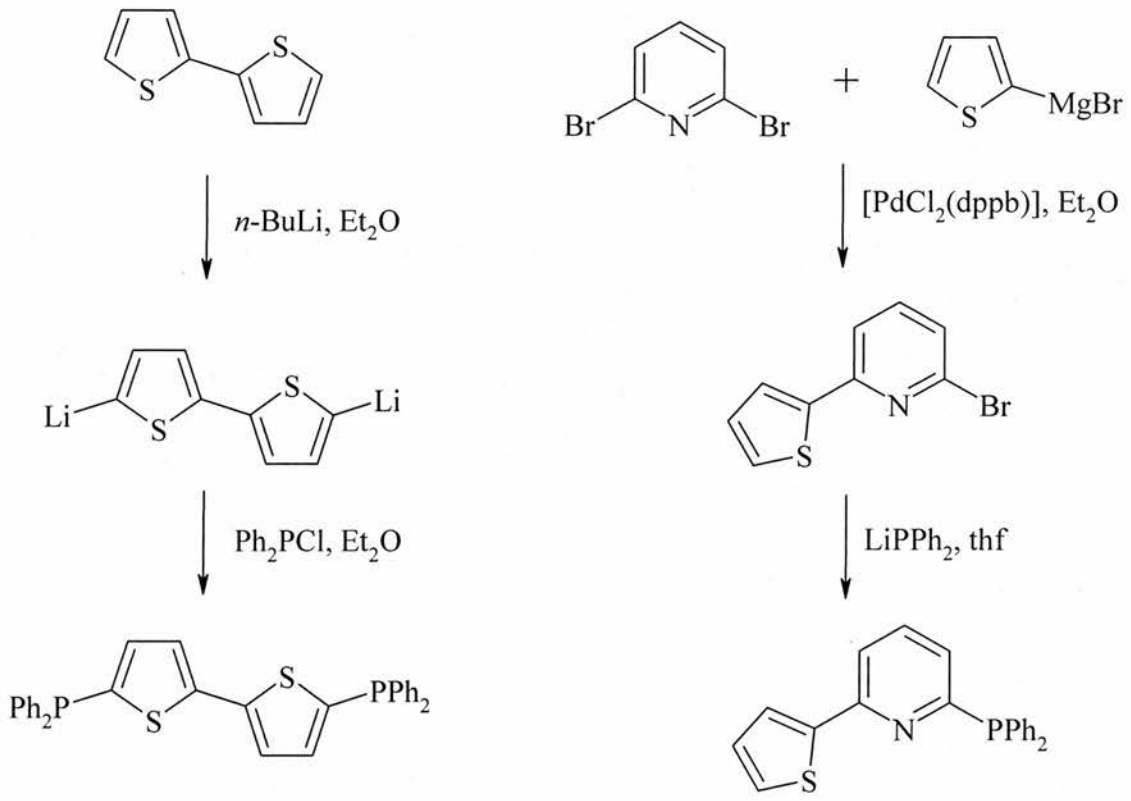

***Figure 1.25**: Example syntheses of thiophene ligands.*

1.16 Hemilabile P-N(or O) ligands and steric effects.

Based on possible catalytic activity with regard to hydrogenation of ketones Mathieu *et al* prepared a family of chiral ligands which introduced steric hindrance around the pyridyl N of the ligands[97,98]. This steric aspect is explored by complexation to Rh(I)[99]. ^{31}P NMR and crystallographic investigations by these workers showed that by increasing the steric hindrance around the pyridyl N (by substitution of H for Me at the 6 position) the lability of the Rh-N bond is also increased.

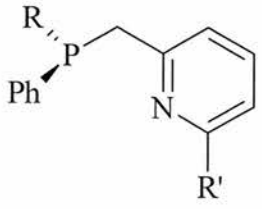

R = Me, R' = H
R = Me, R' = Me
R = *o*-anisyl, R' = H
R = *o*-anisyl, R' = Me
R = Ph, R' = Me

***Figure 1.26**: Sterically hindered phosphorus-nitrogen ligands.*

A variable temperature ^{1}H NMR study of the reaction between $[Rh(cod)(thf)_2][BF_4]$ and the anisyl/methyl ligand was carried out. This ligand also contains a competitive binding site, the O form the anisyl group, and it was suggested that a dynamic equilibrium exists between the two separate hemilabile binding sites. Their investigations led them to conclude that the η^2-P,O bound species was the dominant of the two species.

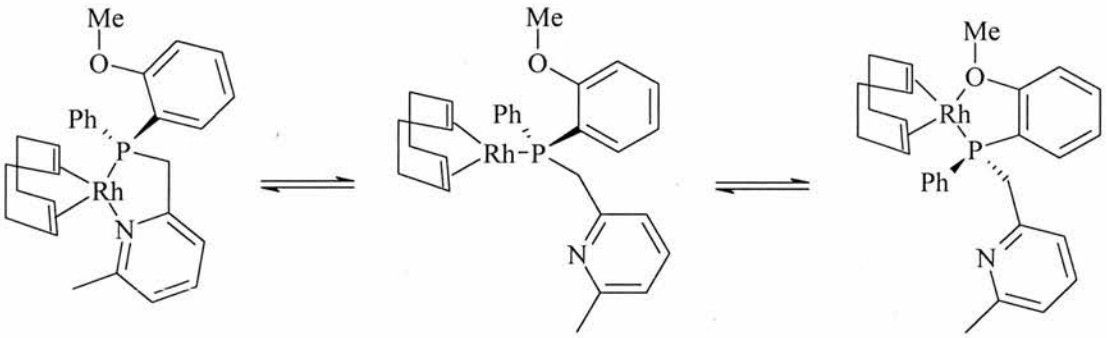

***Figure 1.27:** Complexation of a sterically hindered ligand.*

REFERENCES.

1. W. C. Davis, F. G. Mann, *J. Chem Soc.,* 1944, 276.
2. F. G. Mann, J. Watson, *J. Org. Chem.,* 1948, **13**, 502.
3. F. A. Cotton, M. Matusz, *Polyhedron*, 1988, **7**, 2201.
4. J. E. Parks, B. E. Wagner, R. E. Holm, *J. Organomet. Chem.*, 1973, **56**, 53.
5. Y. Inoguchi, B. Milewski-Marhrla, H. Schimidbaur, *Chem. Ber.*, 1982, **115**, 3085. (Ger).
6. K. Issleib, L. Brusehaber, *Z. Naturfosch.*, 1965, **20b**, 181.
7. E. Uhlig, M. Maaser, *Z. Anorg. Allg. Chem.*, 1966, **334**, 205.
8. R. Ziessel, *Tetrahedron Lett.*, 1989, **577**, 74.
9. A. Maisonnet, J. P. Farr, M. M. Olmstead, C. T. Hunt, A. L. Balch, *Inorg. Chem.*, 1982, **21**, 3961.
10. H. C. E. McFarlane, W. McFarlane, *Polyhedron*, 1988, **7**, 1875.
11. H. C. E. McFarlane, W. McFarlane, A. S. Muir, *Polyhedron*, 1990, **9**, 1757.
12. W. S. J. Kelly, G. H. Ford, S. M. Nelson, *J. Chem. Soc.*, 1971, 388.
13. R. B. King, R. N. Kapoor, M. S. Saran, M. S. Kapoor, *Inorg. Chem.*, 1971, **10**, 1851.
14. H. G. Ang, W. L. Kwik, P. T. Lau, *Polyhedron*, 1990, **9**, 1479.
15. K. W. Hermanowicz, F. P. Pruchnik, *Transition Met. Chem.*, 1988, **13**, 22.
16. C. Moreno, M. J. Macazaga, S. Delgado, *J. Organomet. Chem.*, 1990, **397**, 93.
17. G. Bruzo, S. Lo Schiavo, E. Rotondo, C. G. Arena, F. Farone, *Organometallics*, 1989, **8**, 886.

18. J. L. Ronstan, N. Ansari, F. Lee, J. P. Charland, *Inorg. Chim. Acta.*, 1989, **155**, 11.

19. H. Schmidbaur, Y. Inorguchi, *Z. Naturforsch.*, 1980, **35b**, 1329.

20. J. P. Farr, M. M. Olmstead, F. E. Wood, A. L. Balch, *J. Am. Chem. Soc.*, 1983, **105**, 792.

21. J. P. Farr, F. E. Wood, A. L. Balch, *Inorg. Chem.*, 1983, **22**, 3387.

22. V. K. Jain, V. S. Jakkal, R. Bohra, *J. Organomet. Chem.*, 1990, **389**, 417.

23. C. G. Arena, E. Rotondo, F. Farone, *Organometallics*, 1991, **10**, 3877.

24. A. Maisonnat, J. P. Farr, A. L. Balch, *Inorg. Chim. Acta.*, 1981, **53**, L217.

25. J. P. Farr, M. M. Olmstead, A. L. Balch, *Inorg. Chem.*, **22**, 1229.

26. W. R. Robinson, D. E. Wigley, R. A. Walton, *Inorg. Chem.*, 1985, **24**, 918.

27. Z. Z. Zhang, H. K. Wang, Z. Xi, X. K. Yao, R. J. Wang, *J. Organomet. Chem.*, 1989, **376**, 123.

28. M. M. Olmstead, A. Maisonnat, J. P. Farr, A. L. Balch, *Inorg. Chem.*, 1981, **20**, 4060.

29. J. L. Roustan, N. Ansari, F. R. Ahmed, *Inorg. Chim. Acta.*, 1987, **129**, L11.

30. J. P. Farr, M. M. Olmstead, C. H. Hunt A. L. Balch, *Inorg. Chem.*, 1981, **20**, 1182.

31. K. W. Hermanowicz, F. P. Pruchnik, *Transition Met. Chem.*, 1988, **13**, 101.

32. W. R. Robinson, D. E. Wigley, R. A. Walton, *Inorg. Chem.*, 1985, **24**, 918.

33. Y. Inoguchi, B. Milewski-Mahrla, D. Neugebaur, P. G. Jones, H. Schmidbaur, *Chem. Ber.*, 1983, **116**, 1487. (Ger).

34. H. J. Wasserman, D. C. Moody, R. T. Paine, R. R. Ryan, K. V. Salazar, *J. Chem. Soc., Chem. Commun.*, 1984, 533.

35. E. Uhlig, M. Schafer, *Z. Anorg. Allg. Chem.*, 1968, **359**, 67.

36. W. J. Knebel, R. J. Anjelici, *Inorg. Chim. Acta.*, 1973, **7**, 713.

37. W. J. Knebel, R. J. Anjelici, *Inorg. Chem.*, 1974, **13**, 632.

38. G. U. Spiegel, O. Stelzer, *Z. Naturfosch*, 1987, **42b**, 579.

39. H. T. Dieck, G. Hahn, *Z. Anorg. Allg. Chem.*, 1989, **577**, 74.

40. W. Seidel, H. Scholer, *Z. Chem.*, 1967, **11**, 431.

41. W. Seidel, *Z. Chem.*, 1967, **12**, 462.

42. W. Ainscough, L. K. Peterson, *Inorg. Chem.*, 1970, **9**, 2699.

43. S. M. Aucott, A. M. Z. Slawin and J. D. Woollins, *J. Chem. Soc., Dalton Trans*, 2000, 2559.

44. W. Schirmer, U. Florke, H. J. Haupt, *Z. Anorg. Allg. Chem.*, 1989, **574**, 239.

45. F. E. Wood, M. M. Olmstead, A. L. Batch, *J. Am. Chem. Soc.*, 1983, **105**, 6332.

46. F. E. Wood, J. Hvoslef, H. Hope, A. L. Batch, *Inorg. Chem.*, 1984, **23**, 4309.

47. P. Giannoccaro, G. Vasapollo, A. Sacco, *J. Chem. Soc., Chem. Commun.*, 1980, 1136.

48. W. Keim, *Chem. Ing. Techn.*, 1984, **56**, 850.

49. E. Lindner, J-P. Reber, P. Wegner, *Z. Naturforsch. Teil B*, 1980, **43**, 1269.

50. E. Lindner, A. Sickinger, P. Wegner, *J. Organomet. Chem.*, 1988, **349**, 75.

51. E. Lindner, U. Schrober, E. Glaser, H. Norz, P. Wegner, *Z. Naturforsch. Teil B*, 1987, **42**, 1527.

52. E. Lindner, H. A. Mayer, P. Wegner, *Chem. Ber.*, 1986, **119**, 2616.

53. J-P. Reber, *Dissertation*, Universitat Tubingen, 1991.

54. W. S. Knowles, *Acc. Chem. Res.*, 1983, **16**, 106.

55. H. Brunner, *Angew. Chem. Int. Ed. Engl.*, 1983, **22**, 897.

56. J. M. Brown, S. J. Cook, R. Kahn, *Tetrahedron*, 1986, **42**, 5105.

57. L. Horner, G. Simons, *Z. Naturforsch. Teil. B.*, 1984, **39**, 497.

58. J. C. Jeffrey, T. B. Rauchfuss, *Inorg. Chem.*, 1979, **18**, 2658.

59. E. Lindner, S. Meyer, P. Wegner, B. Karle, A. Sickinger, B. Steger, *J. Organomet. Chem.*, 1987, **335**, 59.

60. E. Lindner, P. Wegner, A. Sickinger, *J. Organomet. Chem.*, 1986, **312**, C37.

61. E. Lindner, H. Rauleder, C. Scheytt, H. A. Mayer, W. Hiller, R. Fawzi, P. Wegner, *Z. Naturforsch. Teil. B.*, 1984, **39**, 632.

62. G. K. Anderson, R. Kumar, *Inorg. Chem.*, 1984, **23**, 4064.

63. T. Okano, M. Yamamoto, T. Noguchi, H. Konishi, J. Kiji, *Chem. Lett.*, 1982, 977.

64. W. S. Knowles, M. J. Sabacky, B. D. Vineyard, *J. Chem. Soc. Chem. Commun.*, 1972, 10.

65. H. B. Kagan, T-P. Dang, *J. Am. Chem. Soc.*, 1972, **94**, 6429.

66. J. M. Brown, B. A. Murrer, *Tetrahedron Lett.*, 1980, **21**, 581.

67. D. Lafont, D. Sinou, G. Descotes, *Nouv. J. Chim.*, 1983, **7**, 283.

68. D. Lafont, D. Sinou, G. Descotes, *J. Organomet. Chem.*, 1978, **150**, C14.

69. T. H. Fife, *J. Am. Chem. Soc.*, 1967, **89**, 3228.

70. G. Doyle, *J. Organomet. Chem.*, 1973, **61**, 235.

71. G. Booth, *Adv. Inorg. Chem. Radiochem.*, 1964, **6**, 1.

72. G. R. Dobson, I. W. Stolz, R. K. Sheline, *Adv. Inorg. Chem. Radiochem.*, 1966, **8**, 1.

73. R. Poli, H. D. Mui, *J. Am. Chem. Soc.*, 1990, **112**, 2446.

74. M. J. Boylan, J. D. Black, P. S. Braterman, *J. Chem. Soc. Dalton Trans.*, 1980, 1646.

75. J. D. Black, M. J. Boylan, P. S. Braterman, A. Fullarton, *J. Chem. Soc. Dalton Trans.*, 1980, 1651.

76. G. L. Geoffroy, M. S. Wrighton, *Organometallic Photochemistry, Academic Press, New York*, 1980.

77. E. Lindner, C. Scheytt, P. Wegner, *J. Organomet. Chem.*, 1986, **308**, 311.

78. E. Lindner, U. Schober, R. Fawzi, W. Hiller, U. Englert, P. Wegner, *Chem. Ber.*, 1987, **120**, 1621.

79. E. Lindner, B. Karle, *Chem. Ber.*, 1990, **123**, 1469.

80. E. Lindner, B. Karle, *Z. Naturforsch. Teil. B.*, 1990, **45**, 1108.

81. T. B. Rauchfuss, *J. Am. Chem. Soc.*, 1979, **101**, 1045.

82. E. Lindner, U. Schober, M. Stangle, *J. Organomet. Chem.*, 1983, **331**, C13.

83. E. Lindner, B. Andres, *Chem. Ber.*, 1987, **120**, 761.

84. E. Lindner, B. Andres, *Chem. Ber.*, 1988, **121**, 829.

85. E. Lindner, H. Norz, *Chem. Ber.*, 1990, **123**, 459.

86. E. Lindner, H. Norz, *Z. Naturforsch. Teil. B.*, 1989, **44**, 1493.

87. G. K. Anderson, R. Kumar, *Inorg. Chim. Acta.*, 1988, **146**, 89.

88. M. Ciampolini, P. Dapporto, N. Nardi, F. Zanobini, *J. Chem. Soc. Chem. Commun.*, 1980, 177.

89. E. Lindner, R. Speidel, R. Fawzi, W. Hiller, *Chem. Ber.*, 1990, **123**, 2255.

90. N. W. Alcock, A. W. G. Platt, P. G. Pringle, *J. Chem. Soc. Dalton Trans.*, 1989, 2069.

91. E. Lindner, R. Speidel, *Z. Naturforsch. Teil. B.*, 1989, **44**, 437.

92. J. M. Brown, S. J. Cook, A. G. Kent, *Tetrahedron*, 1986, **42**, 5097.

93. S. E. Bouaoud, P. Braunstein, D. Grandjean, D. Matt, D. Nobel, *Inorg. Chem.*, 1986, **25**, 3765.

94. P. Braunstein, M. D. Fryzuk, M. Le Dall, F. Naud, S. Rettig, F. Speiser, *J. Chem. Soc. Dalton Trans.*, 2000, 1067.

95. O. Clot, M. O. Wolf, G. P. A. Yap, B. O. Patrick, *J. Chem. Soc. Dalton Trans.*, 2000, 2729.

96. J. S. Field, R. J. Haines, E. I. Lakoba, M. Hal Sosabowski, *J. Chem. Soc. Perkin Trans.*, 2001, 3352.

97. H. Yang, M. Alvarez, N. Lugan, R. Mathieu, *Organometallics*, 1997, **16**, 1401.

98. J. M. Brunel, T. Constantieux, A. Labande, F. Lubatti, G. Buono, *Tetrahedron Lett.*, 1997, **38**, 5971.

99. H. Yang, N. Lugan, R. Mathieu, *Organometallics*, 1997, **16**, 2089.

100. Z. Z. Zhang, H. P. Xi, W. J. Zhao, K. J. Jiang, R. J. Wang, H. G. Wang, Y. Wu, *J. Organomet. Chem.*, 1993, **454**, 221.

Chapter Two: Synthesis and Coordination of 2-Diphenylphosphinopicolinamide (dpppa).

2.1: Introduction

There has been much work based on a variety of hemilabile phosphorus-nitrogen ligands, which has been discussed in detail in chapter 1. In brief, this interest has focused on the presence of both 'hard' (nitrogen) and soft (phosphorus) donor atoms on one ligand. The key to the hemilabile nature of these ligands is also based around the presence of spacer atoms between the phosphorus and the pyridyl nitrogen donor atom, such as N-H (**A**)[1], CH_2-CH_2 (**B**)[2], NH-NH (**C**)[3].

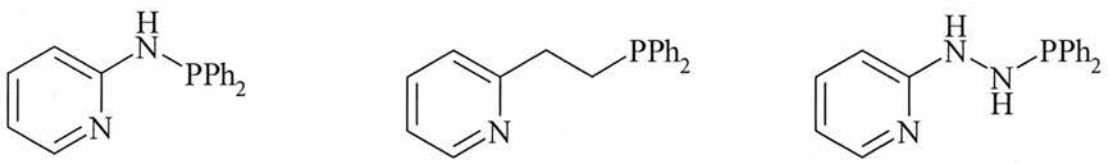

A **B** **C**

Figure 2.1: *Pyridylphosphines.*

Also there has been considerable interest in phosphorus-oxygen ligands, with oxygen acting as the 'hard' donor atom. There are numerous examples where oxygen

has been incorporated into a ligand, examples include etherphosphines (**D**)[4], 1,3-dioxolane derivatives (**E**)[5], phosphino-enolate (**F**)[6] and furylphosphines (**G**)[7] systems.

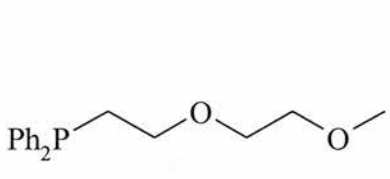

D

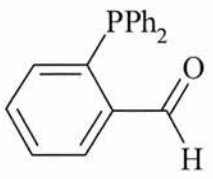

F

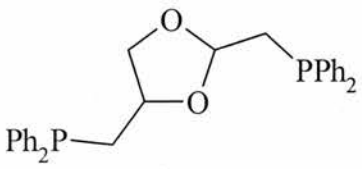

E

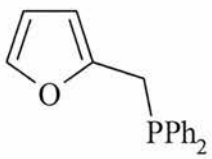

G

***Figure 2.2**: Phosphorus-oxygen ligands.*

In this chapter we will describe our investigations into an amalgamation of two of these aspects of coordination chemistry; aminopyridylphosphines and phosphino-enolates with reactions on a variety of pertinent transition metals. Described are a range of coordination modes incorporating both the pyridylphosphine and phosphino-enolate character of our ligand. The ligand, its derivatives and the complexes generated have been principally characterised by multi-element NMR spectroscopy and X-ray crystallography.

2.2:Results and Discussion.

2.2.1:Synthesis and Chalcogen derivatives of dpppa.

The synthesis of dpppa is straightforward and involves the dropwise addition of Ph_2PCl in tetrahydrofuran, to a tetrahydrofuran solution of 2-picolinamide and a small excess of Et_3N. Subsequent overnight reflux results in the formation of dpppa (Equation 2.1).

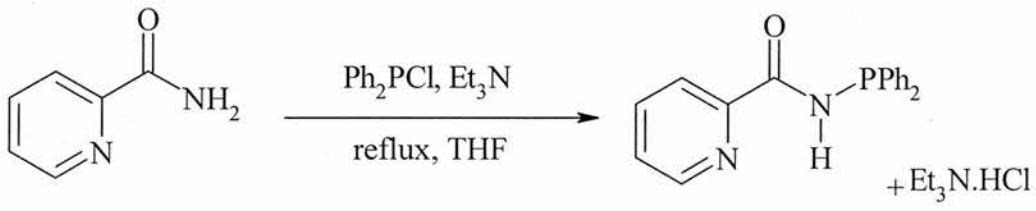

2.1

Equation 2.1

The ligand was recrystallised from boiling methanol to give a colourless crystalline solid in a tolerable yield (55%) and is relatively air stable; however exposure to air for prolonged periods resulted in degradation. It is readily soluble in chlorinated solvents, acetone, thf, but somewhat less so in toluene, methanol and diethyl ether. A singlet is observed in the ^{31}P spectrum of dpppa (in $CDCl_3$) at δ(P) 22.0 ppm. The ^1H NMR (also $CDCl_3$) clearly shows the presence of an amide proton at δ(H) 8.6 ppm, as a doublet $^2J_{P\text{-}H}$ = 4 Hz. The IR spectra shows the expected peaks, a weak ν(N-H) band is present at 3297 cm^{-1}, and bands attributable to ν(pyCN) and ν(P-N) are found at 1589 cm^{-1} and 996 cm^{-1} respectively. The expected ν(C=O) signature is visible at 1691 cm^{-1}. Satisfactory microanalysis was also obtained. Crystals suitable for X-ray crystallography were grown by vapour diffusion of diethyl ether into a concentrated $CDCl_3$ solution of dpppa. Selected structural data for dpppa are given in Table 2.1.

Table: 2.1 *Selected bond lengths (Å) and angles (°) for Dpppa* ***(2.1).***

P(1)-N(2)	1.702(3)	N(2)-C(3)	1.355(5)
P(1)-C(16)	1.834(4)	C(3)-O(3)	1.221(5)
C(3)-C(4)	1.500(6)	N(5)-C(4)	1.325(6)
C(4)-C(9)	1.379(6)	P(1)-C(10)	1.825(4)
N(2)-N(5)	2.67(5)		
N(2)-P(1)-C(10)	102.97(18)	N(2)-P(1)-C(16)	98.84(17)
C(16)-P(1)-C(10)	102.34(19)	C(3)-N(2)-P(1)	126.1(3)
P(1)-N(2)-H(2)		O(3)-C(3)-N(2)	122.1(4)
O(3)-C(3)-C(4)	121.7(4)	N(2)-C(3)-C(4)	116.2(4)
C(3)-C(4)-N(5)	115.5(4)	N(2)-H(2)...N(5)	129(3)

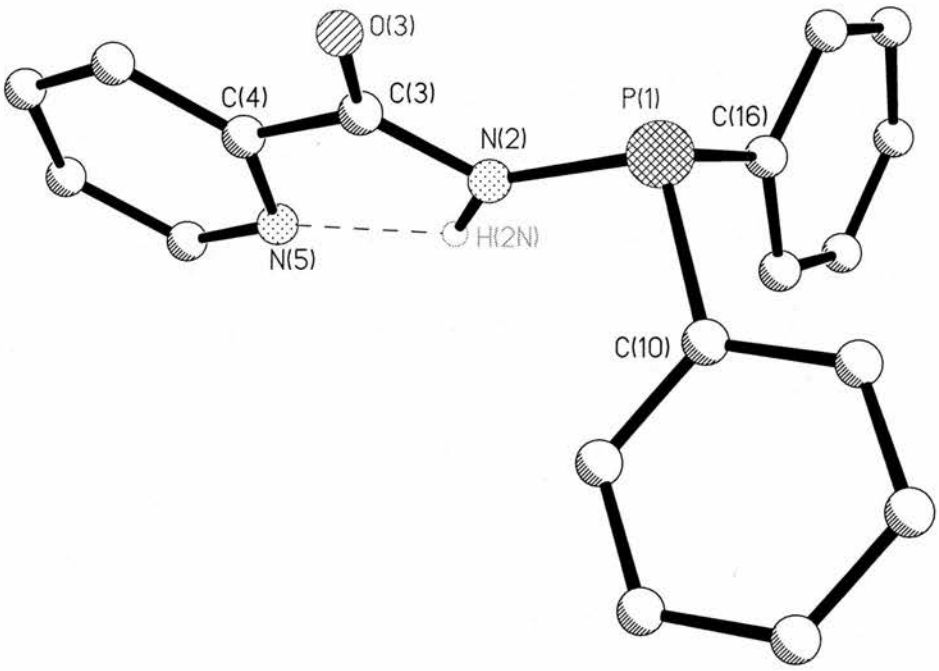

***Figure 2.3**: Crystallographic representation of Dpppa (**2.1**).*

This molecular structure reveals that the P(1)-N(2)-C(3)-O(3) backbone is essentially planar. In addition to this the crystal determination shows that there is an intramolecular hydrogen bonding interaction between the amide proton and the pyridyl nitrogen, this generates an effective five-membered ring that is almost planar. The N(2)-N(5) intramolecular separation is 2.67 Å. It can be imagined that dpppa could have existed in dimer arrangement with a intermolecular hydrogen-bond linking a second dpppa, as has been described in previous examples of pyridylaminophosphines found in literature[3]. It is possible that the ring arrangement is favoured as it generates an energetically favourable five-membered ring as opposed to the unfavourable four membered ring that would have been generated in many of the previous examples. The phosphorus-nitrogen bond length of 1.702(3) Å is well within acceptable boundaries previously established in aminophosphine chemistry in

the literature, confirming there is no change in the single bond nature found in previous examples.

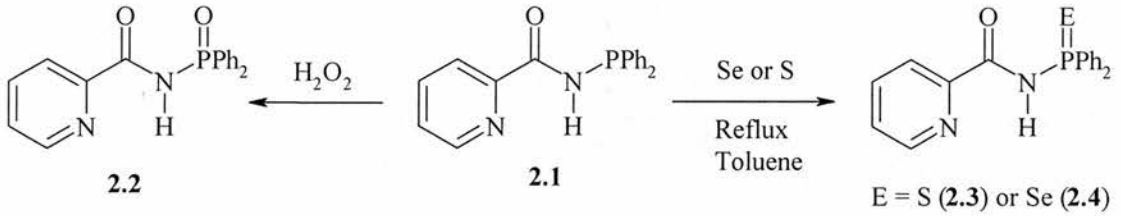

Equation 2.2

The oxide, sulfide and selenide of dpppa were also synthesised as seen in equation 2.2. The oxide (**2.2**) was easily prepared by the addition of a small excess of H_2O_2 (aq), to a solution of dpppa in thf, and isolated as a white solid in good yield. The sulfide **2.3** and selenide **2.4** were prepared by refluxing dpppa in toluene with a stoichiometric amount of sulfur or selenium for 20 min. Both generated the desired oxidized ligand in good yields (82% for **2.3**, 48 % for **2.4**) as colourless solids. The expected downfield shift is found in the ^{31}P NMR spectra of all three compounds. Selected data for $Ph_2P(E)C(E)NHpy$ (E = O, S or Se) can be found in Table 2.2. One item to note is the $^{1}J_{P\text{-}Se}$ value of 788 Hz, this represents a typical value for a phosphorus-selenium double bond.

***Table 2.2**: Spectroscopic data for $Ph_2P(E)C(O)NHpy$.*

Compound	*δ (^1H)*		*δ(^{31}P)*	*IR (cm^{-1})*			
	NH	Aromatics	P	P=E	C=O	NH	CN(py)
2.1	8.7	8.5-7.2	22.0	N/A	1691	3297	1452
2.2	9.4	8.5-7.3	22.1	1215	1694	3302	1451

2.3	9.3	8.6-7.4	54.4	837	1689	3268	1447
2.4	9.3	8.6-7.1	48.7*	Obscured	1698	3288	1391

* - $^{1}J_{P\text{-}Se}$ = 788 Hz

Crystals of **2.2** suitable for X-ray determinations were generated by vapour diffusion of diethyl ether into a concentrated $CDCl_3$ solution. The C(4)-C(3)-N(2)-P(1) back-bone is essentially planar with a mean deviation of 0.0391 Å. As was seen in the unoxidised free ligand the oxide forms the H-bonded five-membered ring linking N(5) and H(2), the intramolecular distance N(2)-N(5) is 2.653 Å which is again typical and comparable to that of the unoxidised ligand. The angle of the bond is again typical being 109° for N(2)-H(2)…N(5).

Table: 2.3 *Selected bond lengths (Å) and angles (°) for Dpppa-O* ***(2.2)****.*

P(1)-O(1)	1.478(2)	P(1)-N(2)	1.683(2)
P(1)-C(11)	1.800(3)	P(1)-C(17)	1.801(3)
O(3)-C(3)	1.217(3)	N(2)-C(3)	1.370(4)
N(5)-C(4)	1.345(4)	C(3)-C(4)	1.506(4)
C(4)-C(9)	1.372(4)	N(2)-N(5)	2.653
N(2)-P(1)-O(1)	115.03(12)	C(17)-P(1)-O(1)	112.68(12)
C(11)-P(1)-O(1)	113.07(12)	C(17)-P(1)-C(11)	106.98(13)
N(2)-P(1)-C(11)	100.96(12)	N(2)-P(1)-C(17)	107.16(13)
C(3)-N(2)-P(1)	124.09(19)	P(1)-N(2)-H(2)	121.01(19)
N(2)-C(3)-C(4)	114.4(2)	O(3)-C(3)-N(2)	123.1(3)

O(3)-C(3)-C(4)	122.6(3)	C(3)-C(4)-C(9)	120.4(3)
C(3)-C(4)-N(5)	115.5(2)	N(5)-C(4)-C(9)	124.11

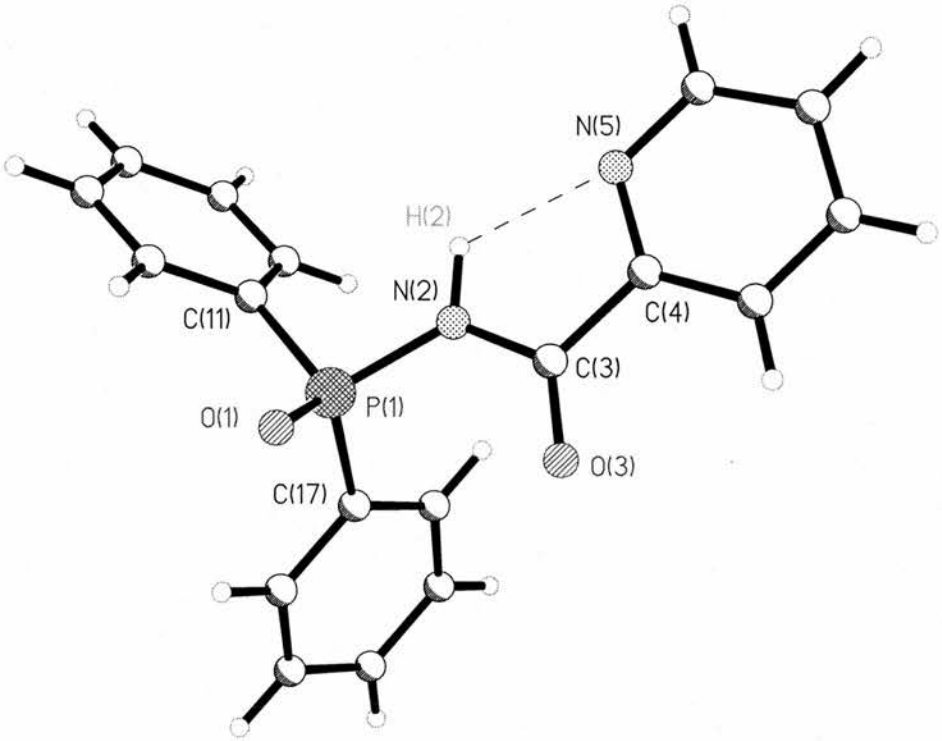

***Figure 2.4**: Crystallographic representation of Dpppa-O (**2.2**).*

It has been shown in previous literature examples that the oxides and sulfides of phosphorus(III) ligands can display different solid state motifs, based around the ability of the oxygen to be protonated by means of a rearrangment[8]. However in this case the amide proton for which such a rearrangement is vital is already involved in intermolecular H-bonding, so it was of interest to examine this example for any differences.

Cooling a hot toluene solution of **2.3** produced crystals suitable for the X-ray analysis. Immediately we see the expected change of motif, with the sulfide existing in a dimer arrangement rather than favouring the internal bonding seen in the oxide.

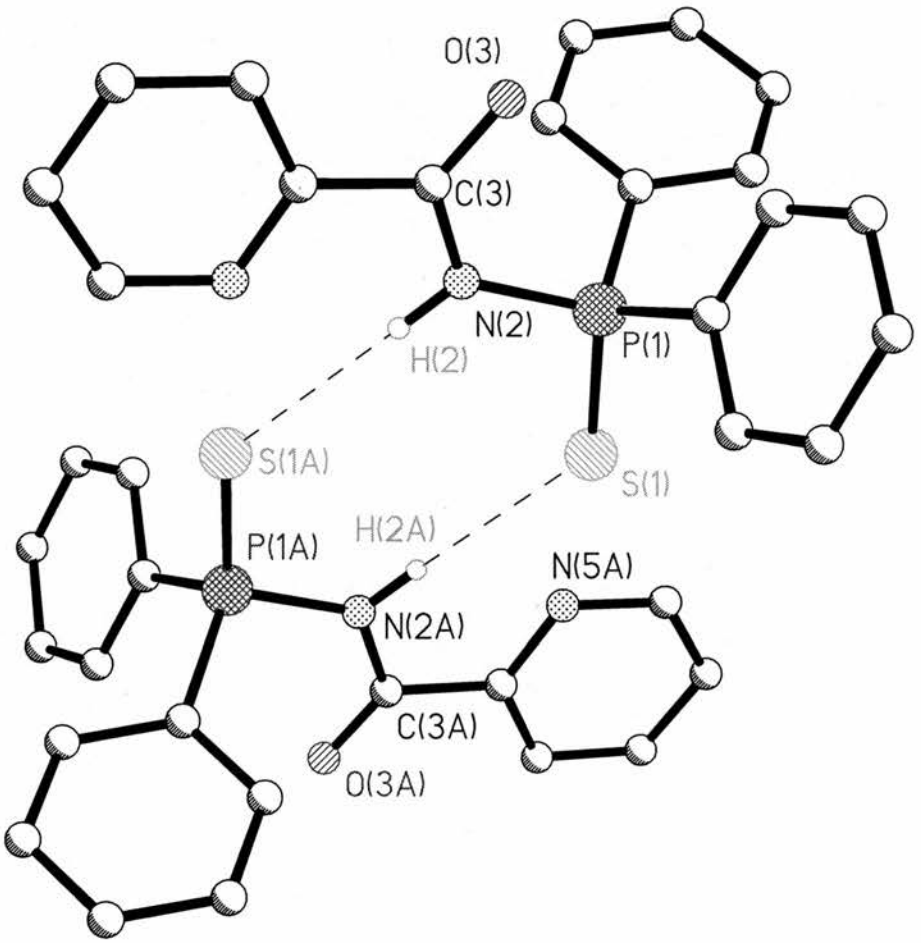

Figure 2.5: *Crystallographic Representation of dpppa-S* ***(2.4)****.*

It is interesting to see what changes this different form of bonding has on the rest of the molecule. The backbone of the molecule remains mostly planar, and also the distance between N(2) and N(5) remains very close (2.65 Å) and thus a N(2)-H(2)…N(5) hydrogen bond interaction is retained.

2.2.2: *Monodentate dpppa coordination mode complexes.*

Dpppa reacts with $[PtCl_2(cod)]$ in dichloromethane to generate *cis*-$[PtCl_2(dpppa\text{-}P)_2]$ (**2.5**) a white crystalline solid in good yield 80 % (figure 2.6). This is the only coordination mode found in the initial reaction, no *trans*-bis(dpppa) or mono(dpppa) binding was observed. This is in marked contrast to 2-(diphenylphosphino)aminopyridine (dppap). Two equivalents of dppap react with $[PtCl_2(cod)]$ (where X = Cl or Me) to form a cationic compound where one ligand is monodentate (*P*), and the second chelates (*P,N*), generating $[PtX(Ph_2PNHpy\text{-}P,N)(Ph_2PNHpy\text{-}P)][Cl]$ (X = Cl or Me). The ^{31}P NMR ($CDCl_3$) of **2.5** shows a singlet at δ(P) 31.2 ppm with the expected Pt satellites, the sizable coupling constant of $^1J_{Pt\text{-}P}$ = 3984 Hz is consistent with the phosphorus *trans* to chloride. ^1H NMR ($CDCl_3$) displays some significant changes from the free ligand. The amine proton is shifted to δ(H) 10.7 ppm; also the coupling constant increases to $^2J_{P\text{-}H}$ = 15 Hz. The pyC[6]H remains unchanged at δ(H) 8.5 ppm, this is evidence to suggest that the ligand is unchelated, as a downfield shift is expected in a chelated complex. The ν(N-H) in the IR spectrum shifts to a lower wave number, suggesting the possibility of hydrogen bonding interactions in the solid state, however the ν(C=O) stretch remains unchanged indicating no such interactions. Two Pt-Cl stretches are visible in the spectrum (320 and 302 cm^{-1}), further evidence of a *cis*- conformation for **2.5**. In contrast, reaction of $[PdCl_2(cod)]$ with dpppa generates $[PdCl_2(dpppa\text{-}P)_2]$ (**2.6**), which is insoluble and displays only one Pd-Cl stretch (310 cm^{-1}), suggesting a *trans*-arrangement, the other expected IR peaks are observed clearly, ν(N-H) at 3232, ν(C=O) at 1694, ν(P-N) at 997 cm^{-1}. This *trans*- arrangement is consistent with previous examples of pyridylaminophosphines found in literature[1].

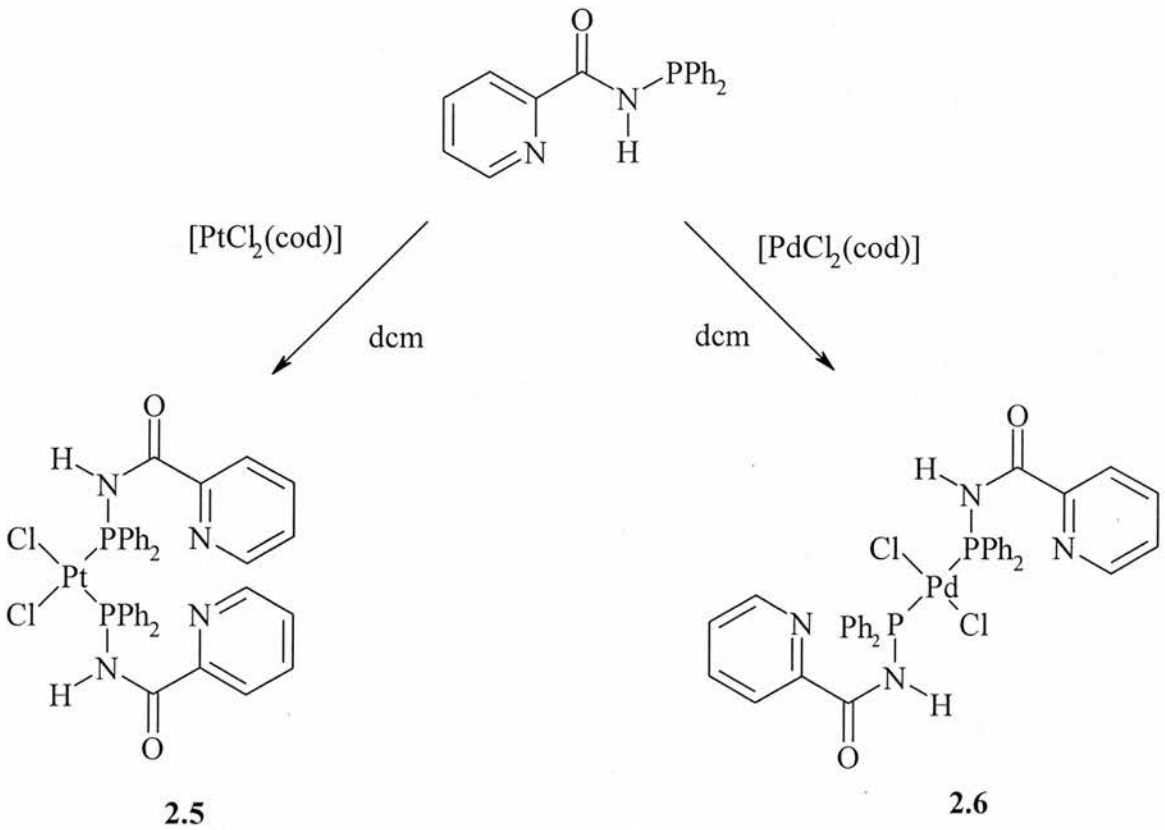

***Figure 2.6**: Synthesis of two monodentate dpppa complexes.*

A series of palladium complexes were synthesised bearing only one dpppa monodentate bound via the phosphorus. Complexes [PdCl(allyl)(dpppa-*P*)] (**2.7**), [PdCl($C_{10}H_6NO$)(dpppa-*P*)] (**2.8**), [PdCl($C_9H_{12}N$)(dpppa-*P*)] (**2.9**), [PdCl($C_{12}H_{12}N$)(dpppa-*P*)] (**2.10**), were all synthesised via bridge cleavage reactions of the respective dimer starting materials. **2.7** was synthesised as a yellow solid in good yield (87%), it's ^{31}P NMR ($CDCl_3$) shows the expected singlet at δ(P) 54.5 ppm. The amide proton is shifted downfield in the ^1H NMR spectra ($CDCl_3$), to δ(H) 10.7 ppm, this mirrors the shift of the amide proton in **2.5**, and also in common with **2.5** the $^2J_{P\text{-}H}$ coupling constant is enlarged, stretching to 22 Hz. The IR spectrum shows

the ν(N-H) stretch has shifted to a much greater extent than seen in **2.5**, this could be due to much stronger hydrogen bonding interaction being present in **2.7**, and once again the ν(C=O) is relatively unmoved in comparison with the free ligand being found at 1686 cm^{-1}. Excellent microanalysis was obtained for **2.7**, as well as a crystal suitable for X-ray analysis by vapour diffusion of diethyl ether to a concentrated $CDCl_3$ solution of **2.7**.

***Table 2.5**: Selected bond lengths (Å) and angles (°) for [PdCl(allyl)(dpppa-P)](**2.7**).*

P(1)-Pd(1)	2.2786(8)	Pd(1)-Cl(1)	2.3800(8)
P(1)-N(2)	1.703(3)	N(2)-C(3)	1.366(4)
O(3)-C(3)	1.216(4)	C(3)-C(4)	1.512(4)
N(5)-C(4)	1.336(4)	C(4)-C(9)	1.381(5)
P(1)-C(11)	1.811(3)	P(1)-C(17)	1.821(3)
Pd(1)-C32(2)	2.150(6)	Pd(1)-C33(2)	2.211(4)
Pd(1)-C31(2)	2.087(4)	N(2)...Cl(1)	3.204
N(2)...N(5)	2.669		
P(1)-Pd(1)-Cl(1)	96.52(3)	N(2)-P(1)-Pd(1)	107.90(9)
C(11)-P(1)-Pd(1)	114.09(10)	C(17)-P(1)-Pd(1)	116.75(11)
N(2)-P(1)-C(11)	106.21(13)	N(2)-P(1)-C(17)	105.87(13)
C(17)-P(1)-C(11)	105.26(14)	P(1)-N(2)-H(2)	115(2)
C(3)-N(2)-P(1)	130.3(2)	N(2)-C(3)-C(4)	114.1(3)
O(3)-C(3)-C(4)	121.4(3)	O(3)-C(3)-N(2)	124.5(3)
N(5)-C(4)-C(9)	123.6(3)	C(3)-C(4)-C(9)	120.1(3)

C(3)-C(4)-N(5)	116.3(3)	N(2)-H(2)...Cl(1)	138
N(2)-H(2)...N(5)	110		

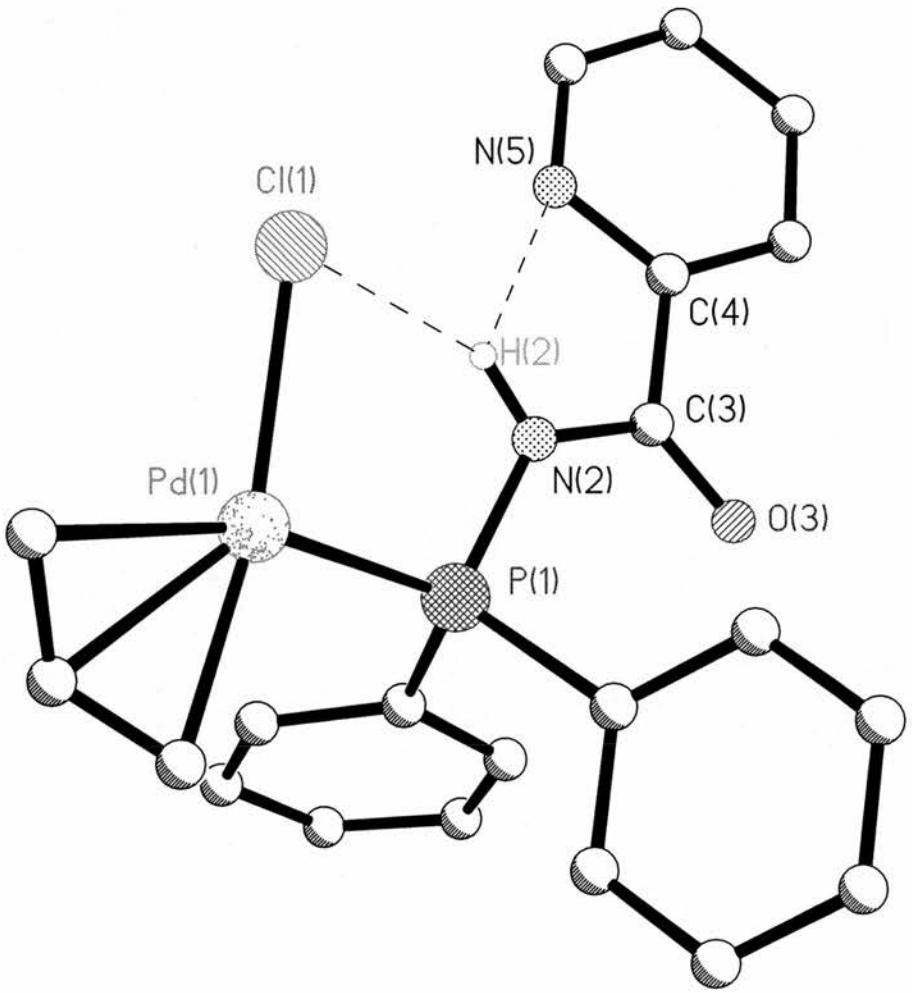

***Figure 2.7**: Crystallographic representation of [PdCl(allyl)(dpppa-P)]* (**2.7**).

In the solid state, **2.7** has a hydrogen-bonding interaction between not only H(2)-N(5), but also between H(2)-Cl(1) with the interatomic distances being N(2)-

Cl(1) 3.204 Å and N(2)-N(5) 2.669, the latter is almost identical to the previously observed values for dpppa and dpppa-O. It should be noted the interaction with Cl(1) causes the previously planar five-membered ring formed by the H(2)-N(5) H-bond to distort with a N(5)-C(4)-C(3)-N(2) torsion angle of –15.08 °. We investigated comparable hydrogen-bonds involving metal bound chlorides to determine whether the value seen in **2.7** is representative. In **2.7** the N(2)-H(2)-N(5) angle is 110.16 and N(2)-H(2)-Cl(1) 138.13°, comparison of these values with examples of single rather than multi hydrogen bond motifs may show some deviation and will be explored later in the chapter. The increased hydrogen-bonding observed in the crystal structure confirms the observations made from the IR data about the extent of the hydrogen-bonding. Investigation into the bonding in the other palladium complexes of dpppa should prove enlightening.

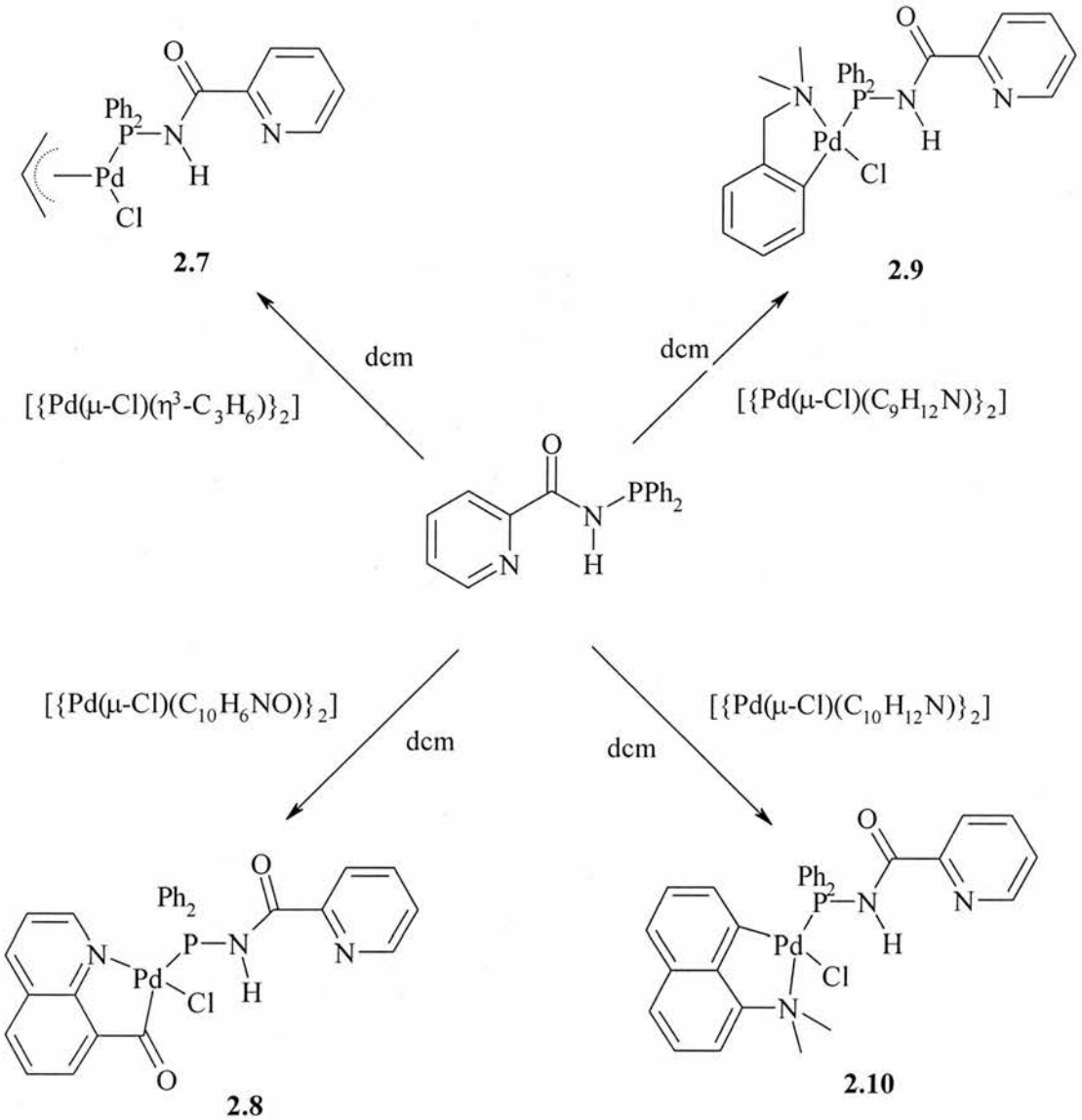

***Figure 2.8**: Reaction of dpppa with Palladium Dimers.*

Complexes **2.8**, **2.9** and **2.10** are on the face of it very similar, however a significant difference can be seen in their solubility. **2.8** is insoluble in all common organic solvents; where as **2.10** is sparingly soluble, and **2.9** reasonably soluble in chlorinated solvents. The IR spectrum of **2.8** displays the expected peaks, ν(N-H) 3231 cm^{-1}, and the two ν(C=O) and 1685 and 1673 cm^{-1} it was isolated as a tan solid in excellent yield (95%) and mass spectral and microanalytical analysis proved its identity. The ^{31}P NMR ($CDCl_3$) of **2.9** and **2.10** is very similar δ(P) 63 and 64 ppm

for **2.9** and **2.10** respectively. Peaks at δ(P) 63.3 (**2.9**) and 64.3 (**2.10**) ppm in the ^{31}P spectrum along with the other spectral evidence confirm monodentate geometry for these complexes. The ^{1}H spectra of **2.9** and **2.10** are similar to each other and that of **2.7**. A shift of the amide proton is again visible, in **2.9** it shifts to 10.9 ppm with a $^{2}J_{P-H}$ of 19 Hz, and in **2.10** it shifts to 11.3 ppm with a $^{2}J_{P-H}$ of 18 Hz. The similarities continue in the proton spectra when the pyC[6]H resonance is investigated, peaks at 8.7 ppm ($^{1}J_{H-H}$ = 4 Hz, for **2.9**, 5 Hz for **2.10**) are observed, giving the impression that the pyridyl protons are in similar environments. The IR data is consistent, ν(N-H) = 3203 (**2.9**) and 3190 (**2.10**), ν(C=O) = 1678 (**2.9**) and 1684 cm^{-1} (**2.10**) respectively. Both were isolated as yellow solids in moderate yields (**2.9**, 64 %; **2.10**, 44 %). Crystals of **2.9** suitable for X-ray analysis were obtained by vapour diffusion of diethyl ether into a concentrated $CDCl_3$ solution. This analysis showed that the C(3)-N(2)-P(1)-Pd(1) backbone is essentially planar with a mean deviation of 0.0353Å and a P-N bond distance of 1.703(3) Å. Hydrogen bonding is again prevalent in the complex, based around N(2) and Cl(1) and also N(2) and N(5), the separation of N(2)-Cl(1) is 3.099 Å which is considerably shorter than the analogous interaction seen in **2.7** (3.204 Å); the N(2)-H(2)-Cl(1) angle is 138.16°. . The N(2)-N(5) separation is 2.674, with a N(2)-H(2)-N(5) angle of 103.68°, both of these values are similar to those seen with **2.7**.

Table 2.5: *Selected bond lengths (Å) and angles (°) for [PdCl($C_9H_{12}N$)(dpppa-P)]* ***(2.9)****.*

P(1)-Pd(1)	2.2786(8)	Pd(1)-Cl(1)	2.3800(8)
P(1)-N(2)	1.703(3)	N(2)-C(3)	1.366(4)

O(3)-C(3)	1.216(4)	C(3)-C(4)	1.512(4)
N(5)-C(4)	1.336(4)	C(4)-C(9)	1.381(5)
P(1)-C(11)	1.811(3)	P(1)-C(17)	1.821(3)
Pd(1)-C(33)	2.211(4)	N(2)-Cl(1)	3.20
Pd(1)-C(31)	2.087(4)	Pd(1)-C(32)	2.150(6)
N(2)-N(5)	2.66		
P(1)-Pd(1)-Cl(1)	96.52(3)	N(2)-P(1)-Pd(1)	107.90(9)
C(11)-P(1)-Pd(1)	114.09(10)	C(17)-P(1)-Pd(1)	116.75(11)
N(2)-P(1)-C(11)	106.21(13)	N(2)-P(1)-C(17)	105.87(13)
C(17)-P(1)-C(11)	105.26(14)	P(1)-N(2)-H(2)	114
C(3)-N(2)-P(1)	130.3(2)	N(2)-C(3)-C(4)	114.1(3)
O(3)-C(3)-C(4)	121.4(3)	O(3)-C(3)-N(2)	124.5(3)
N(5)-C(4)-C(9)	123.63(3)	C(3)-C(4)-C(9)	120.1(3)
C(3)-C(4)-N(5)	116.3(3)	N(2)-H(2)...Cl(1)	138
N(2)-H(2)...N(5)	110		

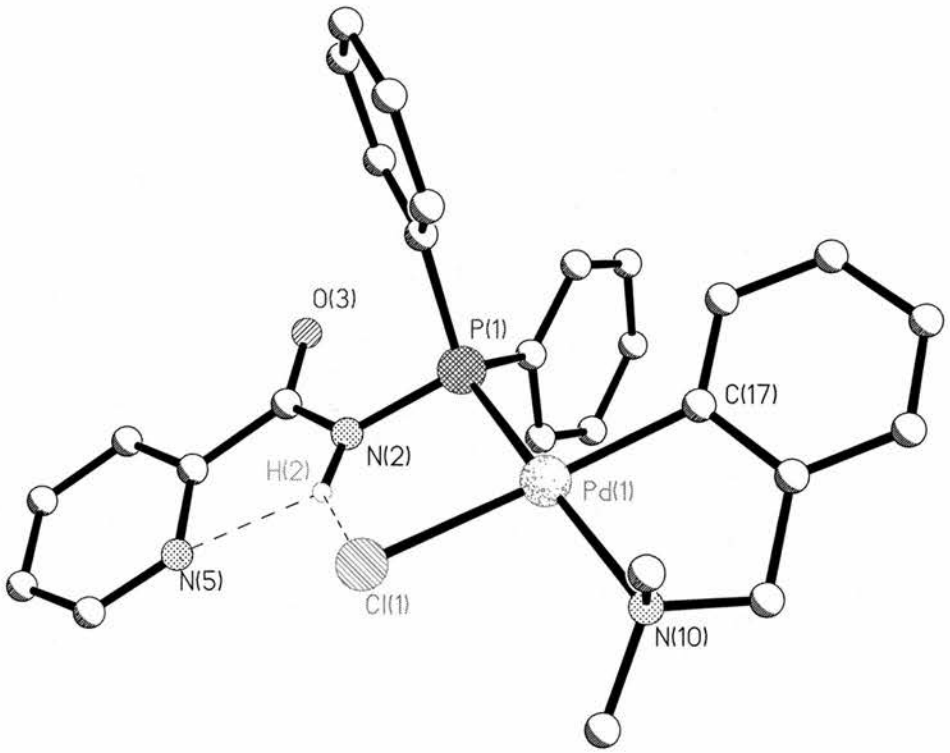

Figure 2.9**: Crystallographic representation of [PdCl($C_9H_{12}N$)(dpppa-P)]* ***(2.9).

For an extended comparison of these palladium systems a crystal of **2.10** was also grown by vapour diffusion of diethyl ether into a concentrated $CDCl_3$ solution; it is essentially isostructural to **2.9**. The same multi hydrogen bond motif is found in this complex, the N(2)-Cl(1) separation is 3.11 Å, which fits between the values observed for **2.7** and **2.9** the N(2)-H(2)…Cl(1) angle of the bond is similar to the figures reported for **2.7** and **2.9** at 134.14°. The N(2)-N(5) distance 2.70 Å and the N(2)-H(2)-N(5) angle 104.44° which is also consistent.

***Table 2.6**: Selected bond lengths (Å) and angles (°) for [PdCl($C_{12}H_{12}N$)(dpppa-P)] **(2.10)**.*

P(1)-Pd(1)	2.2482(13)	Pd(1)-Cl(1)	2.3944(13)
Pd(1)-N(32)	2.159(4)	P(1)-N(2)	1.706(4)
O(3)-C(3)	1.217(6)	N(2)-C(3)	1.383(7)
N(5)-C(4)	1.345(7)	C(3)-C(4)	1.507(7)
C(4)-C(9)	1.395(8)	P(1)-C(17)	1.821(5)
N(2)-Cl(1)	3.114(4)	P(1)-C(11)	1.825(5)
N(2)-N(5)	2.70		
P(1)-Pd(1)-Cl(1)	93.43(5)	P(1)-Pd(1)-N(32)	163.38(12)
N(2)-P(1)-Pd(1)	109.02(15)	C(17)-P(1)-Pd(1)	118.91(17)
C(11)-P(1)-Pd(1)	110.17(16)	Cl(1)-Pd(1)-N(32)	92.17(12)
N(2)-P(1)-C(11)	103.8(2)	N(2)-P(1)-C(17)	104.2(2)
C(3)-N(2)-P(1)	124.8(3)	C(17)-P(1)-C(11)	109.5(2)
P(1)-N(2)-H(2)	116(4)	O(3)-C(3)-N(2)	124.2(5)
O(3)-C(3)-C(4)	121.5(4)	N(2)-C(3)-C(4)	114.3(4)
C(3)-C(4)-N(5)	117.7(4)	C(3)-C(4)-C(9)	118.4(5)
N(5)-C(4)-C(9)	123.25(5)	N(2)-H(2)...Cl(1)	134(5)
N(2)-H(2)...N(5)	104		

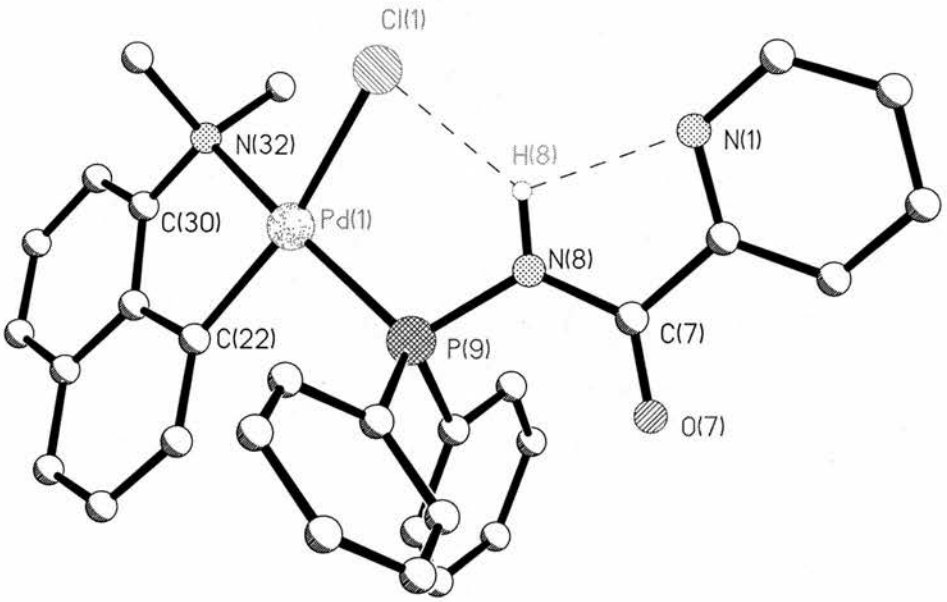

***Figure 2.10**: Crystallographic representation of [PdCl($C_{12}H_{12}N$)(dpppa-P)] (**2.10**).*

The major difference between the three crystal structures of **2.7**, **2.9** and **2.10** is the backbone of the ligand in the complexes. As was stated **2.7** has torsion angles of N(2)-C(3)-C(4)-N(5) of –15.08° and N(2)-P(1)-Pd(1)-Cl(1) of –1.04°. However the other complexes do not duplicate these values. With **2.9** the angles are reversed with the N(2)-C(3)-C(4)-N(5) torsion angle –4.12°, much more planar, and N(2)-P(1)-Pd(1)-Cl(1) –28.07° with the Cl(1) being pushed out of the plane. When one considers the analogous values for **2.10**, a pattern begins to emerge, the N(2)-C(3)-C(4)-N(5) torsion angle is –18.65 and the N(2)-P(1)-Pd(1)-Cl(1) torsion angle is 1.63. If the other ligands around the metal are examined it can be observed that when the metal is crowded the Cl is pushed out of the plane and the other hydrogen-bond is planar as is seen in **2.10**. When the crowding is reduced as seen in **2.9** the Cl returns closer to the plane of the hydrogen-bond and this has the subsequent effect of

distorting the plane of the other hydrogen-bond. Taking the pattern further one would imagine that when the steric crowding around the metal is all but removed (as in **2.7**) the Cl containing angle will become almost planar, and this is observed, furthermore the predicable distortion of the N(2)-C(3)-C(4)-N(5)-H(2) ring also occurs in **2.7**. From this information it could be assumed that the N(2)-Cl(1) H-bond is the dominant interaction in the molecule as the changes in this interaction affect the entire molecule, and ligand's conformation is directly effected by the Cl(1)-H(2) interaction.

2.2.3: Complexes of Ruthenium, Rhodium and Iridium.

Complexes of ruthenium, rhodium and iridium were synthesised to further investigate the coordination of dpppa. $[RuCl_2(p\text{-Cymene})(dpppa\text{-}P)]$ **2.11** was generated by reaction of $[RuCl(\mu\text{-}Cl)(p\text{-Cymene})]_2$ with dpppa and isolated as a red solid. The rhodium and iridium complexes were synthesised by reaction with $[MCl(\mu\text{-}Cl)(\eta^5\text{-}C_5Me_5)]_2$ (where M = Rh or Ir), and dpppa, to give complexes of the type $[MCl_2(\eta^5\text{-}C_5Me_5)(dpppa\text{-}P)]$ (where M = Rh (**2.12**) or Ir (**2.13**)) **2.12** was isolated as a deep red crystalline solid and **2.13** as an orange solid. As can be seen from the IR data, the ν(N-H) of **2.12** and **2.13** are relatively unchanged in comparison with the stretches found for the free ligand. In contrast the peak for **2.11** is significantly lower than the band found for free ligand indicating hydrogen bonding consistent with the previous examples. Inspection of the ν(C=O) stretches for **2.12** and **2.13** shows a considerable shift. This and the small ν(N-H) band could indicate a different type of hydrogen bonding interaction present in **2.12** and **2.13** than that seen in previous complexes such as **2.5** and that is present in **2.11**.

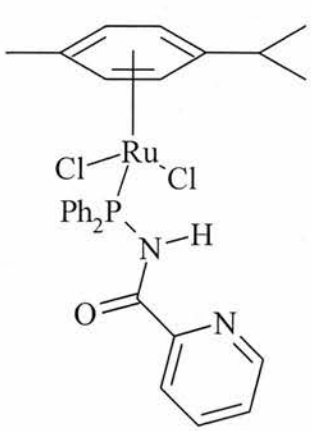

2.11

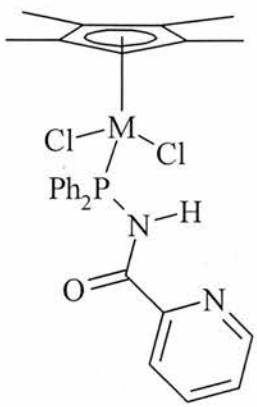

M = Rh (**2.12**) or Ir (**2.13**)

***Figure 2.11**: Complexes of dpppa.*

The data for **2.11**, **2.12** and **2.13** is available for comparison (Table 2.7).

***Table 2.7**: Selected spectroscopic data for **2.11**, **2.12** and **2.13**.*

Compound	*NMR*		*IR*			
	^{1}H ($CDCl_3$)	^{31}P ($CDCl_3$)	N-H cm^{-1}	C=O cm^{-1}	P-N cm^{-1}	Yield/%
2.11	9.7	59.3	3261	1684	997	84
2.12	9.9	62.8	3298	1678	997	91
2.13	10.2	32.7	3288	1678	998	91

The ^{31}P NMR of **2.11**, **2.12** and **2.13** is as expected, with singlets observed for **2.11** and **2.13**, and a doublet for **2.12** ($^{1}J_{Rh\text{-}P}$ = 150.2 Hz) and all are shifted downfield from that of the free ligand this data can be seen in table 2.7. Also the ^{1}H NMR shows that the $^{2}J_{P\text{-}H}$ amine couplings are very similar for **2.11**, **2.12** and **2.13** being 18, 18 and 17 Hz respectively. The amine shifts follow the expected pattern for the complexed ligand with a considerable downfield shift as seen in table 2.7. Crystals of

2.12 and **2.13** have been studied by X-ray analysis; these crystals were grown by slow vapour diffusion of diethyl ether into a concentrated $CDCl_3$ solution of the relevant complex. These structures also proved to be isomorphous; here we will consider **2.13** for discussion. On inspection of the ligand backbone we observed a modest shift out of plane, with the mean deviation of C(3)-N(2)-P(1)-Ir(1) being 0.1160Å, this is the highest deviation seen so far with monodentate dpppa complexes but is not unexpected. The analogous complex formed with 2-(diphenylphosphino)hydrazinopyridine displays a similar deviation[9]. Also as seen with the 2-(diphenylphosphino)hydrazinopyridine example, there are two types of hydrogen bonding displayed, the first is between the amine proton and one of the chlorides. The N(2)-Cl(2) distance in **2.13** is 3.123 Å, which is a marked increase in the bond length compared to the palladium examples we have already discussed, and in comparson with 2(diphenylphosphino)hydrazinopyridine it is also an increase, this could be due the presence of the carbonyl rather than a N-H spacer group. Equally when considering earlier dpppa examples, it could be a simple result of the octahedral coordination around the metal rather than the square planar motif we have concentrated on earlier. This argument could be reinforced if the bond angle was of smaller magnitude, and this is indeed the case with the N(2)-H(2)...Cl(1) angle 116.51°, this is a large reduction compared to the palladium analogues, however in comparison again with 2(diphenylphosphino)hydrazinopyridine a very similar angle is observed in the analogous complex. The second type of hydrogen bonding observed in the complex is of a similar motif to that found in the free ligand, oxide and sulphide, with a bond present between N(2)-N(5), the distance 2.71 Å is similar to the free ligand bond length, as is the bond angle N(2)-H(2)...N(5) being 110.39°. The torsion angle N(2)-C(3)-C(4)-N(5) is significant, it is 19.41°. Following our

discussion of the palladium complexes (**2.7**, **2.8**, **2.9** and **2.10**) this suggests that the other hydrogen-bond interaction is strained, forcing the non-planar angle, and this is substantiated by the observed angle, this N(2)-C(3)-Ir(1)-Cl(2) angle has a significant twist of 35.03°.

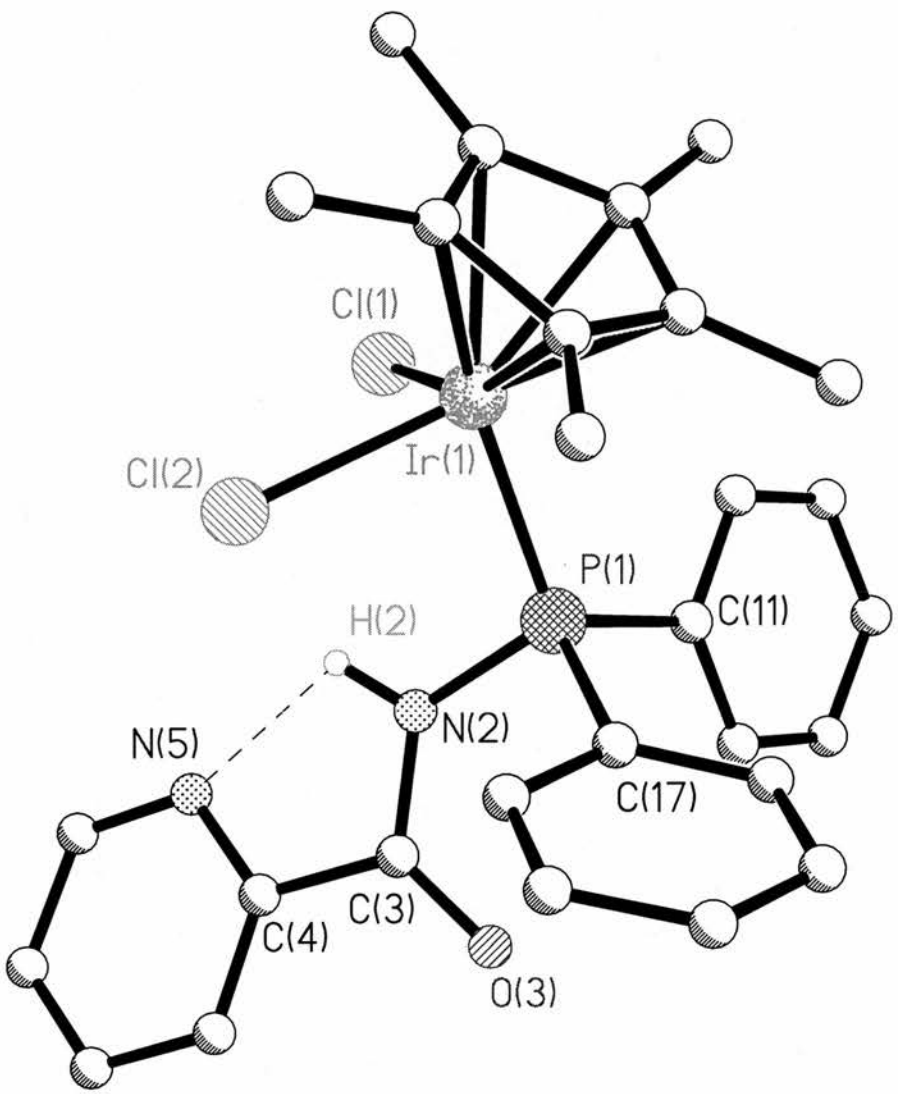

***Figure 2.12**: Crystallographic representation of [$IrCl_2(\eta^5\text{-}C_5Me_5)$ (dpppa-P)] (**2.13**).*

Table 2.8**: Selected bond lengths (Å) and angles (°) for [$IrCl_2(\eta^5\text{-}C_5Me_5)$ (dpppa-P)] **(2.13)

P(1)-Ir(1)	2.287(2)	Ir(1)-Cl(1)	2.4126(19)
Ir(1)-Cl(2)	2.4034(18)	P(1)-N(2)	1.699(7)
O(3)-C(3)	1.233(9)	N(2)-C(3)	1.379(10)
N(5)-C(4)	1.333(10)	C(3)-C(4)	1.494(11)
P(1)-C(11)	1.815(8)	P(1)-C(17)	1.820(8)
N(2)-Cl(2)	2.94(7)	C(4)-C(9)	1.383(11)
N(2)-N(5)	2.24(8)		
P(1)-Ir(1)-Cl(1)	88.49(7)	P(1)-Ir(1)-Cl(2)	87.72(7)
N(2)-Ir(1)-P(1)	110.2(2)	C(17)-Ir(1)-P(1)	111.7(2)
C(11)-Ir(1)-P(1)	117.8(3)	Cl(1)-Ir(1)-Cl(2)	87.57(7)
N(2)-P(1)-C(11)	104.2(3)	N(2)-P(1)-C(17)	104.2(3)
C(3)-N(2)-P(1)	129.0(5)	C(17)-P(1)-C(11)	107.7(3)
P(1)-N(2)-H(2)	119(6)	O(3)-C(3)-N(2)	123.3(7)
O(3)-C(3)-C(4)	122.1(7)	N(2)-C(3)-C(4)	114.6(6)
C(3)-C(4)-N(5)	117.3(7)	C(3)-C(4)-C(9)	118.3(7)
N(5)-C(4)-C(9)	124.4(8)	N(2)-H(2)...Cl(2)	114
N(2)-H(2)...N(5)	112(6)		

2.2.4. Mixed diphosphine Pt complexes of dpppa.

Dpppa reacts with [{PtCl(μ-Cl)(PR_3)}$_2$] (PR_3 = PMe_2Ph or PEt_3), to give complexes of the type *cis*-[$PtCl_2$(dpppa-*P*)(PR_3)] (PR_3 = PMe_2Ph (**2.14**) or PEt_3 (**2.15**)). Monodentate binding was the only observed mode of coordination in both instances. Complexes of **2.14** and **2.15** were isolated as white solids in acceptable yields of 65 and 66 % respectively. Selected NMR data can be found in table 3. Again we observe a significantly shifted amine proton, shifting to δ(H) 11.1 and 11.4 ppm for **2.14** and **2.15** respectively. The ^{31}P NMR shows the expected AM spectra and the large $^1J_{Pt\text{-}P}$ coupling constants and the small $^2J_{P\text{-}P}$ couplings are consistent with a *cis*- arrangement of phosphorus around the Pt metal centre this geometry continues the trend seen with other phosphorus-nitrogen ligands of this type, this data can be seen in table 2.9.

***Table 2.9**: Spectroscopic data for **2.14** and **2.15**.*

Compound	*^{1}H (CDCl$_3$)*			*^{31}P (CDCl$_3$)*				
	N-H	$^2J_{P\text{-}N\text{-}H}$	Aromatics	P1	P2	$^1J_{Pt\text{-}P1}$	$^1J_{Pt\text{-}P2}$	$^2J_{P\text{-}Pt\text{-}P}$
2.14	11.1	15	8.6-7.0	30.9	-14.5	3930	3500	18.78
2.15	11.4	16	8.7-7.1	30.0	7.6	4010	3360	18.77

(P1 = dpppa; P2 = PMe_2Ph or PEt_3), (All J in Hz)

The IR data shows the anticipated peaks; with ν(N-H) at 3162 cm^{-1} for **2.15** (obscured for **2.14**); ν(C=O) at 1686 (**2.14**), 1687 cm^{-1} (**2.15**). Suitable crystals of **2.15** were grown for X-ray crystallography; growth was facilitated by vapour diffusion of diethyl ether into concentrated dichloromethane solution of the complex.

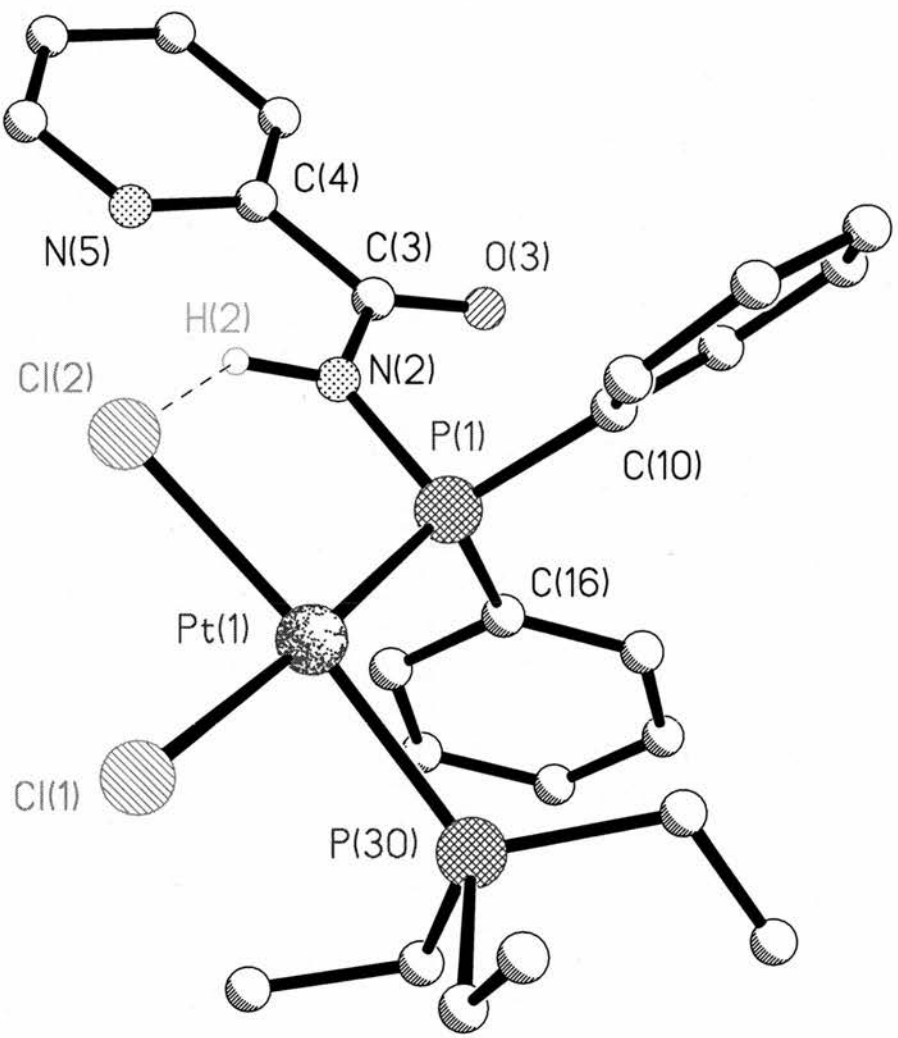

***Figure 2.13**: Crystallographic representation of [$PtCl_2$(dpppa-P)(PEt_3)] (**2.15**).*

The C(3)-N(2)-P(1)-Pt(1) backbone is essentially planar, with a mean deviation of 0.0334 Å, which is consistent with what we have seen so far. Two different hydrogen bonding motifs are again observed within the complex, they are the expected interactions, with N(2)-Cl(2) bonding with a interatomic distance of 3.011 Å. This is in accord with similar separations observed for the earlier square planar palladium complexes. However the bond angle is somewhat smaller than the earlier square planar complexes at N(2)-H(2)...Cl(2) 126.55°. The second motif observed is again consistent with the Pd complexes earlier, with N(2)-N(5) interacting with a distance of 2.641 Å, and N(2)-H(2)-N(5) angle of 112.26°, which is closer to **2.7** than the other palladium examples, this could be due to the fact that Cl(2) is raised out of the plane, displaying a N(2)-P(1)-Pt(1)-Cl(2) torsion angle of –19.16°, as we have seen earlier the position of the Cl has a profound effect on the hydrogen-bonding throughout the rest of the molecule. The N(2)-C(3)-C(4)-N(5) torsion angle is almost planar, this is as we might expect as our previous examples have illustrated a similar pattern between the two hydrogen-bonds when the Cl is distorted as in this complex.

Table: 2.10: *Selected bond lengths (Å) and angles (°) for [$PtCl_2$(dpppa-P)(PEt_3)] **(2.15)**.*

P(1)-Pt(1)	2.2389(14)	Pt(1)-Cl(1)	2.3446(14)
Pt(1)-Cl(2)	2.3554(13)	P(1)-N(2)	1.693(4)
O(3)-C(3)	1.211(6)	N(2)-C(3)	1.377(7)
N(5)-C(4)	1.335(7)	C(3)-C(4)	1.507(8)
P(1)-C(11)	1.814(6)	P(1)-C(17)	1.826(5)
P(30)-Pt(1)	2.2631(14)	C(4)-C(9)	1.376(8)

N(2)-Cl(2)	3.012(5)	N(2)-N(5)	2.64(7)
P(1)-Pt(1)-Cl(1)	175.94(5)	P(1)-Pt(1)-Cl(2)	91.05(5)
N(2)-P(1)-Pt(1)	109.33(16)	C(17)-P(1)-Pt(1)	115.45(18)
C(11)-P(1)-Pt(1)	113.29(29)	Cl(1)-Pt(1)-Cl(2)	85.05(5)
N(2)-P(1)-C(11)	105.7(2)	N(2)-P(1)-C(17)	103.0(2)
C(3)-N(2)-P(1)	126.6(4)	C(17)-P(1)-C(11)	109.2(2)
P(1)-N(2)-H(2)	120(5)	O(3)-C(3)-N(2)	124.3(5)
O(3)-C(3)-C(4)	122.6(5)	N(2)-C(3)-C(4)	113.1(5)
C(3)-C(4)-N(5)	116.3(5)	C(3)-C(4)-C(9)	120.1(5)
N(5)-C(4)-C(9)	123.6(5)	P(1)-Pt(1)-P(30)	94.17(5)
N(2)-H(2)...Cl(2)	127(6)	N(2)-H(2)...N(5)	111(5)

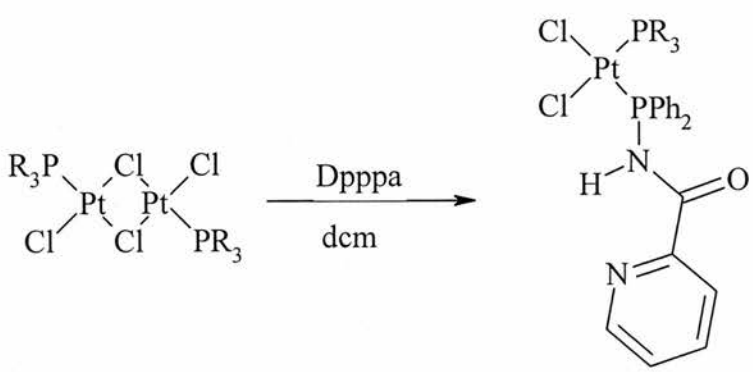

PR_3 = Me_2PhP (**2.14**) or PEt_3 (**2.15**)

***Figure 2.14**: Reaction of dpppa to from Platinum diphosphines.*

***2.2.5.** Rh^I complexes of dpppa.*

Reaction of dpppa with $[RhCl(cod)]_2$ in dichloromethane gave the expected product: [RhCl(cod)(dpppa-*P*)] (**2.16**) as a yellow solid in moderate yield (63%). ^{31}P NMR ($CDCl_3$) shows a doublet at δ(P) 58.3 $^{1}J_{Rh\text{-}P} = 161.98$. ^{1}H NMR ($CDCl_3$) shows a typical amine shift to δ(H) 10.4 ppm, and monodentate coordination is confirmed by the unshifted pyC[6]H at δ(H) 8.6 ppm. Carbonyl and amine signatures are clearly shown in the IR spectrum at 3194 (ν(N-H)) and 1698 cm^{-1} (ν(C=O)). The ν(N-H) band is shifted by a considerable amount, again indicating the likelihood of hydrogen-bonding interactions. The carbonyl stretch remains relatively unmoved.

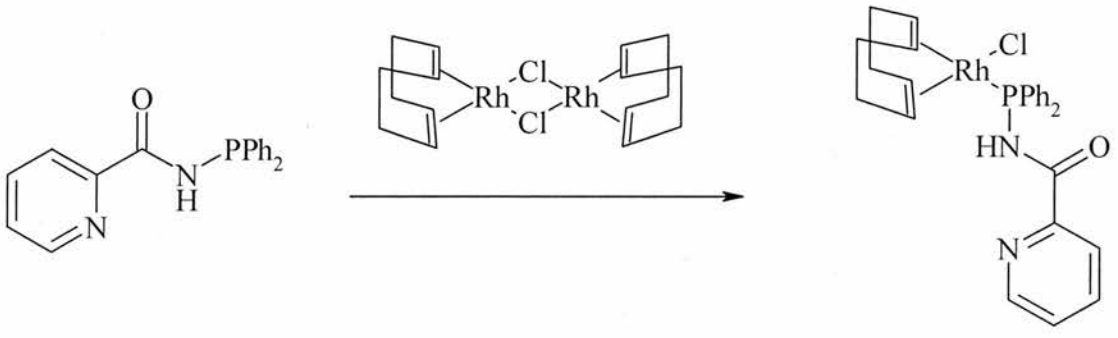

2.16

***Figure 2.15**: Formation of [RhCl(cod)(dpppa-P)].*

2.2.6. Au Complexes of dpppa.

When dpppa was reacted with [AuCl(tht)] in dichloromethane the anticipated monodentate [AuCl(dpppa-*P*)] (**2.17**) complex was generated as a colourless solid. This complex displays the anticipated singlet at δ(P) 53.5 ppm in the ^{31}P NMR, this is in the expected range we have designated for monodentate dpppa complexes. The proton spectra also follows the previous examples of monodentate bound dpppa. The amide proton is shifted down field and is found at δ(H) 9.1 ppm, with an increased

$^2J_{P\text{-}H}$ of 13 Hz. The pyC[6] proton is also visible in the spectrum at δ(H) 8.6 ppm. The ν(N-H) stretch is consistent with these findings being at 3289 cm^{-1}. This is only a minor shift from the free ligand, indicating a similar bonding pattern which is confirmed by the crystal data. The ν(C=O) band is found at 1698 cm^{-1}, again similar to the free ligand. A ν(Au-Cl) stretch is located in the expected region at 326 cm^{-1}. Crystals suitable for X-ray analysis were produced by slow evaporation of a $CDCl_3$ solution of the complex.

Table 2.11: *Selected bond lengths (Å) and angles (°) for [AuCl(dpppa-P)]* ***(2.17)****.*

P(1)-Au(1)	2.2168(18)	Au(1)-Cl(1)	2.2993(17)
P(1)-C(11)	1.816(7)	P(1)-C(17)	1.810(6)
P(1)-N(2)	1.694(5)	N(2)-C(3)	1.395(8)
C(3)-C(4)	1.495(9)	C(3)-O(3)	1.215(8)
C(4)-C(9)	1.382(9)	C(4)-N(5)	1.349(9)
N(2)-N(5)	2.64(7)		
P(1)-Au(1)-Cl(1)	177.82(6)	N(2)-P(1)-Au(1)	112.02(19)
C(11)-P(1)-C(17)	105.1(3)	H(2)-N(2)-P(1)	124(4)
H(2)-N(2)-C(3)	110(4)	N(2)-C(3)-O(3)	124.1(6)
O(3)-C(3)-C(4)	122.6(6)	N(2)-C(3)-C(4)	113.3(6)
C(3)-C(4)-N(5)	116.3(6)	N(2)-H(2)...N(5)	114(5)

On inspection of the crystal data we see the now familiar hydrogen-bonding pattern between N(2) and N(5), again with a value well within acceptable parameters

for a hydrogen-bond being 2.64 Å. The angle of the bond N(2)-H(2)-N(5) is 114° which is consistent with the other dpppa complexes where only one mode of hydrogen-bonding is present within the complex apparatus.

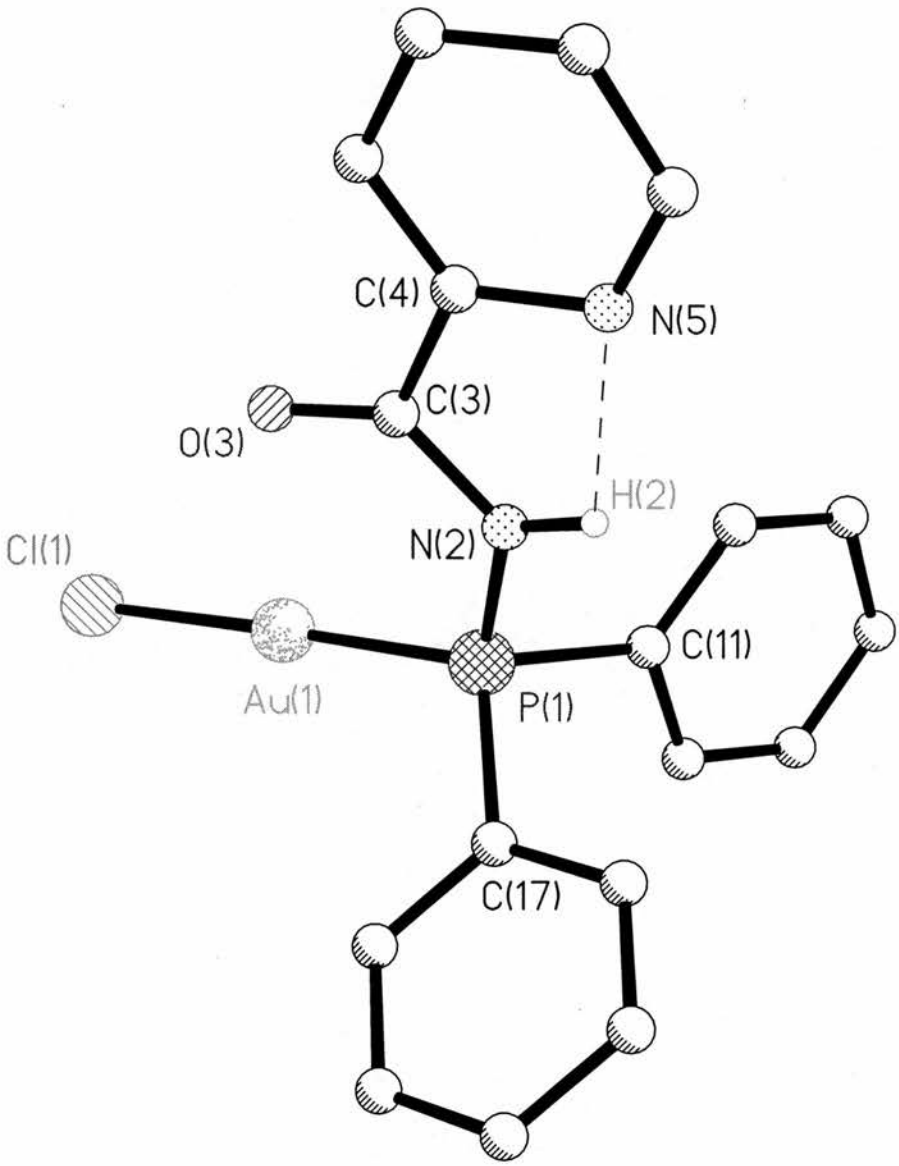

Figure 2.16: *Crystallographic representation of [AuCl(dpppa-P)]* ***2.17****.*

2.2.7. *P-O* Chelate complexes of dpppa.

Chelation of dpppa can be achieved by reaction of a chloride containing monodentate complex with K^+ $^-O^tBu$ and then subsequent reflux in methanol. A successful reaction of this type has been performed on [$RuCl_2$(*p*-Cymene)(dpppa-*P*)], and generated [RuCl(*p*-Cy)(dpppa-*P,O*)] (**2.18**) (equation 2.3)

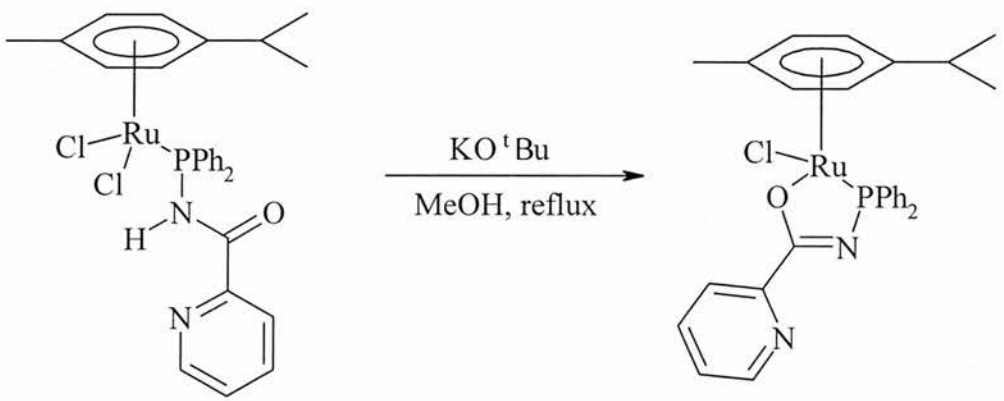

2.11 **2.18**

Equation 2.3

As can be seen, this generates a 5-membered heterocycle, with the oxygen binding to the metal centre. The ^{31}P NMR shows a downfield shift in the complex, to δ(P) 101.5 ppm; this is an expected shift, indicating chelation. As expected the amide proton disappears from the ^1H spectra, and the pyC[6]H sift and coupling constant is relatively unchanged. The IR spectrum also confirms the loss of the amide proton, and shows a ν(C-O) stretch at 1351 cm^{-1}, this confirms that it is C-O that is present and not C=O that binds to the metal. Acceptable microanalytical data was obtained. A crystal suitable for X-ray analysis was grown for **2.18** by layering a concentrated dcm solution of the complex with diethyl ether.

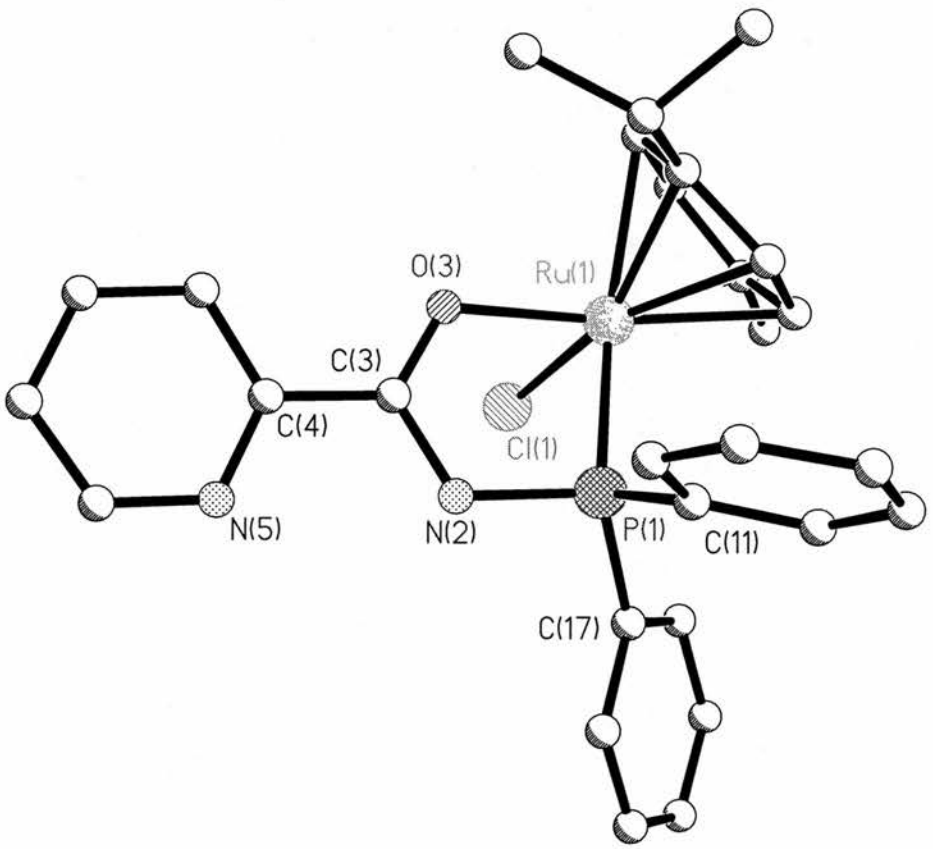

***Figure 2.17**: Crystallographic representation of [RuCl(p-Cy)(dpppa-P,O)] (**2.18**).*

The five-membered ring that is formed is essentially planar. It is clear that the deprotonation of the ligand inhibits its ability to for internal or external hydrogen bonds as it removes the amide proton. If we take a look at the angles involved in the ligands backbone we can clearly see that once the influence of the hydrogen-bonds straining the backbone has been removed these angles return to a much closer alignment to what would be expected of sp^2 hybridised bonds, with all angles being close to 120°.

Table 2.12: *Selected bond lengths (Å) and angles (°) for [RuCl(p-Cy)(dpppa-P,O)] **(2.18)**.*

P(1)-Ru(1)	2.2812(19)	Ru(1)-O(3)	2.097(5)
P(1)-C(11)	1.808(7)	P(1)-C(17)	1.805(7)
P(1)-N(2)	1.715(6)	N(2)-C(3)	1.380(10)
C(3)-O(3)	1.276(9)	C(3)-C(4)	1.465(10)
C(4)-C(9)	1.423(10)	C(4)-N(5)	1.315(9)
Ru(1)-Cl(1)	2.3910(18)		
P(1)-Ru(1)-O(3)	80.28(14)	P(1)- Ru(1)-Cl(1)	86.32(6)
O(3)-Ru(1)-Cl(1)	81.53(14)	C(11)-P(1)-C(17)	104.7(3)
Ru(1)-P(1)-N(2)	101.2(2)	P(1)-N(2)-C(3)	116.3(5)
N(2)-C(3)-O(3)	120.6(6)	C(3)-O(3)-Ru(1)	112.0(5)
N(2)-C(3)-C(4)	117.5(7)	O(3)-C(3)-C(4)	121.9(7)
C(3)-C(4)-C(9)	119.2(7)	C(3)-C(4)-N(5)	117.0(7)
C(9)-C(4)-N(5)	123.8(7)		

2.2.8: *P-N Chelate complexes of dpppa.*

A second mode of chelation is possible for dpppa, as with a typical phosphorus-nitrogen ligand chelation via the pyridyl nitrogen is expected. This is facilitated by reaction of the appropriate monodentate complex with a halide abstractor; in this case both $AgBF_4$ and $AgPF_6$ can be used to facilitate this. This

transformation was performed on **2.11** and **2.12**. Generating the cationic species [RuCl(*p*-Cy)(dpppa-*P,N*)][BF_4] (**2.19**) and [RhCl(η^5-C_5Me_5)(dpppa-*P,N*)][BF_4] (**2.20**) in good yield (93 and 74% respectively). The reaction involves stirring a solution of the initial complex with the Ag salt in dichloromethane, then filtering the AgCl that precipitates and isolating the product by precipitation with diethyl ether from a concentrated dichloromethane solution. The ^{31}P NMR shows the downfield shift generated by chelate ring formation with the peak moving to δ(P) 98.1 and 85.2 ppm for **2.19** and **2.20** respectively. Also the amine proton is shifted back toward its position in the free ligand with it being found at δ(H) 8.6 ppm in both cases, this peak has a $^2J_{P\text{-}H}$ of 5 and 4 Hz respectively. This must be due to the fact that as the pyridyl nitrogen is now bound to the metal, the N(2)-H(2)...N(5) hydrogen bond interaction can no longer take place. The IR data show a downfield shift in the ν(C-N(py)) stretch this is consistent with a ligand chelating via the pyridyl nitrogen, with the band moving to 1603 cm^{-1}. A comparison of the monodentate and bidentate complexes can be seen in table **2.13**.

A final chelation experiment was attempted but with one of the Pd complexes that we discussed earlier. This complex is in a different geometry to that of **2.19** and **2.20**, and as such provides an insight into the flexibility of dpppa when chelated. Under the same conditions as **2.19** and **2.20** [Pd($C_9H_{12}N$)(dpppa-*P,N*)][BF_4] (**2.21**) was formed by reaction of [PdCl($C_9H_{12}N$)(dpppa-*P*)] with $AgBF_4$, this compound shows the same shifts as the two previous examples, with the δ(P) 77.7 ppm being a considerable shift from the peak of δ(P) 63.3 ppm in the monodentate example. However this is not as substantial as for **2.19** and **2.20**, this could be a result of the change of geometry we mentioned before.

***Table 2.13**: Spectroscopic data for comparison of chelated and non-chelated complexes.*

Complex	***2.11***	***2.19***	***2.12***	***2.20***	***2.9***	***2.21***
^{31}P (δ)	59.3	98.1	62.8	85.2	63.3	77.7
^{1}H N-H (δ)	9.6	8.6	9.9	8.6	10.9	8.7
ν(C-N)py (cm^{-1})	1587	1603	1589	1603	1589	1603

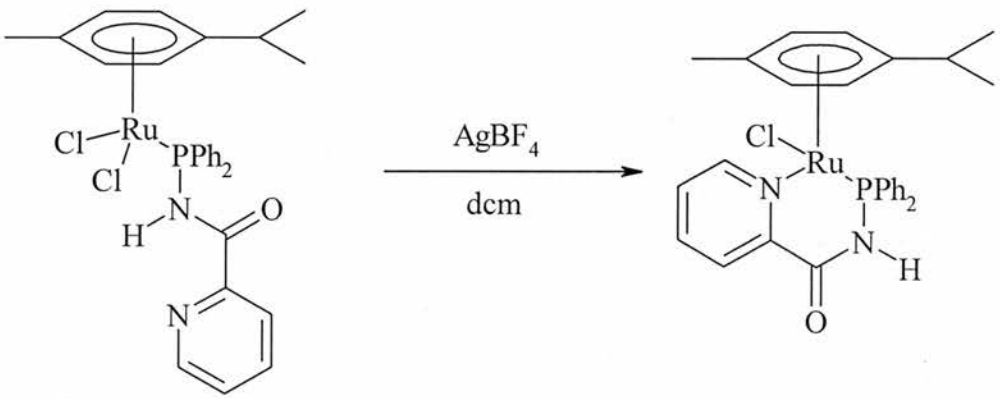

2.11 **2.19**

Equation 2.4

From this chapter we can determine that dpppa has a varied coordination chemistry, form the simple monodentate binding as seen in $[PtCl_2(dpppa\text{-}P)_2]$, to the two possible forms of chelation as shown by [RuCl(*p*-Cy)(dpppa-*P,O*)] and [RuCl(*p*-Cy)(dpppa-*P,N*)][BF_4]. This chemistry is summarised in figure 2.19.

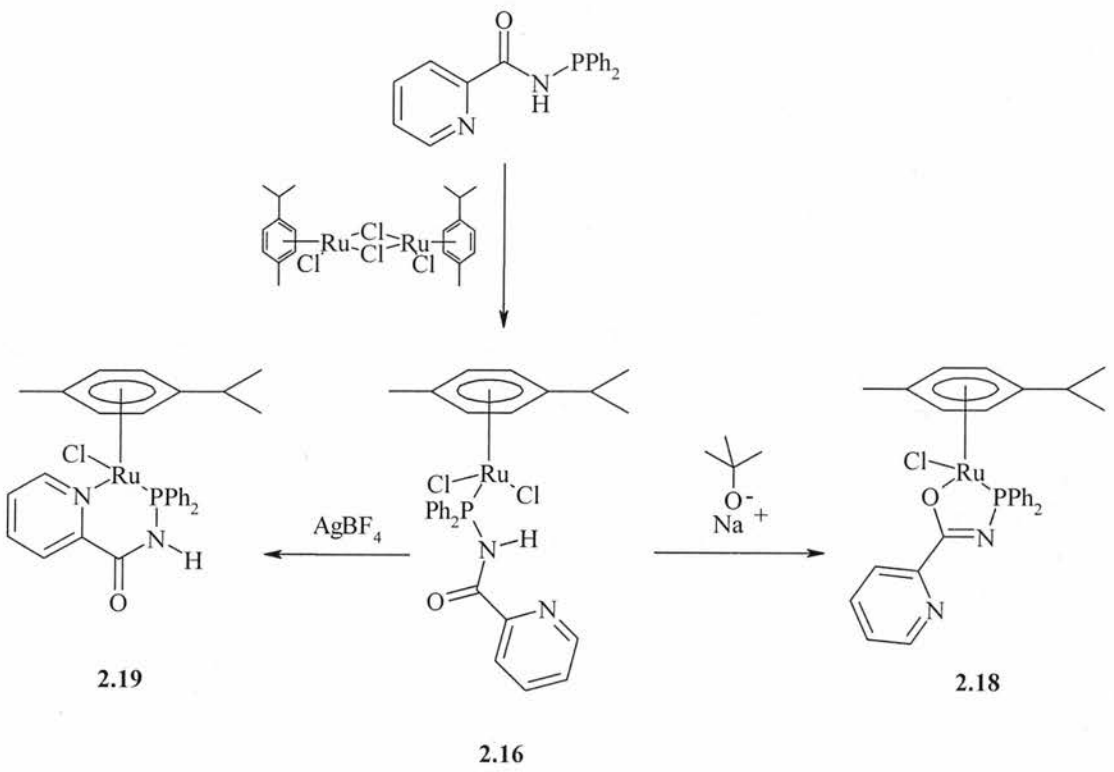

Figure 2.19: *Summary of the coordination chemistry of dpppa.*

Experimental: Chapter Two.

General Conditions

All manipulations were carried out in an atmosphere of nitrogen, unless stated otherwise. All solvents were either freshly distilled from an appropriate drying agent (thf, Et_2O, dcm) or obtained as anhydrous grade from Aldrich. ^1H and ^{31}P NMR spectra were recorded using a Jeol Delta FT (270 MHz) spectrometer. IR spectra were recorded as KBr discs (prepared in air) on a Perkin Elmer 2000 FTIR/RAMAN spectrometer. All significant peaks (>800 cm^{-1}) are quoted to serve as a fingerprint. Silver salts, 2-picolinamide (Aldrich Chemical Co.) and BuLi (2.5M, Lancaster) were purchased and used as received. Triethylamine and chlorodiphenylphosphine were distilled prior to use. Dimethylaminopyridine (DMAP) was sublimed before use. The various metal starting materials were made by the appropriate literature methods, [AuCl(tht)][10], $[MCl_2(cod)]$ (M = Pt or Pd, cod = cycloocta-1,5-diene)[11,12], [PtMeCl(cod)][13], $[\{PtCl(\mu\text{-}Cl)(PMe_2Ph)\}_2]$[14], $[\{MCl(\mu\text{-}Cl)(Cp^*)\}_2]$ (M = Rh or Ir)[15], $[\{Rh(\mu\text{-}Cl)(cod)\}_2]$[16], $[\{RuCl(\mu\text{-}Cl)(\eta^6\text{-}p\text{-}MeC_6H_4{}^iPr)\}_2]$[17], $[\{RuCl(\mu\text{-}Cl)(\eta^3\text{:}\eta^3\text{-}C_{10}H_{16})\}_2]$[18], $[\{PdCl(\mu\text{-}Cl)(\eta^3\text{-}C_3H_5)\}_2]$[19], $[PtMe_2(cod)]$[20].

2-Diphenylphosphinopicolinamde (2.1): Chlorodiphenylphosphine (3.7 cm^3, 20 mmol) was added to a solution of 2-picolinamide (2.5 g, 20 mmol), triethylamine (3.0 cm^3, 21 mmol) and DMAP (240 mg, 2.0 mmol) in thf (100 cm^3) and refluxed overnight. The reaction mixture was filtered to remove a white solid (Et_3NHCl) and

washed with thf (50 cm^3). The solvent was removed *in vacuo* leaving a pale yellow solid. This solid was recrystallised by cooling a concentrated methanol solution at 4 °C overnight (yield: 3.38 g, 55 %). $C_{18}H_{15}N_2OP$ requires: C, 70.6, H, 4.9, N, 9.1. Found: C, 70.29, H, 4.58, N, 8.95%. ν_{max}/cm^{-1}: 3297, 1691, 1452, 1412, 996. ^{31}P NMR δ 22.0 ppm ^1H NMR ($CDCl_3$), 8.65 (1H, d, J = 4Hz, N-H), 8.54 (1H, d, J = 5Hz, pyC[6]H), 8.26 (1H, d, J = 8Hz, pyC[3]H), 7.85 (1H, t, J = 8Hz, pyC[5]H), 7.6-7.2 (10H, m, aromatic).

2-Diphenylphosphinopicolinamde oxide (2.2): Aqueous H_2O_2 (30 % w/w, 0.0071 cm^3, 0.065 mol) was added dropwise over 5 min to a solution of dpppa (200 mg, 0.065 mol) in thf (10 cm^3) and the mixture stirred for 30 min and then reduced to dryness. The residue was dissolved in dcm, and filtered while hot and subsequently dried over $MgSO_4$. The filtrate was stored at –4°C during which time a crystalline solid was deposited and filtered and dried. Yield: 85 mg, 41 %. $C_{18}H_{15}N_2O_2P$ requires: C, 67.1, H, 4.69, N, 8.69. Found: C, 66.7, H, 4.26, N, 8.41 %. ν_{max}/cm^{-1}: 3302, 1694, 1451, 1403, 1215, 998. ^{31}P NMR δ 22.1 ppm. ^1H NMR ($CDCl_3$), δ 9.46 (1H, d, J = 9 Hz, N-H), 8.58 (1H, d, J = 4 Hz, pyC[6]H), 8.1-7.7 (6H, m, aromatic), 7.5-7.2 (7H, m, aromatic).

2-Diphenylphosphinopicolinamde sulfide (2.3): Sulfur (105 mg, 3.30 mmol) was added to a solution of 2-Diphenylphosphinopicolinamde (1.00 g, 3.30 mmol) in toluene (100 cm^3) and refluxed overnight. The solvent was removed *in vacuo* leaving an off-white solid. This solid was recrystallised by cooling a concentrated toluene solution at 4°C overnight (yield: 900 mg, 82 %). $C_{18}H_{15}N_2OPS$ requires: C, 63.9, H, 4.47, N, 8.28. Found: C, 63.6, H, 4.22, N, 8.26 %. ν_{max}/cm^{-1}: 3268, 1689, 1387, 997.

^{31}P NMR δ 54.4 ppm. ^{1}H NMR ($CDCl_3$), δ 9.3 (1H, d, J = 11 Hz, N-H), 8.6 (1H, d, J = 1 Hz, pyC[6]H), 8.1-7.8 (6H, m, aromatic), 7.6-7.4 (7H, m, aromatic).

2-Diphenylphosphinopicolinamde selenide (2.4): Selenium (52 mg, 0.65 mmol) was added to a solution of 2-Diphenylphosphinopicolinamde (200 mg, 0.65 mmol) in toluene (5 cm^3) and refluxed overnight. The solvent was removed *in vacuo* leaving an off-white solid. This solid was recrystallised by cooling a concentrated toluene solution at 4°C overnight (yield: 105 mg, 48 %). $C_{18}H_{15}N_2OPSe$ requires: C, 56.1, H, 3.92, N, 7.27. Found: C, 56.4, H, 3.77, N, 7.05 %. ν_{max}/cm^{-1}: 3288, 1698, 1391, 998. ^{31}P NMR ($CDCl_3$) δ 47.8, $^{1}J_{P\text{-}Se}$ = 788 Hz. ^{1}H NMR ($CDCl_3$), δ 9.3 (1H, d, J = 13 Hz, N-H), 8.6 (1H, d, J = 1 Hz, pyC[6]H), 8.2-7.7 (6H, m, aromatic), 7.5-7.3 (7H, m, aromatic).

[$PtCl_2$(dpppa-P)$_2$] (2.5): Dpppa (50 mg, 0.16 mmol) and [$PtCl_2$(cod)] (30 mg, 0.08 mmol) were weighed into a schlenk type flask and dcm (5 cm^3) added. The solution was stirred for 10 min and the majority of the solvent removed *in vacuo*. A white solid was precipitated after addition of Et_2O (20 cm^3) then isolated by filtration and washed with further ether (10 cm^3) (yield: 57 mg, 80 %). $C_{36.5}H_{31}N_4O_2P_2Cl_3Pt$ requires: C, 47.6, H, 3.39, N, 6.08. Found: C, 47.5, H, 3.20, N, 5.81%. ν_{max}/cm^{-1}: 3251, 1692, 1446, 1391, 998, 320, 302. ^{31}P NMR ($CDCl_3$) δ 31.2 ppm, $^{1}J_{Pt\text{-}P}$ = 3984 Hz. ^{1}H NMR ($CDCl_3$), 10.7 (2H, d, J = 15 Hz, N-H), 8.5 (2H, d, J = 4 Hz), pyC[6]H), 7.7-7.2 (26H, m, aromatic).

[$PdCl_2$(dpppa-P)$_2$] (2.6): Dpppa (258 mg, 0.86 mmol) and [$PdCl_2$(cod)] (120 mg, 0.43 mmol (2.6)) were weighed into a schlenk type flask and dcm (10 cm^3) added. The solution was stirred for 10 min. This resulted in precipitation of the desired product, which was filtered and washed with ether (10 cm^3). Yield: 307 mg, 92 %. $C_{36}H_{30}N_4O_2P_2Cl_2Pd$ requires: C, 54.6, H, 3.83, N, 7.09. Found: C, 53.9, H, 3.64, N, 6.85 %. ν_{max}/cm^{-1}: 3232, 1694, 1446, 1392, 997, 310.

[PdCl(allyl)(dpppa-P)] (2.7): Reaction followed as for 2.5. Dpppa (84 mg, 0.27 mmol) and [{Pd(μ-Cl)(η^3-C_3H_6)}$_2$] (50 mg, 0.13 mmol) gave a pale yellow solid, (yield: 117 mg, 87 %). $C_{21}H_{20}N_2OPClPd$ requires: C, 51.5, H, 4.12, N, 5,72. Found: C, 51.8, H, 3.93, N, 5.61%. ν_{max}/cm^{-1}: 3193, 1685, 1446, 1396, 1103, 998. ^{31}P NMR ($CDCl_3$) δ 54.5 ppm. ^{1}H NMR ($CDCl_3$), 10.5 (1H, d, J = 22 Hz, N-H), 8.7 (1H, d, J = 4 Hz, pyC[6]H), 7.8-7.4 (19H, m, aromatic), 5.5 (1H, m, allyl), 4.7 (1H, t, J = 7 Hz, allyl), 3.7 (1H, t, J = 13 Hz, allyl), 3.3 (1H, d, J = 7 Hz, allyl), 2.6 (1H, d, J = 13 Hz, allyl).

[PdCl($C_{10}H_6NO$)(dpppa-P)] (2.8): Dpppa (205 mg, 0.66 mmol) and [Pd(μ-Cl)($C_{10}H_6NO$)]$_2$ (200 mg, 0.33 mmol) were weighed into a schlenk type flask and dcm (10 cm^3) added. The solution was stirred for 10 min. This resulted in precipitation of the desired product, which was filtered and washed with ether (10 cm^3) (yield: 371 mg, 95 %). $C_{28}H_{21}N_3O_2PClPd$ requires: C, 55.6, H, 3.50, N, 6.95. Found: C, 49.7, H, 3.18, N, 6.04 %. ν_{max}/cm^{-1}: 3231, 1673, 1446, 1394, 996, 322. FAB MS: *m/z* 568 ([M-Cl]$^+$).

[PdCl($C_9H_{12}N$)(dpppa-P)] (2.9): Reaction followed as for 2.5. Dpppa (223 mg, 0.72 mmol) and [Pd(μ-Cl)($C_9H_{12}N$)]$_2$ (200 mg, 0.36 mmol) gave a yellow solid, (yield: 136 mg, 64 %). $C_{27.5}H_{26}N_3OPCl_2Pd$ requires: C, 52.9, H, 4.51, N, 6.73. Found: C, 54.3, H, 4.46, N, 6.07 %. ν_{max}/cm^{-1}: 3187, 1683, 1449, 1391, 997. ^{31}P NMR ($CDCl_3$) δ 63.3 ppm. ^{1}H NMR ($CDCl_3$) δ 10.9 (1H, d, J = 19 Hz, N-H), 8.6 (1H, d, J = 4 Hz, pyC[6]H), 8.1 (1H, m, aromatic), 8.0 (1H, m, aromatic), 7.8 (1H, m, aromatic), 7.4 (8H, m, aromatic) 7.0, (1H, m, aromatic), 6.8 (1H, m, aromatic), 6.4 (1H, m, aromatic), 2.8 (6H, d, J = 3 Hz, NMe-H). FAB MS: *m/z* 546 ([M-Cl]$^+$).

[PdCl($C_{12}H_{12}N$)(dpppa-P)] (2.10): Reaction followed as for 2.5. Dpppa (197 mg, 0.64 mmol) and [Pd(μ-Cl)($C_{12}H_{12}N$)]$_2$ (200 mg, 0.32 mmol) gave a yellow/green solid, (yield: 176 mg, 44 %). $C_{30}H_{27}N_3OPClPd$ requires: C, 58.2, H, 3.40, N, 6.80. Found: C, 58.09, H, 2.92, N, 6.62 %. ν_{max}/cm^{-1}: 3203, 1678, 1446, 1388, 997. ^{31}P NMR ($CDCl_3$) δ 64.3 ppm. ^{1}H NMR ($CDCl_3$) 11.3 (1H, d, J = 18 Hz, N-H), 8.7 (1H, d, J = 5 Hz, pyC[6]H), 8.2 (4H, m, aromatic), 8.0 (1H, d, aromatic), 7.8 (1H, d, aromatic), 7.6 (1H, d, aromatic), 7.5-7.4 (10H, m, aromatic), 6.7 (1H, m, aromatic), 6.5(1H, m, aromatic), 3.5 (6H, d, J = 3 Hz, NMe-H).

[$RuCl_2$(p-Cy)(dpppa-P)] (2.11): Prepared as for 2.5. Dpppa (200 mg, 0.66 mmol) and [{RuCl(μ-Cl)(*p*-Cymene)}$_2$] (200 mg, 0.33 mmol) gave a red solid, (yield: 324 mg, 84 %). $C_{28}H_{29}N_2OPCl_2Ru$ requires: C, 54.9, H, 4.77, N, 4.57. Found: C, 55.8, H, 4.82, N, 4.07 %. ν_{max}/cm^{-1}: 3261, 1684, 1449, 1406, 997, 292. ^{31}P NMR ($CDCl_3$) δ 59.3 ppm. ^{1}H NMR ($CDCl_3$) δ 9.6 (1H, d, J = 18 Hz, N-H), 8.6 (1H, d, J = 7 Hz, pyC[6]H), 8.0 (4H, m, aromatic), 7.8 (1H, m, aromatic), 7.6 (1H, m, aromatic) 7.4

(4H, m, aromatic), 7.2 (1H, m, aromatic), 5.3 (2H, m, aromatic [*p*-Cy]), 5.2 (2H, m, aromatic [*p*-Cy]), 2.6 (1H, m, Pr^i-H), 1.8 (3H, m, Me-H), 0.8 (6H, d, J = 7 Hz, Pr^i-Me).

[$RhCl_2(\eta^5\text{-}C_5Me_5)(dpppa\text{-}P)$] (2.12): Prepared as for 2.5. Dpppa (198 mg, 0.65 mmol) and [{RhCl(μ-Cl)(η^5-C_5Me_5)}$_2$] (200 mg, 0.32 mmol) gave a orange solid, (yield: 363 mg, 91 %). $C_{28}H_{30}N_2OPCl_2Rh$ requires: C, 54.6, H, 4.91, N, 4.55. Found: C, 54.0, H, 4.65, N, 4.40 %. ν_{max}/cm^{-1}: 3298, 1678, 1449, 1410, 997, 282. ^{31}P NMR ($CDCl_3$) δ 62.8 ppm. ^1H NMR ($CDCl_3$) δ 9.9 (1H, d, J = 18 Hz, N-H), 8.6 (1H, d, J = 5 Hz, pyC[6]H), 8.1 (4H, m, aromatic), 7.9 (1H, d, aromatic), 7.7 (1H, m, aromatic), 7.5 (6H, m, aromatic), 7.3 (1H, m, aromatic), 1.4 (15H, d, J = 12 Hz, Cp*-H).

[$IrCl_2(\eta^5\text{-}C_5Me_5)(dpppa\text{-}P)$] (2.13): Prepared as for 2.5. Dpppa (77 mg, 0.25 mmol) and [{IrCl(μ-Cl)(η^5-C_5Me_5)}$_2$] (100 mg, 0.13 mmol) gave a yellow/orange solid, (yield: 162 mg, 91 %). $C_{28}H_{30}N_2OPCl_2Ir$ requires: C, 47.6, H, 4.29, N, 3.98. Found: C, 47.1, H, 4.27, N, 3.83 %. ν_{max}/cm^{-1}: 3288, 1678, 1450, 1412, 997. ^{31}P NMR ($CDCl_3$) δ 32.7 ppm. ^1H NMR ($CDCl_3$) δ 10.2 (1H, d, J = 17 Hz, N-H), 8.6 (1H, d, J = 4 Hz, pyC[6]H), 8.1-7.7 (6H, m, aromatic), 7.4 (6H, m, aromatic), 1.4 (15H, d, J = 2 Hz, Cp^*-H).

[$PtCl_2(Me_2PhP)(dpppa\text{-}P)$] (2.14): Prepared as for 2.5. Dpppa (76 mg, 0.25 mmol) and [{PtCl(μ-Cl)(PMe_2Ph)}$_2$] (100 mg, 0.12 mmol) gave a white solid, (yield: 114 mg, 65 %). $C_{26}H_{26}N_2OP_2Cl_2Pt$ requires: C, 44.0, H, 3.69, N, 3.95. Found: C, 43.77, H, 3.61, N, 3.82 %. ν_{max}/cm^{-1}: 1686, 1447, 1384, 1107. ^{31}P NMR ($CDCl_3$) δ 30.9 ($^1J_{Pt\text{-}P}$ = 3930), -14.5 ($^1J_{Pt\text{-}P}$ = 3500), $^2J_{P\text{-}P}$ = 19 Hz. ^1H NMR ($CDCl_3$) δ 11.1 (1H, d, J

= 15 Hz, N-H), 8.6 (1H, d, J = 4 Hz, pyC[6]H), 8.0-7.7 (6H, m, aromatic), 7.5-7.0 (12H, m, aromatic), 1.6-1.5 (6H, d, J = 11 Hz, Me-H).

[$PtCl_2(Et_3P)(dpppa\text{-}P)$] (2.15): A solution of [{PtCl(μ-Cl)(PEt_3)}$_2$] (50 mg, 0.07 mmol), in dcm (10 cm^3) was added dropwise to a solution of dpppa (40 mg, 0.13 mmol) in dcm (10 cm^3). The solution was stirred for 10 min and the majority of the solvent removed *in vacuo*. A white solid was precipitated after addition of Et_2O then isolated by filtration and washed with further ether (10 cm^3) (yield: 55 mg, 66 %). $C_{24}H_{30}N_2OP_2Cl_2Pt$ requires: C, 41.9, H, 4.38, N, 4.06. Found: C, 42.8, H, 3.60, N, 4.15 %. ν_{max}/cm^{-1}: 3162, 1687, 1446, 1385, 998, 310. ^{31}P NMR ($CDCl_3$) δ 30.0 ($^1J_{Pt\text{-}P}$ = 4010), 7.6 ($^1J_{Pt\text{-}P}$ = 3360), $^2J_{P\text{-}P}$ = 19 Hz. ^{1}H NMR (270MHz, $CDCl_3$) δ 11.4 (1H, d, J = 16 Hz, N-H), 8.7 (1H, d, J = 1 Hz, pyC[6]H), 8.2 (3H, m, aromatic), 7.9-7.7 (13H, m, aromatic), 7.5-7.3 (6H, m, aromatic), 7.1 (1H, m, aromatic), 1.5 (6H, m, -CH_2-), 0.9 (9H, m, Me-H).

[RhCl(cod)(dpppa-P)] (2.16): Dpppa (125 mg, 0.41 mmol), and [{Rh(μ-Cl)(cod)}$_2$] (100 mg, 0.20 mmol) were weighed into a schlenk type flask and toluene (5 cm^3) added. The solution was stirred for 10 min and the majority of the solvent removed *in vacuo*. A yellow solid was precipitated after addition of *n*-heaxne (20 cm^3) then isolated by filtration and washed with further hexane (10 cm^3) (yield: 142 mg, 63 %). $C_{26}H_{27}N_2OPClRh$ requires: C, 56.5, H, 4.92, N, 5.07. Found: C, 56.05, H, 4.76, N, 4.90 %. ν_{max}/cm^{-1}: 3194, 1698, 1448, 1407, 997. ^{31}P NMR ($CDCl_3$) δ 58.3 ($^1J_{Rh\text{-}P}$ = 162 Hz). ^{1}H NMR (270 MHz, $CDCl_3$) δ 10.4 (1H, d, J = 21Hz, N-H), 8.6 (1H, d, J = 2Hz, pyC[6]H), 8.0-7.8 (6H, m, aromatic), 7.6-7.2 (6H, m, aromatic), 2.3 (4H, br.s, cod), 2.0 (8H, br.s, cod).

[AuCl(dpppa-P)] (2.17). Prepared as for 5, Dpppa (67 mg, 0.021 mmol) and [AuCl(tht)] (70 mg, 0.021 mmol) reacted in dcm gave a white solid, (yield: 78 mg, 70 %). $C_XH_XN_2OPClAu$ requires: C, 40.0, H, 2.80, N, 5.20. Found: C, 39.5, H, 1.75, N, 5.09 %. ν_{max}/cm^{-1}: 3288, 1698, 1391, 998. ^{31}P NMR ($CDCl_3$) 53.5 ppm. ^1H NMR ($CDCl_3$) δ 9.1 (1H, d, J = 13 Hz, N-H), 8.6 (1H, d, J = 1 Hz, pyC[6]H), 8.2-7.5 (13H, m, aromatic).

[RuCl(p-Cy)(dpppa-P,O)] (2.18): A solution of BuLi (65 µl, .0.16 mmol) in THF (2 cm^3) was added dropwise to a solution of [$RuCl_2$(*p*-Cy)(dpppa-*P*)] (100 mg, 0.16 mmol) in THF (5 cm^3) at 0°C. The solution was stirred for 10 min and allowed to reach room temperature, and filtered through a bed of celite. The majority of the solvent removed *in vacuo*. A dull beige solid was precipitated after addition of Et_2O then isolated by filtration and washed with further ether (10 cm^3) (yield: 47 mg, 52 %). $C_{26.5}H_{29}N_2OPCl_2Ru$ requires: C, 51.0, H, 4.28, N, 4.17. Found: C, 51.9, H, 4.00, N, 4.38 %. ν_{max}/cm^{-1}: 3312, 1351, 249. ^{31}P NMR ($CDCl_3$) δ 101.5. ^1H NMR (270 MHz, $CDCl_3$) δ 8.4 (1H, d, J = 8 Hz, pyC[6]H), 7.9-7.7 (3H, m, aromatic), 7.6-7.2 (10H, m, aromatic), 6.0 (1H, d, J = 6 Hz, *p*-Cy-H), 5.7 (1H, d, J = 4 Hz, *p*-Cy-H), 5.4 (1H, d, J = 6 Hz, *p*-Cy-H), 5.0 (1H, d, J = 4 Hz, *p*-Cy-H), 2.5 (1H, m, C-H), 2.0 (3H, s, Me-H), 1.1 (6H, d, J = 10 Hz, Pr^i-H).

[RuCl(p-Cy)(dpppa-P,N)] (2.19): $AgClO_4$ (32 mg, 0.16 mmol) was added under dark conditions to a solution of [$RuCl_2$(*p*-Cy)(dpppa-*P*)] (100 mg, 0.16 mmol) in DCM (5 cm^3). The solution was stirred overnight and filtered through a celite bed. The

majority of the solvent was removed *in vacuo*. An orange solid was precipitated after addition of Et_2O then isolated by filtration and washed with further ether (10 cm^3) (yield: 87 mg, 0.15 mmol, 93 %). $C_{28.5}H_{29}N_2O_5PCl_3Ru$ requires: C, 47.6, H, 4.21, N, 3.90. Found: C, 47.2, H, 4.00, N, 3.89%. ν_{max}/cm^{-1}: 1482, 1084. ^{31}P NMR ($CDCl_3$) δ 98.1 ppm. ^1H NMR (270 MHz, $CDCl_3$) δ 8.6 (1H, d, J = 5 Hz, N-H), 8.2 (1H, d, J = 8 Hz, pyCH), 8.0 (1H, t, J = 8 Hz, pyCH), 7.8 (2H, m, aromatic), 7.7-7.5 (9H, m, aromatic), 5.8 (2H, m, *p*-Cy-H), 5.6 (2H, m, *p*-Cy-H), 2.8 (1H, m, C-H), 2.1 (3H, s, Me-H), 1.3 (6H, t, J = 6 Hz, Pr^i-H).

[RhCl(η^5-C_5Me_5)(dpppa-P,N)] (2.20): $AgClO_4$ (32 mg, 0.16 mmol) was added under dark conditions to a solution of [$RhCl_2$(η^5-C_5Me_5)(dpppa-*P*)] (100 mg, 0.16 mmol) in DCM (5 cm^3). The solution was stirred overnight and filtered through a celite bed. The majority of the solvent was removed *in vacuo*. An orange solid was precipitated after addition of Et_2O then isolated by filtration and washed with further ether (10 cm^3) (yield: 70 mg, 0.12 mmol, 74 %). $C_{27}H_{27}N_3OPPd$ requires: C, 49.5, H, 4.45, N, 4.12. Found: C, 49.8, H, 4.25, N, 4.04 %. ν_{max}/cm^{-1}: 1684, 1477, 1421. ^{31}P NMR ($CDCl_3$) δ 85.2 ppm. ^1H NMR (270 MHz, $CDCl_3$) δ 8.6 (1H, d, J = 4 Hz, pyC[6]H), 8.3 (1H, d, J = 8 Hz, pyC[3]H), 8.0 (1H, t, J = 8 Hz, pyC[5]H), 7.8 (2H, m, aromatic), 7.6 (8H, m, aromatic), 1.6 (15H, d, J = 4 Hz, Cp^*-H).

[Pd($C_9H_{12}N$)(dpppa-P,N)][BF_4] (2.21): $AgBF_4$ (22 mg, 0.112 mmol) was added under dark conditions to a solution of [PdCl($C_9H_{12}N$)(dpppa-*P*)] (65 mg, 0.112 mmol) in DCM (5 cm^3). The solution was stirred overnight and filtered through a celite bed. The majority of the solvent was removed *in vacuo*. A yellow solid was precipitated after addition of Et_2O then isolated by filtration and washed with further ether

($10cm^3$) (yield: 44 mg, 71 %). $C_{27}H_{27}N_3OPPd$ requires: C, 50.17, H, 4.21, N, 6.50. Found: C, 50.28, H, 3.97, N, 6.50%. ν_{max}/cm^{-1}: 1684, 1603, 1477, 1421, 1060. ^{31}P NMR ($CDCl_3$) δ 77.7 ppm. ^1H NMR (270 MHz, $CDCl_3$) δ 8.7 (1H, d, J_{P-H} = 4 Hz, N-H), 8.3 (1H, d, J_{H-H} = 6 Hz, aromatic), 8.0-7.0 (17H, m, aromatic), 3.1 (6H, d, J_{H-H} = 2 Hz, Me), 2.9 (2H, d, J_{H-H} = 2 Hz, CH_2).

REFERENCES: Chapter Two

1. S. M. Aucott, A. M. Z. Slawin and J. D. Woollins, *J. Chem. Soc., Dalton Trans*, 2000, 2559
2. E. Uhlig, M. Maaser, *Z. Anorg. Allg. Chem.*, 1966, 334, 205.
3. M. L. Clarke, A. M. Z. Slawin, M. V. Wheatley and J. D. Woollins, *J. Chem. Soc., Dalton Trans.*, 2001, 3421.
4. T. Okano, M. Yamamoto, T. Noguchi, H. Konishi, J. Kiji, *Chem. Lett.*, 1982, 977.
5. D. Lafont, D. Sinou, G. Descotes, *Nouv. J. Chim.*, 1983, 7, 283.
6. T. B. Rauchfuss, *J. Am. Chem. Soc.*, 1979, 101, 1045.
7. E. Lindner, C. Scheytt, P. Wegner, *J. Organomet. Chem.*, 1986, 308, 311.
8. P. Bhattacharyya, A. M. Z. Slawin, M. B. Smith, D. J. Williams, J. D. Woollins, *J. Chem. Soc., Dalton Trans.*, 1996, 3647.
9. A. M. Z. Slawin, J. Wheatley, M. V. Wheatley, J. D. Woollins, *Polyhedron*, 2003, 22, 1397.
10. R. Uson, A. Laguna and M. Laguna, *Inorg. Synth.*, 1989, 26, 85.
11. D. Drew and J. R. Doyle, *Inorg. Synth*, 1991, 28, 346.
12. J. X. McDermott, J. F. White and G. M. Whiteside, *J. Am. Chem. Soc.*, 1976, 60, 6521.
13. H. C. Clark and L. E. Manzer, *J. Organomet. Chem.*, 1973, 59, 411.
14. W. Baratta and P. S. Pregosin, *Inorg. Chem Acta.*, 1993, 209, 85.
15. C. White, A. Yates, P. M. Maitlis, *Inorg. Synth.*, 1992, 29, 228.
16. G. Giordano, R. H. Crabtree, *Inorg. Synth.*, 1979, 19, 218.

17. M. A. Bennett, T. N. Huang, T. W. Matheson, A. R. Smith, *Inorg. Synth.*, 1982, 21, 74.

18. L. Porri, M. C. Gallazzi, A. Colombo, G. Allegra, *Tetrahedron Lett.*, 1965, 47, 4187.

19. A. L. Balch, L. S. Benner, *Inorg. Synth.*, 1990, 28, 340.

20. H. C. Clark, L. E. Manzer, *J. Orgnaomet. Chem.*, 1973, 59, 411.

CHAPTER THREE: Synthesis and Coordination of Two Derivatives of Dpppa, 2-Diphenylphosphinothiophenocarboxamide and Bis(2,5-diphenylphosphinepicolinamide)

3.1. Introduction.

Much of the work in this chapter is based around comparisons between the chemistry of dpppa with two new derivatives; 2-diphenylphosphinothiophenocarboxamide (dpptc) and bis(2,5-diphenylphosphinepicolinamide) (bdpppa). This will take the form of investigating the coordination of these ligands in similar circumstances to the coordination chemistry of dpppa discussed in the previous chapter. However these new ligands also resemble a few other ligands which have been found in literature and which have been discussed in Chapter One, and which we will briefly summarise here.

There are few known examples of phosphino-thiophenes, and even fewer that act as bidentate phosphino-thiophene ligands. Clot *et al* described the major examples in 2000[1]. These were 2-(2'-{diphenylphosphino}phenyl)thiophene (dpppth) (**A**) and 3'-diphenylphosphino-2,2':5',2''-terthiophene (dppterth) (**B**).

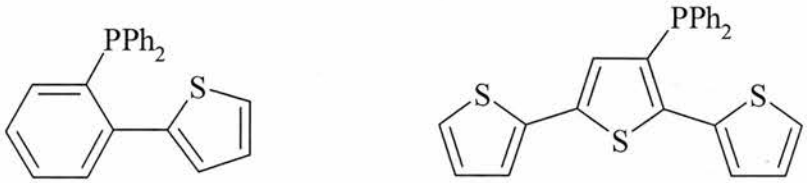

A **B**

***Figure 3.1**: Thiophene based phosphines.*

These ligands were both shown to bind with a bidentate motif on reaction with $[RuCl_2(PPh_3)_3]$.

Early bridging diphosphines are 2,6-bis(diphenylphosphino)pyridine ($(Ph_2P)_2py$) (**C**)[2], 2,6-(diphenylphosphinomethyl)pyridine (**D**)[3] and N,N'-bis(diphenylphosphino)-2,6-diaminopyridine (**E**)[4] which are displayed in diagram 3.2. These ligands are commonly found as bridging ligands and bidentate ligands with a variety of transition metals, these were discussed in Chapter One.

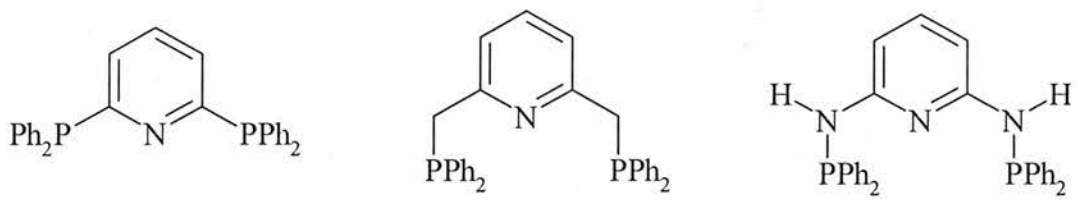

C **D** **E**

***Figure 3.2**: Bridging diphosphinopyridine ligands.*

Our ligands show the characteristics of all of the these ligands and those of dpppa, we will investigate which of the characteristics of the ligands are dominant and how the coordination compares to each of the ligands discussed, especially dpppa.

3.2. Results and Discussion.

3.2.1. Synthesis and Chalcogen derivatives of dpptc.

The synthesis of dpptc (**3.1**) is analogous to that of dpppa and involves the dropwise addition of chlorodiphenylphosphine in tetrahydrofuran to a tetrahydrofuran solution of 2-thiophenocarboxamide and a small excess of triethylamine. Subsequent overnight reflux, results in the formation of dpppa (figure 1).

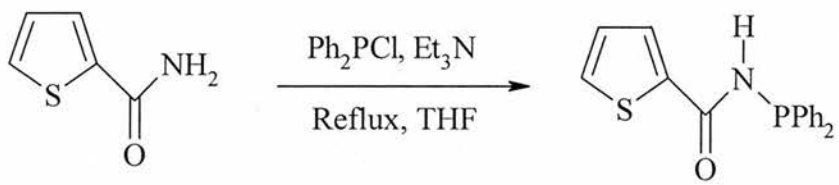

3.1

Figure 3.3: *Synthesis of dpptc.*

The ligand was recrystallised from boiling methanol to give a colourless crystalline solid in an moderate yield (54%) which is air stable. It is readily soluble in chlorinated solvents, acetone, tetrahydrofuran, somewhat less so in toluene, methanol and diethyl ether. A singlet is observed in the ^{31}P spectra of dpptc at δ(P) 25.9 ppm, this is comparable with the value for dpppa. The ^{1}H NMR spectrum (also $CDCl_3$) does not show the presence of an amide proton, as we see from some of the successive complexes it is clear that it is obscured by the main body of the aromatic protons. The IR spectra shows the expected peaks, a weak ν(N-H) band is present at 3265 cm^{-1}, also bands attributable to ν(thCS) and ν(P-N) are found at 1096 cm^{-1} and

996 cm^{-1} respectively, with ν(C-N) coming at 1522 cm^{-1}. The expected ν(C=O) signature is visible at 1624 cm^{-1}.

Due to the similarities in the oxidised forms of dpppa, only the sulfide of dpptc was synthesised as a representative example of the oxidised form. However a crystal of the oxide derivative was obtained via air oxidation of the free ligand in a $CDCl_3$ solution, and this structure and its data are considered here.

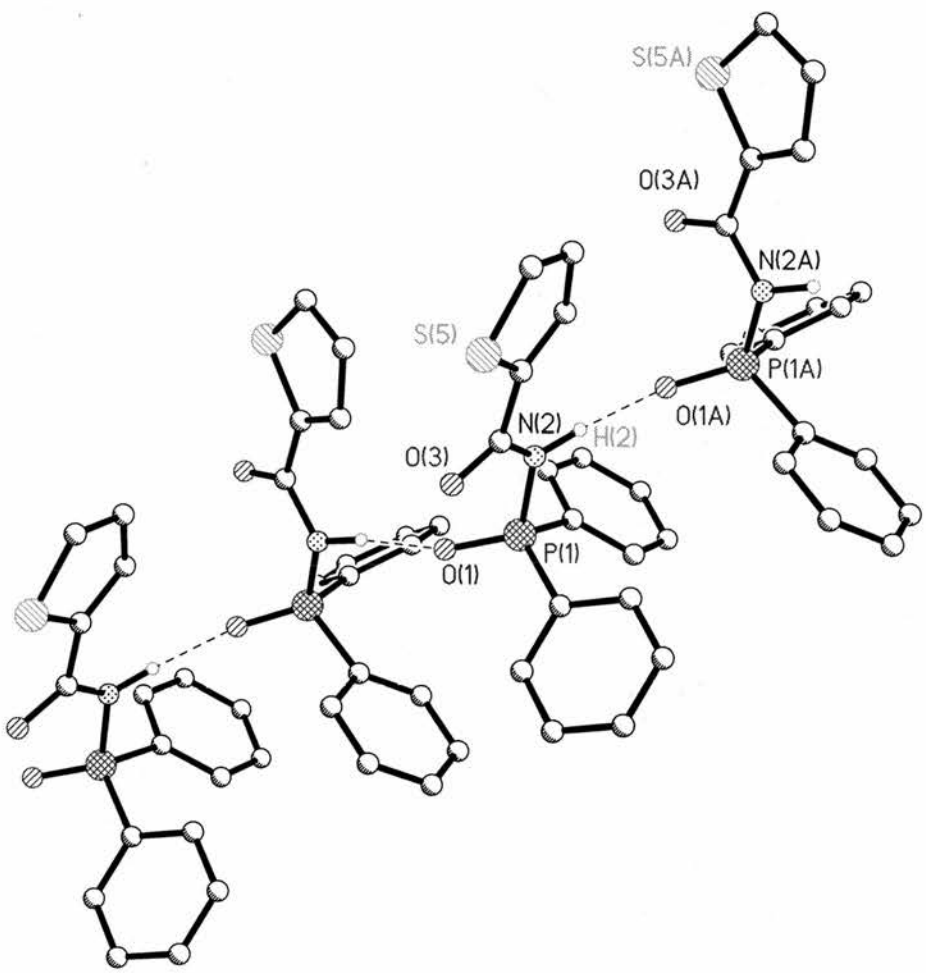

Figure 3.4: *Crystallographic representation of dpptc-O* ***(3.2)****.*

As can be seen directly from the diagram there is great similarity in the structure of **3.2** when compared with **2.2**, which is consistent with the spectroscopic data we have already considered. When one considers the crystallographic data, again there are many consistencies to be found, but the major difference is based around the difference of the thiophene ring compared to the pyridyl, in some much that the former is a five-membered ring as oppose to the six of the pyridyl, but also that the bonding is also different, with the thiophene's bonding is less delocalised than that in pyridyl giving the different lengths.

***Table**: **3.1** Selected bond lengths (Å) and angles (°) for dpptc-O **3.2**.*

P(1)-O(1)	1.456(3)	P(1)-N(2)	1.692(3)
P(1)-C(11)	1.801(4)	P(1)-C(17)	1.795(4)
O(3)-C(3)	1.229(4)	N(2)-C(3)	1.373(5)
C(3)-C(4)	1.463(5)	S(5)-C(4)	1.725(4)
C(4)-C(8)	1.365(5)	N(2)-O(1)	2.80
N(2)-P(1)-O(1)	115.10(16)	C(17)-P(1)-O(1)	112.61(16)
C(11)-P(1)-O(1)	112.17(17)	C(17)-P(1)-C(11)	109.77(17)
N(2)-P(1)-C(11)	100.64(16)	N(2)-P(1)-C(17)	105.73(16)
C(3)-N(2)-P(1)	121.2(3)	P(1)-N(2)-H(2)	119(3)
N(2)-C(3)-C(4)	118.0(3)	O(3)-C(3)-N(2)	121.1(3)
O(3)-C(3)-C(4)	120.9(3)	C(3)-C(4)-C(8)	131.2(3)
C(3)-C(4)-S(5)	117.6(3)	S(5)-C(4)-C(8)	111.2(3)
N(2)-H(2)...O(1)	171		

The sulfide was synthesised in the same way as for dpppa, reaction of dpptc with elemental sulfur in toluene generated the desired product dpptc-S (**3.3**). **3.3** shows a singlet in the ^{31}P spectrum, located at δ(P) 57.2 ppm, which is in the expected range, slightly higher than the dpppa analogue. The ^{1}H spectrum shows considerable similarity with dpppa-S, with the amide proton found at 7.0 ppm with a $^{2}J_{P\text{-}H}$ of 8 Hz. Peaks at 3167, 1624, 1436 and 1000 cm^{-1} in the IR spectrum, demonstrate similarities with the free ligand, with only the N-H bond being slightly lower.

3.2.2: Monodentate dpptc complexes.

Dpptc reacts with $[PtCl_2(cod)]$ in dichloromethane to generate *cis*-$[PtCl_2(dpptc\text{-}P)_2]$ (**3.4**) in reasonable yield, 72% (figure 3.5). This is the only coordination mode found in the initial reaction, no *trans*-bis(dpptc) or mono(dpptc) binding was observed. Also no bidentate binding was initially observed, which is consistent with earlier observations on dpppa. The ^{31}P NMR of **3.4** shows a singlet at δ(P) 27.9 ppm with the expected platinum satellites, the coupling constant of $^{1}J_{Pt\text{-}P}$ = 3870 Hz is consistent with the phosphorus *trans* to the chloride. The ^{1}H NMR spectrum displays the anticipated changes from the free ligand. The amine proton is shifted to δ(H) 9.7 ppm, and the coupling constant has increased to $^{2}J_{P\text{-}H}$ = 11 Hz., which mirrors the shift seen in the dpppa analogue where the constant was enlarged to 15 Hz. The ν(N-H) stretch in the IR spectrum has shifted to a lower wave number (3214 cm^{-1}), suggesting the possibility of intermolecular hydrogen bonding

interactions within the complex. The ν(C=O) also shifts considerably from 1624 cm^{-1} to 1672 cm^{-1}. Here is another variation, the dpppa example shows no discernable difference. Again this may suggest a difference in the hydrogen-bonding pattern within the complexes of dpptc as well is the free ligand. Two Pt-Cl stretches are visible in the spectrum (304 and 273 cm^{-1}), another indication of a *cis*- configuration in **3.4**.

Reaction of dpptc with $[\{Pd(\mu\text{-}Cl)(\eta^3\text{-}C_3H_5)\}_2]$ produced the expected mondentate dpptc complex $[PdCl(\eta^3\text{-}C_3H_5)(dpptc\text{-}P)]$ (**3.5**) as a yellow solid in good yield (87 %). The ^{31}P NMR displays a singlet at δ(P) 54.3 ppm, this is remarkably close to that observed for the equivalent dpppa complex, suggesting that in this complex the aromatic R group plays little part in the monodentate binding of the phosphorus to the metal. The amine proton is again shifted downfield in the ^1H NMR spectrum to 9.4 ppm, and in common with dpppa the $^2J_{P\text{-}H}$ coupling constant, is again enlarged to 20 Hz, this is a typical result as we have witnessed before. The IR spectrum shows the ν(N-H) stretch has again shifted to a lower wavenumber (3208 cm^{-1}), and the ν(C=O) has shifted to higher wavenumber (1671 cm^{-1}), which continues the trend first seen in **3.4** and proliferates the first real contrast found between the coordination chemistry of dpptc and dpppa observed, by giving information on hydrogen-bonding. The metal-chloride band is clearly visible at 277 cm^{-1} in the IR data, providing more supporting evidence for mondentate binding. Excellent microanalysis was obtained for **3.5**. Crystallographic studies were performed on a crystal obtained by vapour diffusion of diethyl ether into a concentrated solution of **3.5**.

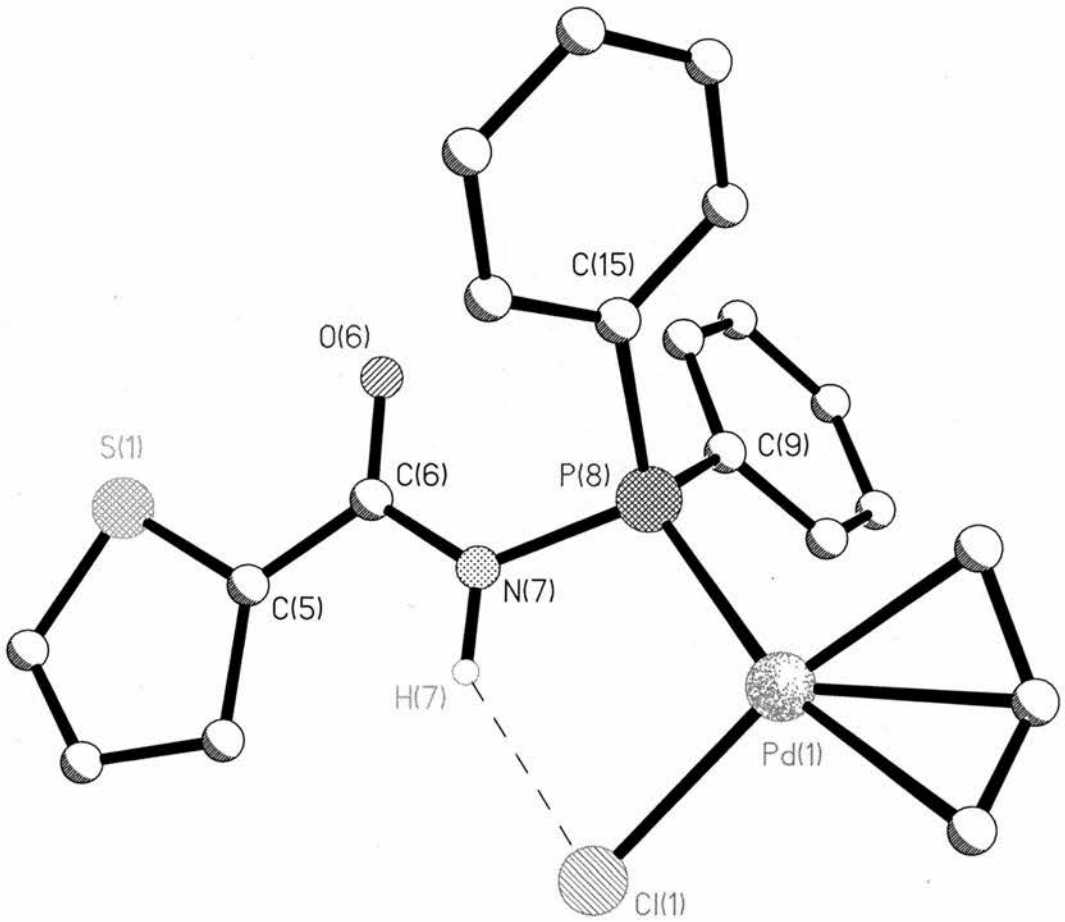

Figure 3.5: *Crystallographic representation of [PdCl(η^3-C_3H_5)(dpptc-P)]* ***(3.5)****.*

Figure 3.5 displays the expected hydrogen bonding, with the sulfur playing no part. This leaves the N(7)-H(7)…Cl(1) interaction dominant, the distance is 3.166 Å, with a N(7)-H(7)…Cl(1) angle of 131°.

Table*: **3.2** Selected bond lengths (Å) and angles (°) for [PdCl(η^3-C_3H_5)(dpptc-P)]* ***(3.5)***

P(81)-Pd(1)	2.2937(14)	Pd(1)-Cl(1)	2.3780(13)

P(8)-N(7)	1.706(4)	N(7)-C(6)	1.377(6)
O(6)-C(6)	1.227(6)	C(6)-C(5)	1.455(8)
S(1)-C(5)	1.712(6)	P(8)-C(9)	1.818(5)
P(8)-C(15)	1.825(4)	C(5)-C(4)	1.536(8)
N(7)...Cl(1)	3.166(4)		
P(8)-Pd(1)-Cl(1)	97.18(4)	C(15)-P(8)-Pd(1)	116.93(15)
N(7)-P(8)-Pd(1)	106.26(14)	C(9)-P(8)-Pd(1)	114.06(16)
C(6)-N(7)-P(8)	127.1(8)	C(15)-P(8)-C(9)	105.8(2)
P(8)-N(7)-H(7)	122(3)	O(6)-C(6)-N(7)	122.9(4)
O(6)-C(6)-C(5)	121.1(4)	N(7)-C(6)-C(5)	116.0(4)
C(6)-C(5)-S(1)	118.8(4)	N(7)-H(7)...Cl(1)	131(4)

The mixed phosphine complex $[PtCl_2(PEt_3)(dpptc\text{-}P)]$ (**3.6**) was synthesised in poor yield (50%) from $[\{PtCl(\mu\text{-}Cl)(PEt_3)\}_2]$ and dpptc in dichloromethane. The expected *cis* (P-P) configuration was confirmed by the ^{31}P NMR, which showed two doublets with the appropriate platinum satellites, one set comes at δ(P) 29.7 ppm ($^2J_{P\text{-}P}$ = 18.78 Hz, $^1J_{Pt\text{-}P}$ = 3890 Hz) and the other δ(P) –15.6 ppm ($^2J_{P\text{-}P}$ = 18.78 Hz, $^1J_{Pt\text{-}P}$ = 3500 Hz), these coupling constants are consistent with two phosphorus *cis*- to each other and *trans*- to a chloride. Also the IR provides further evidence with two Pt-Cl stretches observed at 316 and 281 cm^{-1}. The C=O, and N-H stretches (1671 and 3226 cm^{-1} respectively) are found in the expected range with regards to the peaks already seen for dpptc coordination, including the now consistent shift in the carbonyl peak (due again to hydrogen-bonding). The proton data follow the example of our previous

complexes, the amine proton can be seen at δ(H) 11.4 ppm, as a doublet with $J_{P\text{-}H}$ = 16 Hz, and the alkyl protons from PEt_3 can be seen from δ(H) 1.6-0.8 ppm. These spectral data are entirely consistent with those for the equivalent dpppa complex, suggesting a very similar configuration, and again suggesting that the 'R' group does not effect the monodentate coordination.

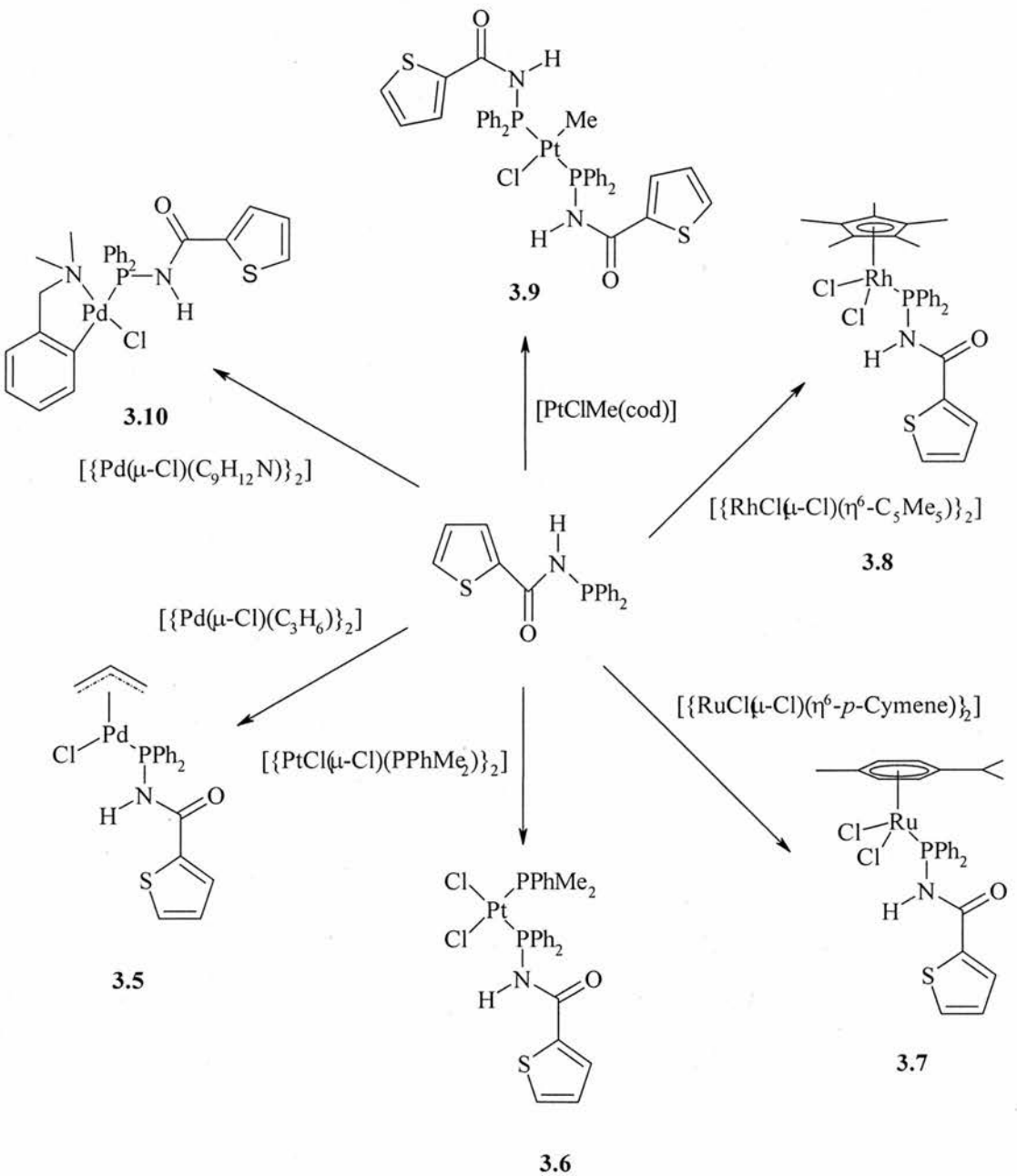

***Figure 3.6**: Formation of monodentate complexes of dpptc.*

Further monodentate complexes were synthesised; both ruthenium and rhodium examples were generated as for the earlier examples by dissolving dpptc and the metal starting materials ([{RuCl(μ-Cl)(η^6-*p*-cymene)}$_2$] and [{RhCl(μ-Cl)(η^5-C_5Me_5)}$_2$]) in dichloromethane and stirring for ten minutes followed by precipitation of the products with diethyl ether. These reactions generated [$RuCl_2$(*p*-cymene)(dpptc-*P*)] (**3.7**) and [$RhCl_2$(η^5-C_5Me_5)(dpptc-*P*)] (**3.8**). ^{31}P NMR shows a singlet for **3.7** (δ(P) 59.9 ppm) and a doublet for **3.8** (δ(P) 63.5 ppm, $^1J_{Rh\text{-}P}$ = 147.9 Hz). The ^{1}H NMR spectrum displays an amide shift similar to the shifts already observed for the dpppa monodentate complexes of ruthenium for **3.7**, the amide proton is seen at δ(H) 7.9 ppm with the expected enlarged $^2J_{P\text{-}H}$, being 14 Hz. The proton data for the rhodium complex (**3.8**) displays similar characteristics, with the amide proton shifting to δ(H) 8.2 ppm, with a $^2J_{P\text{-}H}$ coupling of 14 Hz. The IR data for the complexes is also relevant, as we have already seen it can be a valuable indicator of the coordination of the ligand. The ruthenium complex shows a N-H stretch at 3312 cm^{-1}, and the ν(C=O) stretch is present at 1665 cm^{-1}, which is a typical value in comparison with the previously examined monodentate dpptc complexes. The data for the rhodium complex are somewhat more straightforward. The N-H stretch is observed at 3299 cm^1. This brings an interesting conundrum: these N-H values are higher than those seen for the free ligand, which is the first example of this seen in this chemistry, and if the trend follows, indicates a smaller amount of H-bonding is present in these complexes in contrast to the other dpptc complexes and the dpppa analogues seen in the previous chapter. The ν(C=O) value for **3.8** is almost exactly the same as for **3.7**, at 1668 cm^{-1} again suggesting a consistency in hydrogen-bonding in these similar complexes. In an effort to investigate these possibly novel

hydrogen-bonding interactions, a crystal of **3.8** was grown via vapour diffusion of diethyl ether into a concentrated $CDCl_3$ solution of **3.8**.

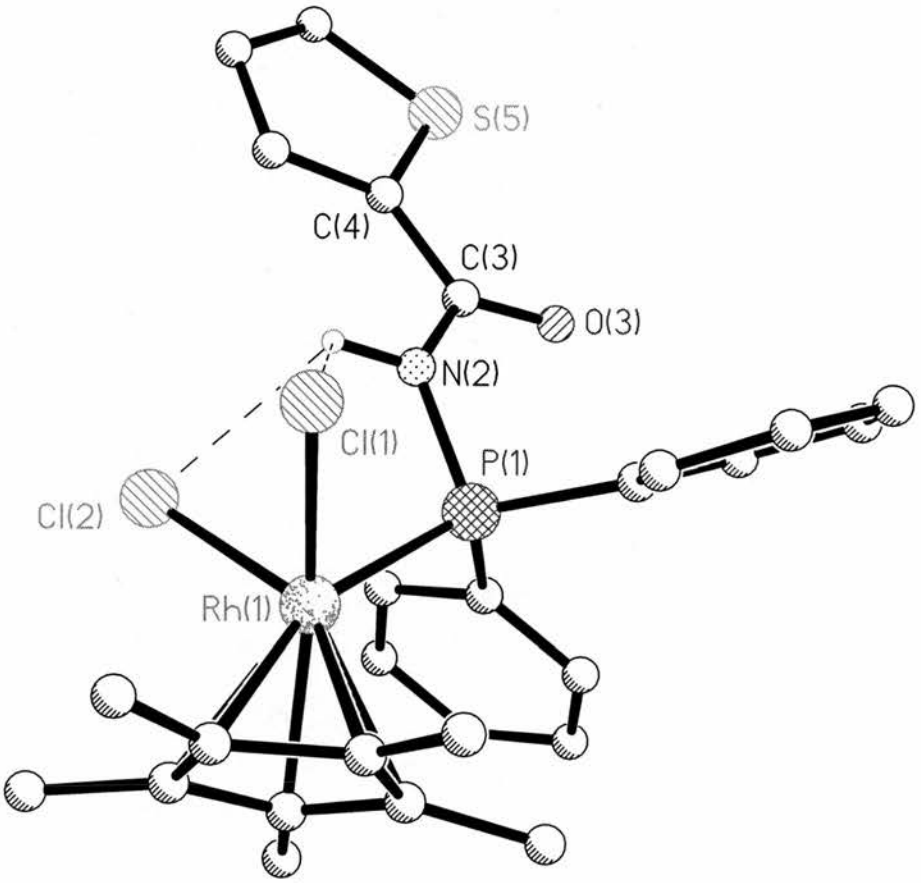

Figure 3.7: *Crystallographic Representation of* $[RhCl_2(\eta^5\text{-}C_5Me_5)(dpptc\text{-}P)]$ **(3.8)**.

As can be seen from the diagrammatic representation of **3.8** there is an interaction between the amide proton and both chlorides attached to the metal. Also, it is worthy of note that there is no interaction involving the oxygen or the sulfur heteroatom in the ring. This could be due to the fact that the sulfur is less likely to form a hydrogen bond, or that the geometry of the five membered ring as opposed to

that of the six membered ring is less favourable for a N(2)-H(2)...S(5) interaction. These issues and the easy availability of the chlorides account for the chosen motif in this molecule. Now, if we tie in these findings with the IR data from earlier, the data do fit into place. The carbonyl stretch being in the higher 1600's suggested a different motif in comparison with the free ligand and its derivatives that were in the lower 1600's, and from the crystal data of **3.2** we did determine that the carbonyl was involved in the hydrogen-bonding motif.

Closer inspection of the hydrogen-bonds in **3.8** reveals that one is slightly longer than the other, this could be due to possible steric interference between the two chlorides. However both are within an acceptable range with regard to hydrogen-chloride interactions.

***Table**: **3.3** Selected bond lengths (Å) and angles (°) for* $[RhCl_2(\eta^5\text{-}C_5Me_5)(dpptc\text{-}P)]$ (**3.8**).

P(1)-Rh(1)	2.3077(10)	Rh(1)-Cl(1)	2.3998(9)
Rh(1)-Cl(2)	2.4163(9)	P(1)-N(2)	1.695(3)
O(3)-C(3)	1.218(4)	N(2)-C(3)	1.387(4)
S(5)-C(4)	1.719(4)	C(3)-C(4)	1.466(5)
P(1)-C(11)	1.811(3)	P(1)-C(17)	1.829(4)
C(4)-C(8)	1.393(5)	N(2)-Cl(1)	3.379(3)
N(2)-Cl(2)	3.113(3)		
P(1)-Rh(1)-Cl(1)	89.44(3)	P(1)-Rh(1)-Cl(2)	89.19(3)

Rh(1)-P(1)- N(2)	106.88(10)	Rh(1)-P(1)- C(17)	118.42(12)
Rh(1)-P(1)- C(11)	111.91(12)	Cl(1)-Rh(1)-Cl(2)	87.96(3)
N(2)-P(1)-C(11)	104.30(15)	N(2)-P(1)-C(17)	104.96(13)
C(3)-N(2)-P(1)	127.3(2)	C(17)-P(1)-C(11)	109.15(15)
P(1)-N(2)-H(2)	114(3)	O(3)-C(3)-N(2)	122.1(4)
O(3)-C(3)-C(4)	122.7(3)	N(2)-C(3)-C(4)	115.2(3)
C(3)-C(4)-S(5)	117.8(3)	C(3)-C(4)-C(8)	131.0(3)
S(5)-C(4)-C(8)	111.2(3)	N(2)-H(2)...Cl(1)	112(3)
N(2)-H(2)...Cl(2)	121(3)		

Reaction of dpptc with [PtMeCl(cod)] in dichloromethane generated the expected complex *trans*-[PtMeCl(dpptc-*P*)$_2$] (**3.9**). The *trans*- geometry can be inferred in a number of ways. Firstly, in the case of a *cis*- product the ^{31}P NMR would display two doublets, but only a singlet is displayed. Also the crystal structure has been obtained confirming this geometry. The ^{31}P spectrum indeed shows a single resonance at δ(P) 49.1 ppm and the $^{1}J_{Pt\text{-}P}$ = 3220 Hz, is in the expected range for a phosphorus *trans* to another phosphorus. The ^{1}H data show agreement for the proposed structure, as there is no noticeable difference between the two ligands. The amine resonance has shifted to δ(H) 9.7 ppm. The IR spectra also suggests identical ligands as only one ν(N-H) stretch is visible at 3209 cm^{-1}, also only a single ν(C=O) stretch is observed, at 1671 cm^{-1}.

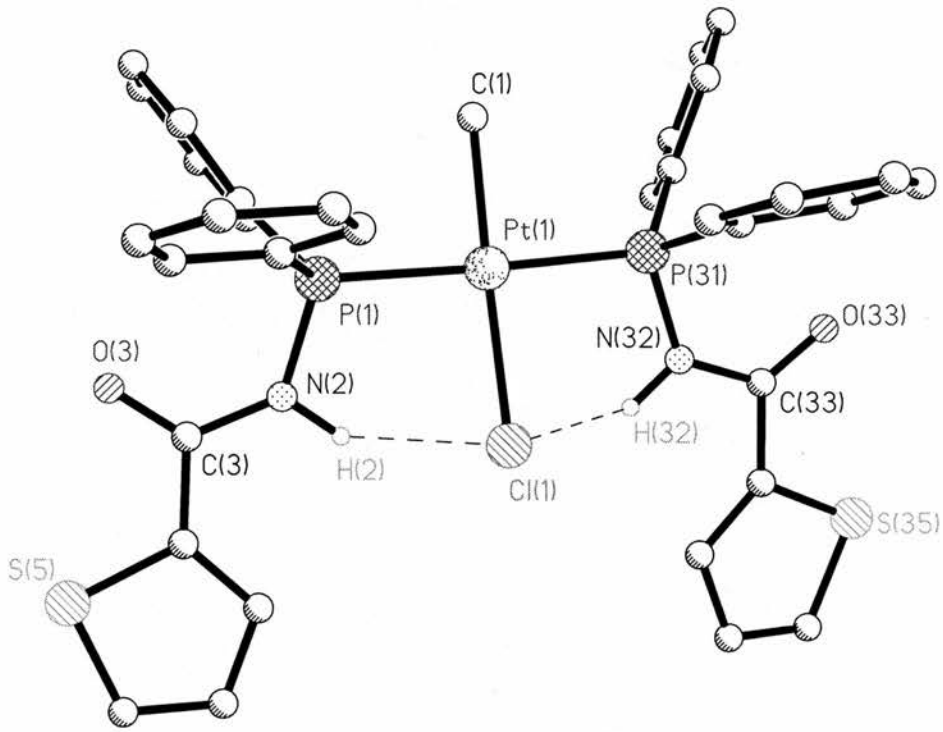

Figure 3.8: *Crystallographic representation of [PtMeCl(dpptc-P)$_2$] (**3.9**).*

As covered above, the *trans-* configuration is preferred to the initially expected *cis-* due to the advantageous hydrogen-bond motif this offers, this is clearly illustrated in diagram 3.7.

***Table**: **3.4** Comparison of selected bond lengths (Å) for [PtMeCl(dpptc-P)$_2$] (**3.9**).*

P(1)-Pt(1)	2.2902(15)	P(31)-Pt(1)	2.2902(15)
P(1)-N(2)	1.702(5)	P(31)-N(32)	1.700(5)
P(1)-C(11)	1.819(6)	P(31)-C(41)	1.817(7)
P(1)-C(17)	1.819(6)	P(31)-C(47)	1.801(7)
N(2)-C(3)	1.371(8)	N(32)-C(33)	1.365(7)

C(3)-O(3)	1.227(7)	C(33)-O(33)	1.227(7)
C(3)-C(4)	1.473(9)	C(33)-C(34)	1.470(8)
C(4)-S(5)	1.716(6)	C(34)-S(35)	1.716(6)
C(4)-C(8)	1.374(9)	C(34)-C(38)	1.369(9)
Pt(1)-Cl(1)	2.4343(16)	Pt(1)-C(1)	2.074(6)
N(2)-Cl(1)	3.085(6)	N(32)-Cl(1)	3.045(5)

As can be seen in table 3.3, the two hydrogen bonds present are almost identical, showing again the favourable motif that can be produced by the *trans*-arrangement. Both are well within the normal boundaries accepted for this type of interaction. Table 3.3 also provides a useful comparison between the two separate ligand molecules present within the complex. As can be seen on closer inspection, there is little variation in the two ligands, with there being little more than a few percentage difference between the values for each ligand.

***Table**: **3.5** Comparison of selected bond angles (°) for [PtMeCl(dpptc-P)$_2$] (**3.9**).*

P(1)-Pt(1)-Cl(1)	91.72(5)	P(31)-Pt(1)-Cl(1)	90.34(5)
P(1)-Pt(1)-C(1)	89.79(18)	P(31)-Pt(1)-C(1)	88.58(18)
P(1)-Pt(1)-P(31)	173.57(6)	C(1)-Pt(1)-Cl(1)	176.0(3)
N(2)-P(1)-Pt(1)	106.14(18)	N(32)-P(31)-Pt(1)	106.14(18)
P(1)-N(2)-H(2)	114(4)	P(31)-N(32)-H(32)	113(3)
P(1)-N(2)-C(3)	132.0(4)	P(31)-N(32)-C(33)	129.3(4)
N(2)-C(3)-O(3)	121.9(6)	N(32)-C(33)-O(33)	123.8(5)
N(2)-C(3)-C(4)	115.4(5)	N(32)-C(33)-C(34)	114.0(5)

O(3)-C(3)-C(4)	122.6(5)	O(33)-C(33)-C(34)	122.2(5)
C(3)-C(4)-S(5)	116.9(4)	C(33)-C(34)-S(35)	118.4(4)
N(2)-H(2)…Cl(1)	139(4)	N(32)-H(32)...Cl(1)	139(5)

Similar observations can be noted in table 3.4. The two hydrogen bonds are again very similar, as is every analogous angle found in each ligand in the complex. This again strengthens the thought that the hydrogen-bond motif found in the *trans*-arrangement is very stable, and this is why this stereochemistry is favoured over the other.

Another monodentate complex was formed from reaction of dpptc with [Pd(μ-Cl)($C_9H_{12}N$)}$_2$], which generated the analogous complex to the one seen in chapter two, [PdCl($C_9H_{12}N$)(dpptc-*P*)] (**3.10**). A singlet is observed in the ^{31}P NMR at δ(P) 62.4 ppm, which is very close to **2.9**. The ^{1}H NMR delivers more data that is consistent with the dpppa analogue. The amide proton can be found at δ(H) 10.1 ppm as a broad singlet. Peaks at 3171 and 1672 cm^{-1} in the infra-red spectrum are typical for the ν(N-H) and ν(C=O) stretches expected for the monodentate geometry. However this is the lowest amide stretch seen for the dpptc complexes but this is not unexpected as the value for the dpppa analogue was also low. This agrees well with the high amide shift in the ^{1}H spectrum with accompanying broadening indicating extensive hydrogen bonding. A crystal of **3.10** was isolated from slow evaporation of a $CDCl_3$ solution in air. This crystal was analysed and generated the structure as seen in figure 3.8.

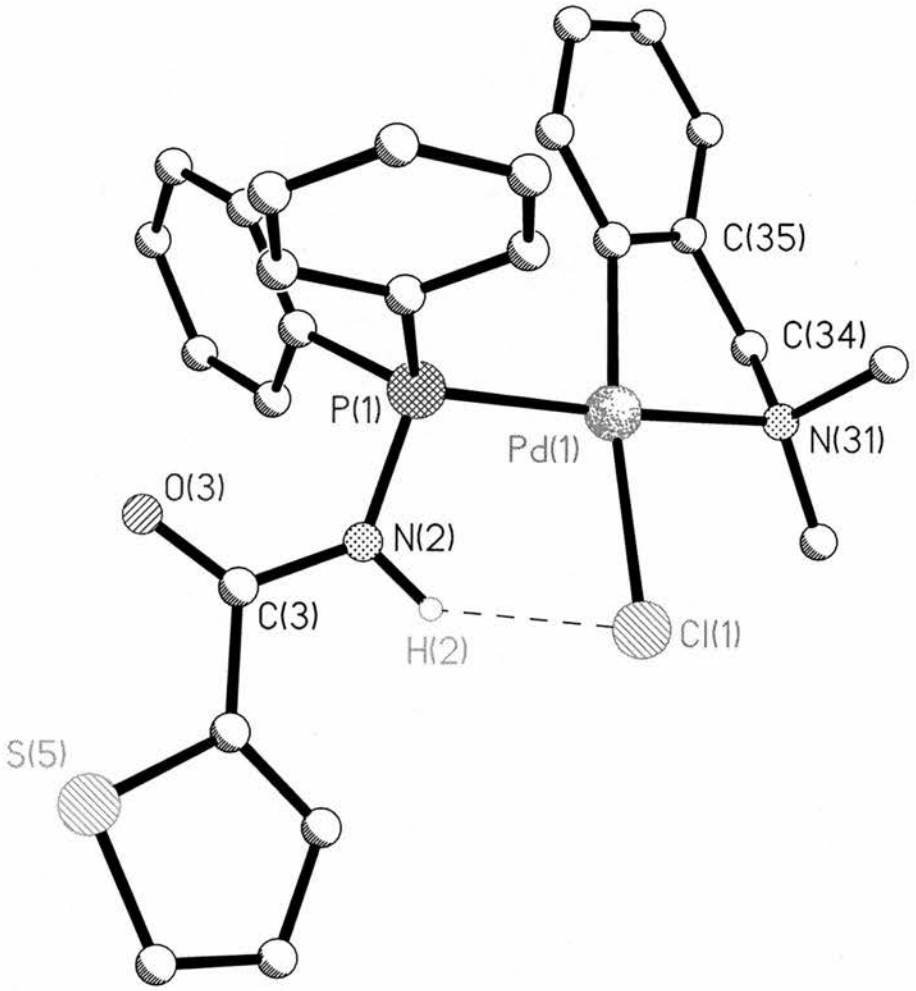

Figure 3.9: *Crystallographic representation of [PdCl($C_9H_{12}N$)(dpptc-P)]* ***(3.10)***.

This diagram shows the expected interactions with a N(2)-H(2)…Cl(1) hydrogen bond controlling the ligands geometry, forming a psuedo five-membered ring, similar to the ones we have seen previously. Again the sulfur has no part in the bonding motif. A list of the bond lengths and angles is displayed in table 3.5.

***Table**: 3.6 Selected bond lengths (Å) and angles (°) for [PdCl($C_9H_{12}N$)(dpptc-P)] (3.10).*

P(1)-Pd(1)	2.2479(12)	Pd(1)-N(31)	2.143(4)
Pd(1)-Cl(1)	2.4249(12)	P(1)-C(11)	1.819(4)
P(1)-C(17)	1.820(4)	P(1)-N(2)	1.697(4)
C(3)-O(3)	1.219(5)	N(2)-C(3)	1.382(5)
C(4)-C(8)	1.388(6)	C(3)-C(4)	1.471(6)
N(2)...Cl(1)	3.027(4)	C(4)-S(5)	1.713(4)
P(1)-Pd(1)-Cl(1)	93.58(4)	P(1)-Pd(1)-N(31)	173.10(10)
Cl(1)-Pd(1)-N(31)	91.83(10)	C(11)-P(1)-C(17)	107.56(19)
C(11)-P(1)-N(2)	106.12(18)	C(17)-P(1)-N(2)	104.09(19)
P(1)-N(2)-H(2)	115(3)	P(1)-N(2)-C(3)	129.9(3)
H(2)-N(2)-C(3)	115(3)	N(2)-C(3)-O(3)	123.1(4)
N(2)-C(3)-C(4)	114.0(4)	O(3)-C(3)-C(4)	122.9(4)
C(3)-C(4)-S(5)	119.0(3)	C(3)-C(4)-C(8)	129.5(4)
C(8)-C(4)-S(5)	111.5(3)	N(2)-H(2)-Cl(1)	141(4)

The bond lengths here are consistent with the other monodentate complexes in the chapter. This confirms the findings from the spectroscopic evidence, and once again displays that there is very little deviation in the monodentate-binding motif, between the dpptc and dpppa examples. Inspection of the bond angles also provides evidence to further this thinking. As with **3.9** (our other square planar crystal analysis), the geometry around the metal also slightly deviated from ideal geometry with a few degrees difference from ideal 90° angles. Also the backbone of the ligand

shows angles around 120° which is consistent with the other examples of dpptc complexation. Finally the value of 140° for the hydrogen bond is almost identical to that seen in **3.9**.

***Table 3.7**: Summary of the Spectroscopic Data for monodentate dpptc complexes.*

	IR/cm^{-1}		*NMR/ppm*	
	N-H	C=O	^{31}P δ(P)	N-H δ(H)
$[PtCl_2(dpptc\text{-}P)_2]$	3214	1672	27.9	9.7
[PdCl(allyl)(dpptc-P)]	3208	1671	54.3	9.4
$[PtCl_2(PEt_3)(dpptc\text{-}P)]$	3226	1671	29.7*	16
$[RuCl_2(\eta^6\text{-p-cymene})(dpptc\text{-}P)]$	3312	1665	59.9	7.9
$[RhCl_2(\eta^5\text{-}C_5Me_5)(dpptc\text{-}P)]$	3299	1668	63.5	8.2
$[PdCl(C_9H_{12}N)(dpptc\text{-}P)]$	3171	1672	62.4	10.1

*also peak at –15.6 for PEt_3

3.2.3: Bidentate complexes of dpptc.

On exploration of dpptc's bidentate chemistry, we witness a significant difference between the chemistry of dpppa and dpptc. Reaction of a halide abstractor on a monodentate dpppa complex generated the bidentate species bound via the phosphorus and pyridyl nitrogen. However, in the case of dpptc when the same reaction in undertaken one may expect the binding of the thiophene S. However chelation by C=O could also be imagined due to the poor binding characteristics of sulfur. This can be investigated by observing the evidence presented in the IR

spectrum which would show a noticeable shift in the C=O peak, indicating chelation through the oxygen. The example investigated was reaction of [$RuCl_2$(*p*-cymene)(dpptc-*P*)] with $AgBF_4$ in dcm, the silver salt was removed by filtration and the product [RuCl(*p*-Cy)(dpptc-*P,O*)] (**3.11**) precipitated with diethyl ether. The ^{31}P NMR displays the expected downfield shift in the spectra. The peak moves from δ(P) 59.9 to 100.0 ppm, and the chelate ring effect is responsible for this. The proton spectrum shows some interesting characteristics, we see the largest amine shift so far for the dpptc ligand as the amine proton moves from δ(H) 7.9 ppm in the monodentate complex to δ(H) 10.1 ppm in the bidentate complex. Also the amine proton peak changes from a doublet to a broad singlet, which is typical of extensive hydrogen-bonding being present. The amine stretch in the IR is unmoved in comparison with the monodentate complex and is found at 3216 cm^{-1}. The important IR information is the carbonyl. As discussed, C=O chelation would cause a upfield shift and this is observed with the band moving to 1561 cm^{-1}, a shift of 104 cm^{-1} from the monodentate complex, typical of C=O bound, bidentate ligand, as described by Braustein[5], with the increasing single bond nature of the bond being the major contributory factor.

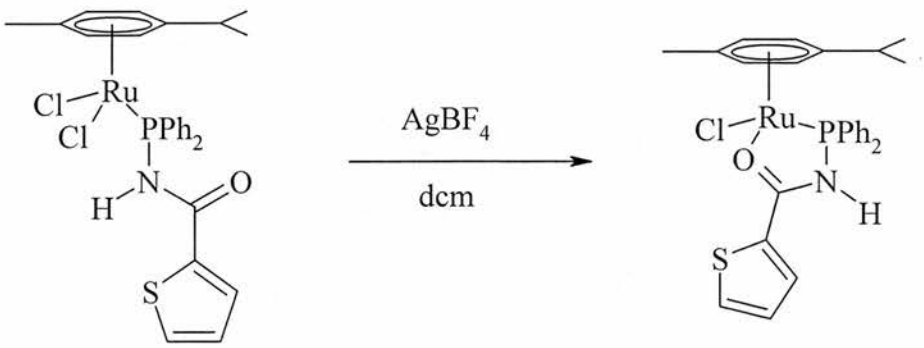

***Figure 3.10**: Chelation of dpptc.*

*3.3: **Part 2:** Bis(2,5-diphenylphosphino)picolinamide (bdpppa).*

3.2.4: Synthesis of bdpppa and its and Chalcogen derivatives.

The synthesis of bdpppa (**3.12**) is very similar to that of dpppa. Addition of two equivalents of Ph_2PCl in tetrahydrofuran to a tetrahydrofuran solution of a small excess of Et_3N and a 10 % molar equivalent of DMAP proceeded by overnight reflux.

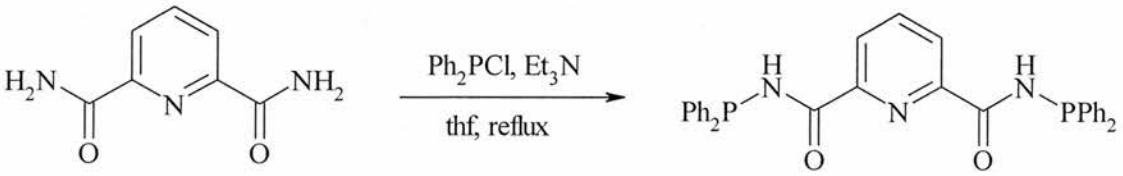

3.12

***Figure 3.11:** Synthesis of bdpppa.*

As with dpppa, bdpppa was successfully recrystallised by cooling a concentrated methanol solution to give a pure product in 61 % yield. Bdpppa is a colourless air stable amorphous solid, which is soluble in chlorinated solvents, tetrahydrofuran and methanol, and relatively soluble in toluene. The expected singlet in the ^{31}P NMR is located at δ(P) 21.9 ppm. This is extremely close to the value for dpppa (22.0 ppm), which is expected, as bdpppa is very similar to dpppa. This singlet also confirms that there is no difference between the two phosphorus atoms in the molecule. We see the same similarities in the proton spectra, the N-H peak appears again as a doublet with a more or less identical shift to dpppa at δ(H) 8.4 ppm. However the coupling constant is significantly larger for bdpppa, being 8 Hz as compared to 4 Hz for dpppa. When one examines the IR spectra for bdpppa we finally see some significant deviation in the characteristics of bdpppa compared to

dpppa. Both ν(N-H) stretches are visible at 3345 and 3262 cm^{-1}, and this trend continues into the ν(C=O) stretches which are visible at 1665 and 1646 cm^{-1}. The ν(C=N) stretches are at 1588 and 1571 cm^{-1}. However there is only one ν(P-N) stretch observed at 999 cm^{-1}, from which we could surmise that there is a slight difference in the to 'arms' of the molecule present in the solid state.

The presence of two P^{III} atoms in this molecule provides an opportunity for a variety of oxidation products to be synthesised. Bis(2,6-diphenylphosphino)picolinamide disulfide (**3.13**) and the diselenide (**3.14**) were prepared by refluxing bdpppa in toluene with a stoichiometric amount of sulfur or selenium for 1 hour. Both were recrystallised by cooling the toluene reaction solutions directly following the initial synthesis. The yields for each reaction were good (78 % for di-S, 81 % for di-Se). The ^{31}P NMR displays the expected downfield shift for each compound, with the disulfide shifting to δ(P) 55.1 ppm and the diselenide to δ(P) 49.7 ppm with $^{1}J_{P=Se}$ = 795 Hz. This coupling constant is typical for with a P=Se bond. These values are almost identical to the values seen for dpppa, again suggesting that there is little or no interaction between the two arms of the ligand. The amide protons in **3.13** and **3.14** are shifted to δ(H) 8.9 and 8.8 ppm respectively, and are both doublets with $^{2}J_{P-H}$ = 9 Hz. These values are similar to the ones witnessed for the unoxidized ligand, which is as expected after inspection of the trends laid out by dpppa and dpptc. The IR data shows no real variation from the dpppa equivalents, for **3.13** the ν(N-H) is observed at 3360 cm^{-1} as a sharp peak. However the ν(C=O) is observed at 1697 cm^{-1} with significant line broadening, and the ν(P-N) peak remains constant at 999 cm^{-1}. A similar pattern is observed for **3.14**, with ν(N-H), ν(C=O) and ν(P-N) coming at 3256, 1698 and 998 cm^{-1} respectively, although the slightly lower value for the amine stretch does suggest more extensive

hydrogen-bonding in **3.14** compared to both the disulfide and the free ligand. A crystal of **3.14** was prepared for X-ray analysis by vapour diffusion of diethyl ether to a concentrated dichloromethane solution of **3.14**.

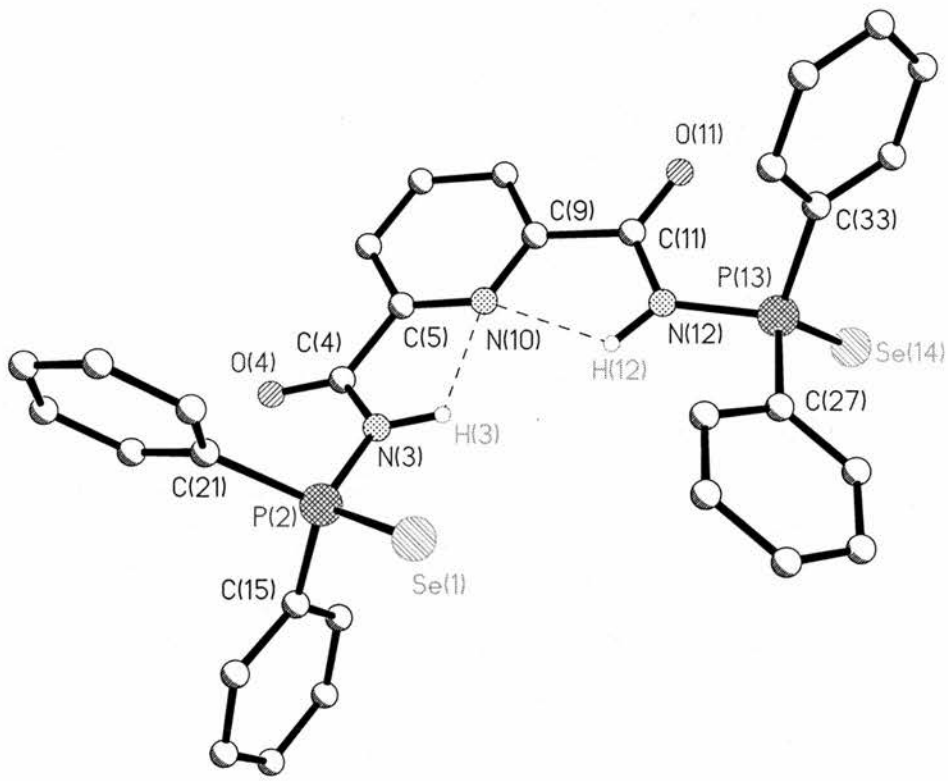

Figure 3.12: *Crystallographic representation of bdpppa-diSe (**3.14**).*

The crystallographic representation of **3.14** shows a return to the hydrogen motifs seen in dpppa. Once again a pseudo five-membered ring is formed by an interaction of the amide hydrogens with the pyridyl nitrogen.

***Table**: **3.8** Selected bond lengths (Å) and angles (°) for bdpppa-diSe (**3.14**).*

Left of molecule		*Right of molecule*	

P(2)-Se(1)	2.0974(14)	P(13)-Se(14)	2.1014(15)
P(2)-C(21)	1.822(5)	P(13)-C(27)	1.821(5)
P(2)-C(15)	1.808(5)	P(13)-C(33)	1.818(5)
P(2)-N(3)	1.687(4)	P(13)-N(12)	1.698(4)
N(3)-C(4)	1.374(6)	N(12)-C(11)	1.373(6)
C(4)-O(4)	1.209(6)	C(11)-O(11)	1.207(6)
C(4)-C(5)	1.513(6)	C(11)-C(9)	1.510(7)
C(5)-N(10)	1.334(6)	C(9)-N(10)	1.334(16)
N(3)...Cl(3)	3.050	N(12)...Cl(3)	3.368
N(3)-N(10)	2.684(5)	N(12)-N(10)	2.721(5)
Se(1)-P(2)-N(3)	107.68(16)	Se(14)-P(13)-N(12)	114.97(16)
P(2)-N(3)-H(3)	120(5)	P(13)-N(12)-H(12)	128(4)
P(2)-N(3)-C(4)	128.7(3)	P(13)-N(12)-C(11)	120.9(3)
H(3)-N(3)-C(4)	111(5)	H(12)-N(12)-C(11)	111(4)
N(3)-C(4)-O(4)	124.4(4)	N(12)-C(11)-O(11)	122.8(5)
N(3)-C(4)-C(5)	113.0(4)	N(12)-C(11)-C(9)	115.5(4)
O(4)-C(4)-C(5)	122.6(4)	O(11)-C(11)-C(9)	121.7(5)
C(4)-C(5)-N(10)	117.8(4)	C(11)-C(9)-N(10)	117.7(4)
N(3)-H(3)...N(10)	113(5)	N(12)-H(12)....N(10)	113(5)
	C(5)-N(10)-C(9)	117.9(4)	

The bond lengths and angles observed within these interactions are consistent with previously observed values, and agree well with the values for dpppa-E. Also

this molecule gives us another opportunity to compare the two sides of a single molecule. On inspection we can observe that for **3.14** the bond lengths within the ligand all correlate well. However, when one considers the angles they are somewhat different in about half of the examples. The reason for this could be that one selenium atom points inwards toward the centre of the molecule and the other points away from the heart of the molecule. This is due to the large size of the selenium atom, and there is not enough space for two to occupy the hole between the amide hydrogens. The angles involved in the hydrogen-bonding are all very similar to each other.

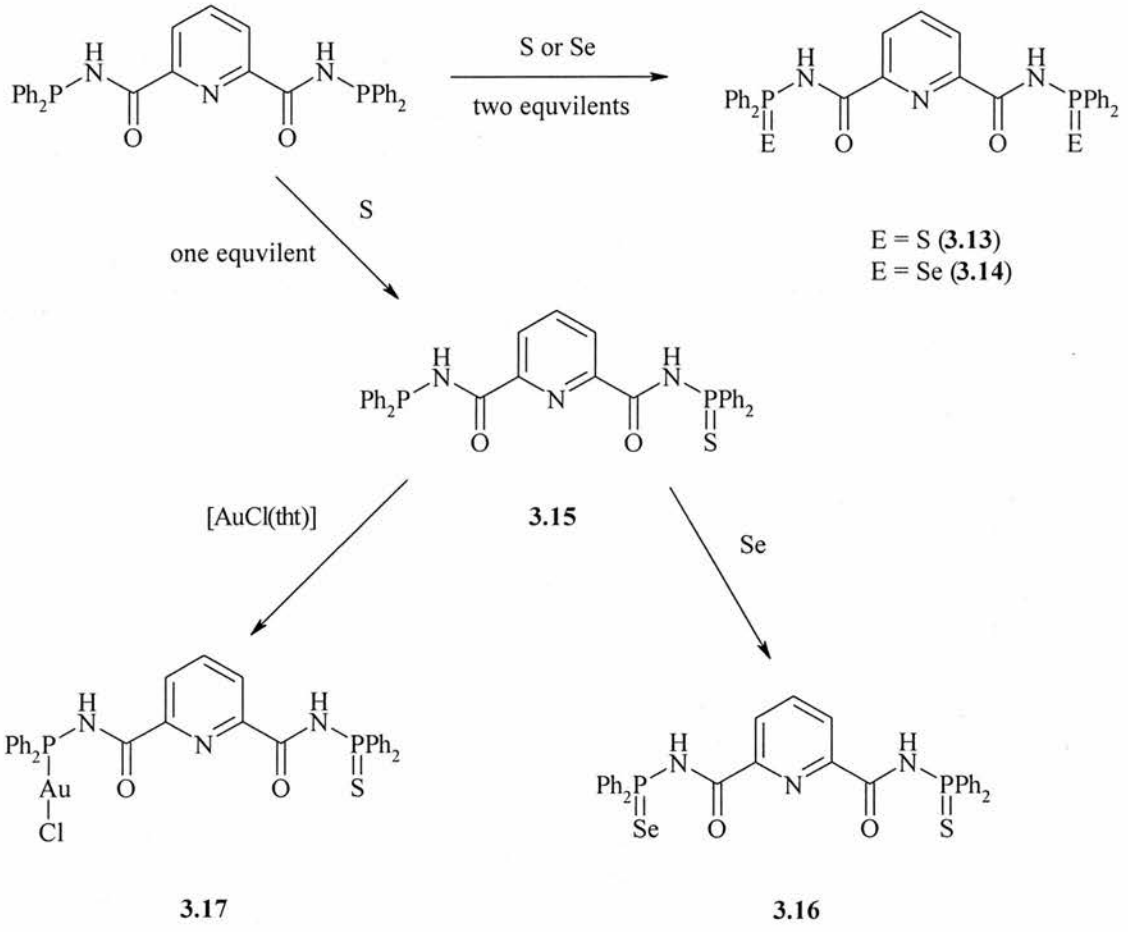

Figure 3.13: *Reactions of bdpppa and its mono-oxidized derivatives.*

It was possible to isolate a mono-oxidized species of bdpppa, by making use of the mild conditions involved in synthesis of the sulfur species one can isolate the mono-sulfur derivative of bdpppa, bdpppa-S (**3.15**). This generates a compound where only one sulfur is bound to phosphorus, leaving one free for further chemistry. The ^{31}P spectrum clearly shows this motif with two singlets being present at δ(P) 56.0 (P=S), and 21.7 ppm (P^{III}). This is a clear distinction between the two phosphorus, with the original P^{III} barely changing from its original shift, and the P=S shift in the same region as the peak observed in the disulfide derivative. The ^{1}H spectrum shows limited deviation from the data observed for the free ligand and that of the disufide. The amine shift is seen at δ(H) 8.8 ppm, with a $^{2}J_{P\text{-}H}$ = 8 Hz, suggesting once more that the oxidation of the phosphorus has little effect on the rest of the ligand. The IR data show the two arms clearly, when observing the ν(N-H) stretch one observes a peak at 3345 cm^{-1} which is consistent with bdpppa, and also a peak at 3262 cm^{-1} is clearly observed, this is in agreement with the peaks for dpppa-S and bdpppa-diS. The same pattern is seen in the ν(C=O), a peak at 1697 cm^{-1} representing the sulfide arm, and a peak at 1665 cm^{-1} represents the P^{III} arm.

As we speculated, the mono-oxidised form of bdpppa can use its unoxidised phosphorus to react further, and reaction with one equivalent of selenium in toluene generates the unsymmetrical bdpppa-S,Se (**3.16**). The ^{31}P NMR again shows clear distinction between the two inequivalent phosphorus resonances, one is found at δ(P) 55.0 ppm (consistent with P=S), and one at δ(P) 49.7 ppm which also has the anticipated selenium satellites with a $^{1}J_{P=Se}$ of 795 Hz. These values are consistent with the previously established values for dpppa and the various bdpppa derivatives. The proton spectrum of **3.16** is entirely consistent with the spectra so far considered. The amine peak is found at δ(H) 8.8 ppm, again as a doublet with coupling constant

($^2J_{P-H}$) of 8 Hz, and again the aromatic protons are found in a cluster, in the same region as the other ligands (δ(H) ~7-8 ppm). The IR spectrum shows similar characteristics to that of the disulfide and diselenium, which is to be expected. Bands for ν(C=O), and ν(P-N) can be clearly seen at 1697 and 997 cm^{-1}. However the ν(N-H) stretch is concealed. These peaks do not show two distinct arms of the ligand as seen in **3.15**. This could be due to the similarities between sulfur and selenium.

3.15 can be reacted with one equivalent of [AuCl(tht)] in dichloromethane to generate the complex [AuCl(bdpppa-S-*P*)] **3.17**. This complex shows the expected peaks in the ^{31}P NMR spectrum, at δ(P) 55.0 (P=S) and δ(P) 50.2 (P-Au), the P=S peak is again in the usual range, and the P-Au peak is consistent with the peak seen for the dpppa-Au complex. The amine proton is found as a broad singlet at δ(H) 10.2 ppm. The IR data shows a broad ν(N-H) stretch at 3256 cm^{-1}. This is a reasonable value given the bands seen for the previous example seen for dpppa, and taking into account the values seen for the sulfide derivatives of bdpppa. The carbonyl stretch once again remains unmoved at 1698 cm^{-1} as has been seen for every example of bdpppa derivatives so far.

3.2.5: Complexes of bdpppa.

Reaction of bdpppa with [AuCl(tht)] in dichloromethane gives two products dependant on the stoichiometry of the reaction. One equivalent of [AuCl(tht)] generates the expected product with one phosphorus bound to gold and one remaining unbound (**3.18**). With two equivalents of [AuCl(tht)] both phosphorus' become bound to a gold atom (**3.19**). In the case of this digold complex we see the expected singlet in the ^{31}P NMR at 50.0 ppm, this agrees well with the one previous gold

complex of dpppa, and the peak seen in **3.17**. The proton spectrum also displays the characteristics of its dpppa example, the amide peak is clearly seen at δ(H) 10.3 ppm with a $^{2}J_{P\text{-}H}$ = 16 Hz and the aromatics are all found in the 8.2-7.2 region. The ν(N-H) stretch in the IR spectrum is a broad peak at 3261 cm^{-1}, also the ν(C=O) band is broad, located at 1698 cm^{-1}, both these values correlate well with [AuCl(dpppa-*P*)] (3288 and 1698 cm^{-1} respectively).

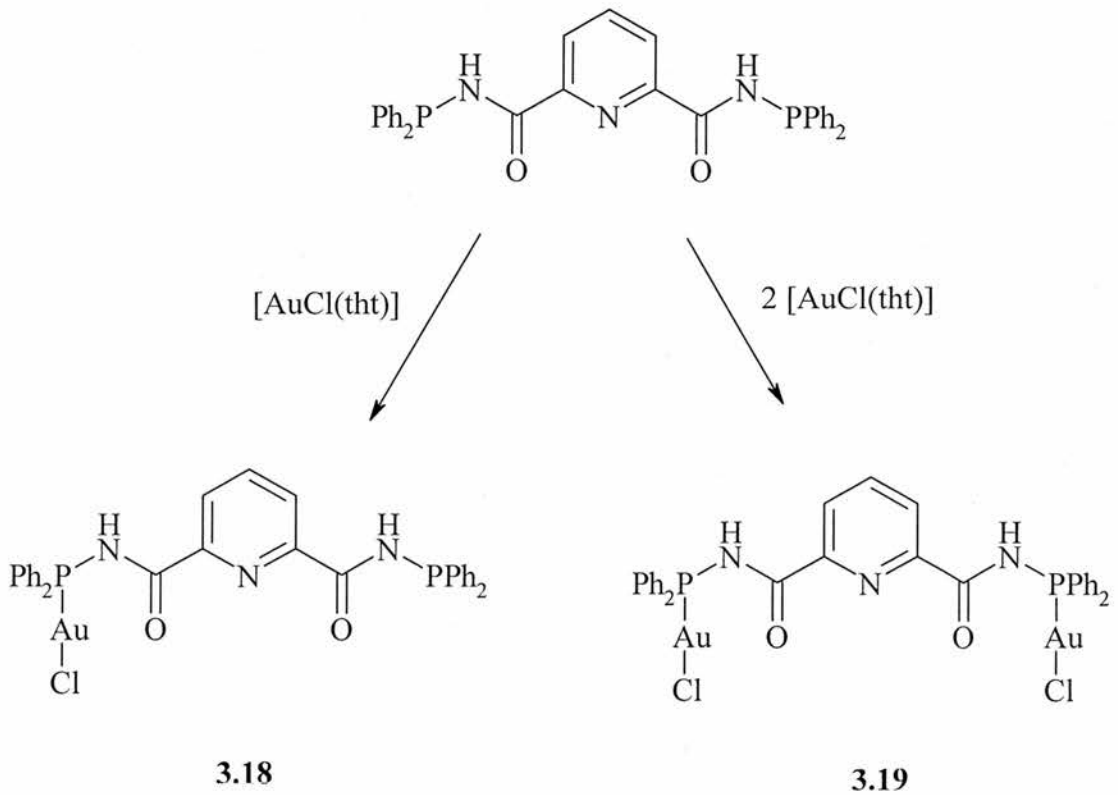

3.18 **3.19**

Figure 3.14: *Reaction of bdpppa with [AuCl(tht)].*

However, when one considers the mono-gold complex it (unlike **3.15**), does not display two separate peaks in the ^{31}P NMR for P-Au and P^{III}, it only generates a singlet at δ(P) 64.3 ppm, which is a significantly higher than anything we have seen earlier, and does not correlate with the shift observed in the monosulfide/gold complex. Inspection of the IR data provides further evidence for a single phosphorus environment, with single peaks being displayed for ν(N-H) and ν(C=O) (3054 and

1698 cm^{-1} respectively). Also the ^1H NMR data shows a single resonance for the amide proton, a broad singlet at δ(H) 11.0 ppm. The most plausible explanation for this data is for **3.18** to exist as a dimer, this is not a unique conformation as a similar system has been reported for dppap.[13] With the ligands surrounding the metal in a top to tail arrangement.

3.2.6: Bridging Complexes of bdpppa.

Reaction of bdpppa with a range of Pt and Pd dimers has generated complexes where the bdpppa ligand bridges two metal atoms. The first example of this type of complex was synthesised via reaction of one equivalent of bdpppa with one equivalent of $[\{Pd(\mu\text{-}Cl)(\eta\text{-}C_3H_6)\}_2]$, generating $[Pd_2Cl_2(\eta\text{-}C_3H_6)_2$(bdpppa-*P,P*)] (**3.20**). The ^{31}P NMR shows a singlet at δ(P) 55.1 ppm, consistent with the duduced structure of the complex when compared to dpppa and dpptc.

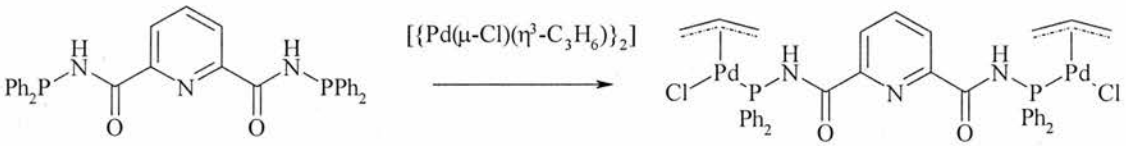

3.20

***Figure 3.15**: Synthesis of a bdpppa bridged Palladium complex.*

The ^1H NMR is as expected, the amine proton can be observed at δ(H) 10.2 ppm as a doublet ($^1J_{P\text{-}H}$ = 18 Hz), this is a large down field shift, which is consistent with the reactions seen with dpppa, the allyl proton spread out between 5.6 and 3.7 ppm. The IR spectrum shows peaks which are again within established boundaries, the ν(N-H) stretch is found at 3209 cm^{-1}, and the ν(C=O) at 1698 cm^{-1}.

The analogous reaction with [{Pt(μ-Cl)(η-C_3H_6)}$_4$] generated a similar product which could be considered isomorphous. The product [Pt_2Cl_2(η-C_3H_6)$_2$(bdpppa-*P,P*)] (**3.21**), shows a peak at δ(P) 51.7 ppm with the expected platinum satellites giving a $^1J_{Pt\text{-}P}$ = 4730 Hz. The proton spectrum is almost identical to that of **3.20**, with the amide proton shifting to δ(H) 10.1 ppm with a $^2J_{N\text{-}H}$ is 10 Hz, the only slight variation is that the allyl protons are slightly shifted; which is a result of the change of metal. Examination of the IR data displays close agreement with **3.20**, the ν(N-H) band is found at 3360 cm^{-1}, and the ν(C=O) at 1700 cm^{-1}.

A crystal of **3.21** was prepared for crystallographic analysis by vapour diffusion of diethyl ether into a concentrated solution of **3.21** in $CDCl_3$. Given our conclusions based on **3.20** we could imagine the two compounds would be almost analogous in the solid state.

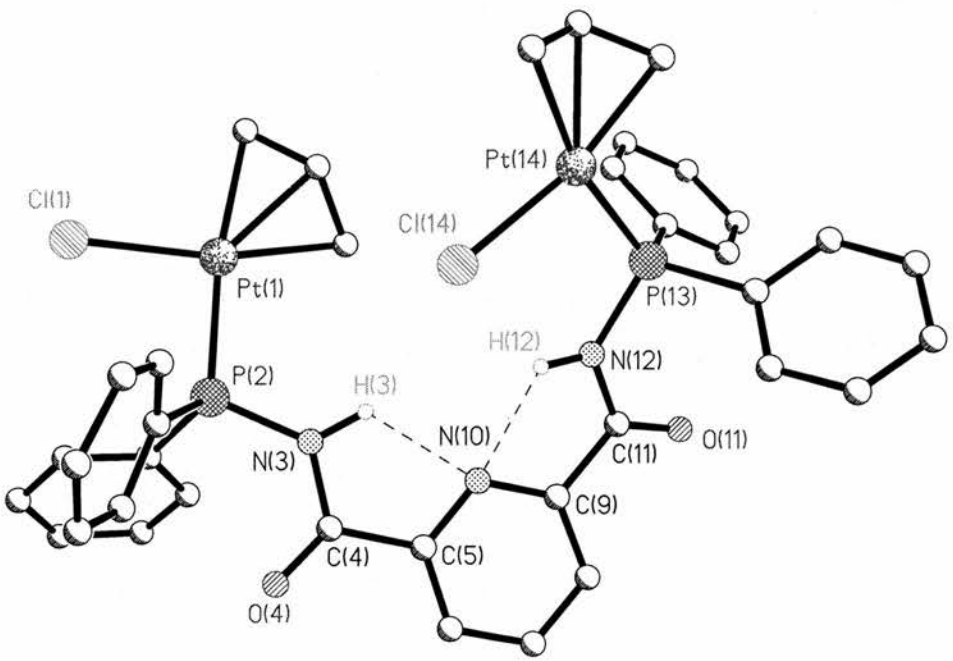

Figure 3.16: *Crystallographic representation of* $[Pt_2Cl_2(\eta\text{-}C_3H_6)_2(bdpppa\text{-}P,P)]$ ***(3.21)***.

Figure 3.15 shows that **3.21** has an arrangement much like that of **3.14**, with the amide protons interacting with the pyridyl nitrogen, and if one considers the chlorides to be analogous to the selenium atoms, then we can see that again one is 'in' and one is 'out' of the hole in the centre of the complex. Similar to **3.14** one can imagine in this scenario that there is probably too much steric bulk involved for both of the chlorides to occupy the 'in' slot as was the case with the seleniums.

Table**: **3.9** Selected bond lengths (Å) and angles (°) for* $[Pt_2Cl_2(\eta\text{-}C_3H_6)_2(bdpppa\text{-}P,P)]$ ***(3.21).

Left of molecule		*Right of molecule*	
P(2)-Pt(1)	2.249(2)	P(13)-Pt(14)	2.250(2)
P(2)-C(21)	1.855(9)	P(13)-C(131)	1.799(9)
P(2)-C(27)	1.824(8)	P(13)-C(137)	1.803(9)
P(2)-N(3)	1.699(7)	P(13)-N(12)	1.720(7)
N(3)-C(4)	1.383(10)	N(12)-C(11)	1.355(10)
C(4)-O(4)	1.206(9)	C(11)-O(11)	1.190(10)
C(4)-C(5)	1.508(11)	C(11)-C(9)	1.502(12)
C(5)-N(10)	1.352(10)	C(9)-N(10)	1.315(10)
N(3)-N(10)	2.689(10)	N(12)-Cl(14)	3.167(7)
		N(12)-N(10)	2.674(9)

Pt(1)-P(2)-N(3)	110.4(2)	Pt(14)-P(13)-N(12)	109.9(3)
P(2)-N(3)-H(3)	127(6)	P(13)-N(12)-H(12)	120(6)
P(2)-N(3)-C(4)	125.9(6)	P(13)-N(12)-C(11)	127.0(6)
H(3)-N(3)-C(4)	106(6)	H(12)-N(12)-C(11)	111(6)
N(3)-C(4)-O(4)	123.8(8)	N(12)-C(11)-O(11)	125.1(8)
N(3)-C(4)-C(5)	113.77(7)	N(12)-C(11)-C(9)	112.5(8)
O(4)-C(4)-C(5)	122.5(7)	O(11)-C(11)-C(9)	122.3(8)
C(4)-C(5)-N(10)	116.9(7)	C(11)-C(9)-N(10)	117.96
N(3)-H(3)...N(10)	119(7)	N(12)-H(12)...N(10)	110(6)
	C(5)-N(10)-C(9)	117.5(7)	

Table 3.8 shows that there is a noticeable difference in the two arms of the ligand. Almost all of the bond lengths show a difference, this must be due to the conformational differences enforced by the geometry of the complexes with the position of the chlorides being the dominant factor. However this is not a difference mirrored in the bond angles. These angles are reasonably consistent throughout the molecule with the major differences based around the hydrogens and the hydrogen bonds. This would tie in with the chlorines controlling the geometry of the complex, as the chlorine may be pushing one of the hydrogens out of their favoured positions in the centre of the complex. Comparison of the bond lengths and angles for **3.21** with the dpppa analogues shows more similarities with the 'left' of the molecule being the arm with the 'chlorine' out of the slot and thus should resemble the dpppa analogue more closely, as the chlorine has little or no interactions with the rest of the molecule.

Throughout this chapter we have witnessed that the chemistry of dpptc and bdpppa is similar to that of dpppa, however there are some significant differences. For example, chelation of dpptc via use of $AgBF_4$ the thiophene sulfur proves unsuitable for chelation and the carbonyl oxygen is favoured. Bdpppa differs in respect that it acts as a bridging ligand but the method, and geometry of each end of the ligand is consistent with that of dpppa, as is displayed in $[Pt_2Cl_2(\eta\text{-}C_3H_6)_2$(bdpppa-*P,P*)]. Also the ability of bdpppa to by mono- and di-oxidised provides an interesting new ability that could not be replicated by dpppa.

Experimental: Chapter Three.

General Conditions.

All manipulations were carried out in a atmosphere of nitrogen, unless stated otherwise. All solvents were either freshly distilled from an appropriate drying agent (thf, Et_2O, dcm) or obtained as anhydrous grade from Aldrich. ^1H and ^{31}P NMR spectra were recorded using a Jeol Delta FT (270 MHz) spectrometer. IR spectra were recorded as KBr discs (prepared in air) on a Perkin Elmer 2000 FTIR/RAMAN spectrometer. All significant peaks (>800 cm^{-1}) are quoted to serve as a fingerprint. Silver salts, 2-thiophenecarboxamide, 2,6-pyridinedicarboxamide (Aldrich Chemical Co.) and BuLi (2.5M, Lancaster) were purchased and used as received. Triethylamine and chlorodiphenylphosphine were distilled prior to use. Dimethylaminopyridine (DMAP) was sublimed before use. The various metal starting materials were made by the appropriate literature methods, $[AuCl(tht)]$[5], $[MCl_2(cod)]$ (M = Pt or Pd, cod = cycloocta-1,5-diene)[6,7], $[PtMeCl(cod)]$[8], $[\{PtCl(\mu\text{-}Cl)(PMe_2Ph)\}_2]$[9], $[\{MCl(\mu\text{-}Cl)(Cp^*)\}_2]$ (M = Rh or Ir)[10], $[\{RuCl(\mu\text{-}Cl)(\eta^6\text{-}p\text{-}MeC_6H_4{}^iPr)\}_2]$[11], $[\{PdCl(\mu\text{-}Cl)(\eta^3\text{-}C_3H_5)\}_2]$[12].

***2-(Diphenylphosphino)thiophenecarboxamide (Dpptc)* (3.1):**

Chlorodiphenylphosphine (3.53 cm^3, 20 mmol) was added to a solution of 2-thiophenecarboxamide (2.5 g, 20 mmol), triethylamine (2.88 cm^3, 20.6 mmol) and DMAP (240 mg, 2 mmol) in THF (100 cm^3) and refluxed overnight. The reaction

mixture was filtered to remove a white solid (Et_3NHCl) and washed with THF (50 cm^3). The solvent was removed *in vacuo* leaving a pale yellow solid. This solid was recrystallised by cooling a concentrated methanol solution in a fridge overnight (yield: 3.28 g, 10.5 mmol, 54 %). $C_{17}H_{14}NOSP$ requires: C, 65.5, H, 4.53, N, 4.50. Found: C, 63.8, H, 4.09, N, 4.70%. ν_{max}/cm^{-1}: 3265, 1624, 1522, 1442, 1270, 1096, 996. ^{31}P NMR (109.3 MHz, $CDCl_3$), δ 25.9. ^1H NMR (270 MHz, $CDCl_3$), 7.6 (2H, m, aromatic), 7.5-7.3 (10H, m, aromatic), 7.1 (2H, m, aromatic).

2-(Diphenylphosphino)thiophenecarboxamide Sulfide (**3.3**): Sulfur (77 mg, 2.4 mmol) was added to a solution of 2-(Diphenylphosphino)thiophenecarboxamide (750 mg, 2.4 mmol) in toluene (20 cm^3) and refluxed overnight. The solvent was removed *in vacuo* leaving an off-white solid. This solid was recrystallised by cooling a concentrated toluene solution at 4°C overnight (yield: 1.39 g, 93 %). $C_{17}H_{14}NOPS_2$ requires: C, 59.5, H, 4.11, N, 4.08. Found: C, 59.2, H, 3.70, N, 4.48 %. ν_{max}/cm^{-1}: 3167, 1624, 1436, 1000. ^{31}P NMR (109.3 MHz, $CDCl_3$), δ 57.2 ppm. ^1H NMR ($CDCl_3$), δ 8.0 (3H, m, aromatic), 7.7-7.3 (6H, m, aromatic), 7.3-7.1 (4H, m, aromatic), 7.0 (1H, d, N-H).

[$PtCl_2$(dpptc-P)$_2$]: (**3.4**): Dpptc (166 mg, 0.53 mmol) and [$PtCl_2$(cod)] (100 mg, 0.27 mmol) were weighed into a schlenk type flask and dcm (5 cm^3) added. The solution was stirred for 10 min and the majority of the solvent removed *in vacuo*. A white solid was isolated after addition of Et_2O then filtered and washed with further ether (yield: 170 mg, 72 %). $C_{34.5}H_{29}N_2O_2P_2S_2Cl_3Pt$ requires: C, 44.5, H, 3.14, N, 3.01.

Found: C, 44.0, H, 3.89, N, 2.95 %. ν_{max}/cm^{-1}: 3214, 1672, 1424, 1398, 1042, 304, 273. ^{31}P NMR (109.3 MHz, $CDCl_3$), δ 27.9 ($J_{P\text{-}Pt}$ = 3870Hz). ^{1}H NMR (270 MHZ, $CDCl_3$), 9.7 (2H, d, J = 11 Hz, N-H), 7.8-6.9 (26H, m, aromatic).

[PdCl(η^3-C_3H_6)(dpptc-P)] (**3.5**): Dpptc (170 mg, 0.54 mmol) and [{Pd(μ-Cl)(η^3-C_3H_6)}$_2$] (100 mg, 0.27mmol) were weighed into a schlenk type flask and DCM (5 cm^3) added. The solution was stirred for 10min and the majority of the solvent removed *in vacuo*. A white solid was isolated after addition of Et_2O then filtered and washed with further ether (yield: 117 mg, 87%). $C_{20}H_{20}NOSPClPd$ requires: C, 48.5, H, 4.07, N, 2.83. Found: C, 48.3, H, 2.35, N, 2.82 %. ν_{max}/cm^{-1}: 3208, 1671, 1435, 1394, 1010, 277. ^{31}P NMR (109.3 MHz, $CDCl_3$), δ 54.3. ^{1}H NMR (270 MHz, $CDCl_3$), 9.4 (1H, d, J = 19Hz, N-H), 7.7 (1H, d, J = 1 Hz, thC[5]H), 7.7-7.6 (4H, m, aromatic), 7.5-7.3 (7H, m, aromatic) 7.1 (1H, dd, J = 3, 6 Hz, thC[4]) 5.5 (1H, m, allyl), 4.8 (1H, t, J = 6Hz, allyl), 3.7 (1H, dd, J = 10, 13 Hz, allyl), 3.3 (1H, obscured, allyl), 2.6 (1H, d, J = 13 Hz, allyl).

[PtCl$_2$(PPhMe$_2$)(dpptc-P)] (**3.6**): Dpptc (58 mg, 0.18 mmol) and [{PtCl(μ-Cl)(Me_2PhP)}$_2$] (75 mg, 0.093 mmol) were weighed into a schlenk type flask and DCM (5 cm^3) added. The solution was stirred for 10 min and the majority of the solvent removed *in vacuo*. A yellow solid was isolated after addition of Et_2O then filtered and washed with further ether (yield: 66 mg, 50 %). $C_{25}H_{25}NOSP_2Cl_2Pt$ requires: C, 39.7, H, 4.20, N, 2.01. Found: C, 40.0, H, 3.31, N, 1.72 %. ν_{max}/cm^{-1}: 3226, 1671, 1435, 948, 316, 281. ^{31}P NMR (109.3 MHz, $CDCl_3$) δ 29.7 (d, $J_{P\text{-}P}$ = 18.78 Hz, $J_{P\text{-}Pt}$ = 3890 Hz), -15.6 (d, $J_{P\text{-}P}$ = 18.78 Hz, $J_{P\text{-}Pt}$ = 3500 Hz). ^{1}H NMR (270MHz, $CDCl_3$) δ 11.4 (1H, d, J = 16 Hz, N-H), 8.6 (1H, d, J = 7 Hz, pyC[6]H), 8.2

(4H, m, aromatic), 7.9-7.4 (9H, m, aromatic), 1.6-1.4 (9H, m, Me-H) 1.0-0.8 (6H, m, -CH_2-).

[RuCl$_2$(p-Cymene)(dpptc-P)] (**3.7**): Dpptc (102 mg, 0.326 mmol) and [{RuCl(μ-Cl)(*p*-Cymene)}$_2$] (100 mg, 0.0163 mmol) were weighed into a schlenk type flask and dcm (5 cm^3) added. The solution was stirred for 10 min and the majority of the solvent removed *in vacuo*. A red solid was isolated after addition of Et_2O then filtered and washed with further ether (yield: 155 mg, 77%). $C_{27}H_{28}NOPCl_2Ru$ requires: C, 52.5, H, 4.57, N, 2.27. Found: C, 52.1, H, 3.48, N, 2.19 %. ν_{max}/cm^{-1}: 3312, 1665, 1435, 1404, 1091, 288. ^{31}P NMR (109.3 MHz, $CDCl_3$), δ 59.9. ^{1}H NMR (270 MHZ, $CDCl_3$), 8.0 (5H, m, aromatic) 7.9 (1H, d, J = 14 Hz, N-H), 7.6 (1H, dd, J = 1, 4 Hz), 7.5-7.3 (10H, m, Aromatic), 5.3-5.2 (4H, m, *p*-Cy), 2.5 (1H, m, C-H), 1.9 (3H, s, Me-H), 0.8 (6H, d, J = 7Hz, ^{i}Pr-H).

[RhCl$_2$(η^5-C$_5$Me$_5$)(dpptc-P)] (**3.8**): Dpptc (101 mg, 0.326 mmol) and [{RhCl(μ-Cl)(η^5-C_5Me_5)}$_2$] (100 mg, .0161 mmol) were weighed into a schlenk type flask and DCM (5 cm^3) added. The solution was stirred for 10 min and the majority of the solvent removed *in vacuo*. A red solid was isolated after addition of Et_2O then filtered and washed with further ether (yield: 159 mg, 80 %). $C_{27.5}H_{30}NSOPCl_3Rh$ requires: C, 49.8, H, 4.56, N, 2.11. Found: C, 50.7, H, 4.17, N, 2.27 %. ν_{max}/cm^{-1}: 3299, 1669, 1435, 1097, 246, 231. ^{31}P NMR (109.3 MHz, $CDCl_3$), δ 63.5 ($^1J_{Rh\text{-}P}$ = 148 Hz).. ^{1}H NMR (270 MHZ, $CDCl_3$), 8.2 (1H, d, J = 14 Hz, N-H) 8.1-8.0 (4H, m, aromatic) 7.7 (1H, d, J = 4 Hz, N-H), 7.5-7.3 (7H, m, aromatic), 7.0 (1H, t, J = 8 Hz, aromatic), 1.4 (15H, d, Cp*Me-H).

[PtClMe(dpptc-P)$_2$] **(3.9)**: Dpptc (39 mg, 0.12 mmol) and [PtClMe(cod)] (22 mg, 0.06 mmol) were weighed into a schlenk type flask and DCM (5 cm^3) added. The solution was stirred for 10 min and the majority of the solvent removed *in vacuo*. A yellow solid was isolated after addition of Et_2O then filtered and washed with further ether (yield: 34 mg, 65 %). $C_{35}H_{31}N_2S_2O_2P_2ClPt$ requires: C, 48.4, H, 3.60, N, 3.23. Found: C, 48.4, H, 3.40, N, 3.17 %. ν_{max}/cm^{-1}: 3209, 1671, 1435, 1094. ^{31}P NMR (109.3 MHz, $CDCl_3$), δ 49.1 ($J_{P\text{-}Pt}$ = 3220 Hz). ^{1}H NMR (270 MHZ, $CDCl_3$), 9.7 (2H, t, $J_{Pt\text{-}H}$ =19 Hz, N-H), 7.9 (10H, m, aromatic), 7.6-7.3 (14H, m, aromatic), 7.1 (2H, d, J = 3 Hz, thiophene), 1.5 (3H, s, Me).

[PdCl($C_9H_{12}N$)(dpptc-P)] **(3.10)**: Dpptc (79 mg, 0.25 mmol) and [Pd(μ-Cl)($C_9H_{12}N$)]$_2$ (70 mg, 0.13 mmol) were weighed into a schlenk type flask and DCM (5 cm^3) added. The solution was stirred for 10 min and the majority of the solvent removed *in vacuo*. A yellow solid was isolated after addition of Et_2O then filtered and washed with further ether (yield: 82 mg, 55 %). $C_{26}H_{26}N_2SOPClPd$ requires: C, 53.0, H, 4.63, N, 4.76. Found: C, 52.3, H, 4.52, N, 4.53 %. ν_{max}/cm^{-1}: 3171, 1672, 1438, 1259, 1101, 286. ^{31}P NMR (109.3 MHz, $CDCl_3$), δ 62.4ppm. ^{1}H NMR (270 MHZ, $CDCl_3$), 10.1 (1H, bs, N-H) 8.2 (4H, m, aromatic) 7.2-7.7 (10H, m, aromatic), 7.1 (1H, dd, J = 1, 4 Hz, aromatic) 7.0 (1H, d, J = 6 Hz, aromatic), 6.8 (1H, t, J = 15 Hz, aromatic) 6.4 (2H, m, aromatic) 2.9 (6H, s, N-Me).

[RuCl(p-Cy)(dpptc-P,O)] **(3.11)**: $AgBF_4$ (22 mg, 0.11 mmol) was added under dark conditions to a solution of [$RuCl_2$(*p*-Cy)(dpptc-*P*)] (70 mg, 0.11 mmol) in DCM (5 cm^3). The solution was stirred overnight and filtered through a celite bed. The majority of the solvent was removed *in vacuo*. An orange solid was isolated after

addition of Et_2O then filtered and washed with further ether (yield: 45 mg, 70%). $C_{28.5}H_{30}NOSPCl_2Ru$ requires: C, 47.3, H, 4.17, N, 1.93. Found: C, 48.0, H, 4.07, N, 2.02 %. ν_{max}/cm^{-1}: 3216, 1561, 1460, 1433, 1084. ^{31}P NMR (109.3 MHz, $CDCl_3$) δ 100.0. ^1H NMR (270 MHz, $CDCl_3$) δ 10.1 (1H, s, N-H), 8.3 (1H, d, J = 3Hz, thC[5]H), 8.0 (2H, m, aromatic), 7.7-7.1 (11H, m, aromatic), 5.9 (1H, dd, J = 7Hz, *p*-Cy-H), 5.6 (1H, dd, J = 6Hz, *p*-Cy-H), 5.3 (1H, m, *p*-Cy), 5.0 (1H, d, J = 6Hz, *p*-Cy) 2.6 (1H, m, C-H), 2.1 (3H, s, Me-H), 1.3 (6H, m, Pr^i-H).

Bis(2,6-diphenylphosphino)picolinamide. (bdpppa) (**3.12**): Chlorodiphenylphosphine (5.44 cm^3, 30.3 mmol) was added to a solution of 2,6-pyridinedicarboxamide (2.5 g, 30.3 mmol), triethylamine (4.44 cm^3, 32 mmol) and DMAP (370 mg, 3.0 mmol) in thf (100 cm^3) and refluxed overnight. The reaction mixture was filtered to remove a white solid (Et_3NHCl) and washed with thf (50 cm^3). The solvent was removed *in vacuo* leaving a pale yellow solid. This solid was recrystallised by cooling a concentrated methanol solution at 4°C overnight (yield: 4.89 g, 61 %). $C_{31.5}H_{26}N_3O_2P_2Cl$ requires: C, 66.0, H, 4.50, N, 7.22. Found: C, 65.7, H, 4.41, N, 7.40 %. ν_{max}/cm^{-1}: 3345, 3262, 1665, 1646,, 1588, 1571, 1408, 999. ^{31}P NMR ($CDCl_3$) 21.9. ^1H NMR ($CDCl_3$), 8.42 (2H, d, J = 8 Hz, N-H), 8.00 (3H, m, py), 7.5-7.1 (21H, m, aromatic).

Bis(2,6-diphenylphosphino)picolinamide disulfide (**3.13**): Sulfur (120 mg, 3.7 mmol) was added to a solution of bis(2,6-diphenylphosphino)picolinamide (1 g, 3.7 mmol) in toluene (20 cm^3) and refluxed for 10 minutes. The solvent was removed *in vacuo* leaving an off-white solid. This solid was recrystillised by cooling a

concentrated toluene solution at 4°C overnight (yield: 876 mg, 78 %). $C_{31}H_{25}N_3O_2P_2S_2$ requires: C, 63.8, H, 4.32, N, 4.80. Found: C, 64.1, H, 4.46, N, 4.50 %. ν_{max}/cm^{-1}: 3360, 1697, 1424, 999. ^{31}P NMR ($CDCl_3$) 55.1 ppm. ^1H NMR ($CDCl_3$), δ 8.9 (2H, d, J = 9Hz, N-H), 8.3 (2H, d, J = 8Hz, pyC[3,5]H), 8.1-7.9 (8H, m, aromatic), 7.6-7.4 (10H, m, aromatic), 7.1-7.3 (3H, m, aromatic).

2,5-bis(Diphenylphosphino)picolinamide diselenide (**3.14**): Selenium (74 mg, 0.9 mmol) was added to a solution of 2,5-bis(Diphenylphosphino)picolinamde (250 mg, 0.47 mmol) in toluene (20 cm^3) and refluxed for 10 min. The solvent was removed *in vacuo* leaving an off-white solid. This solid was recrystillised by cooling a concentrated toluene solution in a fridge overnight (yield: 263 mg, 81 %). $C_{31}H_{25}N_3O_2P_2Se_2$ requires: C, 53.9, H, 3.64, N, 6.08. Found: C, 53.7, H, 3.24, N, 6.17 %. ν_{max}/cm^{-1}: 3256, 1698, 1421, 998. ^{31}P NMR (109.3 MHz, $CDCl_3$), δ 49.6 ($^1J_{P=Se}$ =795 Hz). ^1H NMR (270 MHz, $CDCl_3$), δ 8.8 (2H, d, J = 9Hz, N-H), 8.3 (1H, d, J = 8Hz, pyC[6]H), 8.0 (8H, m, aromatic), 7.5 (13H, m, aromatic).

Bis(2,6-diphenylphosphino)picolinamide monosulfide (**3.15**). Sulfur (36 mg, 0.37 mmol) was added to a solution of bis(2,6-diphenylphosphino)picolinamide (600 mg, 0.37 mmol) in toluene (20 cm^3) and refluxed for 10 minutes. The solvent was removed *in vacuo* leaving an off-white solid. This solid was recrystallised by cooling a concentrated toluene solution at 4°C overnight (yield: 415 mg, 65 %). $C_{31}H_{25}N_3O_2P_2S$ requires: C, 65.7, H, 4.46, N, 7.43. Found: C, 67.4, H, 4.47, N, 7.20 %. ν_{max}/cm^{-1}: 3345, 3262, 1697, 1665, 1646, 1432, 999. ^{31}P NMR ($CDCl_3$) 56.0 (s, P=S), 21.7 (s, P^{III}). ^1H NMR ($CDCl_3$), δ 8.8 (2H, d, J = 9Hz, N-H), 8.4 (4H, m aromatic), 7.8-8.1 (5H, m, aromatic), 7.0-7.6 (14H, m, aromatic).

Bis(2,6-diphenylphosphino)picolinamide monosulfide monoselenide (**3.16**): Selenium (22 mg, 0.26 mmol) was added to a solution of bis(2,6-diphenylphosphino)picolinamide monosulfide (150 mg, 0.26 mmol) in toluene (10 cm^3) and refluxed for 10 minutes. The solvent was removed *in vacuo* leaving an off-white solid. This solid was recrystillised by cooling a concentrated toluene solution at 4°C overnight (yield: 120 mg, 71 %). $C_{31}H_{25}N_3O_2P_2SSe$ requires: C, 57.7, H, 3.91, N, 6.52. Found: C, 58.8, H, 3.68, N, 6.30 %. ν_{max}/cm^{-1}: 3449, 1697, 1421, 997. ^{31}P NMR ($CDCl_3$) 55.0 (s, P=S), 49.7 (s, P=Se, $^1J_{P\text{-}Se}$ = 789 Hz). ^1H NMR ($CDCl_3$), δ 8.8 (2H, d, J = 8 Hz, N-H), 8.3 (2H, dd, J = 8, 1 Hz, pyC[3,5]H), 7.9-8.1 (7H, m, aromatic), 7.6-7.4 (14H, m, aromatic).

[{AuCl} (bdpppa-S)] (**3.17**): [AuCl(tht)] (57 mg, 0.17 mmol) and Bis(2,6-diphenylphosphino)picolinamide (100 mg, 0.17 mmol) were added to a round bottomed flask and dcm (5 cm^3) added. The solvent volume was reduced to ~1 cm^3 and the product precipitated with n-hexane (20 cm^3). Yield 93 mg, 66%. $C_{32}H_{26}N_3O_2P_2SAuCl_3$ requires: C, 41.9, H, 2.80, N, 4.58. Found: C, 41.7, H, 2.74, N, 4.69 %. ν_{max}/cm^{-1}: 3256, 1697, 1437, 999. ^{31}P NMR ($CDCl_3$) δ(P) 55.0 (s, P=S), 50.2 (s, P-Au). ^1H NMR ($CDCl_3$) δ(H) 10.2 (2H, bs, N-H), 7.0-8.0 (23H, m, aromatic).

[{AuCl} (bdpppa)] (**3.18**): A solution of [AuCl(tht)] (120 mg, 0.37mmol) in dcm (10 cm^3) was dropped into a solution of Bis(2,6-diphenylphosphino)picolinamide (200 mg, 0.37 mmol) in dcm (15 cm^3). The solvent volume was reduced to ~1cm^3 and the product precipitated with n-hexane (20cm^3). Yield 240 mg, 83 %. $C_{31}H_{25}N_3O_2P_2AuCl$ requires: C, 48.6, H, 3.29, N, 5.49. Found: C, 48.2, H, 2.91, N,

5.48 %. ν_{max}/cm^{-1}: 3054, 1698, 1436, 999. ^{31}P NMR ($CDCl_3$) δ(P) 64.3. ^{1}H NMR ($CDCl_3$) δ(H) 11.0 (2H, bs, N-H), 9.0 (2H, m, aromatic), 7.1-8.1 (21H, m, aromatic).

[{AuCl}$_2$(bdpppa)] (**3.19**): [AuCl(tht)] (84 mg, 0.26 mmol) and Bis(2,6-diphenylphosphino)picolinamide (70 mg, 0.13 mmol) were added to a round bottomed flask and dcm (5 cm^3) added. The solvent volume was reduced to ~1 cm^3 and the product precipitated with n-hexane (20 cm^3). Yield 125 mg, 95 %. $C_{31}H_{25}N_3O_2P_2Au_2Cl_2$ requires: C, 37.3, H, 2.52, N, 4.21. Found: C, 37.16, H, 2.37, N, 4.12%. ν_{max}/cm^{-1}: 3261, 1697, 1436, 999. ^{31}P NMR ($CDCl_3$) δ(P) 50.0. ^{1}H NMR ($CDCl_3$) δ(H) 10.2 (2H, d, J_{H-H} = 16 Hz, N-H), 8.1 (2H, m, aromatic), 7.9-7.6 (8H, m, aromatic), 7.6-7.1 (13H, m, aromatic).

[Pd$_2$Cl$_2$(allyl)$_2$(bdpppa-P,P)] (**3.20**): Bdpppa (397 mg, 0.7.45 mmol) and [{Pd(μ-Cl)(η^3-C_3H_6)}$_2$] (272 mg, 0.373 mmol) were weighed into a schlenk type flask and dcm (10 cm^3) added. The solution was stirred for 10 min and the majority of the solvent removed *in vacuo*. A white solid was isolated after addition of Et_2O then filtered and washed with further ether (yield: 671 mg, 91 %). $C_{37}H_{37}N_3O_2P_2Cl_2Pd_2$ requires: C, 49.3, H, 4.13, N, 4.66. Found: C, 49.23, H, 3.68, N, 4.57%. ν_{max}/cm^{-1}: 3351, 3209, 1698, 1434, 1385, 999. ^{31}P NMR (109.3 MHz, $CDCl_3$), δ 55.1. ^{1}H NMR (270 MHZ, $CDCl_3$), 10.2 (2H, d, J = 18 Hz, N-H), 8.2 (2H, d, J = 8 Hz), pyC[6]H), 8.0-7.8 (10H, m, aromatic), 7.6-7.4 (10H, m, aromatic), 5.5 (4H, quin, J = 10 Hz, allyl), 4.7 (4H, t, J = 7Hz, allyl), 3.7 (2H, t, J = 10 Hz, allyl).

[$Pt_2Cl_2(allyl)_2$(bdpppa-P,P)] (**3.21**): Bdpppa (59 mg, 0.092 mmol) and [{Pt(μ-Cl)(η^3-C_3H_6)}$_4$] (60 mg, 0.046mmol) were weighed into a schlenk type flask and THF (5 cm^3) added. The solution was stirred for 10 min and the majority of the solvent removed *in vacuo*. A white solid was isolated after addition of Et_2O then filtered and washed with further ether (yield: 43 mg, 43 %). $C_{37}H_{37}N_3O_2P_2Cl_2Pt_2$ requires: C, 41.1, H, 3.46, N, 3.90. Found: C, 40.3, H, 3.59, N, 3.86 %. ν_{max}/cm^{-1}: 3360, 3231, 1700, 1434, 1000. ^{31}P NMR (109.3 MHz, $CDCl_3$), δ 51.7 ($^1J_{Pt\text{-}P}$ = 4730Hz). ^{1}H NMR (270 MHZ, $CDCl_3$), 10.2 (2H, d, J = 10 Hz, N-H), 8.2 (2H, d, J = 8Hz), pyC[6]H), 8.0-7.8 (10H, m, aromatic), 7.7-7.3 (12H, m, aromatic), 5.3 (2H, m, allyl), 5.0 (2H, m, allyl), 4.3 (2H, m, allyl), 3.2 (2H, m, allyl), 3.0 (2H, m, allyl), 2.2 (2H, m, allyl).

REFERENCES: Chapter Three

1. O. Clot, M. O. Wolf, G. P. A. Yap, B. O. Patrick, *J. Chem. Soc. Dalton Trans.*, 2000, 2729.
2. F. E. Wood, J. Hvoslef, H. Hope, A. L. Batch, *Inorg. Chem.*, 1984, **23**, 4309.
3. P. Giannoccaro, G. Vasapollo, A. Sacco, *J. Chem. Soc., Chem. Commun.*, 1980, 1136.
4. W. Keim, *Chem. Ing. Techn.*, 1984, **56**, 850.
5. R. Uson, A. Laguna and M. Laguna, *Inorg. Synth.*, 1989, **26**, 85.
6. D. Drew and J. R. Doyle, *Inorg. Synth*, 1991, **28**, 346.
7. J. X. McDermott, J. F. White and G. M. Whiteside, *J. Am. Chem. Soc.*, 1976, **60**, 6521.
8. H. C. Clark and L. E. Manzer, *J. Organomet. Chem.*, 1973, **59**, 411.
9. W. Baratta and P. S. Pregosin, *Inorg. Chem Acta.*, 1993, **209**, 85.
10. C. White, A. Yates, P. M. Maitlis, *Inorg. Synth.*, 1992, **29**, 228.
11. M. A. Bennett, T. N. Huang, T. W. Matheson, A. R. Smith, *Inorg. Synth.*, 1982, **21**, 74.
12. A. L. Balch, L. S. Benner, *Inorg. Synth.*, 1990, **28**, 340.
13. S. M. Aucott, A. M. Z. Slawin and J. D. Woollins, *J. Chem. Soc., Dalton Trans*, 2000, 2559.

CHAPTER FOUR: Synthesis and Coordination of 7-diphenylphosphinoazaindole (dppai).

4.1 Introduction.

The basis of the work in this chapter is to investigate the chemistry of an analogue of dppap (**A**), which has the ability to rotate around the amine functionality removed by addition of a second ring providing a stabilising influence (**B**). The coordination chemistry of this new ligand will be compared to that of dppap.

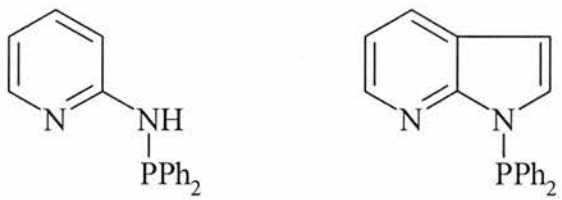

A **B**

Figure 4.1: *Representation of the difference between dppap and dppai.*

The chemistry of dppap has been thoroughly explored by Aucott *et al* and a summary can be seen in figure 4.2[1].

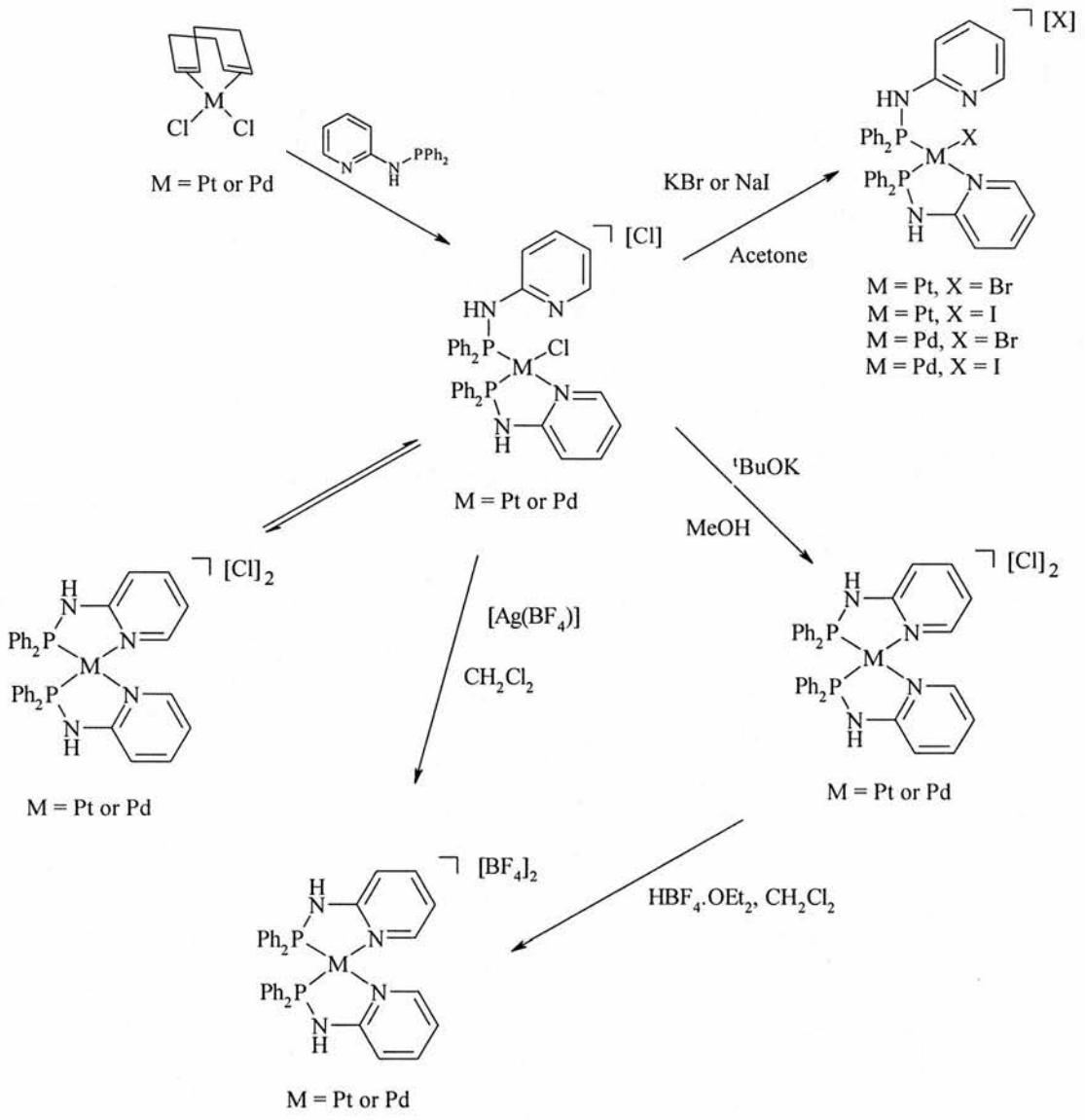

Figure 4.2: *The coordination chemistry of dppap.*

We will investigate the effect this stabilised dppap derivative has when exposed to similar chemistry.

4.2 Results and Discussion.

4.2.1: Synthesis of dppai.

The synthesis of 7-diphenylphosphinoazaindole (dppai, **4.1**) proceeds along the same lines as all the ligand synthesis already discussed throughout this work. Chlorodiphenylphosphine in thf was added dropwise to a tetrahydrofuran solution of 7-azaindole, 10 % excess triethylamine and 10 % DMAP and then refluxed overnight. The crude product obtained from the usual workup was purified by recrystallisation from a concentrated diethyl ether, subsequently cooled to 4°C and the resulting colourless precipitate was filtered to give **4.1**.

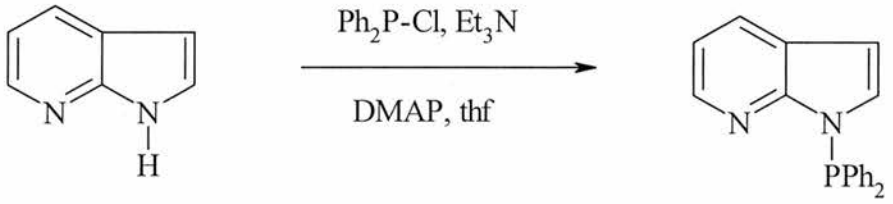

4.1

Figure 4.3: *Synthesis of dppai (**4.1**).*

This colourless solid is the least air stable of all the ligand so far discussed, it will completely degrade when exposed to air for a few days, it is however very soluble in all common laboratory solvents. The yield of the reaction was poor, being 36 %. The ^{31}P NMR ($CDCl_3$) displays a singlet at δ(P) 33.2 ppm, this is a reasonable match with dppap (26.4 ppm). With this ligand we have no amide proton to observe which reduces the usefulness of proton NMR, however the pyC[6] proton is apparent in the spectrum, in the case of **4.1** it appears at δ(H) 8.4 ppm as a double doublet, with coupling constants ($J_{H\text{-}H}$) 5 and 2 Hz. In comparison with our previous ligands, IR is still a useful tool in the case of dppai, but for different reasons. This is mainly due to the lack of an amide proton and carbonyl both of which are important markers in the previous ligands. However we can still observe the ν(P-N) stretch, which for **4.1** falls

at 983 cm^{-1}, this is a small but marked change from our amide examples, which is not overly surprising given that the nitrogen is not part of the amine group. More significantly is that we can still follow the ν(C-N) stretch in the pyridyl ring, which if dppai follows a similar pattern to dppap will show some significant changes. The value for dppai is 1589 cm^{-1}.

4.2.2: *Complexes of dppai.*

Reaction of dppai with [$PtCl_2$(cod)] in dichloromethane generates two products, of which only one could be isolated in a pure form. After analysis it becomes clear that the pure sample is a 1:1 product ([$PtCl_2$(dppai-*P,N*)], **4.2**), and the non-isolated compound is a 2:1 variant. ^{31}P NMR is the most useful tool for monitoring this chemistry. When the 2:1 reaction was performed two products can be observed, one with precise, sharp peaks, the other with broad, shorter peaks. Both display the expected platinum satellites and both only 1 ppm difference being at δ(P) 55 and 54 ppm respectively. The broad peaks indicate a possibility of fluxionality in the molecule. To try to gain more information about the peaks the 1:1 reaction was also performed, this provided a clean reaction generating only one of the two previously seen peaks, the one at δ(P) 55 ppm, with a $^{1}J_{Pt\text{-}P}$ of 4160 Hz which is consistent with a phosphorus *trans*- to a chloride, however its not enough information for us to confirm whether this is one ligand bidentate bound, or two ligands monodentate bound. This is also a significantly larger coupling constant than the average value seen in dppap (3576 Hz) for the equivalent reaction[1]. The ^{1}H NMR is also enlightening with respect to the pyC[6] proton, as predicted on chelation this proton shows a considerable shift. The proton is found at δ(H) 9.4 ppm as a doublet

($^2J_{H\text{-}H}$ = 6 Hz) with platinum satellites giving a $^3J_{Pt\text{-}H}$ = 43 Hz, this is confirmation that we are considering a chelate complex, as platinum satellites can only occur if this is the case. As was indicated earlier the IR data should also provide some confirmation regarding the chelation of the ligand in this system. The *v*(C-N) stretch in **4.2** is found at 1648 cm^{-1}, this is a considerable shift from the value for the free ligand (1589cm^{-1}) and provides any final confirmation about the geometry of this compound. Also there are two *v*(M-Cl) stretches observed in the spectrum at 339 and 318 cm^{-1}, the presence of two peaks again indicates two chlorides bound *cis* to the metal centre.

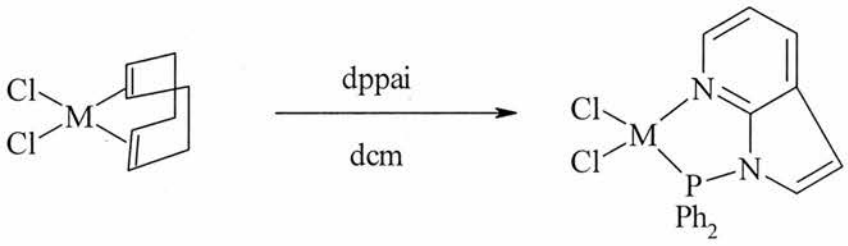

M = Pt (**4.2**) or Pd (**4.3**)

Figure 4.4: *Chelation of dppai.*

The major difference between the dppai and dppap examples is stark, there is no second ligand bound in a monodentate fashion, the only possible reason for this difference is the lack of flexibility in dppai with the second ring providing a great deal of rigidity as opposed to the flexibility inherent in dppap. The conclusions based on the spectroscopic evidence were proved correct by the crystallographic analysis of a crystal formed by vapour diffusion of diethyl ether into a concentrated $CDCl_3$ solution of **4.2**.

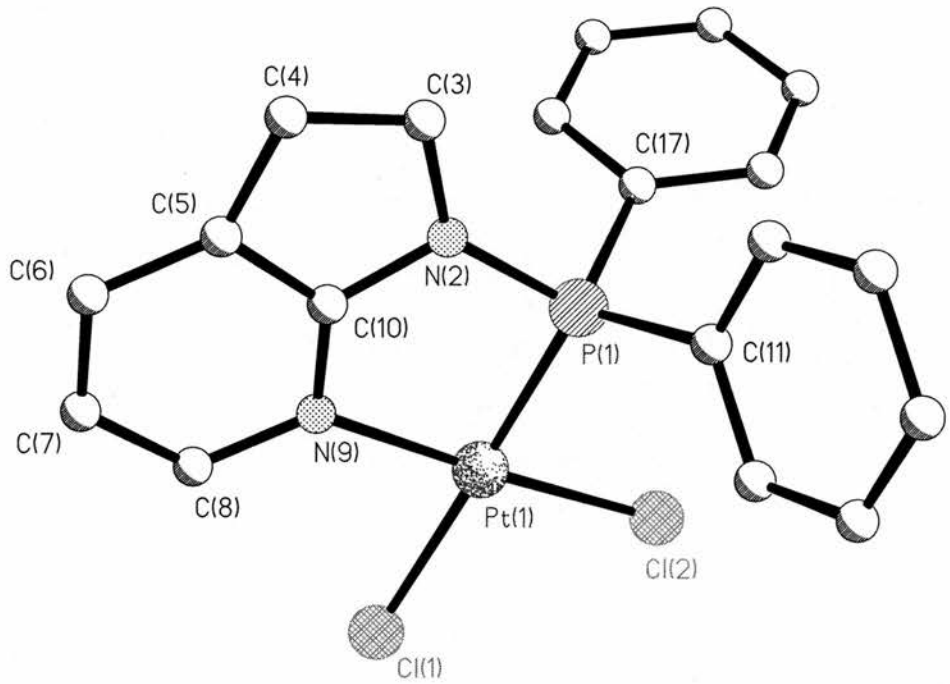

Figure 4.5: *Crystallographic representation of [$PtCl_2$(dppai-P,N)]* ***(4.2)****.*

As can be seen in the diagram there are no hydrogen-bond interactions, mostly because the lack of the amide proton means there are no available protons for such an interaction. However we can see that the square planar geometry is confirmed, and that the expected five-membered ring is indeed present, this ring is effectively planar.

Table*: **4.1** Selected bond lengths (Å) and angles (°) for [$PtCl_2$(dppai-P,N)]* ***(4.2)****.*

P(1)-Pt(1)	2.2003(11)	P(1)-C(11)	1.809(4)
P(1)-C(17)	1.808(4)	P(1)-N(2)	1.716(4)
Pt(1)-Cl(1)	2.3385(11)	Pt(1)-Cl(2)	2.3067(11)
N(2)-C(10)	1.373(5)	N(9)-C(10)	1.326(5)
Pt(1)-N(9)	2.039(3)		

P(1)-Pt(1)-Cl(1)	176.70(4)	P(1)-Pt(1)-Cl(2)	91.05(4)
P(1)-Pt(1)-N(9)	85.93(10)	Pt(1)-P(1)-N(2)	99.70(12)
C(11)-P(1)-C(17)	107.25(18)	C(17)-P(1)-N(2)	104.72(18)
C(11)-P(1)-N(2)	106.48(18)	P(1)-N(2)-C(10)	116.5(3)
N(2)-C(10)-N(9)	123.0(4)	C(10)-N(9)-Pt(1)	114.8(3)

As can be seen from the bond angles listed in table 4.1, there are slight distortions away from an idealised square planar geometry. The main value to note is P(1)-Pt(1)-N(9), being 85.93°, this slightly larger than the value observed in the dppap (chelated) example which was 82.90°. This larger value is most likely due to the reduced steric bulk found in the dppai example due to the lack of a second ligand, with a chloride occupying the coordination site as oppose to a ligand.

To confirm these assumptions, and to improve our understanding of the one ligand phenomenon, the analogous reaction with [$PdCl_2$(cod)] was carried out. The reaction was carried out on a 1:1 scale in dichloromethane, as well as 2:1, however both reactions generating the same product in the pure form in both cases. This product generated was [$PdCl_2$(dppai-*P,N*)] (**4.3**) which displays only a sharp singlet in the ^{31}P NMR at δ(P) 81 ppm. This would indicate that a similar arrangement is found in the solid state; even-though this is a large shift in the peak. Initial observation of the ^{1}H NMR spectrum shows similarity to the data seen for its platinum analogue. The pyridyl proton is again shifted and to a similar position, δ(H) 9.2 ppm and again is a doublet with a J = 6 Hz. From these data we can once again assume the ligand is bidentate bound. Examination of the IR data also provided further confirmation of these assumptions, the ν(C-N) stretch is once again seen at 1640 cm^{-1}, identical to **4.2**,

and two ν(Pd-Cl) stretches are present at 344 and 312 cm^{-1}, this data supports the idea that dppai is again chelated in this complex.

Once again crystallographic analysis was performed on **4.3** in a hope that it would shed some light on the question of rigidity in the ligand. The crystal was grown from slow evaporation of a concentrated dichloromethane solution of the complex.

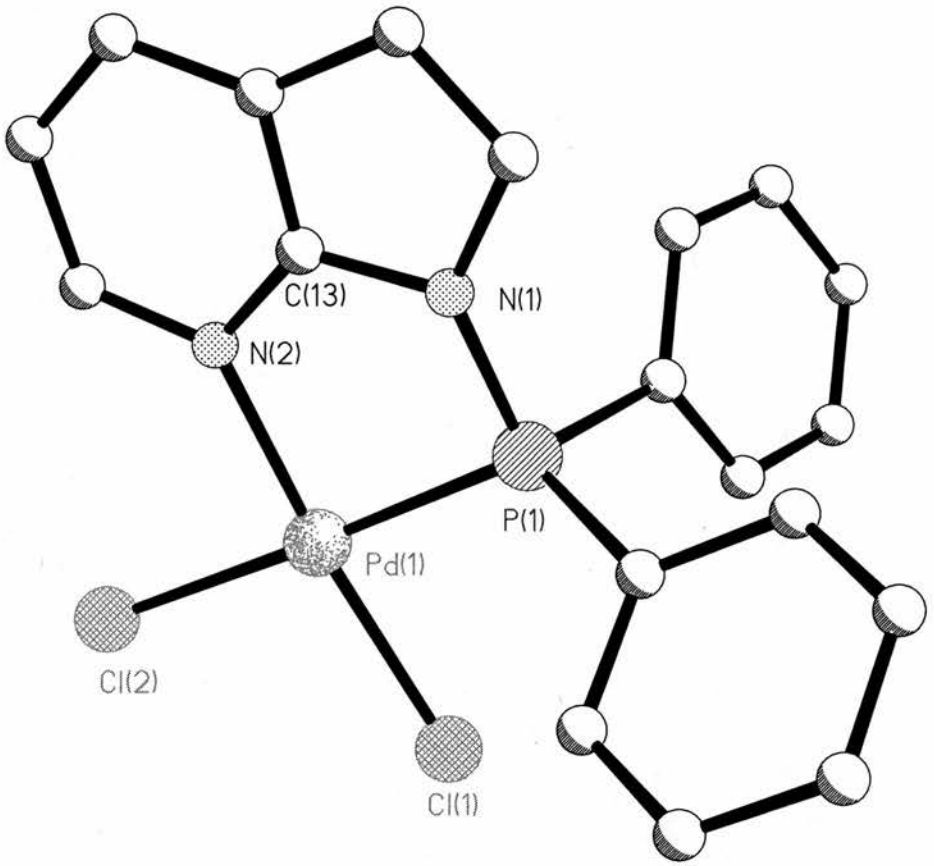

Figure 4.6: *Crystallographic representation of [$PdCl_2$(dppai-P,N)]* ***(4.3)****.*

On initial inspection figure 4.6 looks very similar to figure 4.5, which confirms our conclusions from the spectroscopic data.

***Table**: **4.2** Selected bond lengths (Å) and angles (°) for [$PdCl_2$(dppai-P,N)] (**4.3**).*

P(1)-Pd(1)	2.2159(7)	P(1)-C(11)	1.804(3)
P(1)-C(7)	1.804(3)	P(1)-N(1)	1.719(2)
Pd(1)-Cl(1)	2.2887(8)	Pd(1)-Cl(2)	2.3450(7)
N(1)-C(13)	1.374(4)	N(2)-C(13)	1.337(4)
Pd(1)-N(2)	2.043(2)		
P(1)-Pd(1)-Cl(1)	88.80(3)	P(1)-Pd(1)-Cl(2)	177.66(3)
P(1)-Pd(1)-N(2)	85.38(7)	Pd(1)-P(1)-N(1)	99.44(8)
C(11)-P(1)-C(7)	106.59(12)	C(7)-P(1)-N(1)	107.39(12)
C(11)-P(1)-N(1)	104.59(12)	P(1)-N(1)-C(13)	115.85(19)
N(1)-C(13)-N(2)	122.7(2)	C(13)-N(2)-Pd(1)	114.81(18)

The P(1)-Pd(1)-N(2) angle remains effectively identical to its platinum analogue, as do the majority of the other major angles.

When dppai was reacted with [PtClMe(cod)] and [PtClPh(cod)] the expected bidentate complex was formed, giving [PtClMe(dppai-*P,N*)] (**4.4**) and [PtClPh(dppai-*P,N*)] (**4.5**) respectively. Unfortunately full spectral analysis was difficult to obtain due to both poor yield and purity, however vapour diffusion of diethyl ether into the NMR sample generated a crystal suitable for analysis in both cases. The ^{31}P NMR in both cases showed peaks consistent with the earlier platinum examples with resonances observed at δ(P) 60.9 ppm, and 58.5 ppm for **4.4** and **4.5** respectively, with $^{1}J_{Pt\text{-}P}$ = 5070 Hz for **4.4** and 4960 Hz for **4.5**.

The crystallographic analysis shows two complexes that are isomorphorus in every way but for the difference in the Me and Ph on the platinum centre. Here we will consider **4.4** for discussion.

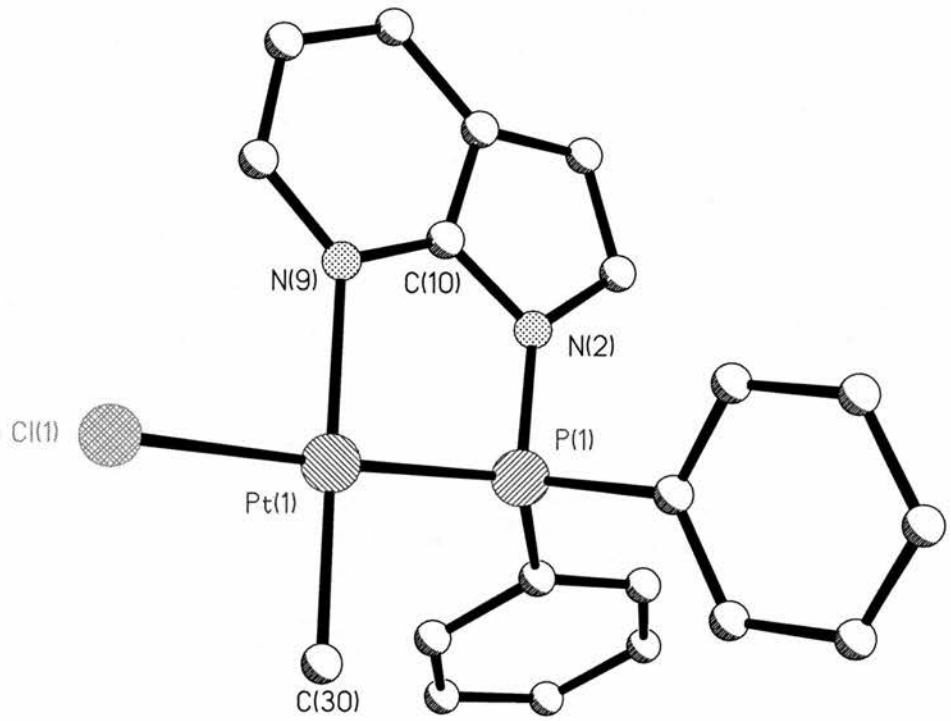

Figure 4.7: *Crystallographic representation of [PtClMe(dppai-P,N)]* ***(4.4)****.*

As can be observed in diagram 4.7 the structure is very similar to the $\{PtCl_2\}$ and $\{PdCl_2\}$ examples seen earlier in this chapter with a planar five-membered ring Also no hydrogen bonding is observed, as there are no available protons.

Table*: **4.3** Selected bond lengths (Å) and angles (°) for [PtClMe(dppai-P,N)]* ***(4.4)****.*

P(1)-Pt(1)	2.168(2)	P(1)-C(11)	1.823(7)

P(1)-C(17)	1.799(7)	P(1)-N(2)	1.730(6)
Pt(1)-Cl(1)	2.349(2)	Pt(1)-C(30)	2.042(8)
N(2)-C(10)	1.369(10)	N(9)-C(10)	1.333(11)
Pt(1)-N(9)	2.145(7)		
P(1)-Pt(1)-Cl(1)	177.37(6)	P(1)-Pt(1)-C(30)	93.7(3)
P(1)-Pt(1)-N(9)	85.35(19)	Pt(1)-P(1)-N(2)	101.1(2)
C(11)-P(1)-C(17)	105.6(4)	C(17)-P(1)-N(2)	104.9(3)
C(11)-P(1)-N(2)	103.0(3)	P(1)-N(2)-C(10)	117.2(5)
N(2)-C(10)-N(9)	123.2(7)	C(10)-N(9)-Pt(1)	112.5(5)

The length of the phosphorus-nitrogen bond is however slightly longer in this example, being 1.730(6) Å compared to 1.719(2) and 1.716(4) Å for our previous examples. However when we consider the bonds around the metal centre we can observe a difference which statistically negligible, **4.4** shows a Pt-N length of 2.145(7) Å where as **4.2** has a length of 2.039(3) Å. However the phosphorus-platinum difference is negligible. These figures could be explained by recognising that the pyridyl nitrogen is *trans* to the new alkyl substituent. The other bond lengths show no significant deviation between the two platinum examples.

The bond lengths displayed in table 4.3 show the same distorted square planar geometry as seen earlier in the chapter, the remaining angles also agrees closely with **4.2** and **4.3**.

It is immediately apparent that the chemistry of dppai is considerably different from that of dppap. Rigidity must be the controlling factor in the difference in

coordination chemistry. It is likely this rigidity causes only one ligand to be bound, as was stated the 2:1 stoichiometry provided a highly fluxional compound that could not be isolated. The added flexibility (through the N-H spacer) must allow the extra space required for a second ligand around the metal.

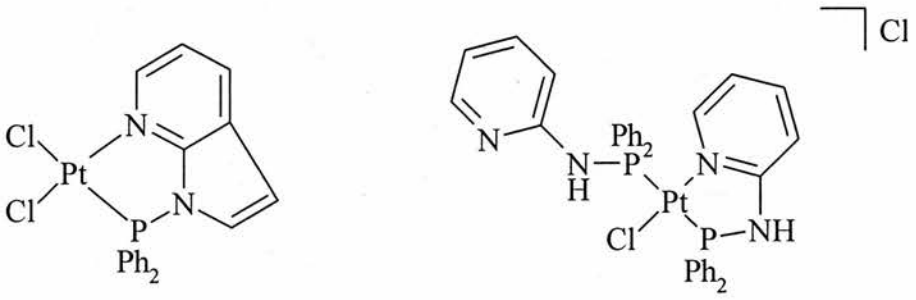

Figure 4.8: *Illustration of the differences on coordination of dppap and dppai.*

Experimental: *Chapter Four*

General Conditions

All manipulations were carried out in an atmosphere of nitrogen, unless stated otherwise. All solvents were either freshly distilled from an appropriate drying agent (thf, Et_2O, dcm) or obtained as anhydrous grade from Aldrich. ^{1}H and ^{31}P NMR spectra were recorded using a Jeol Delta FT (270 MHz) spectrometer. IR spectra were recorded as KBr discs (prepared in air) on a Perkin Elmer 2000 FTIR/RAMAN spectrometer. All significant peaks (>800 cm^{-1}) are quoted to serve as a fingerprint. Silver salts, 1H-indole (Aldrich Chemical Co.) and BuLi (2.5M, Lancaster) were purchased and used as received. Triethylamine and chlorodiphenylphosphine were distilled prior to use. Dimethylaminopyridine (DMAP) was sublimed before use. The various metal starting materials were made by the appropriate literature methods, $[MCl_2(cod)]$ (M = Pt or Pd, cod = cycloocta-1,5-diene)[2,3], [PtMeCl(cod)][4].

7-diphenylphosphinoazaindole **(dppai) (4.1)**: Chlorodiphenylphosphine (3.80 cm^3, 21.1 mmol) was added to a solution of 1H-indole (2.5 g, 21.1 mmol), triethylamine (3.10 cm^3, 22.2 mmol) and DMAP (259 mg, 2.1 mmol) in THF (100 cm^3) and refluxed overnight. The reaction mixture was filtered to remove a white solid (Et_3NHCl) and washed with THF (50 cm^3). The solvent was removed *in vacuo* leaving a pale yellow solid. This solid was recrystallised by cooling a concentrated

diethyl ether solution in a fridge overnight (yield: 2.3 g, 36 %). ν_{max}/cm^{-1}: 1589, 1405, 983. ^{31}P NMR (109.3 MHz, $CDCl_3$), δ 33.2. ^{1}H NMR (270 MHz, $CDCl_3$), 8.4 (1H, dd, J = 5 Hz, 2 Hz, aromatic), 7.9 (1H, dt, J = 8 Hz, 1 Hz, aromatic), 7.4-7.3 (10H, m, aromatic), 7.1 (1H, dd, J = 8 Hz, 5 Hz, aromatic), 7.0 (1H, dd, J = 4 Hz, 2Hz, aromatic), 6.5 (1H, dd, J = 4 Hz, 1 Hz, aromatic).

[PtCl$_2$(dppai-P,N)] (**4.2**): Dppai (81 mg, 0.268 mmol) and [$PtCl_2$(cod)] (100 mg, 0.268 mmol) were weighed into a schlenk type flask and DCM (5 cm^3) added. The solution was stirred for 10 min and the majority of the solvent removed *in vacuo*. A white solid was isolated after addition of Et_2O then filtered and washed with further ether (yield: 56 mg, 37 %). $C_{19}H_{15}N_2PCl_2Pt$ requires: C, 40.1, H, 2.66, N, 4.93. Found: C, 40.7, H, 2.68, N, 4.86%. ν_{max}/cm^{-1}: 1648, 1438, 1107, 996. ^{31}P NMR (109.3 MHz, $CDCl_3$), δ 55.4 ($J_{P\text{-}Pt}$ = 4160 Hz). ^{1}H NMR (270 MHZ, $CDCl_3$), 9.4 (1H, m, $J_{P\text{-}H}$ = 6 Hz, $J_{Pt\text{-}H}$ = 43 Hz, pyC[6]H), 8.1 (2H, m, aromatic), 7.8 (3H, m, aromatic), 7.5 (5H, m, aromatic), 7.2 (4H, m, aromatic).

[PdCl$_2$(dppai-P,N)] (**4.3**): As **4.2**. Dppai (106 mg, 0.35 mmol), and [$PdCl_2$(cod)] (100 mg, 0.35 mmol) gave a yellow solid (yield: 133 mg, 79 %). $C_{19}H_{15}N_2PCl_2Pd$ requires: C, 47.5, H, 3.15, N, 5.84. Found: C, 47.0, H, 2.63, N, 5.95 %. %. ν_{max}/cm^{-1}: 1438, 1104, 994, 344, 312. . ^{31}P NMR (109.3 MHz, $CDCl_3$), δ 80.5. ^{1}H NMR (270 MHZ, $CDCl_3$), 9.2 (1H, dd, $J_{P\text{-}H}$ = 6 Hz, pyC[6]H), 8.1 (1H, m, aromatic), 7.8 (4H, m, aromatic), 7.7-7.6 (2H, m, aromatic), 7.6-7.5 (4H, m, aromatic), 7.3 (1H, dd, aromatic), 7.2 (1H, m, aromatic), 7.0 (1H, m, aromatic).

REFERENCES: Chapter Four.

1. S. M. Aucott, A. M. Z. Slawin and J. D. Woollins, *J. Chem. Soc., Dalton Trans*, 2000, 2559.
2. D. Drew and J. R. Doyle, *Inorg. Synth*, 1991, **28**, 346.
3. J. X. McDermott, J. F. White and G. M. Whiteside, *J. Am. Chem. Soc.*, 1976, **60**, 6521.
4. H. C. Clark and L. E. Manzer, *J. Organomet. Chem.*, 1973, **59**, 411.

CHAPTER FIVE: Investigating The Effects of Steric Hindrance On The Coordination of Three 2-aminothiazoyl based Ligands.

5.1: Introduction.

The chemistry discussed in this chapter is based on a number of different areas. Firstly an initial description could by based around a similar area to that pursued in Chapter Four, namely the chemistry of dppap, but the initial chemistry can also be compared to that of phosphino oxalines, which was described in Chapter One, an example of which is shown in figure 5.1.

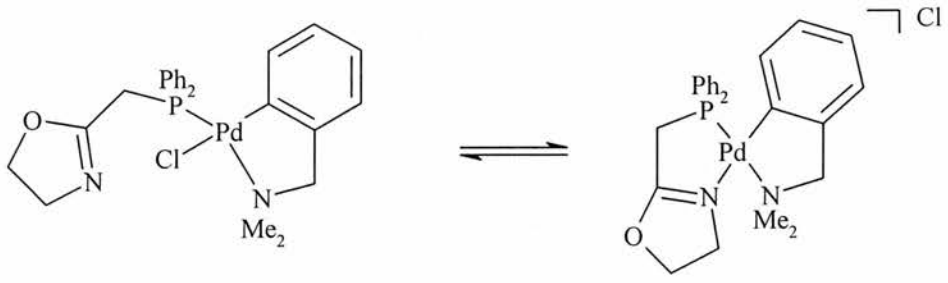

Figure 5.1: *Dynamic coordination of a phosphino-oxaline ligand.*

As the work in this chapter progresses the focus changes to a certain extent. It envelops not only the coordination chemistry, but expands to incorporate chemistry based on the effects of steric interference on the coordination chemistry on the thaizoyl ligands synthesised in this chapter.

The basis of this investigation revolves around increasing the steric bulk around the - nitrogen centre, and observing the result of this change, and trying to interpret it. One example of this kind of investigation in the literature is based around the ligand in figure 5.2.

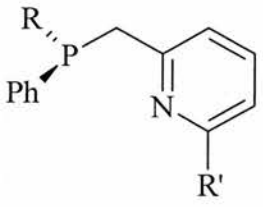

R = Me, R' = H
R = Me, R' = Me
R = *o*-anisyl, R' = H
R = *o*-anisyl, R' = Me
R = Ph, R' = Me

Figure 5.2: *Sterically hindered pyridylphosphines.*

However this chemistry was not fully explored to the same extent that is described in this chapter.

5.2: Results and Discussion

5.2.1: Synthesis and Chalcogen derivatives of 2-diphenylphosphinoaminothiazoyl (dppat)

The synthesis of dppat proceeds as we have seen for the previous phosphorus-nitrogen bond forming reactions, except the reaction was performed at –78°C due to the added complication of a second amine proton. It consisted of the dropwise addition of Ph_2PCl in tetrahydrofuran, to a tetrahydrofuran solution of 2-aminothiazoyl and a small excess of Et_3N at –78°C.

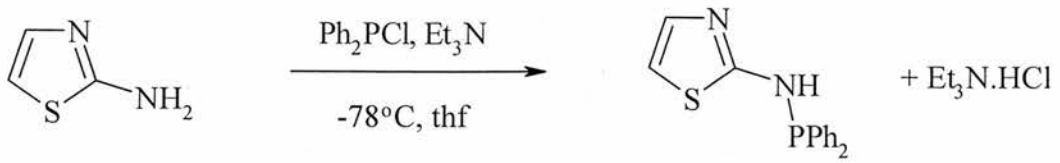

5.1

Figure 5.3: *Synthesis of dppat.*

Subsequent filtration and recrystallisation from $CHCl_3$ afforded a pure sample of dppat (**5.1**), in acceptable yield (37 %). Dppat is a colourless air tolerant solid, it is readily soluble in chlorinated solvents, but less so in solvents such as toluene, acetone and methanol, and not at all soluble in diethyl ether and hexane. The ^{31}P NMR ($CDCl_3$) displays a singlet at δ(P) 41.3 ppm. The ^{1}H spectrum clearly shows the presence of an amine proton at δ(H) 7.9 ppm. However as opposed to the expected doublet (as witnessed for ligands such as dpppa etc), it appears as a broad singlet, this is indicative of extensive hydrogen-bonding within the molecule. Also the thiazoyl protons are worthy of note, they appear at δ(H) 6.7 and 6.5 ppm and are both doublets ($J_{H\text{-}H}$ = 4 Hz). The IR spectrum clearly shows the ν(N-H) band at 3076 cm^{-1}, and the expected ν(C-N) and ν(C-S) stretches at 1541 and 1150 cm^{-1} respectively.

Reaction of dppat with elemental sulfur in toluene generated the expected sulfide of dppat; dppat-S (**5.2**), which was recrystallised from warm toluene to give the desired product as an air stable colourless solid. The ^{31}P NMR shows the expected band, a singlet found at δ(P) 50.2 ppm. We can now recognise this as a typical shift for the sulfide of a phosphorus-nitrogen ligand confirming the success of the reaction. Investigation of the ^{1}H NMR shows the trends we observed for the free ligand and also the trends we have seen for the variety of sulfides seen in this work. Unfortunately the amine proton is hidden behind the aromatic protons, however the

thiazoyl protons are clearly visible at δ(H) 6.4 and 6.2 ppm. The peak at δ(H) 6.4 is a doublet with $^2J_{H\text{-}H}$ = 4 Hz, and the 6.2 ppm peak is a double doublet with $^2J_{H\text{-}H}$ = 2 Hz. The data given in the IR spectrum are consistent with the spectral data above, with ν(N-H) visible at 3140 cm^{-1} and again the ν(C-N) and ν(C-S) stretches found at 1546 and 1115 cm^{-1} respectively.

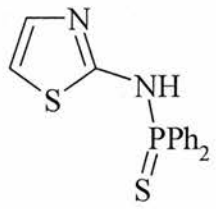

5.2

Figure 5.4: *Dppat-S*

5.2.2: *Square planar complexes of dppat.*

To begin our comparison with the coordination chemistry of dppap we reacted dppat with [$PtCl_2$(cod)] in dichloromethane, this generated a product analogous to the dppap example being [PtCl(dppat-*P,N*)(dppat-*P*)][Cl] (**5.3**). As can be seen it has been assumed that the chelating ligand binds via its nitrogen, rather than its sulfur. This assumption is based on data we will discover later in this chapter when the reactions of the variants of dppat are considered, and also from the IR data. Beyond this it would be expected that it is the nitrogen that would bind, based on the examination of dpppa and dpptc.

It is clear that two ligands are inequivalent via examination of the ^{31}P NMR. If both were chelating or if both were monodentate bound then a singlet would be

observed. In fact a pair of doublets is seen, suggesting one bidentate, one monodentate geometry. There is however a fourth possibility, if both ligands were chelating, but one via a nitrogen and the other via the sulfur then a similar pattern could be observed in the ^{31}P spectrum. I believe that if this was the case then the peaks would be very close together, this is not the case, so the initial geometry speculated for **5.3** remains valid.

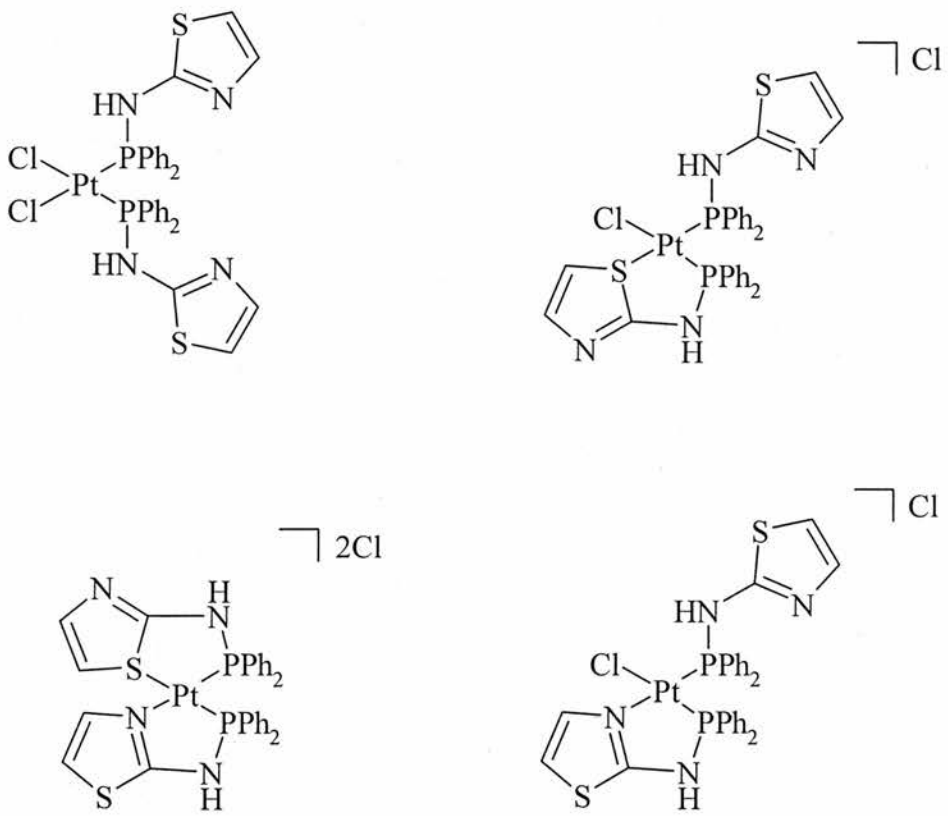

5.3

Figure 5.5: *The four possible isomers of [PtCl(dppat-P,N)(dppat-P)][Cl].*

The actual values for the complex are δ(P) 65 ppm ($^1J_{Pt\text{-}P}$ = 4058 Hz), 23 ppm ($^1J_{Pt\text{-}P}$ = 3646 Hz), ($^2J_{P\text{-}P}$ = 12 Hz). The presence of the doublets as we have said

confirms that both ligands are bound to the metals, and the coupling constants are consist with the geometrical arrangement we have put forward for **5.3**.

The ^{1}H NMR of **5.3** continues to substantiate the geometry of the complex. As with all the previous complexes of this type the ^{1}H spectrum shows a significant shift in the amine protons, in this case they are found at δ(H) 11.0 and 10.4 ppm, both as broad singlets as in the free ligand. This spectrum also clearly displays the thiazoyl protons from both ligands as broad peaks, they are observed at δ(H) 6.5, 6.0, 5.5 and 5.0 ppm. The IR spectrum of **5.3** shows a variety of peaks, bands attributable to ν(N-H) can be seen in the 3100-2900 cm^{-1} region, two peaks for ν(C-N) are found at 1577 and 1551 cm^{-1}, the ν(C-S) bands from the thiazoyl ring are seen at 1159 and 1103 cm^{-1}. The 26 cm^{-1} difference in the ν(C-N) peaks is consistent for the chelated and non-chelated forms of the ligand.

To reinforce these findings dppat was also reacted with [$PdCl_2$(cod)] in dichloromethane to see if the same spectral data could be generated to confirm our initial findings. The reaction indeed generated the analogous compound [PdCl(dppat-*P,N*)(dppat-*P*)][Cl] (**5.4**). The two peaks in the ^{31}P NMR are found at δ(P) 83.1 and 50.0 ppm with a $^{2}J_{P\text{-}P}$ = 14 Hz, these peaks are consistent with the structure proposed for **5.3**. The continuity continues in the^{1}H spectrum, again the two amine resonances are displayed as broad singlets which have been significantly shifted to δ(H) 10.3 and 10.1 ppm. The thiazoyl protons from each ligand are again observed separately, the aromatic protons obscure one from view but the other three are clearly visible at δ(H) 6.1, 5.7 and 5.3 ppm. These proton data are again consistent with the proposed geometry.

The IR data for **5.4** are again very similar to that observed for **5.3**, the ν(N-H) are again found in the 3100-2900 cm^{-1} range as a set of peaks. The ν(C-N) stretches

are much closer in this complex, with peaks at 1542 and 1570 cm^{-1}, but this is still a difference enough. Two well separated peaks are once again observed for the ν(C-S) stretches at 1158 and 1103 cm^{-1}.

For a further comparison and investigation of this motif dppat was reacted with [$PdBr_2$(cod)] to generate the analogous [$PdBr_2$(dppat-*P,N*)(dppat-*P*)][Br] (**5.5**) complex as a orange solid. The ^{31}P NMR shows the identical pattern to **5.4** with peaks as doublets at δ(P) 82.0 and 51.5 ppm with $^2J_{P\text{-}P}$ = 19 Hz. The ^{1}H NMR shows the two amine protons, overlapping each at δ(H) 10.5 ppm, one as a very broad singlet, one as a slightly broad singlet. Only three thiazoyl protons are visible, this is due to one again being hidden behind the aromatic protons, however three is enough to prove that two distinct dppat ligands are bound to the metal centre. The peaks can be seen at δ(H) 6.4, 6.2 and 5.7 ppm, all as broad singlets. The broadness of these (thiazoyl) peaks and of the amine peaks suggests that there is a small amount of fluxionallity in this complex, centred on the ligands. The ν(N-H) stretches are clearly visible in the IR spectrum of **5.5**, they are found the same region as for **5.4**; between 3100 and 2900 cm^{-1}, also the pyridyl peaks are identical to **5.4** being found at 1542 and 1570 cm^{-1} this is acceptable for a bidentate/monodentate motif. There is a minor shift in the ν(C-S) stretches, they are visible at 1155 and 1103 cm^{-1}. This data suggests a close similarity between the two structures for **5.4** and **5.5**. This is in line with our expectations and with the other spectral data we have accumulated on the two complexes.

5.2.3: *Single ligand complexes of dppat.*

Reaction of dppat with [{Pd(μ-Cl)(η^3-C_3H_6)}$_2$] in acetonitrile could generate a mono- or a bidentate complex depending on the ligand's behaviour. The reaction generated a yellow solid which displays a singlet at δ(P) 84.4 ppm in the ^{31}P NMR, this value is very close to the value seen for the chelated ligand in **5.5** and gives our first indication that the product of the reaction is indeed chelated being [Pd(η^3-C_3H_6)(dppat-*P,N*)][Cl] (**5.6**). This is a reasonable assumption as there was a large difference between the two peaks in **5.5** and in previous examples discussed in this work there has been reasonable correlation between the peaks for {$PdCl_2$} and {PdCl(allyl)} complexes with phosphorus-nitrogen ligands. The ^{1}H NMR spectrum shows the usual peaks, however it can shed to real light as to the geometry of the dppat ligand. The amine proton has disappeared from the spectrum. This is a common characteristic of a complex with a large amount of hydrogen bonding. Also there is a possibility that the amine proton is in fact shifted between the amine proton and the second nitrogen from the thiazoyl ring, this will be fully explored on examination of crystal data for a future complex (**5.12**). However the thiazoyl protons are visible at δ(H) 7.1 and 6.6 ppm, and the allyl protons found between δ(H) 5.7 and 3.5 ppm.

Inspection of the IR data for **5.6** shows few useful additions to our data. The ν(N-H) band is broad as seen for the previous examples, found between 3100-2900 cm^{-1}. The ν(C-H) stretches generated by the allyl group are found as three bands between 2589 and 2696 cm^{-1}. A surprising weak ν(C-N) stretch is observed at 1518 cm^{-1}. The ν(C-S) band is located at 1164 cm^{-1}.

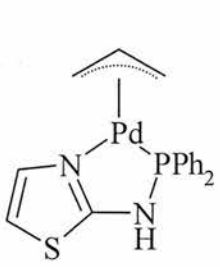

5.6

Figure 5.6: *[Pd(η³-C_3H_6)(dppat-P,N)][Cl]* ***(5.6)****.*

Reaction of dppat with [{RhCl(μ-Cl)(η^6-C_5H_5)}$_2$] in acetonitrile generated another chelated complex; [RhCl(η^6-C_5H_5)(dppat-*P,N*)][Cl] (**5.7**). The ^{31}P NMR shows a doublet at δ(P) 94.2 ppm ($^1J_{Rh\text{-}P}$ = 141 Hz), as was stated in the case of **5.6** this high shift is a first indication of dppat binding in a bidentate fashion. The ^{1}H NMR is consistent with the patterns seen in **5.6** with the amine proton disappearing from the spectra and the thiazoyl protons clearly visible at δ(H) 7.0 and 6.8 ppm. The IR spectrum shows the ν(C-N) at 1572 cm^{-1}, this agrees with the figures seen in **5.3**, **5.4** and **5.5** and strongly suggests a metal bound nitrogen.

For a final look at this class of complex dppat was reacted with [{RuCl(μ-Cl)(η^6-*p*-cymene)}$_2$] in acetonitrile to generate the now expected complex [RuCl(η^6-*p*-cymene)(dppat-*P,N*)][Cl] (**5.8**). This complex on spectroscopic investigation compares well with **5.7**, and little difference can be seen between the two. The ruthenium complex shows a singlet in its ^{31}P NMR at δ(P) 62.7 ppm, but once again the amine proton is missing from the ^{1}H NMR spectra. A slight difference can be seen in this spectrum as that is the thiazoyl protons while they are clearly visible at δ(H) 6.8 and 6.4 ppm, they are broad peaks, as oppose to the sharp ones we have seen in the previous two examples. The IR shows the familiar ν(N-H) stretches at 3043

and 2956 cm^{-1}, the ν(C-N) and ν(C-S) are clearly visible at 1523 and 1130 cm^{-1} respectively.

5.2.4: A monodentate complex of dppat.

In many previous literature examples complexes of $[RuCl_2(\eta^3:\eta^3\text{-}C_{10}H_{16})(L)]$ (where L = a phosphorus-nitrogen ligand) generates a monodentate bound phosphorus bound ligand, this is due to the steric concerns based around the allyl ligand on the metal. The reaction of $[RuCl(\mu\text{-}Cl)(C_{10}H_{16})]$ with dppat in acetonitrile generated $[RuCl_2(C_{10}H_{16})(\text{dppat-}P)]$ (**5.9**) as a brown solid in good yield. The ^{31}P NMR spectrum shows the expected singlet at δ(P) 42.5 ppm. The ^1H NMR clearly shows the 'missing' amine proton at δ(H) 8.6 ppm as a doublet with $^2J_{P\text{-}H}$ = 15 Hz, these figures are reminiscent of the monodentate behaviour witnessed for dpppa and its derivatives. The thiazoyl protons are visible at δ(P) 7.1 and 6.6 ppm, which we can now say are reasonably standard values. The allyl protons are spread throughout the spectra between δ(H) 5.0 and 0.8 ppm.

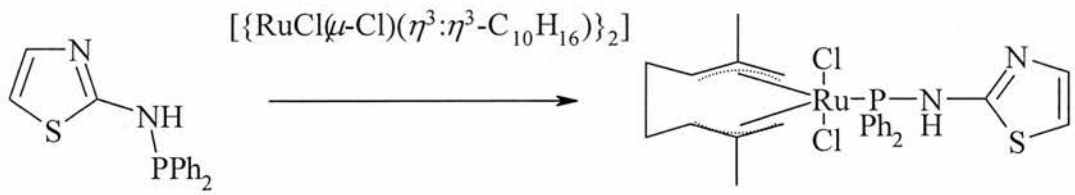

5.9

Figure 5.7: *A monodentate complex of dppat; [RuCl$_2$(C$_{10}$H$_{16}$)(dppat-P)].*

The IR spectrum continues to show close similarities with the monodentate complexes previously described. The ν(N-H) band is seen as a sharp peak once more

at 3173 cm^{-1}, the allyl ν(C-H) stretches are seen in the range 2845-2956 cm^{-1}. The ν(C-N) and ν(C-S) stretches are clearly visible at 1519 and 1134 cm^{-1} respectively. Considering the spectroscopic evidence one can be reasonably sure that this complex does indeed contain a monodentate phosphorus bound dppat ligand.

5.3.1: *Synthesis and chacolgen derivatives of 2-diphenylphosphinoamino-5-methylthiazoyl (Me-dppat).*

The synthesis of the methyl derivative of dppat; Me-dppat (**5.10**) proceeds in a similar fashion to that of dppat itself. The major difference is that the solubility of Me-dppat is greatly increased compared to dppat. This is obviously due to the extra methyl group.

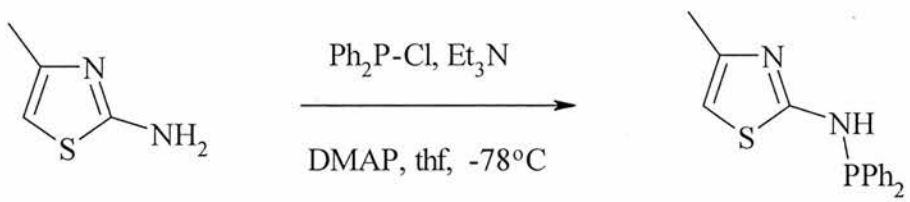

Figure 5.8: *Synthesis of Me-dppat.*

Due to this increased solubility a 100 % pure sample was difficult to produce,. However an example was gained from cooling a very concentrated diethyl ether solution to 4 °C and filtering the generated off-white solid that was produced. This solid showed a singlet at δ(P) 40.2 ppm in the ^{31}P NMR. The ^{1}H NMR shows that the aromatic region obscures the amine peak and the one remaining thiazoyl proton is observed as a doublet at δ(H) 6.1 ppm ($^{2}J_{H\text{-}H}$ = 1 Hz). The new $-CH_3$ peak is

observed at δ(H) 2.0 ppm as a singlet. The IR spectrum shows the expected bands; ν(N-H) at 3068, ν(C-N) at 1524, ν(C-S) at 1135 and ν(P-N) at 986 cm^{-1}.

As has been described before the chalcogen derivatives can be very similar, and again in this case only the sulfide will be considered. Me-dppat-S (**5.11**) was synthesised in toluene by addition of elemental sulfur to Me-dppat and recrystallisation from toluene generates a pure sample as a colourless solid. The expected singlet is produced on examination with ^{31}P NMR, it occurs at δ(P) 48.2 ppm, this quite a small shift from the free ligand but still significant enough to prove the reaction proceeded as expected. The ^{1}H NMR shows few differences from that of the free ligand, again the amine band is concealed behind the aromatic protons, the thiazoyl proton again seen as a doublet at δ(H) 5.7 ($^{2}J_{H-H}$ = 1 Hz), and again consistant with the free ligand the methyl protons are found at δ(H) 2.0 ppm as a singlet. The data seen in the IR spectra are very similar to those seen for the free ligand, which is to be expected, the ν(N-H) stretch is visible at 3098 cm^{-1}, the ν(C-N) band at 1554, the ν(C-S) at 1112 cm^{-1}.

5.3.2: *Complexes of Me-dppat.*

To compare the coordination chemistry of Me-dppat to that of dppat, a series of complexes have been synthesised. The reaction of Me-dppat with [$PtCl_2$(cod)] was performed. This was a first indication of the coordination characteristics of Me-dppat, would it chelate in the same way as dppat, or would the steric hindrance caused by the extra methyl group prove to be too much of a barrier. Another possibility is apparent, as discussed earlier the position of the methyl group places little or no hindrance on

the sulfur in the thiazoyl ring, could this allow the sulfur to bind preferentially to both the nitrogen and the possibility of monodentate binding.

On inspection of the data it was determined that Me-dppat does coordinate in much the same way as dppat, generating [PtCl(Me-dppat-*P,N*)(Me-dppat-*P*)][Cl] (**5.12**), however in the crystal structure we see some strange activity based around the amine proton, we will consider this when analysing the crystal data. On initial inspection of the ^{31}P NMR data we see the expected peaks in a AM type spectra, with the first set of peaks at δ(P) 62.1 ppm ($^{1}J_{Pt\text{-}P}$ = 4089 Hz) and the second set at δ(P) 20.9 ppm ($^{1}J_{Pt\text{-}P}$ = 3700 Hz) and a $^{2}J_{P\text{-}P}$ = 9 Hz. These values are very similar to the ones seen for **5.3**. The expected trend continues in the ^{1}H NMR spectrum, the amine protons have disappeared, and two separate thiazoyl protons are observed at δ(H) 6.9 and 5.6 ppm.. The IR data show that there is no considerable difference in one of the ν(N-H) shift compared to the free ligand (3093 cm^{-1}). However a second ν(N-H) stretch located at 2790 cm^{-1} indicates either increased hydrogen-bonding in the complex, or a more dramatic shift in the amine proton. The phenomenon is more clearly understood on examination of the crystal data. The trend of two distinct ligands is continued by the shifts seen for the ν(C-N) and ν(C-S) stretches. These are seen at 1576, 1555, 1147 and 1105 cm^{-1}. A crystal suitable for X-ray analysis was produced by slow evaporation of a concentrated $CDCl_3$ solution.

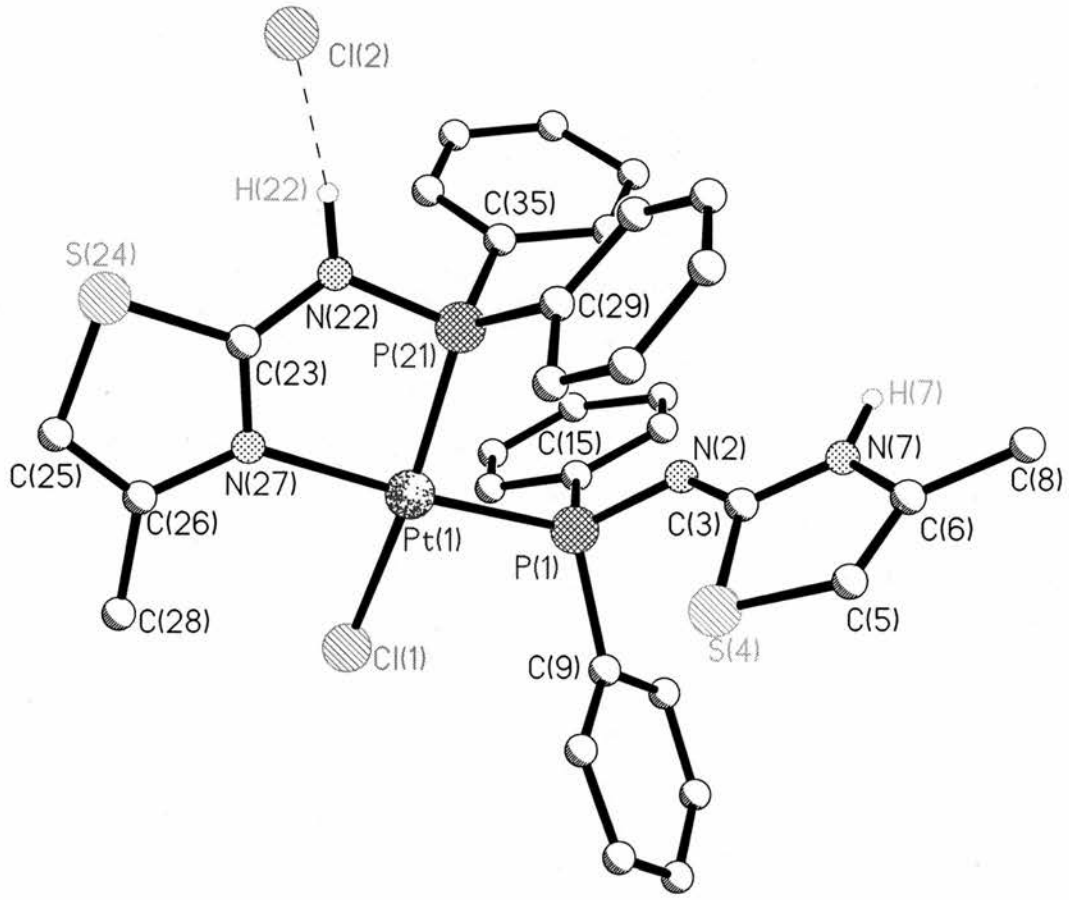

Figure 5.9: *Crystallographic Representation of [PtCl(Me-dppat-P,N)(Me-dppat-P)][Cl]* ***(5.12)****.*

The first thing to notice on examination of the crystal structure is that the amine proton on the monodentate bound ligand has shifted from the N-H spacer group to the nitrogen found in the thiazoyl ring. The reason for this is unclear, however one could consider a possible resonance effect. This would start to explain some of the strange spectroscopic data we have seen, so far in the equivalent complexes for dppat. These data suggests the strange results we have been seeing attributable to the amine proton, is because the proton is in fact 'in motion', certainly it explains the broadening

seen in the ^{1}H NMR of the complexes we have been studying thus far. Also if we again consider the ν(N-H) stretches we have been seeing in the IR spectra of these complexes, we can again start to further understand that this phenomenon may not just be attributable to just this one compound but the majority of the compounds in the thiazoyl family.

***Table**: **5.1** Selected bond lengths (Å) and angles (°) for [PtCl(Me-dppat-P,N)(Me-dppat-P)][Cl].*

Pt(1)-P(1)	2.256(3)	Pt(1)-P(21)	2.214(3)
Pt(1)-Cl(1)	2.332(3)	Pt(1)-N(27)	2.141(8)
P(1)-N(2)	1.616(9)	P(21)-N(22)	1.674(10)
N(2)-C(3)	1.292(12)	N(22)-C(23)	1.333(13)
C(3)-S(4)	1.763(10)	C(23)-S(24)	1.739(11)
C(3)-N(7)	1.332(17)	C(23)-N(27)	1.311(11)
N(22)-Cl(2)	3.053(10)	N(7)-Cl(2)	3.144(10)
P(1)-Pt(1)-P(21)	93.57(9)	P(1)-Pt(1)-Cl(1)	88.26(10)
P(1)-Pt(1)-N(27)	175.8(3)	P(21)-Pt(1)-N(27)	85.5(3)
N(27)-Pt(1)-Cl(1)	95.4(3)	P(21)-Pt(1)-Cl(1)	171.50(12)
Pt(1)-P(1)-N(2)	116.8(3)	Pt(1)-P(21)-N(22)	101.3(4)
Pt(1)-N(27)-C(23)	114.3(7)	Pt(1)-N(27)-C(26)	135.5(8)
P(21)-N(22)-H(22)	120	C(3)-N(7)-H(7)	121
P(1)-N(2)-C(3)	130.7(8)	P(21)-N(22)-C(23)	118.8(9)
N(2)-C(3)-S(4)	129.5(9)	N(22)-C(23)-S(24)	123.1(10)

N(2)-C(3)-N(7)	123.4(10)	N(22)-C(23)-N(27)	122.6(11)
N(7)-C(3)-S(4)	107.2(8)	N(27)-C(23)-S(24)	114.2(10)
N(7)-H(7)...Cl(2)	158.3	N(22)-H(22)...Cl(2)	162.4

We can see from table 5.1 that there is effectively a square planar geometry based around the platinum. There are some significant differences between the two ligands in the complex, as we go through these differences it will become clear that we need to consider that the monodentate bound ligand is deprotonated at N(7), much of the data supplied from the crystallography is consistent with previous examples of deprotonated phosphorus-nitrogen ligands. The first indication is that the P(1)-N(2) bond is much shorter in the mondentate ligand than for its bidentate partner (P(21)-N(22) being reduced to 1.616 from 1.674 Å, similar to this the C(3)-N(2) bond length is also reduced, in the deprotonated ligand. Also there is a slight increase in the C(23)-N(27) bond length on comparison with C(3)-N(7), 1.332 from 1.311 Å. This is consistent with the bond becoming more like a single bond. In the example of dppap we see a significant difference between the P-N-C angles, this is mirrored with this example of dppat coordination, there is an 11.9° difference between these values in **5.12**. This is due to the forming of the chelate ring. At this point we could speculate about the reasons behind this proton shift, it could be simply that the two nitrogens are very similar and because the thiazoyl ring is poorly delocalised there are few barriers preventing a tautomeric exchange of the proton. From this we must assume the pK_a values for the nitrogen atoms must be very similar.

As with dppat, Me-dppat was also reacted with $[PdCl_2(cod)]$ to give [PdCl(Me-dppat-*P,N*)(Me-dppat-*P*)][Cl] (**5.13**) as a yellow solid. The ^{31}P NMR

spectrum is analogous with that seen for **5.5**, with a pair of doublets observed at δ(P) 80.0 and 50.6 ppm with a $^2J_{P\text{-}P}$ = 23 Hz, these are very comparable values and suggests again that Me-dppat is behaving in the same manner as dppat and has one ligand bidentate bound and one monodentate bound. In the ^{1}H NMR we again see a broadening of the amine peak, with the two protons being indistinguishable as a broad singlet found at δ(H) 10.5 ppm. We can however use the thiazoyl and methyl protons to again confirm that there are indeed two different ligands present in the complex. The thiazoyl protons can be observed at δ(H) 5.8 and 5.1 ppm as broad singlets, and the methyl protons are present at δ(H) 2.2 and 1.6 ppm. The IR data provides an interesting detail, the band for the second, 'mobile' amine proton is again shifted in a similar fashion to **5.12**, it is observed at 2914 cm^{-1} as a broad band, with the 'stable' amine barely moving at 3085 cm^{-1}. The other shifts in the spectra again confirm the presence of two separate ligands around the metal centre; two ν(C-N) stretches are clearly seen at 1574 and 1551 cm^{-1}, the difference between the two is consistent with the difference required to suggest chelation in one ligand, and monodentate binding for the other. The two ν(C-S) bands are observed at 1145 and 1102 cm^{-1}.

Further exploration of the coordination chemistry of Me-dppat led us to react it with [{RuCl(μ-Cl)(η^6-*p*-cymene)}$_2$] to see if the octahedral geometry will provide any change in the coordination motif of Me-dppat. This reaction in acetonitrile produced [RuCl(η^6-*p*-cymene)(Me-dppat-*P,N*)][Cl] (**5.14**), this geometry is assumed from the ^{31}P NMR from the peak witnessed at δ(P) 99.9 ppm, which is considerably higher than the monodentate aminophosphine ligands previously seen and very close to the chelated aminophosphines.. The ^{1}H NMR confirms this geometry when we observe the now characteristic broadening of the amine proton at δ(H) 10.2 ppm. We also observe one thiazoyl proton at δ(H) 6.4 ppm. The ν(N-H) stretch in the IR

spectrum is located at 3046 cm^{-1}, a band attributable to ν(C-N) is observed at 1561 cm^{-1} and a ν(C-S) band at 1101 cm^{-1}.

5.4.1: *Synthesis and chacolgen derivatives of 2-diphenylphosphinoamino-5-tert-butylthiazoyl (Bu-dppat).*

To further investigate steric influence on the properties of these thiazoyl ligands we synthesised 2-diphenylphosphinoamino-5-tert-butylthiazoyl (Bu-dppat) (**5.15**) by the same method as for dppat and Me-dppat. However as we observed for Me-dppat, the solubilities of these ligands increases on addition of the alkyl groups, one would presume that ^{t}butyl would increase this belief. This is the case, and this solubility made it difficult to obtain a pure sample, as recrystallisation was impossible from any solvent due to this increased solubility. A sample of roughly 98 % purity was obtained from a petroleum ether (40-60) solution extract of the crude ligand, from which the solvent was subsequently removed *in vacuo*. This pale yellow solid gave the expected singlet in the ^{31}P NMR at δ(P) 39.7 ppm and this correlates well with the values for dppat and Me-dppat (41.3 and 40.2).

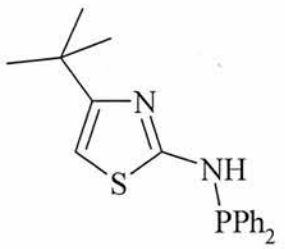

Figure 5.10: *b-dppat.*

The amine peak is seen as a doublet ($^2J_{P\text{-}H}$ = 7 Hz) at δ(H) 8.2 in the ^{1}H NMR spectrum of **5.15**, the thaizoyl proton is visible as a sharp singlet at δ(H) 6.2 ppm, and the ^{t}Bu protons are seen at δ(H) 1.2 ppm again as a sharp singlet. The IR data gave the expected resonances with bands at 3343 cm^{-1} for ν(N-H), 1524 for ν(C-N), 1098 for ν(C-S) and 996 for ν(P-N)

5.4.2: Complexes of ^{t}Bu-dppat.

The obvious reaction to perform to investigate the coordination of ^{t}Bu-dppat in comparison to the other members of the dppat family is to react it with [$PtCl_2$(cod)] as was done with both dppat and Me-dppat. This reaction was indeed carried out, in acetonitrile, the reaction generated a very soluble white solid (**5.16**) which could only be isolated by cooling a saturated diethyl ether solution of **5.16**. The investigation of **5.16** by ^{31}P NMR clearly shows a significant difference in the spectra, in comparison to the set of doublets witnessed for the dppat and Me-dppat derivatives, we see a singlet which is indicative of the monodentate binding we have seen for the likes of dpppa and dpptc. The singlet is found at δ(P) 53.5 ppm with $^1J_{Pt\text{-}P}$ = 4040 Hz, the large coupling constant is also expected for a complex of this type. Purely based on the ^{31}P data we can state that **5.16** is [$PtCl_2$(^{t}Bu-dppat-*P*)$_2$], the only other possibility is that both ligands are chelating and based on the chemistry we have seen in the dppat family this is exceptionally unlikely.

The next question is whether the ^{1}H NMR data will back up the assumption we have made following examination of the ^{31}P data. The amine proton is immediately visible as a broad singlet at δ(H) 11.2 ppm, the one remaining thiazoyl proton is also easily observed at δ(H) 5.9 as a sharp singlet. This data does indeed

provide further evidence to support the proposed structure, as the other possibility would place two inequivalent ligands within the complex; this is obviously not the case. The IR data for **5.16** show that there is some differences in the solid state, we see ν(N-H) stretches at 3055 and 2693 cm^{-1}, also the ν(C-N) and ν(C-S) stretches are also visible bands at 1592, 1561 and 1104, 1017 cm^{-1}. These data does suggest that the two ligands are independent in the solid state.

We now have the variation in coordination chemistry we were searching for. The extra bulk provided by the ^{t}Bu group is indeed sufficient to prevent binding by the nitrogen of the thiazoyl ring. However there is a possibility that was mentioned in the introduction that has not been investigated thus far because it is not plausible, however we will mention it for completeness.. Had we seen two inequivalent ligands in the complex despite the ^{t}Bu group then we would have needed to consider if the ligand is binding via the sulfur in the thiazoyl ring. From this we can confirm that sulfur is indeed a poor atom for coordination and despite the five-membered ring formation, which is generally very favourable the sulfur will still not bind. There has already been much discussion about why this should be the case, but primarily it is due to the weak electron density based on the sulfur, and although the delocalisation in thiazoyl is poor in comparison with other aromatic rings (such as benzene or pyridyl), it still reduces the electron density available at the sulfur atom.

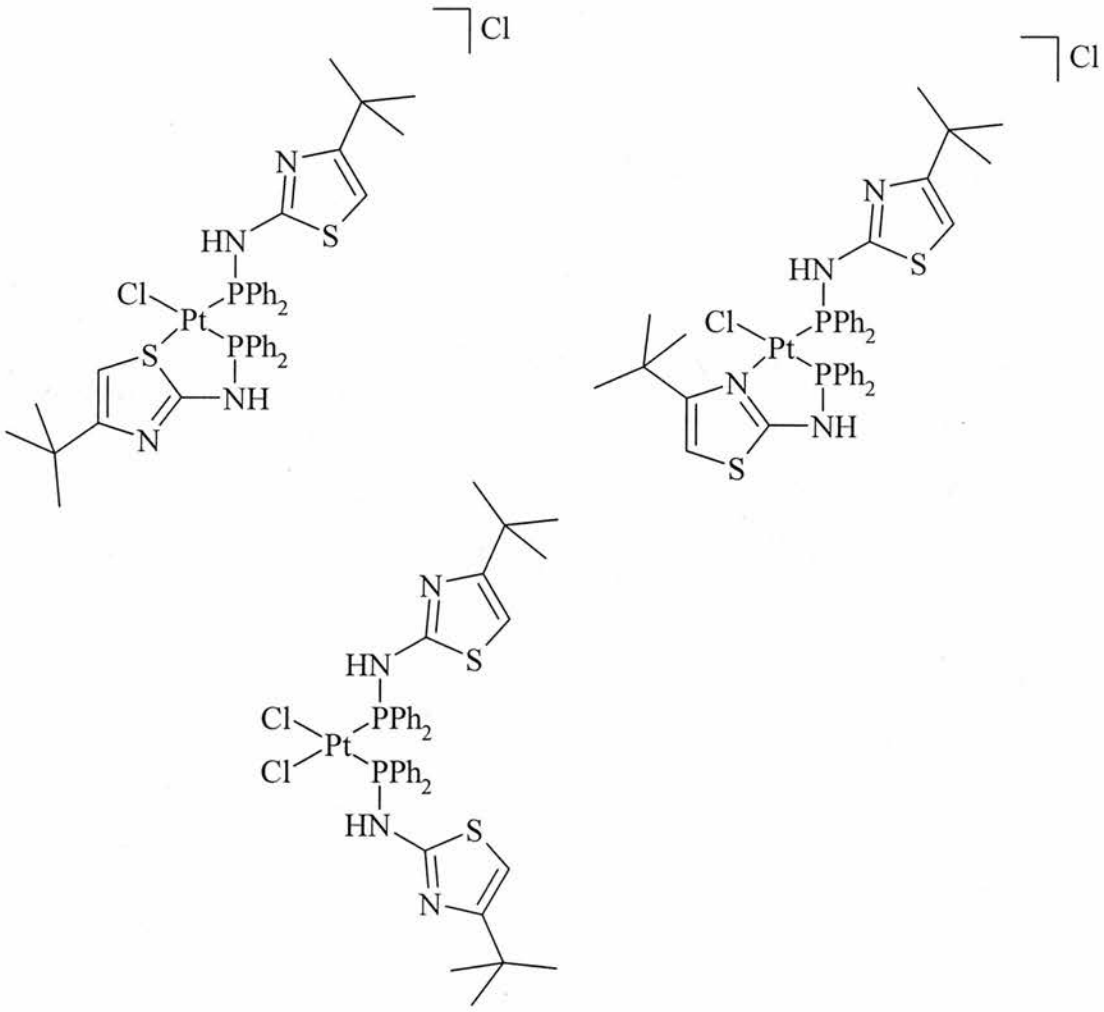

5.16

Figure 5.11: *Possible conformations of [PtCl$_2$(^{t}Bu-dppat-P)$_2$].*

Further complexes of b-dppat were synthesised to investigate the change in ligand geometry. Reaction with [{Pd(μ-Cl)(η^3-C_3H_6)}$_2$] generated the now expected monodentate complex [PdCl(η^3-C_3H_6)(b-dppat-*P*)] (**5.17**) with the ligand bound by the phosphorus. This can be verified by observing the NMR spectroscopy. The ^{31}P NMR shows a peak at δ(P) 58.3 ppm, which is much lower than the peak at δ(P) 84.4 ppm that was seen for dppat and is also in the range that we have grown familiar with for monodentate bound aminophosphines. Also the ^{1}H NMR shows peaks consistent with monodentate binding, the amine proton can is again absent and the thiazoyl

proton found at δ(H) 6.1 ppm as the expected singlet. The major aspect of the IR data which is crucial is the ν(C-N) stretch which would indicate whether the ligand was chelated via the thiazoyl nitrogen or not. In this case it is observed at 1527 cm^{-1}, which is only 2 cm^{-1} from the value seen for the free ligand, indicating monodentate coordination.

Reaction with [{RuCl(μ-Cl)(η^6-*p*-cymene)}$_2$] produced [$RuCl_2$(η^6-*p*-cymene)(b-dppat-*P*)] (**5.18**), again it is a complex with the ligand mondentate bound via the phosphorus, this is indicated by the peak in the ^{31}P NMR at δ(P) 62.3 ppm. The ^{1}H spectrum shows the thiazoyl proton as a singlet at δ(H) 5.9 ppm. The IR data strongly suggests a monodentate coordination, this is based around the ν(C-N) peak, which is found at 1531 cm^{-1}, which is very similar to the value earlier quoted for the free ligand., suggesting it is not chelated. If we consider the different geometry around the metal centre we can suggest that because the tetrahedral conformation provides slightly more space around the metal, it is conceivable that b-dppat can chelate. This possibility must be considered due the spectral analysis.

The coordination chemistry of dppat and its derivatives correlates quite well. It is clear that the addition of a methyl group in the 4- position is not sufficient to prevent the chelation of the thiazoyl nitrogen. The addition of a ^{t}Bu group in the 4-position however does have an effect. In square planar complexes it is apparent that the butyl group blocks the chelating mode of coordination and in turn due to the poor binding characteristics of sulfur the ligand binds in a monodentate fashion. However it is possible that in the tetrahedral geometry that this is sufficient room for the nitrogen to bind.

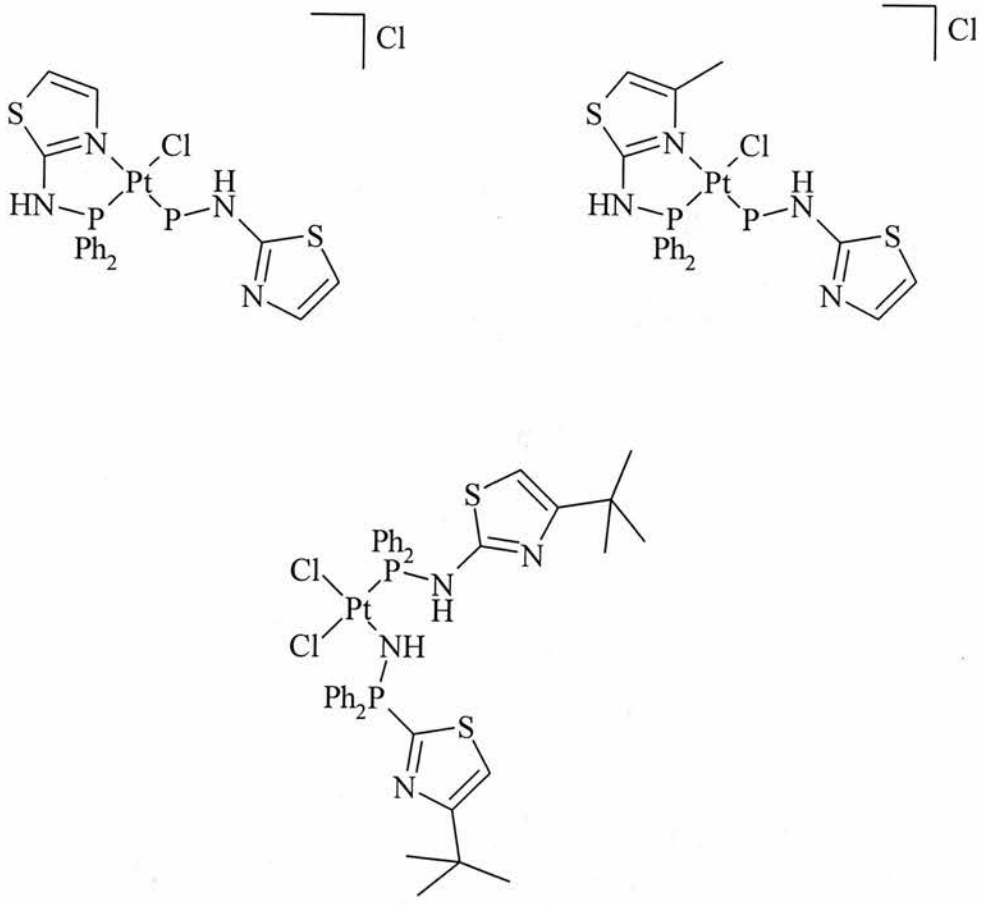

Figure 5.12: *Illustration of the coordination chemistry of dppat and its derivatives.*

Experimental: Chapter Five.

General Conditions

All manipulations were carried out in an atmosphere of nitrogen, unless stated otherwise. All solvents were either freshly distilled from an appropriate drying agent (thf, Et_2O, dcm) or obtained as anhydrous grade from Aldrich. ^1H and ^{31}P NMR spectra were recorded using a Jeol Delta FT (270 MHz) spectrometer. IR spectra were recorded as KBr discs (prepared in air) on a Perkin Elmer 2000 FTIR/RAMAN spectrometer. All significant peaks (>800 cm^{-1}) are quoted to serve as a fingerprint. Silver salts, 2-aminothiazole, 2-amino-4-methylthiazole, 2-amino-4-*tert*-butylthiazole (Aldrich Chemical Co.) and BuLi (2.5M, Lancaster) were purchased and used as received. Triethylamine and chlorodiphenylphosphine were distilled prior to use. Dimethylaminopyridine (DMAP) was sublimed before use. The various metal starting materials were made by the appropriate literature methods, $[MCl_2(cod)]$ (M = Pt or Pd, cod = cycloocta-1,5-diene)[2,3], $[\{MCl(\mu\text{-}Cl)(Cp^*)\}_2]$ (M = Rh or Ir)[6], $[\{Rh(\mu\text{-}Cl)(cod)\}_2]$[7], $[\{RuCl(\mu\text{-}Cl)(\eta^6\text{-}p\text{-}MeC_6H_4{}^iPr)\}_2]$[8], $[\{RuCl(\mu\text{-}Cl)(\eta^3\text{:}\eta^3\text{-}C_{10}H_{16})\}_2]$[9], $[\{PdCl(\mu\text{-}Cl)(\eta^3\text{-}C_3H_5)\}_2]$[10].

2-(diphenylphosphino)aminothiazole (**dppat**) (**5.1**): Chlorodiphenylphosphine (4.23 cm^3, 24 mmol) in 30 cm^3 of thf was added dropwise to a mixture of 2-aminothiazole (2.36 g, 24 mmol) and triethylamine (3.44 cm^3, 25 mmol) in 100 cm^3 of thf at –78°C. After addition was complete the mixture was allowed to warm to room temperature overnight. The resultant white precipitate was filtered and the filtrate reduced to

dryness *in vacuo*. The crude product was recrystallised by cooling a concentrated chloroform solution at 4°C overnight giving a white solid, (yield: 2.5 g, 37 %). $C_{15}H_{13}N_2SP$ requires: C, 63.2, H, 4.51, N, 9.86. Found: C, 62.2, H, 3.68, N, 9.32. ν_{max}/cm^{-1}: 3076, 1541, 1492, 1432, 1150, 999. ^{31}P NMR ($CDCl_3$) δ 41.3 ppm. ^1H NMR ($CDCl_3$), 7.9 (1H, bs, N-H), 7.5-7.2 (10H, m, aromatic), 6.7 (1H, dd, J = 1, 4 Hz, thiazoyl), 6.5 (1H, d, J = 4 Hz, thiazoyl).

2-(diphenylphosphino)aminothiazole sulfide (**5.2**): Sulfur (23 mg, 0.7 mmol) was added to 2-(diphenylphosphino)aminothiazole (200 mg, 0.7 mmol) and the mixture refluxed in toluene (10 cm^3) for 30 min. The resulting solution was stored at 4°C overnight generating a white solid. The product was filtered and isolated as a white solid (yield: 184 mg, 83 %). $C_{15}H_{13}N_2S_2P$ requires: C, 56.9, H, 4.14, N, 8.85. Found: C, 56.8, H, 4.15, N, 8.88. ν_{max}/cm^{-1}: 3141, 3097, 3050, 1576, 1432, 1412, 947. ^{31}P NMR ($CDCl_3$) δ 50.2 ppm. ^1H NMR ($CDCl_3$), δ 8.1-7.9 (4H, m, aromatic), 7.3-7.5 (6H, m, aromatic), 6.35 (1H, d, J = 4 Hz, thiazoyl), 6.2 (1H, dd, J = 2, 4 Hz, thiazoyl).

[PtCl(dppat-P)(dppat-P,N)][Cl] (**5.3**): Dppat (301 mg, 1 mmol) and [$PtCl_2$(cod)] (200 mg, 1 mmol) were weighed into a round bottomed flask and acetonitrile (10 cm^3) added. This mixture was stirred for 2 hours, and a colourless precipitate was generated. The solid was filtered and isolated as a colourless solid, (yield: 333 mg, 80 %). $C_{30}H_{26}N_4S_2P_2Cl_2Pt$ requires: C, 43.2, H, 3.15, N, 6.72. Found: C, 42.3, H, 2.80, N, 6.49. ν_{max}/cm^{-1}: 3054, 2786, 1577, 1551, 1481, 1435, 1159, 1103, 998, 249. ^{31}P NMR ($CDCl_3$), δ 65.1 ($^2J_{P\text{-}P}$ = 14 Hz, $^1J_{Pt\text{-}P}$ = 4060 Hz), 23.9 ($^2J_{P\text{-}P}$ = 14 Hz, $^1J_{Pt\text{-}P}$ = 3650 Hz). ^1H NMR ($CDCl_3$) δ 11.1 (1H, bs, N-H), 10.4 (1H, s, N-H), 7.6-7.4 (4H, m,

aromatic), 7.3-6.9 (16H, m, aromatic), 6.5 (1H, d, J = 1 Hz, thiazoyl), 6.0 (1H, d, J = 1 Hz, thiazoyl), 5.5 (1H, d, J = 1 Hz, thiazoyl), 5.0 (1H, s, thiazoyl).

[PdCl(dppat-P)(dppat-P,N)][Cl] (**5.4**): Dppat (100 mg, 0.34 mmol) and [$PdCl_2$(cod)] (50 mg, 0.17 mmol) were weighed into a round bottomed flask. Acetonitrile (5 cm^3) was added and the mixture heated until the entire solid was dissolved, this mixture was then allowed to return to room temperature. An orange precipitate was formed during cooling and this was filtered isolating the product as an orange solid, (yield: 94 mg, 74 %). $C_{30}H_{26}N_4S_2P_2Cl_2Pd$ requires: C, 48.3, H, 3.52, N, 7.53. Found: C, 47.8, H, 3.05, N, 7.31. ν_{max}/cm^{-1}: 2923, 2719, 1542, 1482, 1434, 1158, 1103, 996, 279. ^{31}P NMR ($CDCl_3$), δ 83.0 ($^2J_{P\text{-}P}$ = 14.1 Hz), 50.0 ($^2J_{P\text{-}P}$ = 14.1 Hz). ^1H NMR ($CDCl_3$), δ 10.3 (1H, s, N-H), 10.1 (1H, bs, N-H) 7.0-6.4 (21H, m, aromatic), 6.2 (1H, d, J = 4 Hz, thiazoyl), 5.7 (1H, d, J = 4 Hz, thiazoyl), 5.3 (1H, d, J = 5 Hz, thiazoyl).

[PdBr(dppat-P)(dppat-P,N)][Br] (**5.5**): Dppat (76 mg, 0.27 mmol) and [$PdBr_2$(cod)] (50 mg, 0.135 mmol) were weighed into a round bottomed flask. Acetonitrile (5 cm^3) was added and the mixture heated until the solid was dissolved, this mixture was then allowed to return to room temperature. An orange precipitate was formed during cooling and this was filtered isolating the product as an orange solid, (yield: 73 mg, 33 %). $C_{30}H_{26}N_4S_2P_2Br_2Pd$ requires: C, 43.2, H, 3.14, N, 6.71. Found: C, 43.4, H, 2.78, N, 6.72 %. ν_{max}/cm^{-1}: 2938, 2799, 1570, 1542, 1483, 1433, 1156, 998, 381. ^{31}P NMR ($CDCl_3$), δ 82.0 ppm($^2J_{P\text{-}P}$ = 18.78 Hz), 51.5 ppm ($^2J_{P\text{-}P}$ = 18.78 Hz). ^1H NMR ($CDCl_3$), δ 10.5 (1H, s, N-H), 10.4 (1H, bs, N-H) 7.8-6.9 (21H, m, aromatic), 6.4 (1H, d, J = 5 Hz, thiazoyl), 6.2 (1H, d, J = 5 Hz, thiazoyl), 5.7 (1H, d, J = 5 Hz, thiazoyl).

[Pd(η^3-C_3H_6)(dppat-P,N)][Cl] (**5.6**): Dppat (78 mg, 0.28 mmol) and [{Pd(μ-Cl)(η^3-C_3H_6)}$_2$] (50 mg, 0.14 mmol) were weighed into a round bottomed flask. Acetonitrile (5 cm^3) was added and the mixture heated until the entire solid was dissolved, this mixture was then allowed to return to room temperature. A yellow precipitate was formed during cooling and this was filtered isolating the product as a yellow solid, (yield: 60 mg, 46 %). $C_{18}H_{19}N_2SPClPd$ requires: C, 46.2, H, 4.10, N, 6.00. Found: C, 45.3, H, 3.27, N, 6.08. ν_{max}/cm^{-1}: 2928, 2589, 1474, 1433, 1164, 1104, 997, 252. ^{31}P NMR ($CDCl_3$), δ 84.4 ppm. ^{1}H NMR ($CDCl_3$) 7.9-7.7 (4H, m, aromatic), 7.5-7.3 (6H, m, aromatic), 7.15 (1H, d, J = 4 Hz, thiazoyl), 6.6 (1H, dd, J = 2, 4 Hz, thiazoyl), 5.7 (1H, m, allyl), 4.9 (1H, bs, allyl), 3.8 (1H, bs, allyl), 3.5 (2H, bs, allyl).

[RhCl(dppat-P,N)(η-C_5Me_5)][Cl] (**5.7**): Dppat (49 mg, 0.17 mmol) and [{RhCl(μ-Cl)(η-C_5Me_5)}$_2$] (53 mg, 0.17 mmol) were weighed into a round bottomed flask. Acetonitrile (5 cm^3) was added and the mixture heated until the entire solid was dissolved, this mixture was then allowed to return to room temperature. A red precipitate was formed during cooling and this was filtered isolating the product as a red solid, (yield: 94 mg, 94 %). $C_{25}H_{28}N_2SPCl_2Rh$ requires: C, 50.7, H, 4.77, N, 4.73. Found: C, 50.4, H, 4.62, N, 4.81. ν_{max}/cm^{-1}: 3052, 2432, 1487, 1434, 1146, 1101, 998, 234. ^{31}P NMR ($CDCl_3$), δ 94.2 ($^1J_{Rh\text{-}P}$ = 141 Hz). ^{1}H NMR ($CDCl_3$), δ 7.9 (2H, m, aromatic), 7.6-7.4 (6H, m, aromatic), 7.3-7.2 (2H, m, aromatic), 7.0 (1H, d, J = 4 Hz, thiazoyl), 6.8 (1H, dd, J = 2.2 Hz, thiazoyl), 1.55 (15H, d, J = 3.7 Hz, C_5Me_5).

[RuCl(p-Cymene)(dppat-P,N)][Cl] (**5.8**): Dppat (56 mg, 0.19 mmol) and [{RuCl(μ-Cl)(η^6-p-Cymene)}$_2$] (61 mg, 0.95 mmol) were weighed into a round bottomed flask and dcm (10 cm^3) added. This mixture was stirred for 2 hours, and a red precipitate

was generated. The solid was filtered and isolated as a red solid, (yield: 86 mg, 77 %). $C_{25}H_{27}N_2SPCl_2Ru$ requires: C, 50.8, H, 4.61, N, 4.75. Found: C, 49.8, H, 3.92, N, 4.60. ν_{max}/cm^{-1}: 3043, 2957, 1523, 1474, 1434, 1130, 1000. ^{31}P NMR ($CDCl_3$), δ 62.7 ppm. ^1H NMR ($CDCl_3$), 8.0 (4H, m, aromatic), 7.5-7.2 (6H, m, aromatic), 6.8 (1H, bs, thiazoyl), 6.4 (1H, bs, thiazoyl), 5.3-5.1 (4H, m, *p*-Cy (aromatic)) 2.5 (1H, m, -CMe_2-H) 1.6 (3H, s, Me-H) 1.0-0.8 (6H, bs, Me-H).

[RuCl$_2$(η^3:η^3-C$_{10}$H$_{16}$)(dppat-P)] **(5.9)**: Dppat (46 mg, 0.17 mmol) and [{RuCl(μ-Cl)(η^3:η^3-$C_{10}H_{16}$)}$_2$] (50 mg, 0.085 mmol) were weighed into a round bottomed flask. Acetonitrile (5 cm^3) was added and the mixture heated until the entire solid was dissolved, this mixture was then allowed to return to room temperature. A brown precipitate was formed during cooling and this was filtered isolating the product as a brown solid, (yield: 36 mg, 36 %). $C_{25}H_{29}N_2SPCl_2Ru$ requires: C, 50.4, H, 5.58, N, 4.70. Found: C, 51.2, H, 4.49, N, 4.70 %. ν_{max}/cm^{-1}: 3173, 1519, 1474, 1438, 1420, 1134, 996. ^{31}P NMR ($CDCl_3$), δ 42.5 ppm. ^1H NMR ($CDCl_3$), δ 8.5 (1H, d, J = 15 Hz, N-H), 8.1-7.9 (4H, m, aromatic), 7.5-7.3 (6H, m, aromatic), 7.1 (1H, d, J = 4 Hz, thiazoyl), 6.5 (1H, d, J = 4 Hz, thiazoyl), 5.0 (2H, m, allyl), 3.7 (2H, d, J = 9 Hz, allyl), 3.4 (2H, m, allyl), 3.00 (2H, d, J = 4 Hz, allyl), 2.6 (2H, m, allyl), 2.0, (6H, s, allyl-Me).

2-(diphenylphosphino)amino-4-methylthiazole **(Me-dppat) (5.10)**:

Chlorodiphenylphosphine (3.93 cm^3, 22 mmol) in 40 cm^3 of thf was added dropwise to a mixture of 2-amino-4-methylthiazole (2.5 g, 22 mmol), DMAP (268 mg, 2.2

mmol) and triethylamine (3.36 cm^3, 24mmol) in 80 cm^3 of thf at –78°C. After addition was complete the mixture was allowed to warm to room temperature overnight. The resultant white precipitate was filtered and the filtrate reduced to dryness *in vacuo* over the course of five days to give the desired product (Yield: 4.3 g, 69 %). $C_{15}H_{13}N_2SP$ requires: C, 64.3, H, 5.07, N, 9.39. Found: C, 62.9, H, 5.31, N, 9.18. ν_{max}/cm^{-1}: 3068, 1524, 1480, 1432, 1135, 986. ^{31}P NMR ($CDCl_3$), δ 40.2 ppm. ^1H NMR ($CDCl_3$), δ 7.5-7.2 (10H, m, aromatic), 6.1 (1H, d, J = 1 Hz, thiazoyl), 2.0 (3H, s, Me).

2-(diphenylphosphino)amino-4-methylthiazole sulfide (**5.11**): Sulfur (21 mg, 0.67 mmol) was added to 2-amino-4-methylthiazole (200 mg, 0.7 mmol) and the mixture refluxed in toluene (10 cm^3) for 30 min. The resulting solution was stored at 4°C overnight generating a white solid. The product was filtered and isolated as a white solid (yield: 175 mg, 79 %). $C_{16}H_{15}N_2S_2P$ requires: C, 58.2, H, 4.58, N, 8.48. Found: C, 56.8, H, 4.45, N, 8.14. ν_{max}/cm^{-1}: 3098, 1577, 1554, 1433, 1401, 1112, 1018. ^{31}P NMR ($CDCl_3$), δ 48.2 ppm. ^1H NMR ($CDCl_3$), δ 8.1-7.9 (4H, m, aromatic), 7.5-7.2 (6H, m, aromatic), 5.7 (1H, d, J = 3 Hz, thiazoyl) 2.0 (3H, s, Me).

[PtCl(Me-dppat-P)(Me-dppat-P,N)][Cl] (**5.12**): Me-dppat (80 mg, 0.27 mmol) and [$PtCl_2$(cod)] (50 mg, 0.135 mmol) were weighed into a round bottomed flask and acetonitrile (5 cm^3) added. This mixture was stirred for 2 hours, and a colourless precipitate was generated. The solid was filtered and isolated as a colourless solid, (yield: 71 mg, 62 %). $C_{32}H_{30}N_4S_2P_2Cl_2Pt$ requires: C, 44.5, H, 3.51, N, 6.49. Found: C, 44.0, H, 3.42, N, 6.42. ν_{max}/cm^{-1}: 3093, 2790, 2551, 1576, 1555, 1480, 1437, 1147,

1105, 999. ^{31}P NMR ($CDCl_3$), δ 62.0 ($^2J_{P\text{-}P}$ = 9 Hz, $^1J_{Pt\text{-}P}$ = 4090 Hz), 20.9 ($^2J_{P\text{-}P}$ = 9 Hz, $^1J_{Pt\text{-}P}$ = 3805 Hz). ^{1}H NMR ($CDCl_3$), δ 7.8-7.2 (22H, m, aromatic), 6.9 (1H, bs, thiazoyl), 5.6 (1H, bs, thiazoyl), 1.6 (3H, bs, Me), 1.2 (3H, bs, Me).

[PdCl(Me-dppat-P)(Me-dppat-P,N)][Cl] (**5.13**): Me-dppat (104 mg, 0.35 mmol) and [$PdCl_2$(cod)] (50 mg, 0.175 mmol) were weighed into a round bottomed flask. Acetonitrile (5 cm^3) was added and the mixture heated until the solid was dissolved, this mixture was then allowed to return to room temperature. An orange precipitate was formed during cooling and this was filtered isolating the product as an orange solid, (yield: 86 mg, 63 %). $C_{32}H_{30}N_4S_2P_2Cl_2Pd$ requires: C, 49.6, H, 3.91, N, 7.24. Found: C, 48.8, H, 3.71, N, 7.07. ν_{max}/cm^{-1}: 3085, 2914, 2570, 1574, 1551, 1477, 1434, 1101, 998. ^{31}P NMR ($CDCl_3$), δ 80.1 ($^2J_{P\text{-}P}$ = 23 Hz), 50.6 ($^2J_{P\text{-}P}$ = 23 Hz). ^{1}H NMR ($CDCl_3$), δ 10.5 (2H, s, N-H), 7.7-6.6 (20H, m, aromatic), 5.8 (1H, s, aromatic), 5.1 (1H, s, aromatic), 2.2 (3H, s, Me), 1.6 (3H, s, Me).

[RuCl(p-Cymene)(Me-dppat-P,N)][Cl] (**5.14**): Me-dppat (68 mg, 0.23 mmol) and [{RuCl(μ-Cl)(*p*-Cymene)}$_2$] (70 mg, 0.115 mmol) were weighed into a round bottomed flask. Acetonitrile (5 cm^3) was added and the mixture heated until the solid was dissolved, this mixture was then allowed to return to room temperature. A red precipitate was formed during cooling and this was filtered isolating the product as a red solid, (yield: 97 mg, 70 %). $C_{26}H_{29}N_2SPCl_2Ru$ requires: C, 51.6, H, 4.84, N, 4.63. Found: C, 51.1, H, 5.21, N, 4.78. ν_{max}/cm^{-1}: 3046, 2961, 1578, 1561, 1482, 1435, 1101, 994. ^{31}P NMR ($CDCl_3$),δ 99.9 ppm. ^{1}H NMR ($CDCl_3$),δ 10.2 (1H, s, N-H), 8.1-7.9 (4H, m, aromatic (ligand)), 7.6-7.1 (6H, m, aromatic (ligand)), 6.4 (1H, s,

thiazoyl), 5.3-5.1 (2H, m, aromatic (p-Cymene)), 2.3 (1H, m, -CMe_2-H), 1.9 (3H, s, Ar-Me), 1.0-0.7 (15H, m, Me and ^{t}Bu-H).

2-(diphenylphosphino)amino-4-tert-butylthiazole **(bu-dppat) (5.15)**:

Chlorodiphenylphosphine (2.80 cm^3, 16 mmol) in 40 cm^3 of thf was added dropwise to a mixture of 2-amino-4-*tert*-butylthiazole (2.5 g, 16 mmol), DMAP (191 mg, 1.6 mmol) and triethylamine (2.34 cm^3, 17mmol) in 100 cm^3 of thf at –78°C. After addition was complete the mixture was allowed to warm to room temperature overnight. The resultant white precipitate was filtered and the filtrate reduced to dryness *in vacuo* over the course of five days to give the desired product (Yield: 3.4 g, 63 %). $C_{19}H_{21}N_2SP$. ν_{max}/cm^{-1}: 3343, 2959, 1525, 1479, 1432, 1241, 1202, 1098, 996. ^{31}P NMR ($CDCl_3$), 39.7 ppm. ^{1}H NMR ($CDCl_3$), 8.2 (1H, d, J = 7 Hz, N-H), 7.5-7.2 (10H, m, aromatic), 6.1 (1H, s, thiazoyl), 1.2 (9H, s, ^{t}Bu-H).

[PtCl$_2$(^{t}Bu-dppat-P)$_2$] **(5.16)**: ^{t}Bu-dppat (99 mg, 0.29 mmol) and [$PtCl_2$(cod)] (54 mg, 0.145 mmol) were weighed into a round bottomed flask. Acetonitrile (5 cm^3) was added and the mixture heated until the solid was dissolved, this mixture was then allowed to return to room temperature. The solvent was removed *in vacuo* and diethyl ether (5 cm^3) added and the resultant solution cooled to –4°C to generate a solid, this solid was subsequently filtered to isolate a expected colourless solid, (yield: 72 mg, 53 %). $C_{38.5}H_{43}N_4S_2P_2Cl_3Pt$ requires: C, 46.7, H, 4.38, N, 5.66. Found: C, 46.9, H, 4.55, N, 5.24 %. ν_{max}/cm^{-1}: 3055, 2964, 1623, 1592, 1561, 1479, 1435, 1104, 1017, 997. ^{31}P NMR ($CDCl_3$), δ 53.9 ppm ($^1J_{Pt\text{-}P}$ = 4040 Hz). ^{1}H NMR ($CDCl_3$), δ 11.2 (2H, bs, N-H), 8.0-7.1 (20H, m, aromatic), 5.9 (2H, s, thiazoyl), 1.3 (9H, s, ^{t}Bu-H).

***[Pd(η-C_3H_6)(b-dppat-P,N)][Cl]* 5.17**: B-dppat (93 mg, 0.27 mmol) and [{Pd(μ-Cl)(η-C_3H_6)}$_2$] (50 mg, 0.135 mmol) were weighed into a round bottomed flask. DCM (5 cm^3) was added and the mixture stirred for 1 hour. The solvent was reduced *in vacuo* to approx. 1 cm^3 and the product precipitated with petroleum ether (15 cm^3), this solid was subsequently filtered to isolate a pale yellow solid, (yield: 34 mg, 24 %). $C_{22}H_{27}N_2SPClPd$ requires: C, 50.4, H, 5.19, N, 5.34. Found: C, 50.4, H, 5.05, N, 5.31 %. ν_{max}/cm^{-1}: 3203, 2963, 1527, 1436, 1097, 955. ^{31}P NMR ($CDCl_3$), δ 58.3 ppm. ^{1}H NMR ($CDCl_3$), 7.9-7.7 (5H, m, aromatic), 7.5-7.2 (6H, m, aromatic), 6.1 (1H, s, thiazoyl), 5.5 (1H, m, allyl), 4.8 (1H, m, allyl), 3.6 (1H, m, allyl), 3.4 (1H, m, allyl), 3.0 (1H, m, allyl) 2.6 (1H, m, allyl), 1.0 (9H, s, ^{t}Bu-H).

***[$RuCl_2$(p-Cymene)(b-dppat-P)]* 5.18**: B-dppat (78 mg, 0.23 mmol) and [{RuCl(μ-Cl)(*p*-Cymene)}$_2$] (70 mg, 0.115 mmol) were weighed into a round bottomed flask. DCM (5 cm^3) was added and the mixture stirred for 1 hour. The solvent was reduced *in vacuo* to approx. 1 cm^3 and the product precipitated with petroleum ether (15 cm^3), this solid was subsequently filtered to isolate a red solid, (yield: 83 mg, 78 %). $C_{30}H_{35}N_2SPCl_2Ru$ requires: C, 54.6, H, 5.36, N, 4.25. Found: C, 53.6, H, 5.29, N, 4.28 %. ν_{max}/cm^{-1}: 2690, 1532, 1435, 1100. ^{31}P NMR ($CDCl_3$), δ 62.3 ppm. ^{1}H NMR ($CDCl_3$), 8.1-8.0 (4H, m, aromatic (ligand)), 7.5-7.2 (6H, m, aromatic (ligand)), 5.9 (1H, s, thiazoyl), 5.3 (2H, m, aromatic (p-Cymene)), 5.2 (2H, m, aromatic (p-Cymene)), 2.5 (1H, m, -CMe_2-H), 1.9 (3H, s, Ar-Me), 1.0-0.7 (15H, m, Me and ^{t}Bu-H).

REFERENCES.

1. R. Uson, A. Laguna and M. Laguna, *Inorg. Synth.*, 1989, **26**, 85.
2. D. Drew and J. R. Doyle, *Inorg. Synth*, 1991, **28**, 346.
3. J. X. McDermott, J. F. White and G. M. Whiteside, *J. Am. Chem. Soc.*, 1976, **60**, 6521.
4. H. C. Clark and L. E. Manzer, *J. Organomet. Chem.*, 1973, **59**, 411.
5. W. Baratta and P. S. Pregosin, *Inorg. Chem Acta.*, 1993, **209**, 85.
6. C. White, A. Yates, P. M. Maitlis, *Inorg. Synth.*, 1992, **29**, 228.
7. G. Giordano, R. H. Crabtree, *Inorg. Synth.*, 1979, **19**, 218.
8. M. A. Bennett, T. N. Huang, T. W. Matheson, A. R. Smith, *Inorg. Synth.*, 1982, **21**, 74.
9. L. Porri, M. C. Gallazzi, A. Colombo, G. Allegra, *Tetrahedron Lett.*, 1965, **47**, 4187.
10. A. L. Balch, L. S. Benner, *Inorg. Synth.*, 1990, **28**, 340.
11. H. C. Clark, L. E. Manzer, *J. Orgnaomet. Chem.*, 1973, **59**, 411.

APPENDIX ONE:

Crystallographic Data For All Studied Complexes.

(Local ID's in brackets)

Table A1: *Crystal data and structure refinement for [$RhCl_2(\eta^5\text{-}C_5Me_5)$(dpppa-P)].*

Identification code	**2.12** (hmasm7)
Empirical formula	$C_{28}H_{30}Cl_2IrN_2OP$
Formula weight	704.61
Temperature	125(2) K
Wavelength	0.71073 Å
Crystal system	Orthorhombic
Space group	P2(1)2(1)2(1)
Unit cell dimensions	a = 8.2751(16) Å α= 90°.
	b = 17.750(3) Å β= 90°.
	c = 17.892(4) Å γ = 90°.
Volume	2628.1(9) $Å_3$
Z	4
Density (calculated)	1.781 Mg/m_3
Absorption coefficient	5.369 mm^{-1}
F(000)	1384
Crystal size	0.15 x 0.15 x 0.15 mm_3
Theta range for data collection	1.62 to 23.28°.
Index ranges	-6<=h<=9, -19<=k<=18, -19<=l<=19
Reflections collected	11347
Independent reflections	3757 [R(int) = 0.0560]
Completeness to theta = 23.28°	99.8 %
Absorption correction	Multi-scan
Max. and min. transmission	1.00000 and 0.491678
Refinement method	Full-matrix least-squares on F_2
Data / restraints / parameters	3757 / 1 / 321
Goodness-of-fit on F_2	0.979
Final R indices [I>2sigma(I)]	R1 = 0.0297, wR2 = 0.0674
R indices (all data)	R1 = 0.0335, wR2 = 0.0692
Absolute structure parameter	-0.014(9)
Extinction coefficient	0.00065(14)
Largest diff. peak and hole	0.824 and -1.236 $e.Å^{-3}$

Table A2: *Crystal data and structure refinement for dpppa-S..*

Identification code	**2.3** (hmasm8)	
Empirical formula	$C_{18}H_{15}N_2OPS$	
Formula weight	338.35	
Temperature	125(2) K	
Wavelength	0.71073 Å	
Crystal system	Triclinic	
Space group	P-1	
Unit cell dimensions	a = 8.7701(17) Å	α= 77.738(3)°.
	b = 9.0319(17) Å	β= 85.554(3)°.
	c = 11.043(2) Å	γ = 72.540(3)°.
Volume	815.3(3) $Å^3$	
Z	2	
Density (calculated)	1.378 Mg/m^3	
Absorption coefficient	0.302 mm^{-1}	
F(000)	352	
Crystal size	0.30 x 0.25 x 0.10 mm^3	
Theta range for data collection	2.41 to 23.29°.	
Index ranges	-9<=h<=9, -9<=k<=10, -11<=l<=12	
Reflections collected	4092	
Independent reflections	2273 [R(int) = 0.0550]	
Completeness to theta = 23.29°	97.3 %	
Absorption correction	Multi-scan	
Max. and min. transmission	1.00000 and 0.857434	
Refinement method	Full-matrix least-squares on F_2	
Data / restraints / parameters	2273 / 1 / 213	
Goodness-of-fit on F_2	0.864	
Final R indices [I>2sigma(I)]	R1 = 0.0393, wR2 = 0.1018	
R indices (all data)	R1 = 0.0538, wR2 = 0.1105	
Extinction coefficient	0.009(4)	
Largest diff. peak and hole	0.375 and -0.279 $e.Å^{-3}$	

Table A3: *Crystal data and structure refinement for [PdCl($C_{12}H_{12}N$)(dpppa-P)].*

Identification code	**2.10** (hmasm10)	
Empirical formula	$C_{30}H_{27}ClN_3OPPd$	
Formula weight	618.37	
Temperature	125(2) K	
Wavelength	0.71073 Å	
Crystal system	Monoclinic	
Space group	P2(1)/c	
Unit cell dimensions	a = 15.239(3) Å	α= 90°.
	b = 8.6292(16) Å	β= 98.237(3)°.
	c = 20.522(4) Å	γ = 90°.
Volume	2670.8(8) Å$_3$	
Z	4	
Density (calculated)	1.538 Mg/m$_3$	
Absorption coefficient	0.884 mm^{-1}	
F(000)	1256	
Crystal size	0.30 x 0.30 x 0.15 mm$_3$	
Theta range for data collection	2.01 to 23.32°.	
Index ranges	-16<=h<=16, -9<=k<=9, -14<=l<=22	
Reflections collected	10995	
Independent reflections	3792 [R(int) = 0.0596]	
Completeness to theta = 23.32°	97.9 %	
Absorption correction	Multi-scan	
Max. and min. transmission	1.00000 and 0.420177	
Refinement method	Full-matrix least-squares on F_2	
Data / restraints / parameters	3792 / 1 / 339	
Goodness-of-fit on F_2	1.085	
Final R indices [I>2sigma(I)]	R1 = 0.0510, wR2 = 0.1269	
R indices (all data)	R1 = 0.0569, wR2 = 0.1315	
Extinction coefficient	0.0014(4)	
Largest diff. peak and hole	2.396 and -1.352 e.Å^{-3}	

Table A4: *Crystal data and structure refinement for [PdCl($C_9H_{12}N$)(dpppa-P)].*

Identification code	**2.9** (hmasm11)	
Empirical formula	$C_{27}H_{27}ClN_3OPPd$	
Formula weight	582.34	
Temperature	125(2) K	
Wavelength	0.71073 Å	
Crystal system	Monoclinic	
Space group	P2(1)/c	
Unit cell dimensions	a = 15.824(6) Å	α= 90°.
	b = 8.481(3) Å	β= 97.899(6)°.
	c = 19.445(7) Å	γ = 90°.
Volume	2584.9(16) $Å_3$	
Z	4	
Density (calculated)	1.496 Mg/m_3	
Absorption coefficient	0.908 mm_{-1}	
F(000)	1184	
Crystal size	0.30 x 0.30 x 0.30 mm_3	
Theta range for data collection	2.11 to 23.54°.	
Index ranges	-17<=h<=17, -7<=k<=9, -21<=l<=21	
Reflections collected	10665	
Independent reflections	3710 [R(int) = 0.1065]	
Completeness to theta = 23.54°	96.7 %	
Absorption correction	Multi-scan	
Max. and min. transmission	1.00000 and 0.137092	
Refinement method	Full-matrix least-squares on F_2	
Data / restraints / parameters	3710 / 1 / 311	
Goodness-of-fit on F_2	1.015	
Final R indices [I>2sigma(I)]	R1 = 0.0681, wR2 = 0.1705	
R indices (all data)	R1 = 0.0821, wR2 = 0.1874	
Largest diff. peak and hole	1.665 and -2.536 $e.Å_{-3}$	

Table A5: *Crystal data and structure refinement for [PdCl(allyl)(dpppa-P)].*

Identification code	**2.7** (hmasm12)
Empirical formula	$C_{21}H_{20}ClN_2OPPd$
Formula weight	489.21
Temperature	125(2) K
Wavelength	0.71073 Å
Crystal system	Triclinic
Space group	P-1
Unit cell dimensions	a = 9.9452(12) Å α= 118.018(2)°.
	b = 15.3618(19) Å β= 101.038(2)°.
	c = 15.7040(19) Å γ = 95.688(2)°.
Volume	2028.7(4) $Å_3$
Z	4
Density (calculated)	1.602 Mg/m_3
Absorption coefficient	1.138 mm_{-1}
F(000)	984
Crystal size	0.30 x 0.30 x 0.10 mm_3
Theta range for data collection	1.53 to 23.33°.
Index ranges	-11<=h<=11, -12<=k<=17, -17<=l<=17
Reflections collected	10246
Independent reflections	5783 [R(int) = 0.0198]
Completeness to theta = 23.33°	98.3 %
Absorption correction	multi-scan
Max. and min. transmission	1.00000 and 0.885778
Refinement method	Full-matrix least-squares on F_2
Data / restraints / parameters	5783 / 2 / 546
Goodness-of-fit on F_2	1.011
Final R indices [I>2sigma(I)]	R1 = 0.0273, wR2 = 0.0731
R indices (all data)	R1 = 0.0305, wR2 = 0.0756
Extinction coefficient	0.0013(3)
Largest diff. peak and hole	0.528 and -0.435 $e.Å_{-3}$

Table A6: *Crystal data and structure refinement for dpptc-O.*

Identification code	**3.2** (hmasm14)
Empirical formula	$C_{17}H_{14}NO_2PS$
Formula weight	327.32
Temperature	125(2) K
Wavelength	0.71073 Å
Crystal system	Monoclinic
Space group	P2(1)/c
Unit cell dimensions	a = 9.617(2) Å α= 90°.
	b = 16.571(3) Å β= 94.111(4)°.
	c = 9.877(2) Å γ = 90°.
Volume	1570.0(6) $Å_3$
Z	4
Density (calculated)	1.385 Mg/m_3
Absorption coefficient	0.314 mm_{-1}
F(000)	680
Crystal size	0.30 x 0.20 x 0.20 mm_3
Theta range for data collection	2.12 to 23.32°.
Index ranges	-10<=h<=10, -18<=k<=17, -11<=l<=10
Reflections collected	7598
Independent reflections	2219 [R(int) = 0.0687]
Completeness to theta = 23.32°	97.7 %
Absorption correction	Multi-scan
Max. and min. transmission	1.00000 and 0.715659
Refinement method	Full-matrix least-squares on F_2
Data / restraints / parameters	2219 / 1 / 204
Goodness-of-fit on F_2	0.888
Final R indices [I>2sigma(I)]	R1 = 0.0472, wR2 = 0.1120
R indices (all data)	R1 = 0.0821, wR2 = 0.1299
Extinction coefficient	0.0021(15)
Largest diff. peak and hole	0.431 and -0.293 $e.Å_{-3}$

Table A7: *Crystal data and structure refinement for cis-[$PtCl_2$(dpppa-P)(PEt_3)].*

Identification code	**2.15** (hmasm15)
Empirical formula	$C_{24}H_{30}Cl_2N_2OP_2Pt$
Formula weight	690.43
Temperature	125(2) K
Wavelength	0.71073 Å
Crystal system	Monoclinic
Space group	P2(1)/c
Unit cell dimensions	a = 15.771(2) Å α= 90°.
	b = 10.4905(16) Å β= 113.589(2)°.
	c = 17.092(3) Å γ = 90°.
Volume	2591.6(7) $Å_3$
Z	4
Density (calculated)	1.770 Mg/m_3
Absorption coefficient	5.764 mm_{-1}
F(000)	1352
Crystal size	0.30 x 0.15 x 0.06 mm_3
Theta range for data collection	1.41 to 23.41°.
Index ranges	-16<=h<=17, -11<=k<=11, -18<=l<=18
Reflections collected	10858
Independent reflections	3699 [R(int) = 0.0405]
Completeness to theta = 23.41°	97.5 %
Absorption correction	Multi-scan
Max. and min. transmission	1.00000 and 0.579114
Refinement method	Full-matrix least-squares on F_2
Data / restraints / parameters	3699 / 1 / 293
Goodness-of-fit on F_2	0.925
Final R indices [I>2sigma(I)]	R1 = 0.0277, wR2 = 0.0641
R indices (all data)	R1 = 0.0366, wR2 = 0.0674
Largest diff. peak and hole	1.349 and -0.919 $e.Å_{-3}$

Table A8: *Crystal data and structure refinement for dpppa-O.*

Identification code	**2.2** (hmasm17)
Empirical formula	$C_{18}H_{15}N_2O_2P$
Formula weight	322.29
Temperature	125(2) K
Wavelength	0.71073 Å
Crystal system	Monoclinic
Space group	P2(1)/c
Unit cell dimensions	a = 8.4497(15) Å α= 90°.
	b = 17.369(3) Å β= 108.389(3)°.
	c = 11.264(2) Å, γ = 90°.
Volume	1568.8(5) $Å^3$
Z	4
Density (calculated)	1.365 Mg/m^3
Absorption coefficient	0.186 mm^{-1}
F(000)	672
Crystal size	0.30 x 0.30 x 0.10 mm^3
Theta range for data collection	2.24 to 23.28°.
Index ranges	-9<=h<=9, -19<=k<=18, -7<=l<=12
Reflections collected	6672
Independent reflections	2230 [R(int) = 0.0439]
Completeness to theta = 23.28°	98.6 %
Absorption correction	Multi-scan
Max. and min. transmission	1.00000 and 0.680448
Refinement method	Full-matrix least-squares on F_2
Data / restraints / parameters	2230 / 1 / 213
Goodness-of-fit on F_2	0.966
Final R indices [I>2sigma(I)]	R1 = 0.0461, wR2 = 0.1141
R indices (all data)	R1 = 0.0689, wR2 = 0.1252
Extinction coefficient	0.0025(15)
Largest diff. peak and hole	0.418 and -0.465 $e.Å^{-3}$

Table A9: *Crystal data and structure refinement for bdpppa-Se_2*

Identification code	**3.14** (hmasm27)
Empirical formula	$C_{32}H_{26}Cl_3N_3O_2P_2Se_2$
Formula weight	810.77
Temperature	125(2) K
Wavelength	0.71073 Å
Crystal system	Triclinic
Space group	P-1
Unit cell dimensions	a = 9.6167(19) Å α= 87.463(3)°.
	b = 11.620(2) Å β= 74.728(3)°.
	c = 15.679(3) Å γ = 82.062(4)°.
Volume	1673.9(6) $Å_3$
Z	2
Density (calculated)	1.609 Mg/m_3
Absorption coefficient	2.579 mm_{-1}
F(000)	808
Crystal size	0.30 x 0.20 x 0.06 mm_3
Theta range for data collection	1.77 to 23.38°.
Index ranges	-10<=h<=10, -12<=k<=12, -17<=l<=17
Reflections collected	8493
Independent reflections	4727 [R(int) = 0.0519]
Completeness to theta = 23.38°	96.9 %
Absorption correction	Multiscan
Max. and min. transmission	1.00000 and 0.736697
Refinement method	Full-matrix least-squares on F_2
Data / restraints / parameters	4727 / 2 / 406
Goodness-of-fit on F_2	0.637
Final R indices [I>2sigma(I)]	R1 = 0.0393, wR2 = 0.1223
R indices (all data)	R1 = 0.0559, wR2 = 0.1537
Extinction coefficient	0.0011(10)
Largest diff. peak and hole	0.577 and -0.552 $e.Å_{-3}$

Table A10: *Crystal data and structure refinement for* $[Pt_2Cl_2(\eta\text{-}C_3H_6)_2(bdpppa\text{-}P,P)]$.

Identification code	**3.21** (hmasm29)
Empirical formula	$C_{37}H_{35}Cl_2N_3O_2P_2Pt_2$
Formula weight	1076.70
Temperature	293(2) K
Wavelength	0.71073 Å
Crystal system	Monoclinic
Space group	P2(1)/n
Unit cell dimensions	a = 15.9450(9) Å α= 90°.
	b = 9.0240(5) Å β= 98.8180(10)°.
	c = 26.5195(16) Å γ = 90°.
Volume	3770.7(4) $Å_3$
Z	4
Density (calculated)	1.897 Mg/m_3
Absorption coefficient	7.675 mm_{-1}
F(000)	2056
Crystal size	0.15 x 0.15 x 0.06 mm_3
Theta range for data collection	1.40 to 23.27°.
Index ranges	-17<=h<=17, -8<=k<=10, -29<=l<=23
Reflections collected	18435
Independent reflections	5409 [R(int) = 0.0515]
Completeness to theta = 23.27°	99.8 %
Absorption correction	multi-scan
Max. and min. transmission	1.00000 and 0.575985
Refinement method	Full-matrix least-squares on F_2
Data / restraints / parameters	5409 / 2 / 451
Goodness-of-fit on F_2	0.964
Final R indices [I>2sigma(I)]	R1 = 0.0359, wR2 = 0.0750
R indices (all data)	R1 = 0.0697, wR2 = 0.0860
Extinction coefficient	0.00016(3)
Largest diff. peak and hole	0.843 and -0.787 $e.Å_{-3}$

Table A11: *Crystal data and structure refinement for [$PtCl_2$(dppai-P,N)].*

Identification code	**4.2** (hmasm31)
Empirical formula	$C_{19}H_{15}Cl_2N_2PPt$
Formula weight	568.29
Temperature	125(2) K
Wavelength	0.71073 Å
Crystal system	Orthorhombic
Space group	Pbca
Unit cell dimensions	a = 9.0694(15) Å α= 90°.
	b = 15.250(3) Å β= 90°.
	c = 26.813(5) Å γ = 90°.
Volume	3708.3(11) $Å_3$
Z	8
Density (calculated)	2.036 Mg/m_3
Absorption coefficient	7.946 mm_{-1}
F(000)	2160
Crystal size	0.25 x 0.25 x 0.1 mm_3
Theta range for data collection	2.67 to 23.36°.
Index ranges	-10<=h<=8, -16<=k<=14, -29<=l<=29
Reflections collected	14950
Independent reflections	2658 [R(int) = 0.0999]
Completeness to theta = 23.36°	98.7 %
Absorption correction	Multi-scan
Max. and min. transmission	1.00000 and 0.744746
Refinement method	Full-matrix least-squares on F_2
Data / restraints / parameters	2658 / 0 / 227
Goodness-of-fit on F_2	0.856
Final R indices [I>2sigma(I)]	R1 = 0.0240, wR2 = 0.0501
R indices (all data)	R1 = 0.0307, wR2 = 0.0526
Extinction coefficient	0.00030(4)
Largest diff. peak and hole	0.736 and -1.930 $e.Å_{-3}$

Table A12: *Crystal data and structure refinement for [RuCl(p-Cy)(dpppa-P,O)].*

Identification code	**2.18** (hmasm32)
Empirical formula	$C_{29}H_{30}Cl_3N_2OPRu$
Formula weight	660.94
Temperature	125(2) K
Wavelength	0.71073 Å
Crystal system	Orthorhombic
Space group	Pca2(1)
Unit cell dimensions	a = 17.576(3) Å α= 90°.
	b = 9.0772(15) Å β= 90°.
	c = 17.593(3) Å γ = 90°.
Volume	2806.8(8) $Å_3$
Z	4
Density (calculated)	1.564 Mg/m_3
Absorption coefficient	0.927 mm_{-1}
F(000)	1344
Crystal size	0.15 x 0.15 x 0.15 mm_3
Theta range for data collection	2.24 to 23.30°.
Index ranges	-19<=h<=16, -10<=k<=10, -18<=l<=19
Reflections collected	13398
Independent reflections	3965 [R(int) = 0.0673]
Completeness to theta = 23.30°	99.6 %
Absorption correction	multi-scan
Max. and min. transmission	1.00000 and 0.551286
Refinement method	Full-matrix least-squares on F_2
Data / restraints / parameters	3965 / 1 / 352
Goodness-of-fit on F_2	0.994
Final R indices [I>2sigma(I)]	R1 = 0.0447, wR2 = 0.1002
R indices (all data)	R1 = 0.0581, wR2 = 0.1053
Absolute structure parameter	0.07(5)
Largest diff. peak and hole	0.944 and -0.856 $e.Å_{-3}$

Table A13: *Crystal data and structure refinement for [$PdCl_2$(dppai-P,N)].*

Identification code	**4.3** (hmasm33)
Empirical formula	$C_{19}H_{15}Cl_2N_2PPd$
Formula weight	479.60
Temperature	125(2) K
Wavelength	0.71073 Å
Crystal system	Monoclinic
Space group	P2(1)/c
Unit cell dimensions	a = 9.8511(10) Å α= 90°.
	b = 15.5407(16) Å β= 111.174(2)°.
	c = 12.3756(12) Å γ = 90°.
Volume	1766.7(3) $Å_3$
Z	4
Density (calculated)	1.803 Mg/m_3
Absorption coefficient	1.447 mm_{-1}
F(000)	952
Crystal size	0.30 x 0.10 x 0.06 mm_3
Theta range for data collection	2.20 to 23.29°.
Index ranges	-9<=h<=10, -16<=k<=17, -13<=l<=13
Reflections collected	7581
Independent reflections	2527 [R(int) = 0.0256]
Completeness to theta = 23.29°	99.2 %
Absorption correction	multiscan
Max. and min. transmission	1.00000 and 0.718554
Refinement method	Full-matrix least-squares on F_2
Data / restraints / parameters	2527 / 0 / 227
Goodness-of-fit on F_2	1.036
Final R indices [I>2sigma(I)]	R1 = 0.0228, wR2 = 0.0574
R indices (all data)	R1 = 0.0269, wR2 = 0.0587
Extinction coefficient	0.0012(3)
Largest diff. peak and hole	0.398 and -0.376 $e.Å_{-3}$

Table 14: *Crystal data and structure refinement for [PtMeCl(dppai-P,N)].*

Identification code	**4.4**(hmasm35)	
Empirical formula	C20 H18 Cl N2 P Pt	
Formula weight	547.87	
Temperature	125(2) K	
Wavelength	0.71073 Å	
Crystal system	Triclinic	
Space group	P-1	
Unit cell dimensions	a = 9.584(3) Å	α= 88.925(5)°.
	b = 10.289(3) Å	β= 77.471(5)°.
	c = 10.965(4) Å	γ = 62.072(4)°.
Volume	928.3(5) $Å_3$	
Z	2	
Density (calculated)	1.960 Mg/m_3	
Absorption coefficient	7.792 mm^{-1}	
F(000)	524	
Crystal size	0.3 x 0.2 x 0.1 mm_3	
Theta range for data collection	2.25 to 23.30°.	
Index ranges	-10<=h<=9, -11<=k<=11, -12<=l<=12	
Reflections collected	4702	
Independent reflections	2631 [R(int) = 0.0563]	
Completeness to theta = 23.30°	98.0 %	
Absorption correction	Multi-scan	
Max. and min. transmission	1.00000 and 0.697392	
Refinement method	Full-matrix least-squares on F_2	
Data / restraints / parameters	2631 / 0 / 227	
Goodness-of-fit on F_2	1.045	
Final R indices [I>2sigma(I)]	R1 = 0.0394, wR2 = 0.1024	
R indices (all data)	R1 = 0.0430, wR2 = 0.1042	
Extinction coefficient	0.0029(8)	
Largest diff. peak and hole	2.600 and -1.368 $e.Å^{-3}$	

Table A15: *Crystal data and structure refinement for [PtMeCl(dpptc-P)$_2$].*

Identification code	**3.9** (hmasm36)
Empirical formula	$C_{36}H_{32}Cl_4N_2O_2P_2PtS_2$
Formula weight	987.59
Temperature	125(2) K
Wavelength	0.71073 Å
Crystal system	Triclinic
Space group	P-1
Unit cell dimensions	a = 12.2558(10) Å α= 68.1350(10)°.
	b = 12.2862(10) Å β= 77.1500(10)°.
	c = 13.6126(11) Å γ = 82.4070(10)°.
Volume	1851.9(3) Å^3
Z	2
Density (calculated)	1.771 Mg/m^3
Absorption coefficient	4.313 mm^{-1}
F(000)	972
Crystal size	0.2 x 0.1 x 0.06 mm^3
Theta range for data collection	1.64 to 23.34°.
Index ranges	-13<=h<=13, -13<=k<=12, -13<=l<=15
Reflections collected	9348
Independent reflections	5256 [R(int) = 0.0251]
Completeness to theta = 23.34°	98.0 %
Absorption correction	Multi-scan
Max. and min. transmission	1.00000 and 0.867680
Refinement method	Full-matrix least-squares on F_2
Data / restraints / parameters	5256 / 2 / 451
Goodness-of-fit on F_2	0.949
Final R indices [I>2sigma(I)]	R1 = 0.0309, wR2 = 0.0714
R indices (all data)	R1 = 0.0406, wR2 = 0.0740
Extinction coefficient	0.00052(19)
Largest diff. peak and hole	1.040 and -0.954 e.Å^{-3}

Table A16: *Crystal data and structure refinement for [Pd($C_9H_{12}N$)(dpptc-P)].*

Identification code	**3.10**(hmasm37)
Empirical formula	C26 H26 Cl N2 O P Pd S
Formula weight	587.37
Temperature	125(2) K
Wavelength	0.71073 Å
Crystal system	Triclinic
Space group	P-1
Unit cell dimensions	a = 10.043(2) Å α= 87.629(4)°.
	b = 10.325(2) Å β= 69.956(3)°.
	c = 13.541(3) Å γ = 70.801(3)°.
Volume	1241.7(4) $Å^3$
Z	2
Density (calculated)	1.571 Mg/m^3
Absorption coefficient	1.026 mm^{-1}
F(000)	596
Crystal size	0.15 x 0.15 x 0.06 mm^3
Theta range for data collection	1.61 to 23.27°.
Index ranges	-11<=h<=11, -7<=k<=11, -14<=l<=14
Reflections collected	6239
Independent reflections	3522 [R(int) = 0.0295]
Completeness to theta = 23.27°	98.6 %
Absorption correction	Multi-scan
Max. and min. transmission	1.00000 and 0.684340
Refinement method	Full-matrix least-squares on F_2
Data / restraints / parameters	3522 / 1 / 303
Goodness-of-fit on F_2	0.927
Final R indices [I>2sigma(I)]	R1 = 0.0382, wR2 = 0.0961
R indices (all data)	R1 = 0.0456, wR2 = 0.0988
Extinction coefficient	0.0019(8)
Largest diff. peak and hole	0.765 and -1.012 $e.Å^{-3}$

Table A17: *Crystal data and structure refinement for* $[RhCl_2(\eta^5\text{-}C_5Me_5)(dpptc\text{-}P)]$.

Identification code	**3.8** (hmasm41)
Empirical formula	$C_{27}H_{29}Cl_2NOPRhS$
Formula weight	620.35
Temperature	125(2) K
Wavelength	0.71073 Å
Crystal system	Orthorhombic
Space group	P2(1)2(1)2(1)
Unit cell dimensions	a = 13.616(2) Å α= 90°.
	b = 11.8190(17) Å β= 90°.
	c = 16.918(2) Å γ = 90°.
Volume	2722.7(7) $Å_3$
Z	4
Density (calculated)	1.513 Mg/m_3
Absorption coefficient	0.980 mm_{-1}
F(000)	1264
Crystal size	0.15 x 0.15 x 0.15 mm_3
Theta range for data collection	2.28 to 23.27°.
Index ranges	-15<=h<=15, -13<=k<=13, -13<=l<=18
Reflections collected	11848
Independent reflections	3864 [R(int) = 0.0326]
Completeness to theta = 23.27°	99.1 %
Absorption correction	Multi-scan
Max. and min. transmission	1.00000 and 0.886248
Refinement method	Full-matrix least-squares on F_2
Data / restraints / parameters	3864 / 1 / 312
Goodness-of-fit on F_2	0.907
Final R indices [I>2sigma(I)]	R1 = 0.0235, wR2 = 0.0557
R indices (all data)	R1 = 0.0260, wR2 = 0.0566
Absolute structure parameter	0.01(3)
Extinction coefficient	0.00028(14)
Largest diff. peak and hole	0.575 and -0.253 $e.Å_{-3}$

Table A18: *Crystal data and structure refinement for [AuCl(dpppa-P)].*

Identification code	**2.17** (hmasm40)	
Empirical formula	$C_{18}H_{15}AuClN_2OP$	
Formula weight	538.71	
Temperature	398(2) K	
Wavelength	0.71073 Å	
Crystal system	Monoclinic	
Space group	P2(1)/c	
Unit cell dimensions	a = 13.271(4) Å	α= 90°.
	b = 12.119(4) Å	β= 102.124(6)°.
	c = 11.111(4) Å	γ = 90°.
Volume	1747.1(10) $Å_3$	
Z	4	
Density (calculated)	2.048 Mg/m_3	
Absorption coefficient	8.672 mm_{-1}	
F(000)	1024	
Crystal size	0.25 x 0.15 x 0.15 mm_3	
Theta range for data collection	1.57 to 23.55°.	
Index ranges	-14<=h<=14, -13<=k<=13, -12<=l<=8	
Reflections collected	7308	
Independent reflections	2484 [R(int) = 0.0395]	
Completeness to theta = 23.55°	95.3 %	
Absorption correction	Multi-scan	
Max. and min. transmission	1.00000 and 0.708088	
Refinement method	Full-matrix least-squares on F_2	
Data / restraints / parameters	2484 / 1 / 222	
Goodness-of-fit on F_2	0.903	
Final R indices [I>2sigma(I)]	R1 = 0.0301, wR2 = 0.0695	
R indices (all data)	R1 = 0.0373, wR2 = 0.0725	
Extinction coefficient	0.00073(16)	
Largest diff. peak and hole	1.170 and -1.212 $e.Å_{-3}$	

Table A19: *Crystal data and structure refinement for [PdCl(allyl)(dpptc-P)].*

Identification code	**3.5** (hmasm16)
Empirical formula	C20 H19 Cl N O P Pd S
Formula weight	494.24
Temperature	125(2) K
Wavelength	0.71073 Å
Crystal system	Monoclinic
Space group	P2(1)/c
Unit cell dimensions	a = 9.2350(18) Å α= 90°.
	b = 12.097(2) Å β= 100.309(4)°.
	c = 18.302(4) Å γ = 90°.
Volume	2011.5(7) $Å^3$
Z	4
Density (calculated)	1.632 Mg/m^3
Absorption coefficient	1.248 mm^{-1}
F(000)	992
Crystal size	0.30 x 0.20 x 0.15 mm^3
Theta range for data collection	2.24 to 23.36°.
Index ranges	-10<=h<=10, -13<=k<=13, -20<=l<=17
Reflections collected	8199
Independent reflections	2780 [R(int) = 0.1066]
Completeness to theta = 23.36°	94.6 %
Absorption correction	Multiscan
Max. and min. transmission	1.00000 and 0.346746
Refinement method	Full-matrix least-squares on F^2
Data / restraints / parameters	2780 / 1 / 248
Goodness-of-fit on F^2	0.959
Final R indices [I>2sigma(I)]	R1 = 0.0449, wR2 = 0.1114
R indices (all data)	R1 = 0.0524, wR2 = 0.1179
Largest diff. peak and hole	1.377 and -1.812 $e.Å^{-3}$

Table A20: *Crystal data and structure refinement for [PtCl(Me-dppat-P)(Me-dppat-P,N)][Cl].*

Identification code	**5.12** (hmasm51)
Empirical formula	$C_{32}H_{28}Cl_2N_4P_2PtS_2$
Formula weight	860.63
Temperature	293(2) K
Wavelength	0.71073 Å
Crystal system	Orthorhombic
Space group	Pbcn
Unit cell dimensions	a = 15.1534(10) Å α= 90°.
	b = 15.1619(10) Å β= 90°.
	c = 30.1776(19) Å γ = 90°.
Volume	6933.4(8) $Å_3$
Z	8
Density (calculated)	1.649 Mg/m_3
Absorption coefficient	4.443 mm^{-1}
F(000)	3376
Crystal size	0.15 x 0.15 x 0.15 mm_3
Theta range for data collection	1.90 to 25.40°.
Index ranges	-18<=h<=17, -11<=k<=18, -36<=l<=34
Reflections collected	34664
Independent reflections	6322 [R(int) = 0.1604]
Completeness to theta = 25.40°	98.8 %
Absorption correction	Sadabs
Max. and min. transmission	1.00000 and 0.725119
Refinement method	Full-matrix least-squares on F_2
Data / restraints / parameters	6322 / 0 / 388
Goodness-of-fit on F_2	0.804
Final R indices [I>2sigma(I)]	R1 = 0.0515, wR2 = 0.0973
R indices (all data)	R1 = 0.1626, wR2 = 0.1292
Largest diff. peak and hole	2.247 and -1.299 $e.Å^{-3}$

Table A21: *Crystal data and structure refinement for dpppa.*

Identification code	**2.1** (mvw1)	
Empirical formula	$C_{18}H_{15}N_2OP$	
Formula weight	306.29	
Temperature	293(2) K	
Wavelength	1.54178 Å	
Crystal system	Triclinic	
Space group	P-1	
Unit cell dimensions	a = 8.4419(17) Å	α= 110.94(3)°.
	b = 10.271(2) Å	β= 103.74(3)°.
	c = 10.416(2) Å	γ = 90.27(3)°.
Volume	815.3(3) $Å^3$	
Z	2	
Density (calculated)	1.248 Mg/m^3	
Absorption coefficient	1.511 mm^{-1}	
F(000)	320	
Crystal size	0.1500 x 0.1500 x 0.0700 mm^3	
Theta range for data collection	4.70 to 73.36°.	
Index ranges	-10<=h<=8, -11<=k<=12, -6<=l<=12	
Reflections collected	6683	
Independent reflections	2850 [R(int) = 0.0923]	
Completeness to theta = 73.36°	86.9 %	
Absorption correction	MULTISCAN	
Max. and min. transmission	1.0000 and 0.2231	
Refinement method	Full-matrix least-squares on F^2	
Data / restraints / parameters	2850 / 1 / 204	
Goodness-of-fit on F^2	1.061	
Final R indices [I>2sigma(I)]	R1 = 0.0881, wR2 = 0.2260	
R indices (all data)	R1 = 0.1129, wR2 = 0.2499	
Extinction coefficient	0.013(4)	
Largest diff. peak and hole0.834 and	0.326 e.Å	

Table A22: *Crystal data and structure refinement for [PdCl(η^3-C_3H_6)(dpptc-P)].*

Identification code	**3.5**(hmasm16)	
Empirical formula	C20 H19 Cl N O P Pd S	
Formula weight	494.24	
Temperature	125(2) K	
Wavelength	0.71073 Å	
Crystal system	Monoclinic	
Space group	P2(1)/c	
Unit cell dimensions	a = 9.2350(18) Å	α= 90°.
	b = 12.097(2) Å	β= 100.309(4)°.
	c = 18.302(4) Å	γ = 90°.
Volume	2011.5(7) Å^3	
Z	4	
Density (calculated)	1.632 Mg/m^3	
Absorption coefficient	1.248 mm^{-1}	
F(000)	992	
Crystal size	0.30 x 0.20 x 0.15 mm^3	
Theta range for data collection	2.24 to 23.36°.	
Index ranges	-10<=h<=10, -13<=k<=13, -20<=l<=17	
Reflections collected	8199	
Independent reflections	2780 [R(int) = 0.1066]	
Completeness to theta = 23.36°	94.6 %	
Absorption correction	MULTISCAN	
Max. and min. transmission	1.00000 and 0.346746	
Refinement method	Full-matrix least-squares on F^2	
Data / restraints / parameters	2780 / 1 / 248	
Goodness-of-fit on F^2	0.959	
Final R indices [I>2sigma(I)]	R1 = 0.0449, wR2 = 0.1114	
R indices (all data)	R1 = 0.0524, wR2 = 0.1179	
Largest diff. peak and hole	1.377 and -1.812 e.Å^{-3}	

Appendix Two: Compound Key.

2.1	mvw042	mvw1
2.2	mvw058	Hmasm17
2.3	mvw065	Hmasm8
2.4	mvw059	
2.5	mvw044	
2.6	mvw045	
2.7	mvw046	Hmasm12
2.8	mvw047	
2.9	mvw049	Hmasm11
2.10	mvw051	Hmasm10
2.11	mvw055	
2.12	mvw067	
2.13	mvw068	Hmasm7
2.14	mvw090	
2.15	mvw094	Hmasm15
2.16	mvw104	
2.17	mvw166	Hmasm40
2.18	mvw057	Hmasm32
2.19	mvw071	
2.20	mvw081	
2.21	mvw079	
3.1	mvw092	
3.13	mvw120	
3.14	mvw122	Hmasm27
3.15	mvw136	
3.16	mvw152	
3.17	mvw153	
3.18	mvw154	
3.19	mvw138	
3.20	mvw077	
3.21	mvw141	Hmasm29
4.1	mvw101	
4.2	mvw103	Hmasm31
4.3	mvw111	Hmasm33
4.4	mvw145	Hmasm35
4.5	mvw146	
5.1	mvw200	
5.2	mvw234	
5.3	mvw201	
5.4	mvw206	
5.5	mvw210	
5.6	mvw207	
5.7	mvw202	
5.8	mvw208	

3.3	mvw121	
3.4	mvw096	
3.5	mvw098	Hmasm16
3.6	mvw099	
3.7	mvw097	
3.8	mvw114	Hmasm41
3.9	mvw168	Hmasm36
3.10	mvw170	Hmasm37
3.11	mvw105	
3.12	mvw072	

5.9	mvw209	
5.10	mvw221	
5.11	mvw235	
5.12	mvw224	Hmasm51
5.13	mvw226	
5.14	mvw229	
5.15	mvw218	
5.16	mvw219	
5.17	mvw223	
5.18	mvw228	